

# **Investigation of the Interaction between the Single-walled Carbon Nanotubes and Fluorene-based Conjugated Oligomers Using Dispersion Corrected DFT Methods**

by

©Mohammad Zahidul Hossain Khan

A thesis submitted to the School of Graduate Studies in partial fulfillment of the requirements for the degree of Master of Science.

Department of Physics and Physical Oceanography

Memorial University of Newfoundland  
October 2015

St. John's

Newfoundland

**This is dedicated to my beloved parents and my wife Jui**

## ABSTRACT

The area of carbon nanotubes (CNT)-polymer composites has been progressing rapidly in recent years. Pure CNT and CNT-polymer composites have many useful (industry related) properties ranging from good electrical conductivity to superior strength. However the full potential of using pure CNTs has been severely limited because of complications associated with the dispersion of CNTs. CNTs tend to entangle with each other forming materials that have properties that fall short of the expectations. The goal of this work is to enhance the understanding as to which type of conjugated oligomers is best suited for the dispersion of single walled CNTs (SWCNTs). For this purpose, various methods of dispersion corrected density functional theory (DFT-D/B97D, /WB97XD,/CAM-B3LYP) have been used to investigate the interaction between the SWCNT and the fluorene based oligomers with different end groups (aldehyde (ALD) and dithiafulvenyl (DTF)). We investigate the effect of intermolecular interactions on the structure, dipole moments and energetics of the oligomers. Our results indicate that DTF-endcapped oligomers tend to stretch along the nanotube (i.e. they lie parallel to it). On the other hand, ALD-endcapped oligomers tend to lie across the nanotube. As a result of this structural difference, our results also indicate that, DTF-endcapped conjugated oligomers become somewhat more polarized than ALD-endcapped oligomers in the presence of the SWCNTs and the binding energy is smaller for DTF-endcapped than ALD-endcapped oligomers with side chain.

## Acknowledgement

I would never have been able to finish my thesis without protection and ability from Allah to do this work.

I would like to give a million thanks to my supervisor, Prof. Jolanta B. Lagowski. From my M.Sc beginning to now, my supervisor teaches and helps me much more than what a professor does, more like a parent educating and caring for her own children, which makes me really enjoy my research and life. Her serious attitude in science and optimism for life will affect me forever. From the bottom of my heart, I would like to say: “thank you so much, my dear professor, I am so lucky to meet you in my life.”

I would like to convey my thanks to Mr. Fred Perry for his technical help. I would also like to acknowledge the financial assistance from Natural Science and Engineering Research Council of Canada (NSERC) and Memorial University of Newfoundland. I would like to thank the following for making this research possible: WestGrid ([www.westgrid.ca](http://www.westgrid.ca)), Compute Canada and ACENET ([www.acclearatediscovery.ca](http://www.acclearatediscovery.ca)) for providing the computational facilities. ACENET is the regional high performance computing consortium for universities in Atlantic Canada, and the provinces of Newfoundland and Labrador, Nova Scotia and New Brunswick. I also appreciate WestGrid and ACENET for their technical support.

Last but not least, I would like to thank my father, Delwar and mother, Jahanara and my beloved wife, Jui. They have always supported me and encouraged me with their best wishes.



# Table of Contents

|   |           |
|---|-----------|
| Dedication  | ii        |
| Abstract  | iii       |
| Acknowledgements  | iv        |
| Table of Contents   | v         |
| Abbreviations   | viii      |
| List of Tables  | x         |
| List of Figures   | xii       |
| <b>1. Introduction</b>  | <b>1</b>  |
| 1.1 Conjugated Polymers   | 1         |
| 1.2. Carbon Nanotubes   | 4         |
| 1.3 CNT-Polymer Composites and CNTs Dispersion                                      | 6         |
| 1.4 Current Research  | 10        |
| <b>2. Theoretical Approach</b>  | <b>13</b> |
| 2.1 Schrodinger Equation  | 13        |
| 2.2 Hartree-Fock Approximation  | 16        |
| 2.3 Density Functional Theory (DFT)   | 19        |
| 2.3.1 Hohenberg-Kohn (HK) Theorems  | 20        |
| 2.3.2 Kohn Sham Equations   | 20        |
| 2.4 The Exchange Correlation Energy Functional                                      | 22        |
| 2.4.1 Local Spin Density Approximation  | 23        |
| 2.4.2 Generalized Gradient Approximation (GGA)                                      | 24        |
| 2.4.3 B97D  | 26        |
| 2.4.4 CAM-B3LYP   | 28        |
| 2.4.5 wB97XD  | 30        |
| <b>3. Computational details</b>   | <b>33</b> |
| <b>4. Isolated Oligomers - Comparison of Structures Using Different DFT Methods</b> | <b>40</b> |
| 4.1 Introduction  | 40        |

|  |           |
|--|-----------|
| 4.2 Chemical and Molecular Structure of Fluorene-Based<br>Conjugated Oligomers.....                                  | 41        |
| 4.3 End Group Effect on the Oligomer Backbone.....   | 45        |
| 4.3.1 Bond Lengths.....  | 45        |
| 4.3.2 Bond Angles.....   | 47        |
| 4.3.3 Dihedral Angles.....   | 48        |
| 4.4 Side Chain Effect on the Oligomer Backbone.....  | 50        |
| 4.4.1 Bond Lengths.....  | 50        |
| 4.4.2 Bond Angles.....   | 52        |
| 4.4.3 Dihedral Angles.....   | 53        |
| 4.5 Comparison of DFT Methods.....   | 55        |
| 4.5.1 Structural Effects.....  | 55        |
| 4.5.2 Standard Deviation.....  | 59        |
| 4.6 Dipole Moment.....   | 62        |
| 4.7 HOMO, LUMO Eigenvalues and HOMO-LUMO Energy Gaps   | 69        |
| 4.8 Conclusions.....   | 73        |
| <b>5. Interacting Oligomers - Comparison of Structures Using Different Dispersion<br/>Corrected DFT Methods.....</b> | <b>75</b> |
| 5.1 Introduction.....  | 75        |
| 5.2 Molecular Structure of Interacting Fluorene-Based Oligomers.....   | 76        |
| 5.3 End Group Effect on the Oligomer Backbones.....  | 83        |
| 5.3.1 Bond Lengths.....  | 83        |
| 5.3.2 Bond Angles.....   | 85        |
| 5.3.3 Dihedral Angles.....   | 86        |
| 5.4 SCs Effect on the Oligomer Backbones.....  | 88        |
| 5.4.1 Bond Lengths.....  | 88        |
| 5.4.2 Bond Angles.....   | 89        |
| 5.4.3 Dihedral Angles.....   | 91        |
| 5.5 Method Effects.....  | 92        |
| 5.5.1 Structural Effects.....  | 92        |
| 5.5.2 Standard Deviation.....  | 96        |

|  |            |
|--|------------|
| 5.6 Binding Energy.....  | 99         |
| 5.7 Intermolecular Distance between Oligomer and CNT.....  | 102        |
| 5.8 Dipole Moment.....   | 104        |
| 5.8.1 End Group Effect.....  | 108        |
| 5.8.2 Side Chains Effect.....  | 109        |
| 5.9 HOMO, LUMO Eigenvalues and HOMO-LUMO Gaps.....   | 110        |
| 5.9.1 End Group Effect.....  | 113        |
| 5.9.2 Side Chain Effect.....   | 114        |
| 5. 10 Conclusions.....   | 115        |
| <b>6. The Effect of Dispersion on the Geometrical and Electronic Structure of Interacting Oligomers.....</b> | <b>116</b> |
| 6.1 Bond Length Differences.....   | 116        |
| 6.2 Bond Angle Differences.....  | 119        |
| 6.3 Dihedral Angle Differences.....  | 121        |
| 6.4 Dipole Moments.....  | 124        |
| 6.5 HOMO-LUMO Gaps.....  | 131        |
| 6.6 Conclusions.....   | 133        |
| <b>7. Summary and Conclusions.....</b>   | <b>134</b> |
| References.....  | 136        |
| Appendix.....  | 145        |

## Abbreviations

- **CNTs** Carbon Nanotubes
- **SWCNTs** Single-wall Carbon Nanotubes
- **PA** polyacetylene
- **OLED** Organic light-emitting diodes
- **CP** Conjugated polymer
- **EL** Electroluminescence
- **FET** Field-effect transistors
- **OFET** Organic Field-effect transistors
- **DWNT** Double-wall nanotubes
- **MWNT** Multi-wall nanotubes
- **DOS** Density of States
- **ALD** Aldehyde
- **DTF** Dithiafulvene
- **MO** Molecular Orbital
- **HF** Hartree-Fock
- **DFT** Density Functional Theory
- **LDA** Local Density Approximation
- **LSDA** Local Spin Density Approximation
- **BL** Bond lengths
- **BA** Bond angles

- **DA** Dihedral angles
- **ACEnet** Atlantic Computational Excellence Network
- **Westgrid** Western Canadian Research Grid
- **RMS** Root Mean Square
- **SCF** Self Consistent Field
- **HOMO** Highest Occupied Molecular Orbital
- **LUMO** Lowest Unoccupied Molecular Orbital
- **nqs** no-quota scratch
- **CPU** Central Processing Unit
- **GGA** Generalized Gradient Approximation

# List of Tables

|  |     |
|--|-----|
| 3.1: The criteria of the SCF convergence   | 35  |
| 4.1: Standard deviations of bond lengths (in Angstroms) for different dispersion corrected DFT methods as a function of oligomers with different end groups and with and without SCs   | 59  |
| 4.2: Standard deviations of bond angles (in degrees) for different dispersion corrected DFT methods as a function of oligomers with different end groups and with and without SCs      | 60  |
| 4.3: Standard deviations of dihedral angles (in degrees) for different dispersion corrected DFT methods as a function of oligomers with different end groups and with and without SCs  | 60  |
| 4.4: Dipole moments (in debyes) with $x$ , $y$ and $z$ components ( $\mu_x, \mu_y, \mu_z$ ) of different molecule systems as a function of different dispersion corrected DFT methods. | 66  |
| 4.5: HOMO, LUMO eigenvalues and HOMO-LUMO energy gap of different molecule system as a function of different dispersion corrected DFT methods.   | 70  |
| 5.1: Standard deviations of bond length (in Angstroms) for different dispersion corrected DFT methods as a function of interacting oligomers with different end groups and SCs.        | 97  |
| 5.2: Standard deviations of bond angles(in degrees) for different dispersion corrected DFT methods as a function of interacting oligomers with different end groups and SCs.           | 97  |
| 5.3: Standard deviations of dihedral angles (in degrees) for different dispersion corrected DFT methods as a function of interacting oligomers with different end groups and SCs.      | 97  |
| 5.4 Binding energy (eV) of different composite systems as a function of different DFT methods.   | 99  |
| 5.5 Distance of the oligomer relative to CNT for different composite systems as a function of different dispersion corrected DFT methods   | 102 |
| 5.6 Angle of the oligomer relative to CNT for different composite systems as a function of different dispersion corrected DFT methods.   | 103 |

5.7: Dipole moments (in Debyes) with components (along  $x$ ,  $y$ ,  $z$  axis) of different conjugated oligomer as a function of different dispersion corrected DFT methods. 105

5.8: HOMO and LUMO eigenvalues and HOMO-LUMO gaps of different composite systems as a function of different dispersion corrected DFT methods. 111

## List of Figures

|   |    |
|---|----|
| 3.1: Dipole moment direction for single molecule system.....  | 38 |
| 3.2: Blue line is the distance between the CNT center to the oligomer center.....   | 39 |
| 4.1: Chemical structure of fluorene-based ALD-endcapped oligomer.....   | 42 |
| 4.2: Molecular (optimized with DFT/B3LYP) structure of fluorene-based ALD-endcapped oligomer without SCs.....   | 42 |
| 4.3: Molecular (optimized with DFT/B3LYP) structure of fluorene-based ALD-endcapped oligomer with SCs.....  | 43 |
| 4.4: Chemical structure of fluorene-based DTF-endcapped oligomer.....   | 43 |
| 4.5: Molecular (optimized with DFT/B3LYP) structure of fluorene-based DTF-endcapped oligomer without SCs.....   | 44 |
| 4.6: Molecular (optimized with DFT/B3LYP) structure of fluorene-based DTF-endcapped oligomer with SCs.....  | 44 |
| 4.7: Bond length differences between ALD- and DTF-endcapped oligomers as a function of bond length position of oligomers without SCs for different DFT methods.....         | 46 |
| 4.8: Bond length differences between ALD- and DTF-endcapped oligomers as a function of bond length position of oligomers with SCs for different DFT methods. ....           | 46 |
| 4.9: Bond angle differences between ALD- and DTF-endcapped oligomers as a function of bond angle position of oligomers without SCs for different DFT methods.....           | 47 |
| 4.10: Bond angle differences between ALD- and DTF-endcapped oligomers as a function of bond angle position of oligomers with SCs for different DFT methods.....             | 48 |
| 4.11: Dihedral angle differences between ALD- and DTF-endcapped oligomers as a function of dihedral angles position of oligomers without SCs for different DFT methods..... | 49 |
| 4.12: Dihedral angle differences between ALD- and DTF-endcapped oligomers as a function of dihedral angles position of oligomers with SCs for different DFT methods..       | 49 |
| 4.13: Bond length differences between ALD-endcapped oligomers without and with SCs as a function of bond length position of oligomers for different DFT methods.....        | 51 |



|  |    |
|--|----|
| 4.14: Bond length difference between DTF-endcapped oligomers without and with SCs as a function of bond length position of oligomers for different DFT methods.....  | 51 |
| 4.15: Bond angle differences between ALD-endcapped oligomer without and with SCs as a function of bond angle position of oligomers for different DTF methods.....  | 52 |
| 4.16: Bond angle differences between DTF-endcapped oligomer without and with SCs as a function of bond angle position of oligomers for different DFT methods.....  | 53 |
| 4.17: Dihedral angle differences between ALD-endcapped oligomers without and with SCs as a function of dihedral angles position of oligomer for different DFT methods....  | 54 |
| 4.18: Dihedral angle differences between DTF-endcapped oligomers without and with SCs as a function of dihedral angle position of oligomer for different DFT methods.....  | 54 |
| 4.19: Bond lengths for ALD-endcapped oligomers (a) without and (b) with SCs and for DTF-endcapped oligomers (c) without and (d) with SCs along oligomers backbones (see Figure 4.1 and 4.4 respectively) for different DTF methods.....            | 56 |
| 4.20: Bond angles for ALD-endcapped oligomers (a) without and (b) with SCs and for DTF-endcapped oligomers (c) without and (d) with SCs along oligomers backbones (see Figure 4.1 and 4.4 respectively) for different DTF methods.....             | 57 |
| 4.21: Dihedral angles for ALD-endcapped oligomers (a) without and (b) with SCs and for DTF-endcapped oligomers (c) without and (d) with SCs along oligomers backbones (see Figure 4.1 and 4.4 respectively) for different DTF methods.....         | 58 |
| 4.22: Standard deviation for bond length as a function of different oligomer systems for different methods.....  | 60 |
| 4.23: Standard deviation for bond angle as a function of different oligomer systems for different methods.....   | 61 |
| 4.24: Standard deviation for dihedral angle as a function of different oligomer systems for different methods.....   | 61 |
| 4.25 Total dipole moments (indicated by the blue arrow) of ALD- and DTF-endcapped oligomers without SCs for different dispersion corrected and hybrid functional DFT methods. For clarity, only the relevant portion of the oligomer is shown..... | 64 |
| 4.26 Total dipole moments (indicated by the blue arrows) of ALD- and DTF-endcapped oligomers with SCs for different dispersion corrected and hybrid functional DFT methods. For clarity, only the relevant portion of the oligomer is shown.....   | 65 |

|  |    |
|--|----|
| 4.27: Dipole moments as a function of different methods for oligomers with ALD and DTF end groups without SCs.....   | 67 |
| 4.28 Dipole moment magnitudes as a function of different methods for oligomers with ALD and DTF end groups with SCs.....   | 67 |
| 4.29: Dipole moment magnitudes as a function of different methods for oligomers with ALD end group and without and with SCs.....   | 68 |
| 4.30: Dipole moment magnitudes as a function of different methods for oligomers with DTF end group and without and with SCs.....   | 68 |
| 4.31 HOMO, LUMO eigenvalues and -(HOMO-LUMO) gaps as a function of different oligomer systems (1.ALD without SCs, 2.DTF without SCs, 3.ALD with SCs, 4.DTF with SCs) for B97D method.....                  | 70 |
| 4.32 Figure 4.26 HOMO, LUMO eigenvalues and -(HOMO-LUMO) gaps as a function of different oligomer systems (1.ALD without SCs, 2.DTF without SCs, 3.ALD with SCs, 4.DTF with SCs) for wB97XD method.....    | 71 |
| 4.33 Figure 4.26 HOMO, LUMO eigenvalues and -(HOMO-LUMO) gaps as a function of different oligomer systems (1.ALD without SCs, 2.DTF without SCs, 3.ALD with SCs, 4.DTF with SCs) for CAM-B3LYP method..... | 71 |
| 4.34 Figure 4.26 HOMO, LUMO eigenvalues and -(HOMO-LUMO) gaps as a function of different oligomer systems (1.ALD without SCs, 2.DTF without SCs, 3.ALD with SCs, 4.DTF with SCs) for B3LYP method.....     | 71 |
| 4.35: HOMO-LUMO gaps of oligomers with ALD and DTF without SCs oligomers as a function of different DFT methods.....   | 72 |
| 4.36: HOMO-LUMO gaps of oligomers with ALD and DTF with SCs oligomers as a function of different DFT methods. ....   | 72 |
| 4.37: HOMO-LUMO gaps of oligomers with ALD without and with SCs oligomers as a function of different DFT methods.....  | 73 |
| 4.38: HOMO-LUMO gaps of oligomers with DTF without and with SCs oligomers as a function of different DFT methods.....  | 73 |
| 5.1: Molecular structures of composite fluorene-based ALD- and DTF-endcapped oligomers and SWCNs without SCs (a) side view (b) top view (c) top view along the backbone obtained using DTF/B97D.....       | 77 |

|  |    |
|--|----|
| 5.2: Molecular structures of composite fluorene-based ALD- and DTF-endcapped oligomers and SWCNTs without SCs (a) side view (b) top view (c) top view along the backbone obtained using DFT/CAM-B3LYP..... | 78 |
| 5.3: Molecular structures of composite fluorene-based ALD- and DTF-endcapped oligomers and SWCNTs without SCs (a) side view (b) top view (c) top view along the backbone obtained using DFT/wB97XD.....    | 79 |
| 5.4: Molecular structures of composite fluorene-based ALD- and DTF-endcapped oligomers and SWCNTs with SCs (a) side view (b) top view (c) top view along the backbone obtained using DFT/B97D.....         | 80 |
| 5.5: Molecular structures of composite fluorene-based ALD- and DTF-endcapped oligomers and SWCNTs with SCs (a) side view (b) top view (c) top view along the backbone obtained using DFT/CAM-B3LYP.....    | 81 |
| 5.6: Molecular structures of composite fluorene-based ALD- and DTF-endcapped oligomers and SWCNTs with SCs (a) side view (b) top view (c) top view along the backbone obtained using DFT/wB97XD.....       | 82 |
| 5.7: Bond length differences between ALD- and DTF-endcapped oligomers as a function of bond length position of interacting oligomers without SCs for different DFT methods.....                            | 84 |
| 5.8: Bond length differences between ALD- and DTF-endcapped oligomers as a function of bond length position of interacting oligomers with SCs for different DFT methods....                                | 84 |
| 5.9: Bond angle differences between ALD- and DTF-endcapped oligomers as a function of bond angle position of interacting oligomers without SCs for different DFT methods.....                              | 85 |
| 5.10: Bond angle differences between ALD- and DTF-endcapped oligomers as a function of bond angle position of interacting oligomers with SCs for different DFT methods....                                 | 86 |
| 5.11: Dihedral angle differences between ALD- and DTF-endcapped oligomers as a function of dihedral angles position of interacting oligomers without SCs for different DFT methods.....                    | 87 |
| 5.12: Dihedral angle differences between ALD- and DTF-endcapped oligomers as a function of dihedral angles position of interacting oligomers with SCs for different DFT methods.....                       | 87 |
| 5.13: Bond length differences between ALD-endcapped oligomer without and with SCs as a function of bond length position of interacting oligomers for different DFT methods.....                            | 88 |

|   |     |
|---|-----|
| 5.14: Bond length difference between DTF-encapped oligomer without and with SCs as a function of bond length position of interacting oligomers for different DFT methods.....         | 89  |
| 5.15: Bond angle differences between ALD-encapped oligomer without and with SCs as a function of bond angle position of interacting oligomers for different DFT methods...            | 90  |
| 5.16: Bond angle differences between DTF-encapped oligomer without and with SCs as a function of bond angle position of interacting oligomers for different DFT methods...            | 90  |
| 5.17: Dihedral angle differences between ALD-encapped oligomers without and with SCs as a function of dihedral angles position of interacting oligomer for different DFT methods..... | 91  |
| 5.18: Dihedral angle differences between DTF-encapped oligomers without and with SCs as a function of dihedral angle position of interacting oligomer for different DFT methods.....  | 91  |
| 5.19: Bond lengths for ALD-encapped oligomers (a) without SCs and (b) with SCs. Bond lengths for DTF-encapped oligomers (c) without SCs and (d) with SCs.....                         | 93  |
| 5.20: Bond angles for ALD-encapped oligomers (a) without SCs and (b) with SCs. Bond angles for DTF-encapped oligomers (c) without SCs and (d) with SCs.....                           | 94  |
| 5.21: Dihedral angles for ALD-encapped oligomers (a) without SCs and (b) with SCs. Dihedral angles for DTF-encapped oligomers (c) without SCs and (d) with SCs.....                   | 95  |
| 5.22: Standard deviations for bond lengths as a function of different interacting oligomer systems for different methods.....   | 98  |
| 5.23: Standard deviations for bond angles as a function of different interacting oligomers system for different methods.....  | 98  |
| 5.24: Standard deviations for dihedral angles as a function of different interacting oligomers system for different methods.....  | 98  |
| 5.25: End group effect for binding energy of composite systems with (ALD and DTF end group) without SCs as a function of different dispersion corrected DFT methods.....              | 100 |
| 5.26: End group effect for binding energy of composite systems with (ALD & DTF end group) with SC as a function of different dispersion corrected DFT methods.....                    | 100 |
| 5.27: SCs effect for binding energy of composite systems with ALD end group without and with SCs as a function of different dispersion corrected DFT methods.....                     | 101 |

|   |     |
|---|-----|
| 5.28: SCs effect for binding energy of composite systems with DTF end group without and with SCs as a function of different dispersion corrected DFT methods.....   | 101 |
| 5.29 Distance of oligomer and CNT.....  | 103 |
| 5.30: Dipole moments (direction indicated by the blue arrow) for ALD- and DTF -endcapped interacting oligomers without SCs for different dispersion corrected DFT methods. For clarity hydrogens are not shown..... | 106 |
| 5.31: Dipole moment (direction indicated by the blue arrow) for ALD- and DTF -endcapped interacting oligomers with SCs for different dispersion corrected DFT methods. For clarity hydrogens are not shown.....     | 107 |
| 5.32 Dipole moment as a function of different methods for oligomers with ALD and DTF end group without SCs.....   | 108 |
| 5.33 Dipole moment as a function of different methods for oligomers with ALD and DTF end group with SCs.....  | 109 |
| 5.34 Dipole moment as a function of different methods for oligomers with ALD end group without and with SCs.....  | 109 |
| Figure 5.35 Dipole moment as a function of different methods for oligomers with DTF end group without and with SCs.....   | 110 |
| 5.36: HOMO, LUMO eigenvalues and HOMO-LUMO gaps as a function of different composite systems (1. ALD without SCs, 2. DTF without SCs, 3. ALD with SCs, 4. DTF with SCs) for B97D method.....                        | 112 |
| 5.37: HOMO, LUMO eigenvalues and HOMO-LUMO gaps as a function of different composite systems (1. ALD without SCs, 2. DTF without SCs, 3. ALD with SCs, 4. DTF with SCs) for wB97XD method.....                      | 112 |
| 5.38: HOMO, LUMO eigenvalues and HOMO-LUMO gaps as a function of different composite systems (1. ALD without SCs, 2. DTF without SCs, 3. ALD with SCs, 4. DTF with SCs) for CAM-B3LYP method.....                   | 112 |
| 5.39: HOMO-LUMO gaps of interacting ALD- and DTF-endcapped oligomers without SCs as a function of different DFT methods.....  | 113 |
| 5.40: HOMO-LUMO gaps of interacting ALD- and DTF-endcapped oligomers with SCs as a function of different DFT methods.....   | 113 |
| 5.41: HOMO-LUMO gaps of the oligomer with ALD end group without and with SCs as a function of different DFT methods.....  | 114 |

|  |     |
|--|-----|
| 5.42: HOMO-LUMO gaps of the oligomer with DTF end group without and with SCs as a function of different DFT methods.....   | 114 |
| 6.1 Dispersion effect for ALD-endcapped oligomers without SCs for bond length differences as a function of bond length position for different DFT methods.....                             | 117 |
| 6.2 Dispersion effect for DTF-endcapped oligomers without SCs for bond length differences as a function of bond length position for different DFT methods.....                             | 117 |
| 6.3 Dispersion effect for ALD-endcapped oligomers with SCs for bond length differences as a function of bond length position for different DFT methods.....                                | 118 |
| 6.4 Dispersion effect for DTF-endcapped oligomers with SCs for bond length differences as a function of bond length position for different DFT methods.....                                | 118 |
| 6.5 Dispersion effect for ALD-endcapped oligomers without SCs for bond angle differences as a function of bond angle position for different DFT methods.....                               | 119 |
| 6.6 Dispersion effect for DTF-endcapped oligomers without SCs for bond angle differences as a function of bond angle position for different DFT methods.....                               | 120 |
| 6.7 Dispersion effect for ALD-endcapped oligomers with SCs for bond angle differences as a function of bond angle position for different DFT methods.....                                  | 120 |
| 6.8 Dispersion effect for DTF-endcapped oligomers with SC for bond angle differences as a function of bond angle position for different DFT methods.....                                   | 121 |
| 6.9 Dispersion effect for ALD-endcapped oligomers without SCs for dihedral angle differences as a function of dihedral angle position for different DFT methods.....                       | 122 |
| 6.10 Dispersion effect for DTF-endcapped oligomers without SC for dihedral angle differences as a function of dihedral angle position for different DFT methods.....                       | 122 |
| 6.11 Dispersion effect for ALD-endcapped oligomers with SC for dihedral angle differences as a function of dihedral angle position for different DFT methods.....                          | 123 |
| 6.12 Dispersion effect for DTF-endcapped oligomers with SC oligomer for dihedral angle differences as a function of dihedral angle position for different DFT methods.....                 | 123 |
| 6.13: Dipole moment directions (see blue arrows) for ALD-endcapped oligomers without SCs for the isolate and the interacting oligomers for different dispersion corrected DFT methods..... | 125 |
| 6.14: Dipole moment directions (see blue arrows) for DTF-endcapped oligomers without SCs for the isolate and the interacting oligomers for different dispersion corrected DFT methods..... | 126 |

|   |     |
|---|-----|
| 6.15: Dipole moment directions (see blue arrows) for ALD-endcapped oligomers with SCs for the isolate and the interacting oligomers for different dispersion corrected DFT methods..... | 127 |
| 6.16: Dipole moment directions (see blue arrows) for ALD-endcapped oligomers with SCs for the isolate and the interacting oligomers for different dispersion corrected DFT methods..... | 128 |
| 6.17: Dispersion effect on dipole moments of ALD-endcapped oligomers without SCs as a function of different DFT methods.....  | 129 |
| 6.18: Dispersion effect on dipole moments of DTF-endcapped oligomers without SCs as a function of different DFT methods.....  | 129 |
| 6.19: Dispersion effect on dipole moments of ALD-endcapped oligomers with SCs as a function of different DFT methods.....   | 130 |
| 6.20: Dispersion effect on dipole moments of DTF-endcapped oligomers with SCs as a function of different DFT methods.....   | 130 |
| 6.21: Dispersion effect on HOMO-LUMO gaps of ALD-endcapped oligomers without SCs as a function of different DFT methods.....  | 131 |
| 6.22: Dispersion effect on HOMO-LUMO gaps of DTF-endcapped oligomers without SCs as a function of different DFT methods.....  | 132 |
| 6.23: Dispersion effect on HOMO-LUMO gaps of ALD-endcapped oligomers with SCs as a function of different DFT methods.....   | 132 |
| 6.24: Dispersion effect on HOMO-LUMO gaps of DTF-endcapped oligomers with SCs as a function of different DFT methods.....   | 133 |

# Chapter 1

## Introduction

In this chapter, we will state our motivation for this thesis. First, we will introduce conjugated polymers then carbon nanotubes (CNTs) followed by composite systems consisting of conjugated polymers and CNTs. Finally current research will be described.

### 1.1 Conjugated Polymers

An organic polymer, which has a molecular structure consisting of a long chain, is typically an insulator (sometimes a semiconductor). Conjugated polymers are characterized by the overlapping alternating “single” and “double” bonds along the backbones of the polymer chains which results in bond delocalization and allows charges such as electrons to be shared with many atoms along the polymer backbones. These delocalized electrons may become charge carriers since they can move freely throughout the whole molecular system [1]. About three decades ago, scientists discovered that a conjugated polymer such as polyacetylene (PA) when doped can display high electrical



conductivity [2,3]. That is, in 1977, A. G. MacDiarmid and H. Shirakawa with their group members found that doped PA can form a new class of polymers whose electrical conductivity can be continuously and systematically varied and whose conductivity range extends over eleven orders of magnitude [4]. In 1987, H. Naarmann and his colleagues accomplished a breakthrough work on these polymers. They have obtained PA's conductivity as high as that of copper metal [5]. Because of their electrical conductivity, PA and other conjugated polymers are sometimes called conducting polymers. Following the discovery of conductivity of doped PA, in 1990 D.D.C Bradley and his co-workers discovered that CPs such as phenylene-vinylene polymers can also electroluminescence [6]. The main advantages of the polymer electroluminescence (EL) devices are their fast response times, ease of process ability, and low operating voltages [7].

The mechanical properties and elemental processing advantages, coupled with the electronic and optical properties of CPs, means that they are particularly attractive materials for the electronic industry. The excellent light-harvesting and light-amplifying properties of CPs also make them attractive materials in biological fields by dissolving or dispersing in aqueous media to fulfil biological applications [8]. Organic light-emitting diodes (OLEDs) for display represent one of the most successful commercial applications of CPs semiconductors. The light-emitting properties and molecular design can also make them attractive for bio-imaging and bio-sensing applications [9]. Supercapacitors are electrochemical capacitors that are useful for power supply with high dynamic charge propagation and long life [10, 11]. The electrode materials for supercapacitors have been classified to belong to three broad categories and CPs is one of them [12, 13]. In addition, since 1983 [14], CPs-based semiconductors have been used to fabricate field-

effect transistors (FETs). CPs based transistors have already found their applications as, for example, in smart pixels [15] and sensors [16].

Fluorene is a common polycyclic aromatic hydrocarbon known for its violet fluorescence [17]. Fluorene-based conjugated oligomers can emit deep blue light at an efficiency of up to 99% in solution and 90% in thin (solid) films [18]. The decoupling property of bonding site, the fluorene's 9-position, makes it very useful, as side groups (usually long alkyl chains) can be placed at 90° angles to the  $\pi$ -conjugated system. The highest efficiency of OLED was found by Wu C-C and his coworkers after using spiro-terfluorene in a double confinement device structure [19]. For blue-emitting device, its life time is a key concern. Ditolylamine endcapped terfluorene, has been demonstrated in a device with a time to half luminescence of 500 hour at 1100 cd/m<sup>2</sup> [20]. Linearly polarized OLEDs could be used as backlights for LCD displays and liquid crystalline fluorene oligomers have shown excellent performance in polarized OLEDs [21]. Chiral oligofluorenes have also exhibited circularly electroluminescence with highest polarization without optical elements external to the OLED device [22]. Fluorene based oligomers have also laser applications. Bifluorenes [23] up to tetrafluorenes [24] showed excellent lasing performance in the UV to deep blue range when excited by appropriate flash lamps. Many high-performance organic FETs (OFETs) are composed of small molecular weight compounds and fluorene-based oligomers being very prominent amongst them [25]. Oligothiophenes are attractive, but their stability against oxidation at ambient exposure is poor. Instead of oligothiophenes, fluorene-thiophene co-oligomers have emerged as more oxidatively stable materials in p-type OFETs [26]. Oligofluorenes and their derivatives also have solar cell applications [27].

## 1.2 Carbon Nanotubes

Carbon nanotubes (CNTs) are considered to be an allotrope of carbon and can be visualized as a sheet of graphene rolled into a cylinder. They are remarkable objects that will have great impact on the technological advances in the near future. Future world will be shaped by nanotube applications similar to silicon-based technology that dominated the (computer and other applications) industry in the past and continues to do so today. CNTs were discovered by Sumio Iijima in 1991 [28] in the Nippon electronic company (NEC) laboratory in Tsukuba, Japan when the high resolution transmission electron microscopy (TEM) was used to observe the sediment generated from the electrical discharge between two carbon electrodes. Single-wall nanotube (SWCNTs), multi-wall nanotube (MWNTs) and double-wall nanotubes (DWNTs) are the examples of the types of carbon nanotubes produced today. It is relatively easy to visualize a SWCNT which is consider as a perfect graphene sheet (graphene is a polyaromatic, monoatomic layer consisting of  $sp^2$ -hybridized carbon atoms arranged in hexagons; for comparison it should be noted that the more readily available graphite consists of graphene layers) that is rolled into a cylinder. The electronic states in SWCNTs are strongly affected by their one-dimensional cylindrical structures. SWCNT's electronic band structure can be obtained by applying the periodic boundary conditions to the tube under consideration. One-dimensional sub-bands are formed that have strong singularities in its density of states (DOS) (referred to as van Hove singularities). The conduction and the valence bands of the graphene only touch at six corners (K points) of the Brillouin zone [28]. When one of these sub-bands passes through the K point, the CNT is metallic otherwise it is semiconducting. The one-dimensional van Hove singularities have also large influence

on the optical properties of CNTs. It has been observed that a broad band flash in the visible spectral range can lead the spontaneous burning of agglomerated SWCNTs in air at room temperature [29]. SWCNTs are also special due to their strong bonding between the carbons of the curved graphene sheet, which is stronger than the bonding in the diamond. This makes CNTs stable against deformations. Their tensile strengths can be 20 times that of steel [30] and has been measured as approximately 45 GPa. [31]. Dai et al. [32] proposed that because of the high mechanical strength of CNTs, they are very good candidates for use as force sensors in scanning probe microscopy (SPM) (in this application he used MWNTs). These CNTs sensors provided higher durability but their ability to image surfaces with a high lateral resolution had some limitations [32]. Hafner et al. [34] used SWCNTs instead of MWCNTs in the SPM sensors. SWCNTs gave higher resolution than MWCNTs because of their small diameters [33]. de Heer et al. [34] did a pioneering work and showed that CNTs are efficient field emitters [34] and this property has been used several applications including flat panel displays for television sets and computers. The most advanced opportunities demand the ability to form perfectly aligned, horizontal arrays of purely semiconducting, chemically pristine carbon nanotubes. There are several methods for SWCNT sorting such as including DNA wrapping, density gradient ultracentrifugation, gel chromatography [35] and disperse SWCNT using conjugated oligomer (CNT-Polymer Composites).

### 1.3 CNT-Polymer Composites and CNTs Dispersion

The area of CNT-polymer composites has progressed intensely and rapidly in recent years. As mentioned above CNTs have important electrical, thermal and mechanical properties. For example, CNTs have unique electrical properties and their electric current-carrying capacity is 1000 times greater than that for the copper wire [36] and their average conductance is  $1/12.9 \text{ k}\Omega^{-1}$  [37]. Theoretical considerations suggest that CNTs have exceptional mechanical properties as determined by their elastic modulus which indicates that their strength is 20 times greater than that of the strongest steel [30]. These superior characteristics make CNTs optimal candidates for the formation of polymer-CNT or CNT-polymer composites with better electrical conductivity and mechanical properties than those of either of polymers or CNTs alone. It has been shown that CNT-polymer composites have versatile potential applications, ranging from electronic paper to the bullet proof vest [38]. A number of scientists have shown that the combinations of CNTs and polymers offer a novel route to materials with improved electrical properties, for example, J.-H. Du with his colleagues [39] have shown that introduction of CNTs to polymers can increase the conductivity of the original polymers by several orders of magnitude. Shaffer et al [40] also fabricated CNT-polymer composites and measured their electrical conductivity using impedance spectroscopy in a four-point configuration (the percolation threshold for these composites lay between 5 and 10 wt%). At the CNT concentration of 10 wt%, the electrical conductivity of the composites was about 1 S/cm which is an increase of about seven orders of magnitude [42]. In addition to very good electrical and mechanical properties; research indicates that CNTs also have excellent

thermal conductivity. Their thermal conductivity can reach 6600 W/mK at room temperature for SWCNTs [41] and 3000 W/mK for MWNTs [43]. Wei et al. [43] carried out classical molecular dynamics simulations that included intra-nanotube interactions and van der Waals intermolecular forces for the polymer-nanotube interface to investigate the thermal expansion and diffusion characteristics of CNT/PE composites. He found that the glass temperature,  $T_g$ , of the composite material has increased (relative to  $T_g$  of CNTs) and above  $T_g$ , the thermal expansion and diffusion coefficients of the composite also increased [42] in comparison to CNTs.

CNT-polymer composites may give different results for the electrical conductivity or the percolation threshold even when using the same polymer because of the uncertainty of the type and the crystalline orientation, and the quality of nanotubes (as characterized by their different sizes, aspect ratios, purity, entanglement, straightness etc.) [44]. Hence, there is a need for the production of pristine CNTs that can be used in composite materials with (reliably) reproducible properties. Furthermore considering their high surface area and high aspect ratio, intrinsic van der Waals attractions among tubes, typically leads to significant agglomeration which prevents the efficient transfer of their superior properties to the CNT-polymer matrix. This is even more complicated by the lack of adhesion between CNTs and various matrix polymers. The impurity, the agglomeration, and the nonreactive (with polymers) surface of CNTs limits their applications in composites [45,46,47,48]. To overcome some of these problems, the dispersion methods [50] of CNTs were introduced.

Dispersion refers to a system where particles of one kind are intermixed in a continuous phase of another composition or state. In spite of excellent electrical mechanical and optical properties of CNTs, the main challenge in this field is the dispersion and stabilization of CNTs-polymer matrices. As stated above, CNTs often aggregate together due to strong van der Waals interactions between the nanotubes [50]. To maximize the advantages of CNTs as effective reinforcements in high strength composites, there are several ways to improve the dispersion of CNTs in polymer matrices such as optimum physical blending, in situ polymerization and chemical functionalization [51]. Physical blending is the simplest and most convenient dispersion method for polymer-CNT composites. In this method, ultrasound and/or high speed shearing is employed to improve the dispersion CNTs in polymer matrix. Qian and his coworker [52] showed that simple solution-evaporation method assisted by high energy sonication can be used to prepare polystyrene (PS)/MWNT composite films (where MWNTs were dispersed homogeneously in the PS matrix). Similarly, Sandler and his colleagues [53] showed that dispersing CNTs in epoxy under high speed stirring (2000rpm) for 1 hour using excessive stirring was a very good process to obtain CNTs uniformly dispersed in epoxy. Adding an appropriate compatibilizer to polymer/CNT composites is also another good method [52]. In chemical functionalization, to achieve good dispersion in polymer/CNT composites and strong interface adhesion between surrounding polymer chains, the surfaces of CNTs have been chemically functionalized (including grafting copolymerization). Riggs [54] and Lin [55] showed that poly (vinyl-alcohol) PVA grafted CNTs were soluble in PVA solution. As prepared PVA-CNT composites films are of high optical quality without any observable phase separation. The results found that

chemical graft functionalization of CNTs in polymer matrix were an effective way to achieve homogeneous dispersion of high-performance polymer/CNT composites. On the other hand, to improve the optical, magnetic and electrical properties of CNTs, some conjugated polymers were attached to their surfaces by in situ polymerization. Fan and his coworkers [56] synthesized conjugated polypyrrole-coated CNTs and showed that the magnetization of composite CNT- polypyrrole is the sum of two components, polypyrrole and CNTs. Star et al [57] synthesized poly(meta-phenylene-vinylene)-wrapped SWCNTs, and UV-vis absorption spectra confirmed  $\pi$ - $\pi$  interactions between SWCNTs and fully conjugated poly(metaphenylenevinylene) (PmPV) backbones. The results reveal that the photo-excited PmPV has a dipole moment that alters the local electric field at the surface of SWCNTs [57]. Xiao and Zhou [58] deposited polypyrrole (PPY) or poly (3-methylthiophene) (PMeT) on the surfaces of the MWNTs by in situ polymerization and revealed that Faraday effect of the conjugated polymer enhances the performance of super-capacitors with MWNTs deposited with the conjugated polymer [58].

Every method has its own advantages and disadvantages. For the physical blending, the dispersed CNTs will quickly precipitate out again when sonication stops and the dispersion quality is the poorest among the three (discussed above) methods (but it is the simplest and the most cost effective method). For the chemical functionalization, CNTs are exposed to strong oxidizing reagents to attach useful groups, for example carboxylic acids, on the nanotube walls. Although most effective as a dispersion method, such treatment inevitably disrupts the long range  $\pi$ -conjugation of the nanotube, often leading to a decreased electrical conductivity, diminished mechanical strength, and other undesirable properties. In the third method, CNTs are de-bundled and stabilized by



dispersant chemicals (such as conjugated oligomers for example) through non-covalent interactions, therefore keeping the chemical structures, electronic and mechanical properties of the CNTs relatively intact. However, in some cases dispersions have limited solubility and stability because the conjugated polymers themselves face solubility and miscibility issues due to the strong interchain  $\pi$ - $\pi$  interactions [59].

The above discussion on CNT-polymer composites points out that the good dispersion method for CNTs (into polymer matrix) is essential for the production of the materials that can enhance the performance of the various organic-based devices and applications. It also points out that pristine or pure CNTs are the most useful materials in most applications since they lead to reproducible designs that can give rise to increased efficiency of these devices for example. In their natural state CNTs are mixtures of say, semiconducting and metallic tubes of various sizes and lengths [35]. Once again a dispersion process can be used to generate pure CNTs. Of particular interest in this work is the dispersion of SWCNTs with DTF- and ALD-endcapped fluorene-based oligomers [60].

## 1.4 Current Research

The main objective of the research in this thesis is to investigate the intermolecular interactions of aldehyde (ALD)- and dithiafulvene (DTF)-endcapped fluorine-based conjugated oligomers with SWCNT in vacuum. The fluorene-based oligomers consist of fluorene with one doubly substituted benzene ring at each end (this part, for short, is called diphenyl-fluorene (DPF)) capped with an end group (ALD or DFT). Hence, for

brevity, we refer to the oligomers as ALD-DPF and DTF-DPF respectively. Since ALD-DPF or DTF-DPF and SWCNT are not covalently bonded we must use the dispersion corrected density functional theory (DFT) to carry out our computations [61]. DFT implemented in Gaussian 09 software [62] constitutes a computational quantum mechanical approach employed to investigate the electronic structure (especially the ground state) of many-body systems such as atoms, molecules, and the condensed phases such as solids. With the use of this computational tool, the structural, optical and electronic properties of many-electron systems can be obtained. Typical DFT does not take into account intermolecular van der Waals interactions (also referred to as London dispersion, hence the term dispersion in the dispersion corrected DFT) between non-covalently bonded molecules. (It should be noted that the word dispersion has multiple meanings in this thesis and it is hoped that from the context of the discussion it will be clear which meaning is used at any given time.) These molecular interactions are very important for many systems such as graphite [63] (due to its interlayered bonding) and biological systems (typically consisting of more than one molecule). In this thesis, we use three dispersion corrected DFT approximations in our calculations: B97D, CAM-B3LYP and wB97XD. We focus on the structure (bond lengths, bond angles and dihedral angles) of the backbones of the fluorene-based oligomers and determine how they are affected by the presence of the long side chains (SCs), by different end groups (ALD and DTF) and by the presence of SWCNT. We consider their dipole moments, HOMO and LUMO eigenvalues and HOMO-LUMO gaps and how these are influenced by SCs, end groups and the presence of SWCNT. In each case of oligomer-SWCNT combination, we determine its binding energy and intermolecular distance between the oligomer and the

tube. It is hoped that the results of this thesis can be of interest to the experimental scientists involved in building organic electronic devices and to the DFT computational researchers.

The outline of this thesis is as follows: Chapter 1 gives the background and introduction; Chapter 2 provides the general theoretical concepts that are employed in computations (Hartree-Fock (HF) theory and the various DFT methods B97D, CAM-B3LYP and wB97XD are discussed briefly in this chapter); Chapter 3 gives the computational details; Chapters 4-6 present the results of this thesis; Chapter 7 states overall conclusions of this thesis.

# Chapter 2

## Theoretical Approach

In this chapter, we briefly discuss the theoretical framework used in this thesis. Over the past 50 years, density functional theory (DFT) has become a much used tool in the quantum mechanical computations involving molecular and periodic systems in chemistry and physics. We will first briefly review the Hartree-Fock (HF) approximation, the precursor to DFT, then DFT and dispersion corrected DFT (D-DFT) will be discussed. The goal of this thesis is to use D-DFT to investigate structure and interaction between conjugated organic oligomers and SWCNTs (in vacuum).

### 2.1 Schrodinger Equation

A molecule is an accumulation of quantum charged particles [64]. Finding the ground state properties of a molecule such as its geometry, vibrational frequencies, total electronic energy level, ground state energy, electron density distribution etc requires that we solve the non-relativistic Schrodinger equation (SE) [65]

$$\hat{H}\psi(\mathbf{r}, \mathbf{R}) = E\psi(\mathbf{r}, \mathbf{R}) \quad 2.1$$

where  $\hat{H}$  is the Hamiltonian operator,  $\psi$  is the total wave function,  $\mathbf{r}$  and  $\mathbf{R}$  stand for electron and nuclear coordinate respectively. For large molecules which contains  $N$  electrons and  $M$  nuclei, the non-relativistic Hamiltonian can be written as

$$\hat{H} = \hat{T} + \hat{V} \quad 2.2$$

where  $\hat{T}$  is the kinetic energy operator and  $\hat{V}$  is the potential energy operator of the system. Kinetic energy operator (first two terms in Eq. (2.3)) contains the electronic and nuclear kinetic energy terms and potential energy operator (the last three terms in Eq. (2.3)) contains electron-electron repulsion, nucleus-nucleus repulsion and electron-nucleus attraction contributions. That is, more explicitly Eq. (2.2) can be written as

$$\hat{H} = -\sum_{i=1}^N \frac{\hbar^2 \nabla_i^2}{2m_e} - \sum_{A=1}^M \frac{\hbar^2 \nabla_A^2}{2m_A} + \sum_{i=1}^N \sum_{j>i}^N \frac{e^2}{4\pi\epsilon_0 r_{ij}} + \sum_{A=1}^M \sum_{B>A}^M \frac{Z_A Z_B e^2}{R_{AB}} - \sum_{i=1}^N \sum_{A=1}^M \frac{Z_A e^2}{4\pi\epsilon_0 r_{iA}} \quad 2.3$$

where  $m_e$  is the mass of an electron,  $Z_A$  and  $m_A$  are the charge and mass of the  $A^{\text{th}}$  nucleus. The  $R_{AB}$  is the relative nuclear distance between the  $A^{\text{th}}$  and  $B^{\text{th}}$  nuclei,  $r_{ij}$  is the distance between the  $i^{\text{th}}$  and  $j^{\text{th}}$  electrons and  $r_{iA}$  is the distance between the  $i^{\text{th}}$  electron and  $A^{\text{th}}$  nucleus.  $\hbar$  is the Planck's constant divided by  $2\pi$  and  $\epsilon_0$  is the permittivity of free space.

The nuclei are much heavier than the electrons and hence move more slowly than the electrons. In the Born-Oppenheimer (BO) approximation, we can consider the electrons in a molecule to be moving in the field of fixed nuclei [64]. Given this approximation the second term in Eq. (2.3), the kinetic energy of the nuclei, can be neglected and fourth

term of Eq. (2.3), the repulsion between the nuclei, can be considered to be constant. The remaining term constitute the so called the electronic Hamiltonian which can be written as

$$\hat{H} = -\sum_{i=1}^N \frac{\hbar^2 \nabla_i^2}{2m_e} + \sum_{i=1}^N \sum_{j>i}^N \frac{e^2}{4\pi\epsilon_0 r_{ij}} + \sum_{i=1}^N \sum_{A=1}^M \frac{Z_A e^2}{4\pi\epsilon_0 r_{iA}}. \quad 2.4$$

In the BO approximation, the solution to Eq. (2.3) can be approximated as the product of wavefunction for electrons that depends parametrically on the coordinates of nuclei and nuclear wavefunction i.e.

$$\psi(\mathbf{r}, \mathbf{R}) = \psi_{el}(\mathbf{r}, \mathbf{R})X(\mathbf{R})$$

where more explicitly the electronic wave function is

$$\psi_{el} = \psi_{el}(\{\mathbf{r}_i\}, \{\mathbf{R}_A\}). \quad 2.5$$

The SE involving the electronic Hamiltonian can be written as [67]

$$\hat{H}\psi_{el} = E_{el}\psi_{el} \quad 2.6$$

where  $\hat{H}$  is given by Eq. (2.4). We emphasize that Eqs. (2.5 to 2.6) describe the motion of electrons and  $\psi_{el}$  not only depends on electronic coordinates but also parametrically on the nuclear coordinates, this also applies to electronic energy, i.e.

$$E_{el} = E_{el}(\{\mathbf{r}_i\}, \{\mathbf{R}_A\}). \quad 2.7$$

Often for simplicity the nuclear coordinates do not appear explicitly in  $\psi_{el}$ . The total electronic energy for fixed nuclei system includes nuclear repulsion, that is,

$$E_{tot} = E_{el} + \sum_{A=1}^M \sum_{B>A}^M \frac{Z_A Z_B e^2}{R_{AB}}. \quad 2.8$$

Equations 2.4 to 2.8 define the electronic problem to be solved in computational quantum mechanics.

## 2.2 Hartree-Fock Approximation

Two years after Schrodinger equation (S.E.) was published, in 1928, Hartree proposed a method for solving the multi-electron system, the approach today is called the Hartree method [64]. According to this method total eigenenergy is the sum of the orbital energies corresponding to different electronic eigenstates. For example, for two particle system (two electrons)

$$\hat{H}\psi = (\epsilon_1 + \epsilon_2)\phi_1\phi_2 = \epsilon\psi \quad 2.9$$

where  $\epsilon_1$  and  $\epsilon_2$  are the energy eigenvalues for the particle 1 and 2 respectively and  $\psi = \phi_1\phi_2$  is the product of single electron wave functions. However, it was found that the energies given by this method do not take into account the indistinguishability of electrons, which leads to the anti-symmetry principle for identical particles and requires that electronic wave functions be anti-symmetric. In 1930, Fock applied Slater determinant (see Eq. (2.10)) to the Hartree method and proposed the so called Hartree-Fock (HF) method. In my thesis, I consider closed shell systems where all molecular orbital levels are doubly occupied and the Slater determinant for 2n electron system is given by

$$\Psi(r, s) = \frac{1}{\sqrt{2n!}} \begin{pmatrix} \psi_1(1)\alpha(1) & \psi_1(1)\beta(1) & \dots & \dots & \dots & \psi_n(1)\beta(1) \\ \psi_1(2)\alpha(2) & \psi_1(2)\alpha(2) & \dots & \dots & \dots & \psi_n(2)\beta(2) \\ & & & & & \vdots \\ \psi_1(2n)\alpha(2n) & \psi_1(2n)\beta(2n) & \dots & \dots & \dots & \psi_n(2n)\beta(2n) \end{pmatrix} \quad 2.10$$

where  $\frac{1}{\sqrt{2n!}}$  is a normalizing factor.  $\psi(i)$  is a function of the coordinates of the  $i^{\text{th}}$  electron with the spin up  $\alpha(\uparrow)$  or the spin down  $\beta(\downarrow)$  [67] ( $\Psi(i)$  is often referred to as molecular orbital (MO)).

The variational theorem states that the energy calculated with any arbitrary wave functions must be greater than or equal to the exact HF ground-state (gs) energy calculated with the true ground state HF wave function [68]

$$E[\psi] \geq E[\psi_{gs}^{HF}]. \quad 2.11$$

Applying the variational principle on Eq. (2.11), we obtain an equation for a single electron

$$\hat{F}\psi_i = \epsilon_i\psi_i. \quad 2.12$$

This equation is called the HF equation and the operator  $\hat{F}$  is called the Fock operator where  $\hat{F}$  is defined as

$$\hat{F} = \hat{h} + \sum_j^n (2\hat{J}_j - \hat{K}_j) \quad 2.13$$

where  $\hat{J}_j$  and  $\hat{K}_j$  are called Coulomb operator and exchange operator respectively and are defined as

$$\hat{J}_j(\mathbf{r}_1)\psi_i(\mathbf{r}_1) = \int d^3\mathbf{r}_2 \psi_j^*(\mathbf{r}_2)\psi_j(\mathbf{r}_2) \frac{1}{r_{12}} \psi_i(\mathbf{r}_1) \quad 2.14$$



and 
$$\hat{K}_j(\mathbf{r}_1)\psi_i(\mathbf{r}_1) = \int d^3\mathbf{r}_2 \psi_j^*(\mathbf{r}_2)\psi_i(\mathbf{r}_2) \frac{1}{r_{12}} \psi_j(\mathbf{r}_1) . \quad 2.15$$

The orbital energy  $\epsilon_i$  is given as

$$\begin{aligned} \epsilon_i &= \int d^3\mathbf{r}_1 \psi_i^*(\mathbf{r}_1) \hat{F} \psi_i(\mathbf{r}_1) \\ &= h + \sum_j^n (2J_{ij} - K_{ij}). \end{aligned} \quad 2.16$$

Then using this orbital energy as given in Eq. (2.16), the total electron energy is written

as 
$$E = 2 \sum_i^n \epsilon_i - \sum_{i,j}^n (2J_{ij} - K_{ij}) \quad 2.17$$

where the sum is over the occupied orbitals and

$$\begin{aligned} J_{ij} &= \int d^3\mathbf{r}_1 d^3\mathbf{r}_2 \psi_i^*(\mathbf{r}_1) \psi_j^*(\mathbf{r}_2) \frac{1}{r_{12}} \psi_i(\mathbf{r}_1) \psi_j(\mathbf{r}_2) = \langle ij|ij \rangle \\ K_{ij} &= \int d^3\mathbf{r}_1 d^3\mathbf{r}_2 \psi_i^*(\mathbf{r}_1) \psi_j^*(\mathbf{r}_2) \frac{1}{r_{12}} \psi_j(\mathbf{r}_1) \psi_i(\mathbf{r}_2) = \langle ij|ji \rangle. \end{aligned}$$

Roothaan and Hall developed a method for solving the Hartree-Fock equation that is more appropriate for today's computers. They transformed differential equation into an equivalent algebraic form using the so called Roothaan-Hall method [68]. In this method MO  $\psi(i)$  is expanded as a linear combination of basis functions (LACO) [69]

$$\psi_i = \sum_{s=1}^{n_{AO}} C_{si} \chi_s \quad 2.18$$

where  $C_{si}$  are the molecular orbital coefficient and  $\chi_s$  are basis functions modeling atomic orbitals. Using this expansion of molecular orbitals, the HF equation is transformed into a matrix equation,

$$F_{sp}C_{si} = \epsilon S_{sp}C_{si} \quad 2.19$$

where

$$F_{sp} = \int d^3r \chi_s^*(\mathbf{r}) \hat{F} \chi_p(\mathbf{r})$$

and

$$S_{sp} = \int d^3r \chi_s^*(\mathbf{r}) \chi_p(\mathbf{r}). \quad 2.20$$

The total HF energy is given by

$$E_{HF} = 2 \sum_{s=1}^m F_{sp}C_{si} + \sum_{s=1}^m \epsilon_{ij} S_{sp}C_{si} \quad 2.21$$

where  $\epsilon_{ij}$  is the diagonal matrix of orbital energies. Using orthonormalized basis sets, Roothaan equation is solved by the (iterative) self-consistent field (SCF) method. In this method the Eq. (2.19) is repeatedly solved until the initial and final charge density is within some predefined criteria [70] (see chapter 3 for details).

## 2.3 Density Functional Theory (DFT)

Hartree-Fock method was and still is an impressive achievement for calculating the ground state energy, constructing the Random Phase Approximation (RPA) and the Random Phase Approximation with Exchange (RPAE) for investigating the properties of multi-electron objects, such as atoms [71], molecules, clusters and fullerenes. Unfortunately, HF method has some difficulties in its application. It treats exchange energy exactly, however it cannot explain the dynamical correlation or correlation contribution of kinetic energy [72]. To overcome this difficulty in early 1960 the Density Functional Theory (DFT) was proposed. This method has helped to reduce the problem of calculating the ground state characteristics of a many-electron system in a local

external field [73]. In this theory total electron density  $\rho = \psi * \psi$  is the main variable rather than wave function  $\psi$ .

### 2.3.1 Hohenberg-Kohn (HK) Theorems

Hohenberg-Kohn theorems are the heart of the DFT method. These theorems were formulated in 1964 [72]. In DFT the electronic Hamiltonian  $H$  can be written as

$$\hat{H} = \hat{V}(r) + \hat{T} + \hat{V}_{ee} \quad 2.19$$

where  $\hat{V}(r)$ ,  $\hat{T}$ , and  $\hat{V}_{ee}$  are external potential, kinetic energy and electron-electron interaction. The solution of the Schrödinger equation depends on external potential and number of electrons. The first HK theorem stated that the potential  $V(r)$  is, except for a constant, determined by the electron density  $\rho(\mathbf{r})$ . As  $\rho(\mathbf{r})$  also determines  $N$ , it determines all ground state properties. And second theorem stated that any trial density  $\rho(\mathbf{r})$  gives energy that is higher than the true ground state energy calculated with ground state electron density function  $\rho'(r)$  that is

$$\rho'(\mathbf{r}) \text{ with } \rho'(\mathbf{r}) \geq 0 \text{ and } \int \rho'(\mathbf{r}) d\mathbf{r} = N, E_o = E_v[\rho'] < E_v[\rho]. \quad 2.20$$

This is the variational principle for the DFT [75].

### 2.3.2 Kohn Sham Equations

Density functional theory can be implemented in many ways but the most successful approach is one due to Kohn-Sham [75]. They introduced a system with no electron-electron repulsion terms in its Hamiltonian but having the same ground-state electron density as the real system (i.e. they introduced a non-interacting reference system

corresponding to real system [76]). The ground state energy of a many electron system can be given as the energy functional,

$$E_v[\rho] = T[\rho] + U[\rho] + V[\rho] \quad 2.21$$

where  $V[\rho]$  is a universal functional that depends on the  $v(\mathbf{r})$  and can be written in terms of the particle density  $\rho$  as

$$V[\rho] = \int d\mathbf{r} v(\mathbf{r})\rho(\mathbf{r}) . \quad 2.22$$

Applying Lagrange multipliers in Eq. (2.22) the minimization of  $E_v[\rho]$  gives

$$\delta[T[\rho] + U[\rho] + \int d\mathbf{r} v(\mathbf{r})\rho(\mathbf{r}) - \mu(\int d\mathbf{r}\rho(\mathbf{r}) - N)] = 0 \quad 2.23$$

where

$$\mu = \frac{\delta T[\rho]}{\delta \rho} + \frac{\delta U[\rho]}{\delta \rho} + v(\mathbf{r}) \quad 2.24$$

and

$$T[\rho] = T_s[\rho] + T_c[\rho] \quad 2.25$$

here  $T_s[\rho] = \frac{\hbar^2}{2m} \sum_i^N d\mathbf{r} \phi_i^*(\mathbf{r}) \nabla^2 \phi(\mathbf{r})$  = kinetic energy of noninteracting particle of density  $\rho$  (while the exact functional forms for  $T_s[\rho]$  is not known) [77], and  $T_c[\rho]$  represents the correlation between particles, and

$$U[\rho] = J[\rho] + U_r[\rho] \quad 2.26$$

here  $J[\rho]$  = electrostatic interaction of the charge distribution  $\rho$ , and  $U_r[\rho]$  is not known.

The sum between the two unknown terms is called the exchange correlation potential.

$$\begin{aligned} E_{xc}[\rho] &= T_c[\rho] + U_r[\rho] \\ &= T[\rho] - T_s[\rho] + U[\rho] - J[\rho] . \end{aligned} \quad 2.27$$

The Euler-Lagrange Eq. (2.24) can be written as

$$\mu = \frac{\delta T_S[\rho]}{\delta \rho} + v_{KS}(\mathbf{r})$$

where

$$\begin{aligned} v_{KS}(\mathbf{r}) &= v_{ext} + \frac{\delta J[\rho]}{\delta \rho} + \frac{\delta E_{XC}[\rho]}{\delta \rho} \\ &= v_{ext}(\mathbf{r}) + v_H(\mathbf{r}) + v_{xc}(\mathbf{r}) \end{aligned} \quad 2.28$$

The solution is a single determinant of  $N$  orthonormal spin orbitals, with the spatial parts that are the solution of the so called Kohn-Sham equations

$$\left[ -\frac{\hbar^2 \nabla^2}{2m} + v_{KS}(\mathbf{r}) \right] \phi_i(\mathbf{r}) = \varepsilon_i \phi_i(\mathbf{r}) \quad 2.29$$

and

$$\sum_i |\phi_i^2(\mathbf{r})| = \rho(\mathbf{r}) . \quad 2.30$$

Using the self-consistent method, Eqs. (2.29) and (2.30) give the orbitals and orbital energies [76]. The highest occupied molecular orbital (HOMO) has an orbital energy which is the negative of the exact ionization potential [79]. The lowest unfilled molecular orbital is (LUMO) has an orbital energy whose negative value is often used to obtain the electron affinity of a molecular system. The total electronic energy is given by

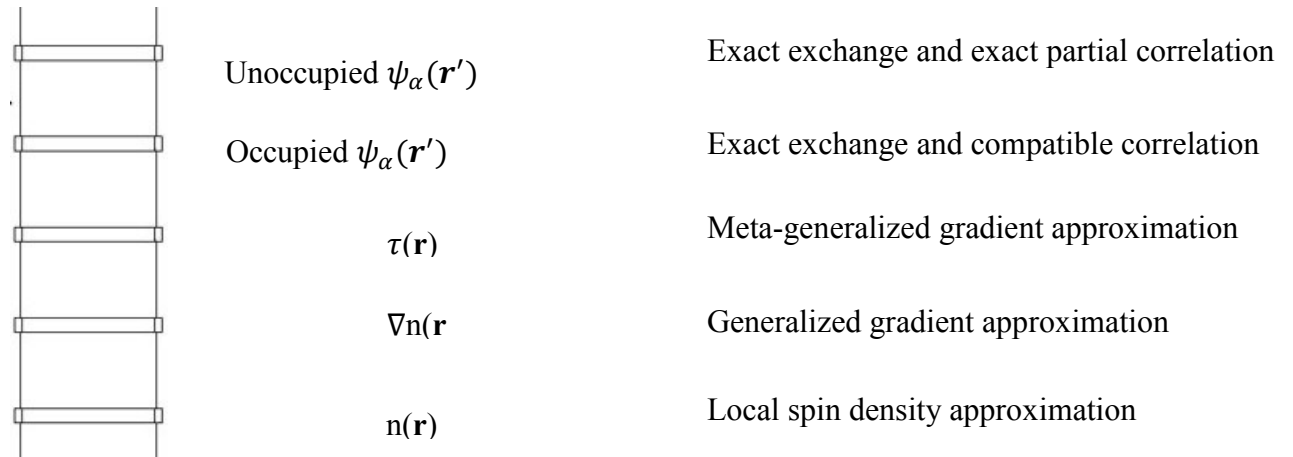
$$E_0 = \sum_i^N \varepsilon_i - \frac{q^2}{2} \int d\mathbf{r} \int d\mathbf{r}' \frac{\rho_0(\mathbf{r})\rho_0(\mathbf{r}')}{r-r'} - \int d\mathbf{r} v_{xc}(\mathbf{r})\rho(\mathbf{r}) + E_{xc}(\rho_0) \quad 2.31$$

The above approach is called the Kohn-Sham method.

## 2.4 The Exchange Correlation Energy Functional

DFT method is a powerful and competitive method for ascertaining the molecular properties after determining two things. First one is the exchange correlation functional

which is very good to produce precise results and the second one is comprehensive testing which already has been done by several computational physicists and chemists [72]. There are several approximations for the exchange correlation functional which can be illustrated with increasing accuracy using the Jacob's ladder [78].



Hartree world

In this thesis we will discuss first local density approximation (**LDA**) then generalized gradient approximation (**GGA**) followed by D-DFT such as B97D, CAM-B3LYP and wB97XD.

### 2.4.1 Local Spin Density Approximation

The local-spin-density-approximation (LSDA) is a straightforward generalization of the local-density-approximation (LDA) by including electron spin dependence in the total density [80, 81]. Both are simplest examples of approximations which are used in Kohn-Sham DFT [82]. General idea is simple; when a uniform electron gas is considered the exchange correlation energy at each point in the system  $e_{xc}$  is calculated and then the

global exchange-correlation energy for a density  $\rho(\mathbf{r})$  is obtained by integrating over all space

$$E_{XC}^{LDA} = \int d\mathbf{r} e_{xc}(\rho(\mathbf{r}))\rho(\mathbf{r}) . \quad 2.32$$

The exchange-correlation energy for each particle  $e_{xc}$  can be separated into exchange and correlation contributions

$$e_{xc}(\rho(\mathbf{r})) = e_x(\rho(\mathbf{r})) + e_c(\rho(\mathbf{r})) . \quad 2.33$$

where the exchange part  $e_x$  for homogeneous electron gas is a functional of the density [83] and can be written as

$$e_x^{LDA} = -\frac{3}{4} \left( \frac{3}{\pi} \rho(\mathbf{r}) \right)^{1/3} \quad 2.34$$

for a uniform electron gas and correlation part can be determined from Monte Carlo quantum calculations [84].

## 2.4.2 Generalized Gradient Approximation (GGA)

For exchange-correlation energy, generalized gradient approximation expands the LSDA and LDA [85]. In 1986, Perdew and Wang developed a functional that treats the exchange hole accurately and defined reduced gradient variable  $s$  as

$$s_\sigma = \frac{|\nabla\rho|}{\rho^{4/3}} . \quad 2.35$$

The per-particle exchange functional is then given by

$$e_x^{GGA} = -\frac{3}{4}\left(\frac{3}{\pi}\right)^{1/3} F(s). \quad 2.36$$

After integration of above equation, final form of the GGA exchange functional can be written as

$$E_x^{GGA} = -\frac{3}{4}\left(\frac{3}{\pi}\right)^{1/3} \int dr \rho^{4/3} F(s) \quad 2.37$$

where

$$F(s) = (1 + 0.0864s^2/m + bs^4 + cs^6)^m \quad 2.38$$

here  $m=1/15$ ,  $b=14$  and  $c=0.2$  [86] .

In quantum chemistry GGAs is used for fitting parameters to test sets of selected molecules whereas in physics it is used for emphasizing exact constraints [75]. After many improvements different expressions of  $F(s)$  were proposed including some new functionals [77]. These days the most reliable GGAs are PBE (Perdew, Burke and Ernzerhof) in solid state physics [85] and BLYP (combination of Becke's exchange functional [87] with the correlation functional of Lee, Yang and Parr [88]) in chemistry. In recent applications, the hybrid functionals are giving the most accurate results [89]. According to hybrid method approximation, the exchange functional is a linear combination of the exact HF exchange energy and DFT exchange functional of the density and density gradients [90], hence  $E_{xc}$  can be written:

$$E_{hybrid}^{xc} = c_{HF} E_{HF}^x + c_{DFT} E_{DFT}^{xc}. \quad 2.39$$

where the  $c_{HF}$  and  $c_{DFT}$  are adjustable coefficients. The main shortcomings of GGA functionals, including hybrid functionals, are the effects that require a nonlocal treatment



of correlation (dispersion force is one of them). In recent publications, different strategies were introduced which can be used to overcome these limitations. For our research work, we consider three methods B97D, CAM-B3LYP, and wB97XD.

### 2.4.3 B97D

In chemical system, the van der Waals (vdW) forces between atoms and molecules play an important role. This interaction balances the electrostatic and exchange-repulsion interactions. van der Waal forces are responsible for long range electron correlations [88-90] which can be described by DFT-D method. B97D is the only available density functional that yields the right sign for the isomerization energy and gives very good performance for the transition metal reactions [91]. The B97 functional is based on the Eq. (2.35) reduced gradient variable

$$s_{\sigma} = \frac{|\nabla\rho_{\sigma}|}{\rho_{\sigma}^{4/3}}$$

where  $\rho$  is the electron density and  $\sigma$  denotes  $\alpha$  and  $\beta$  spins. The exchange-correlation functional can be written as

$$E_{XC} = E_X + E_{C\alpha\beta} + \sum_{\sigma} E_{C\sigma\sigma} \quad 2.40$$

where subscripts x and c represents the exchange and correlation functionals respectively and can be written as:

$$E_x = \sum_{\sigma} \int e_{X\sigma}(\rho_{\sigma}) g_{X\sigma}(s_{\sigma}^2) dr \quad 2.41$$

$$E_{C\alpha\beta} = \int e_{C\alpha\beta}(\rho_{\sigma}, \rho_{\beta}) g_{C\alpha\beta}(s_{av.}^2) dr \quad 2.42$$

$$E_{C\sigma\sigma} = \int e_{C\sigma\sigma}(\rho_\sigma) g_{C\sigma\sigma}(s_\sigma^2) dr. \quad 2.43$$

In Eq. 2.41-2.43  $e(\rho)$  are the local volume energy densities of a uniform electron gas,  $s_{av.}^2 = S_\alpha^2 + S_\beta^2$  and  $g$  denotes the gradient correction factors. The correction factors can be expanded in a power series in the re-mapped variables  $u(s^2)$

$$g(s^2) = \sum_{i=0}^k c_i u^i(s^2). \quad 2.44$$

Each mapping of  $s^2$  to  $u$  is specific:

$$u_{X\sigma}(s_\sigma^2) = \frac{\gamma_{X\sigma} s_\sigma^2}{1 + \gamma_{X\sigma} s_\sigma^2} \quad 2.45$$

$$u_{C\alpha\beta}(s_{av.}^2) = \frac{\gamma_{C\alpha\beta} s_{av.}^2}{1 + \gamma_{C\alpha\beta} s_{av.}^2}. \quad 2.46$$

$$u_{C\sigma\sigma}(s_\sigma^2) = \frac{\gamma_{C\sigma\sigma} s_\sigma^2}{1 + \gamma_{C\sigma\sigma} s_\sigma^2} \quad 2.47$$

here  $\gamma$  is taken from Becke's work [92].

For the dispersion correction, the total energy can be written as

$$E_{DFT-D} = E_{KS-DFT} + E_{disp} \quad 2.48$$

where  $E_{KS-DFT}$  is the self-consistent Kohn-Sham energy and  $E_{disp}$  is an empirical dispersion correction

$$E_{disp} = -s_6 \sum_{i=1}^{N_{at}-1} \sum_{j=i+1}^{N_{at}} \frac{C_6^{ij}}{R_{ij}^6} f_{damp}(R_{ij}) \quad 2.49$$

and damping function is given by

$$f_{damp}(R_{ij}) = \frac{1}{1+e^{-d(R_{ij}/R_r-1)}} \quad 2.50$$

where  $N_{at}$  = no. of atoms in the system,

$C_6^{ij}$  = dispersion coefficient for atom pair ij,

$s_6$  = global scaling factor,

$R_{ij}$  = interatomic distance,

$R_r$  = sum of atomic vdW radii.

The interatomic  $C_6^{ij}$  term is calculated as geometric mean of the form

$$C_6^{ij} = \sqrt{C_6^i C_6^j} \quad 2.51$$

$R_{ij}$  are derived from the radius of the  $0.01a_0^{-3}$  electron density contour from ROHF (Restricted Open Hartree-Fock) /TZV(Triple zeta valence) computations of the atoms in the ground state. This calculation amends the computations of intermolecular distances especially for systems with heavier atoms [91].

#### 2.4.4 CAM-B3LYP

Tawada et al. and his colleagues combined the hybrid qualities of B3LYP and the long range correction [93] for their DFT approximation. Following that Takeshi Yanai proposed a new hybrid exchange-correlation functional named CAM-B3LYP where they used coulomb-attenuating method [94] for the long range correlations. CAM-B3LYP performs similarly to B3LYP whereas it also shows good performance for charge transfer

excitations in a dipeptide model for example. CAM-B3LYP originally follows the Hirao and Hid coworker's related works [95]. A separation of the electron-electron interaction into a long-range and short-range part can be written as

$$\frac{1}{r_{12}} = \frac{1 - \text{erf}(\mu r_{12})}{r_{12}} + \frac{\text{erf}(\mu r_{12})}{r_{12}} \quad 2.52$$

where erf means standard error function. First term consider for the short-range interaction and second term consider for the long-range interaction. In CAM-B3LYP method they add extra two parameters  $\alpha$  and  $\beta$  as,

$$\frac{1}{r_{12}} = \frac{1 - (\alpha + \beta \cdot \text{erf}(\mu r_{12}))}{r_{12}} + \frac{\alpha + \beta \cdot \text{erf}(\mu r_{12})}{r_{12}} \quad 2.53$$

where  $\mu$  is a parameter of dimension  $L^{-1}$  and  $\alpha$  and  $\beta$  are dimensionless parameters satisfying  $0 \leq \alpha + \beta \leq 1$ ,  $0 \leq \alpha \leq 1$ , and  $0 \leq \beta \leq 1$ .

Correspondingly the exchange energy is the sum of long-range (LR) and short-range (SR) components

$$E_X = E_X^{LR} + E_X^{SR} \quad 2.54$$

In this approach the usual exchange functional form,  $E_X = -0.5 \sum_{\sigma} \int \rho^{4/3} K_{\sigma} d^3 \mathbf{r}$  is modified and the short range part of exchange interaction can be written as

$$E_X^{sr} = -0.5 \sum_{\sigma} \int \rho^{4/3} K_{\sigma} \times \left\{ 1 - \frac{8}{3} a_{\sigma} \left[ \sqrt{\pi} \text{erf} \left( \frac{1}{2a_{\sigma}} \right) + 2a_{\sigma} (b_{\sigma} - c_{\sigma}) \right] \right\} d^3 \mathbf{r} \quad 2.55$$

where

$$a_{\sigma} = \frac{\mu K_{\sigma}^{1/2}}{6\sqrt{\pi} \rho_{\sigma}^{1/3}}$$

$$b_{\sigma} = e^{\left(-\frac{1}{4a_{\sigma}^2}\right)} - 1$$

$$c_{\sigma} = 2a_{\sigma}^2 b_{\sigma} + \frac{1}{2}$$

and  $K_{\sigma}$  is the original unattenuated exchange functional [95]. The long range exchange interaction is expressed with the use of HF exchange integral

$$E_x^{lr} = -\frac{1}{2} \sum_{\sigma} \sum_i^{occ} \sum_j^{occ} \int \int \psi_{i\sigma}^*(r_1) \psi_{j\sigma}^*(r_1) \times \frac{\text{erf}(\mu r_{12})}{r_{12}} \psi_{i\sigma}(r_2) \psi_{j\sigma}(r_2) d^3r_1 d^3r_2. \quad 2.56$$

Here  $\psi_{i\sigma}$  is the  $i$ th  $\sigma$  spin molecular orbital. If  $\mu = 0$ , the long range corrected DFT corresponds to the pure (non-LC) DFT calculation, whereas  $\mu = \infty$  corresponds to the HF calculation. It means  $\mu$  extends the DFT to HF [100]. The parameter  $\alpha$  (see Eq. 2.52) allows integrating the HF exchange contribution over the whole range, multiplying by a factor  $\alpha$  for HF whereas the  $\beta$  do the same task for DFT counterpart over the whole range multiplying by a factor of  $1 - (\alpha + \beta)$  [94] for DFT.

### 2.4.5 wB97XD

The popular type of splitting operator used in the long-range corrected (LC) hybrid scheme is the standard error function (erf),

$$\frac{1}{r_{12}} = \frac{\text{erf}(\omega r_{12})}{r_{12}} + \frac{\text{erfc}(\omega r_{12})}{r_{12}} \quad 2.57$$

where,  $r_{12} = |\mathbf{r}_1 - \mathbf{r}_2|$  and in the right hand side of above equation, the first term represents the long range whereas the second term represent for short range.  $\omega$  defines the range of these two parameters [97].

The wB97 functionals as first proposed by Chai and Head-Gordon gave the following expression for the LC hybrid functionals:

$$E_{xc}^{LC-GGA} = E_x^{LR-HF} + E_x^{SR-GGA} + c_x E_x^{SR-HF} + E_c^{GGA} \quad 2.58$$

where long and short-range HF terms are calculated using Savin's Coulomb operator for the two-electron integrals [102],

$$E_x^{LR-HF} = -\frac{1}{2} \sum_{\sigma} \sum_i^{occ} \sum_j^{occ} \int \int \psi_{i\sigma}^*(\mathbf{r}_1) \psi_{j\sigma}^*(\mathbf{r}_1) \times \frac{\text{erf}(\omega r_{12})}{r_{12}} \psi_{i\sigma}(\mathbf{r}_2) \psi_{j\sigma}(\mathbf{r}_2) d\mathbf{r}_1 d\mathbf{r}_2 \quad 2.59$$

$$E_x^{SR-HF} = -\frac{1}{2} \sum_{\sigma} \sum_i^{occ} \sum_j^{occ} \int \int \psi_{i\sigma}^*(\mathbf{r}_1) \psi_{j\sigma}^*(\mathbf{r}_1) \times \frac{\text{erfc}(\omega r_{12})}{r_{12}} \psi_{i\sigma}(\mathbf{r}_2) \psi_{j\sigma}(\mathbf{r}_2) d\mathbf{r}_1 d\mathbf{r}_2 \quad 2.60$$

where  $c_x$  is fractional number to be determined and it is equal to zero for wB97 functional but not equal to zero for the wB97x and wB97XD [78] (erfc is the complimentary error function).

The short range LSDA can be obtained by the integration of the square of the LSDA density matrix with the short range operator,

$$e_x^{SR-LSDA} = -\frac{3}{2} \left( \frac{3}{4\pi} \right)^{1/3} \rho_{\sigma}^{4/3}(\mathbf{r}) F(a_{\sigma}) \quad 2.61$$

where  $F(a_{\sigma})$  is an attenuation function and is given by

$$F(a_{\sigma}) = 1 - \frac{8}{3} a_{\sigma} \left[ \sqrt{\pi} \text{erf} \left( \frac{1}{2a_{\sigma}} \right) - 3a_{\sigma} + 4a_{\sigma}^3 + (2a_{\sigma} - 4a_{\sigma}^3) \exp \left( -\frac{1}{4a_{\sigma}^2} \right) \right]. \quad 2.62$$

To obtain the flexible SR-GGA exchange, they replace  $e_{x\sigma}^{LSDA}$  with  $e_{x\sigma}^{SR-LSDA}$  and giving the name  $E_x^{SR-B97}$

$$E_x^{SR-B97} = \sum_{\sigma} \int e_{x\sigma}^{SR-LSDA}(\rho_{\sigma}) g_{x\sigma}(s_{\sigma}^2) d\mathbf{r} \quad 2.63$$

$$g_{x\sigma}(s_{\sigma}^2) = \sum_{i=0}^k c_{x\sigma,i} u_{x\sigma}^i \quad 2.64$$

$g_{x\sigma}(s_{\sigma}^2)$  is the dimensionless inhomogeneity correction factor depending on the dimensionless reduced spin density gradient (Eq. (2.35))  $u_{x\sigma}^i = \gamma s_{\sigma}^2 / (1 + \gamma s_{\sigma}^2)$  is the expansion function with  $\gamma = 0.004$ . Head-Gordon and his co-workers used the same form which can be written as

$$E_c^{B97} = \sum_{\sigma} E_{c\sigma\sigma}^{B97} + E_{c\alpha\beta}^{B97} \quad 2.65$$

where the first term represent the same spins and the other one represents the opposite spins and

$$E_{c\sigma\sigma}^{B97} = \int e_{c\sigma\sigma}^{LSDA}(\rho_{\sigma}) g_{c\sigma\sigma}(s_{\sigma}^2) d\mathbf{r} , \quad 2.66$$

$$E_{c\alpha\beta}^{B97} = \int e_{c\alpha\beta}^{LSDA} g_{c\alpha\beta}(s_{av.}^2) d\mathbf{r}. \quad 2.67$$

Based on these functional expressions, they suggested two new LC hybrid functionals wB97 and wB97X. First one has no short range (SR) HF exchange whereas the last one contains small amount of the SR HF exchange [97] and can be written as

$$E_{xc}^{\omega B97X} = E_x^{LR-HF} + c_x E_x^{SR-HF} + E_x^{SR-B97} + E_c^{B97} \quad 2.71$$

In 2009 they added another parameter, damped atom-atom dispersion corrections to wB97X and named it wB97XD. This method allows a large number of fixed empirical parameters into the functional.

## Chapter 3

### Computational details

Gaussian is a computer program for physicists, chemists, chemical engineers, biochemists and other scientists for determining the electronic and optical properties of molecular systems. It can be used to obtain the energies, molecular structures, vibrational frequencies and so on. All (electronic structure) calculations in this thesis have been executed with Gaussian 09 software package which is available on the cluster (Placentia) at the Atlantic Computational Excellence Network (ACEnet) and (GreX) in the Western Canadian Research Grid (Westgrid). We took the advantage of non-quota scratch (nqs) space for long calculation and the storage of the large check-point file for continuously running until the molecular structure was fully optimized [98].

For all geometry optimizations, we have used the following DFT approximations: the empirical dispersion corrected B97D; Coulomb attenuating method CAM-B3LYP, and long range corrected dispersion corrected wB97XD. As stated in chapter 2, B97D is the only available density function that yields the right sign for the isomerization energy and



gives good performance for the transition metal reactions [91]. CAM-B3LYP shows a performance of comparable accuracy to other long-range corrected functionals for determining dispersion corrected interaction energies [99]. The functional, wB97XD gives satisfactory results for thermochemistry, non-covalent interactions and thermochemical kinetics. It has been shown that for non-covalent systems, wB97XD shows minor improvement over other empirical dispersion-corrected density functionals, but it performs significantly better for kinetics of noncovalent systems [97].

Geometry optimization is an approach to predict the three-dimensional arrangement of the atoms in a molecule by means of minimization of total energy. The phenomenon of binding is defined as where the atoms and molecules are in stable state to form large molecular structure. All DFT calculations in this work were geometry optimized either fully or partially (mostly using the keyword opt) in order to find the lowest energy state for the ground state. The optimization involves the search for the local minimum on the potential energy surface (PES) which is the point where the gradient of energy with respect to the nuclear coordinates is zero. The method of obtaining the global and local minima is self-consistent field (SCF) approach. It involves consecutive iterations until certain criteria are reached. The criteria of the SCF convergence are defined in Table 3.1. The maximum component of force and the root mean square (RMS) of the force should reach or be below the threshold values. This condition is also applicable for the maximum displacement and the RMS of the displacement.

Table 3.1: The criteria of the SCF convergence

| Item                 | Threshold    |
|----------------------|--------------|
| Maximum Force        | 0.000450 (N) |
| RMS of force         | 0.000300 (N) |
| Maximum Displacement | 0.001800 (Å) |
| RMS of displacement  | 0.001200 (Å) |

In our research we have used two types of optimization keyword one is ‘opt’ another is ‘opt=modredundant’. For single molecular system, we have used opt keyword which requests full geometry optimization. In this case the geometry will be fine-tuned until a stationary point on the potential surface is found. However, for combination system (conjugated oligomer and SWCNT) we used opt=ModRedundant to perform partial geometry optimization. It allows us to explicitly freeze (F) variables (CNT atoms) during the optimization. We freeze the bond lengths, bond angles and dihedral angles of the carbon atoms of the nanotube. We have also used Guess=nosymm means removes all orbital symmetry constraints.

In our research we have used double zeta polarized split-valance basis set 6-31G (d) [100]. It is the expanded version of split-valance 6-31G where for atoms such as carbon, 6 represents the number of Gaussian primitives (Gaussian type orbitals) used to construct the core orbital basis function (the 1s function). The 3 and 1 represent the valence orbitals,  $2s\uparrow$ ,  $2s\downarrow$ ,  $2p\uparrow(3)$  and  $2p\downarrow(3)$ . The first number after the dash in the basis set name indicates the number of Gaussian primitives used to construct the  $2s\uparrow$  and  $2p\uparrow(3)$  basis functions. The second number after the dash gives the number of Gaussian primitives

used to construct the 2s↓ and 2p↓(3) basis functions and d means d-type polarization functions (function of higher angular momentum than the occupied atomic orbitals) that is added to each non-hydrogen atom in the molecule.

To generate the input files and to display and obtain the structures of the output geometrics we used Gaussview 5.0 visualization software. This software can also be used to determine or set up the bond lengths, bond angles and dihedral angles and so on [101]. VMD is a molecular visualization program for displaying, animating and analyzing large molecular systems using 3-D graphics and built-in scripting. To generate the input file for SWCNT calculations, we used VMD software [102]. We also used ACD-Chemsketch free software to draw the chemical structure ALD and DTF endcapped conjugated oligomers. For analyzing the structural behavior, we measure the bond lengths (BLs), bond angles (BAs) and dihedral angles (DAs). We consider only the back-bone of oligomer in the structural analysis. These considered atoms are labelled 1-18 in Figures 4.1 and 4.4. Our aim is to see that how much they change in the presence of SWCNT and how they behave for different methods. We determine  $r_{12}, r_{23} \dots$  for BLs,  $A_{123}, A_{234} \dots$  for BAs and  $D_{1234}, D_{2345} \dots$  for DAs.

To study the amount of variation or dispersion from average BLs, BAs and Das, we calculate the standard deviation.

$$\sigma = \sqrt{\frac{1}{N} \sum_{i=1}^N (X_i - \bar{X})^2} \quad 3.1$$

where N=17. For example, for BLs,  $X_i = r_{12}, r_{23}, \dots, r_{1718}$  and  $\bar{X} = \frac{1}{17} (r_{12} + r_{23} + \dots + r_{1718})$  and similarly for BAs and DAs.

When atoms in a molecule share electrons unequally, the molecule is polarized and has a dipole moment. This happens when one atom is more electronegative than another, then atom pulls more tightly on the shared pair of electrons. If the difference of electronegativity is large then dipole moment is also large. The charge separation is also a deciding factor in determining the size of the dipole moment. The dipole moment is defined as the sum of the products of the charge  $q_i$  and the distance  $\mathbf{r}_i$  between the two charges

$$\boldsymbol{\mu} = \sum_{i=1}^n q_i \mathbf{r}_i . \quad 3.2$$

In our research we analyze the effect of the dispersion on the dipole moments. We consider the dipole moments components (along  $x$ -axis,  $y$ -axis, and  $z$ -axis). For single molecule system, the magnitude of the total dipole moment can be written as,  $\mu = \sqrt{\mu_x^2 + \mu_y^2 + \mu_z^2}$ . Figure 3.1 illustrates the dipole moment direction (blue arrow) for a given molecular system. In Gaussian calculations, dipole moments point toward the positive charge.

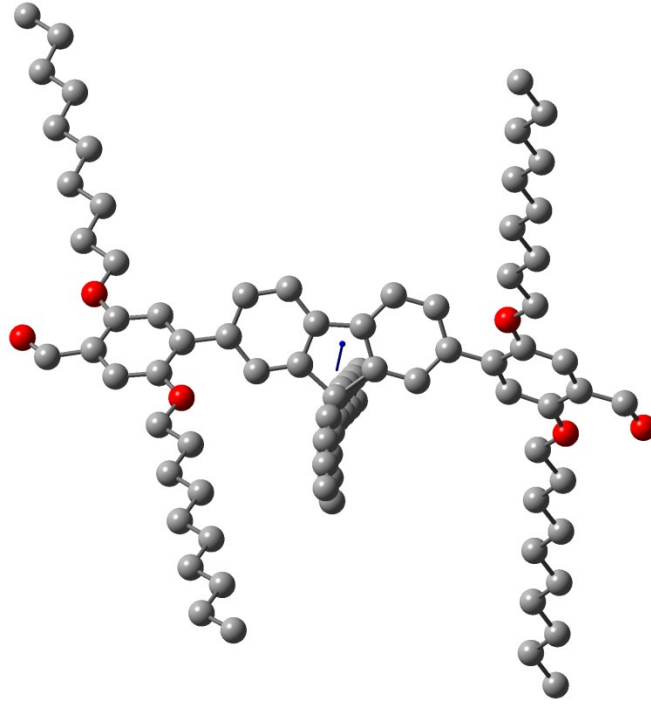


Figure 3.1: Dipole moment direction for single molecule system.

Binding energy (BE) is the energy required to separate a whole system into its constituent's parts. A bound system generally has a lower potential energy than the sum of its constituent parts which keeps the system together. In our calculation BE.

$$BE = (E_o + E_{CNT}) - E_{o+CNT} \quad 3.3$$

where  $E_o$ ,  $E_{CNT}$  and  $E_{o+CNT}$  are the energies of the single oligomer, single nanotube and combination of nanotube and oligomer respectively.

For determining the average distance from oligomer to SWCNT, we have used Mathematica version-9 [104]. First we have to determine the center of mass coordinates of the nanotube and oligomer. We fit planes of nanotube and oligomer using equations.

Formulas of the planes are

$$a_1x_1 + b_1y_1 + c_1z_1 + d_1 = 0 \quad 3.4$$

$$a_2x_2 + b_2y_2 + c_2z_2 + d_2 = 0 \quad 3.5$$

where  $x_1, y_1, z_1$  and  $x_2, y_2, z_2$  are the coordinates of (truncated) nanotube and oligomer respectively and  $a_1, b_1, c_1$  and  $a_2, b_2, c_2$  are the constants (the plane of the nanotube is taken as parallel to the horizontal planes of the coordinate system (see Figure 3.2)). The angle is

$$\theta = \cos^{-1} \frac{a_1a_2 + b_1b_2 + c_1c_2}{\sqrt{a_1^2 + b_1^2 + c_1^2} \sqrt{a_2^2 + b_2^2 + c_2^2}} . \quad 3.6$$

After measuring the angle between planes of nanotube and oligomer we measure the distance between the center of nanotube and oligomer using Euclidian distance formula for two coordinates  $(a_1, b_1, c_1)$  and  $(a_2, b_2, c_2)$

$$\text{Distance} = \sqrt{|a_1 - a_2|^2 + |b_1 - b_2|^2 + |c_1 - c_2|^2} .$$

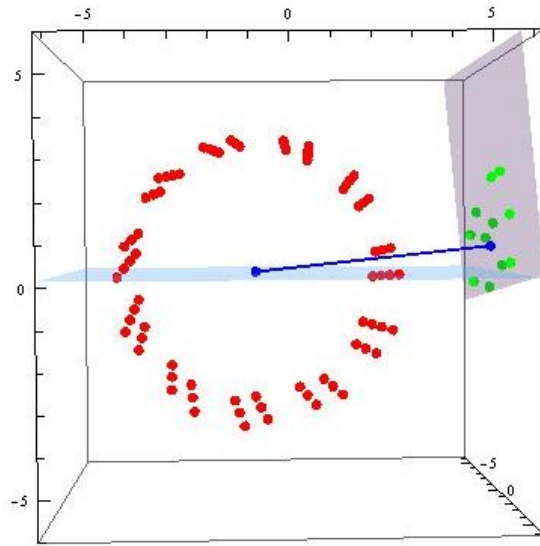


Figure 3.2: Blue line is the distance between the CNT center to the oligomer center.

After that we subtract from the total distance the nanotube radius and we obtain the average distance between nanotube and oligomer (see Figure 3.2).

## **Chapter 4**

### **Isolated Oligomers - Comparison of Structures Using Different DFT Methods**

#### **4.1 Introduction**

In this chapter, we discuss the structures and electronics properties of isolated fluorene-based oligomers (with and without SCs) with two types of end groups (ALD and DTF). As stated in Chapter 1, we refer to them as ALD-DPF and DTF-DPF respectively (DPF stands for the diphenyl-fluorene). We consider only the structures of the backbones of the oligomers in our discussion. For each oligomer, the geometrical parameters such as BLs, BAs and DAs are given (see the Appendix for the respective tables) and the comparison of these results as obtained using the various dispersion corrected (B97D, CAM-B3LYP and wB97XD) and the hybrid (B3LYP) DFT methods is made. The effect of the DFT method, the end group and SCs on the electronic properties such as dipole moments, HOMO and LUMO eigenvalues and energy gaps is also discussed.

## 4.2 Chemical and Molecular Structure of Fluorene-Based Conjugated Oligomers

ALD- and DTF-endcapped fluorene-based conjugated oligomers have linear structures. Figures 4.1 and 4.4 show the chemical structures of ALD-DPF and DTF-DPF respectively where  $R=C_{10}H_{21}$  and  $R'=C_8H_{17}$  are the alkyl SCs. In these oligomers the central part contains fluorene and the each side contains one substituted benzene ring (which constitutes the diphenyl part) with either ALD or DTF end group. In the initial structures, all respective geometrical parameters (BLs, BAs and DAs) are set to be the same along the backbone of oligomers. After geometry optimization, these parameters are modified in agreement with the lowest energy state. In Figures 4.2 and 4.5, representative examples of (B3LYP optimized) oligomers without SCs are shown, and in Figures 4.3 and 4.6, representative examples of (B3LYP optimized) oligomers with SCs are shown (the oligomers with SCs optimized with other DFT methods are shown in the Appendix (Figures A.1-A.6)). In this chapter and chapter 6 and 7, when various differences are calculated, the order of subtractions are as follows, DTF-endcapped system are subtracted from ALD-endcapped systems, systems with SCs from system without SCs and interacting systems from isolated systems.



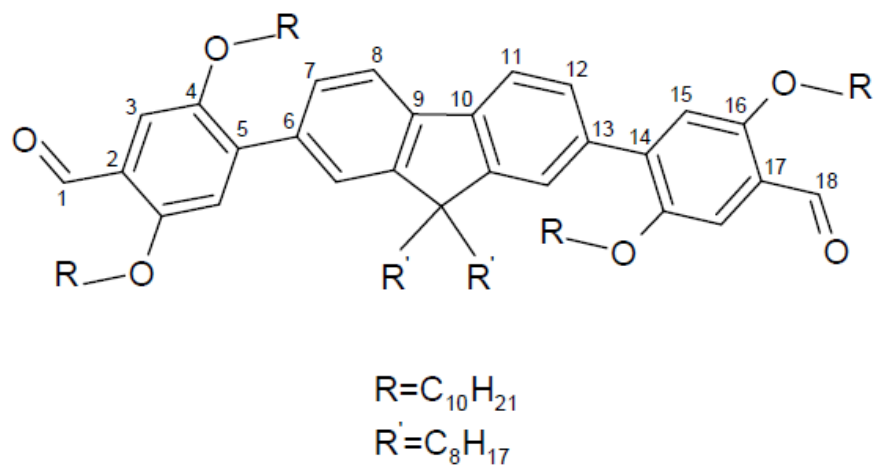


Figure 4.1: Chemical structure of fluorene-based ALD-endcapped oligomer.

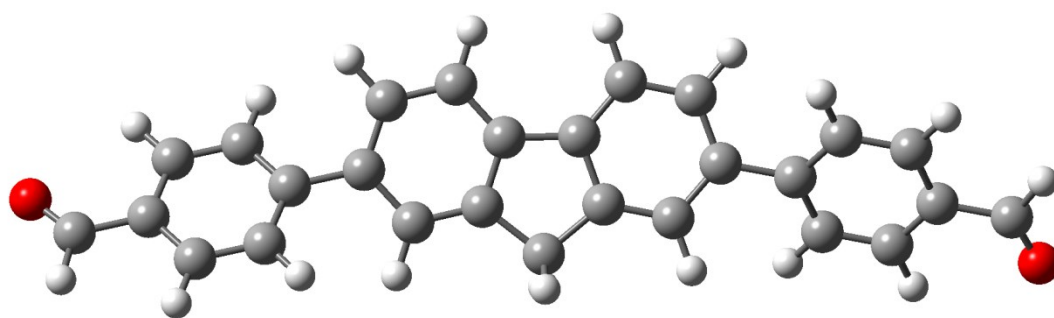


Figure 4.2: Molecular (optimized with DFT/B3LYP) structure of fluorene-based ALD-endcapped oligomer without SCs.

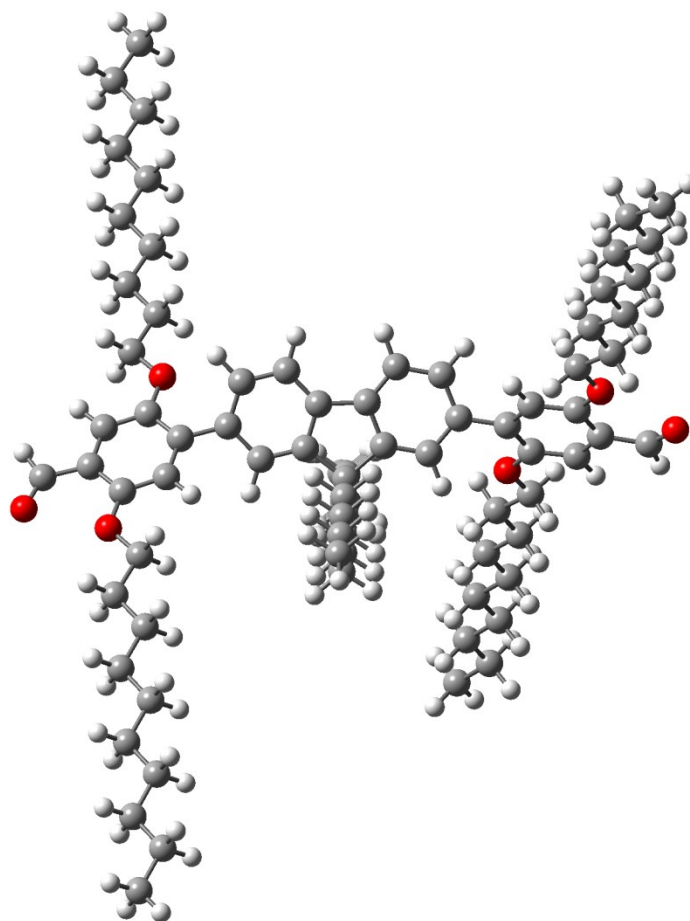


Figure 4.3: Molecular (optimized with DFT/B3LYP) structure of fluorene-based ALD-endcapped oligomer with SCs.

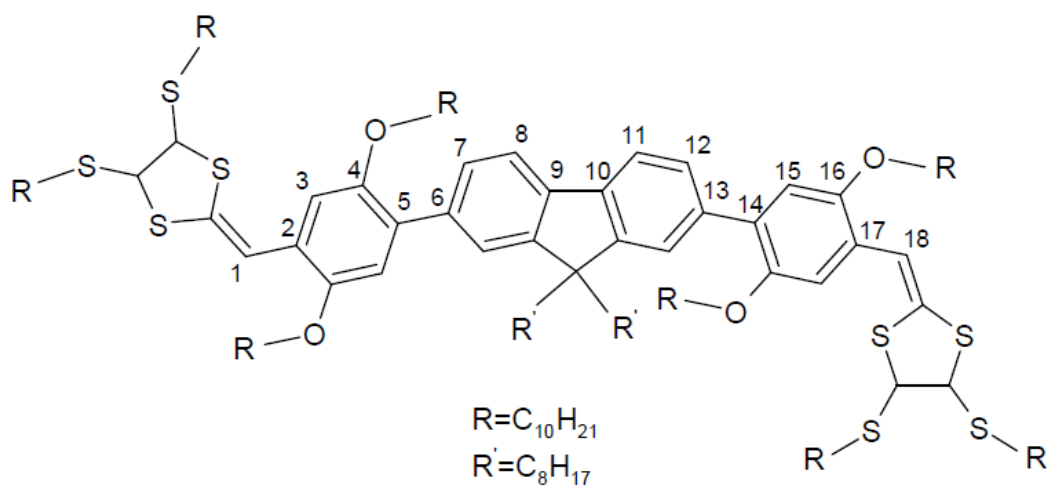


Figure 4.4: Chemical structure of fluorene-based DTF-endcapped oligomer.

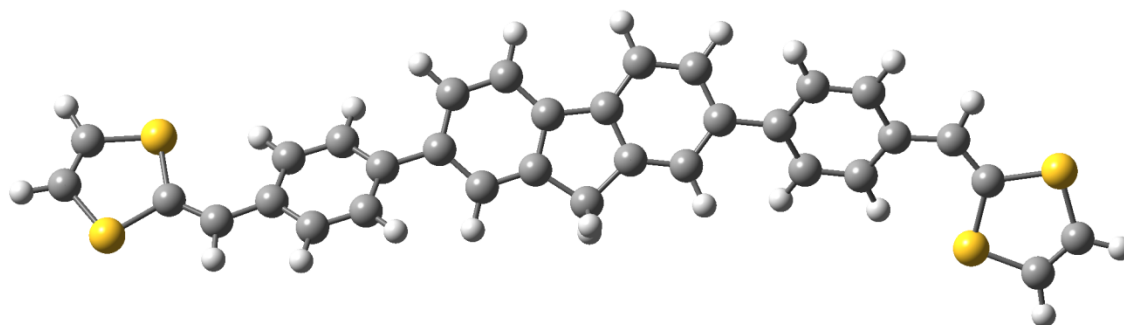


Figure 4.5: Molecular (optimized with DFT/B3LYP) structure of fluorene-based DTF-endcapped oligomer without SCs.

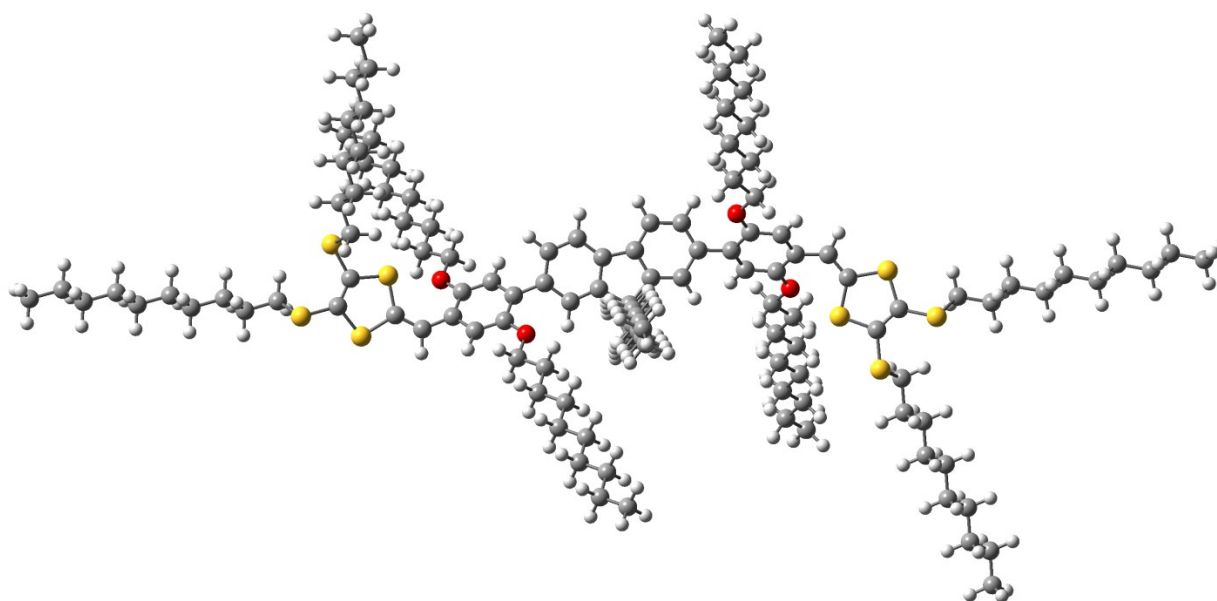


Figure 4.6: Molecular (optimized with DFT/B3LYP) structure of fluorene-based DTF-endcapped oligomer with SCs.

## 4.3 End Group Effect on the Oligomer Backbone

As stated above, for the various comparisons, we consider only the backbone atoms (see Figures 4.1 and 4.4) from C<sub>1</sub> to C<sub>18</sub> of the fluorene-based oligomers when we analyze how the oligomers change when they have different end groups (ALD or DTF).

### 4.3.1 Bond Lengths

C-C bond length differences between ALD- and DTF-endcapped oligomers for different methods (B97D, wB97XD, CAM-B3LYP, B3LYP) are shown in Figures 4.7 and 4.8. Figure 4.7 shows that for oligomers without SCs there are no significant bond length differences. Largest differences occur for C<sub>1</sub>-C<sub>2</sub> and C<sub>17</sub>-C<sub>18</sub> bonds that are closest to the end groups for every DFT method (the maximum value is 0.025 Å for B97D). In Figure 4.8 (for oligomers with SCs) these differences are reduced and maximum difference is less than 0.02 Å (also for B97D). In general, it can be said that the presence of SCs reduces the bond length differences due to different end groups (ALD or DTF) (see Appendix A for the actual bond lengths) and the bonds closest to the end group are somewhat longer in the ALD- than in the DTF-endcapped oligomers.

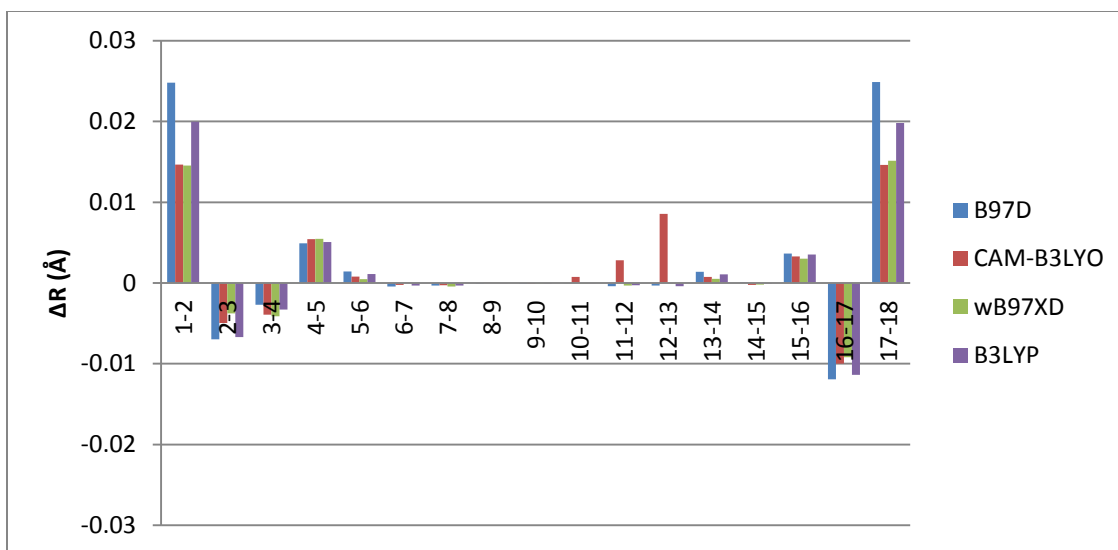


Figure 4.7: Bond length differences between ALD- and DTF-endcapped oligomers as a function of bond length position of oligomers without SCs for different DFT methods.

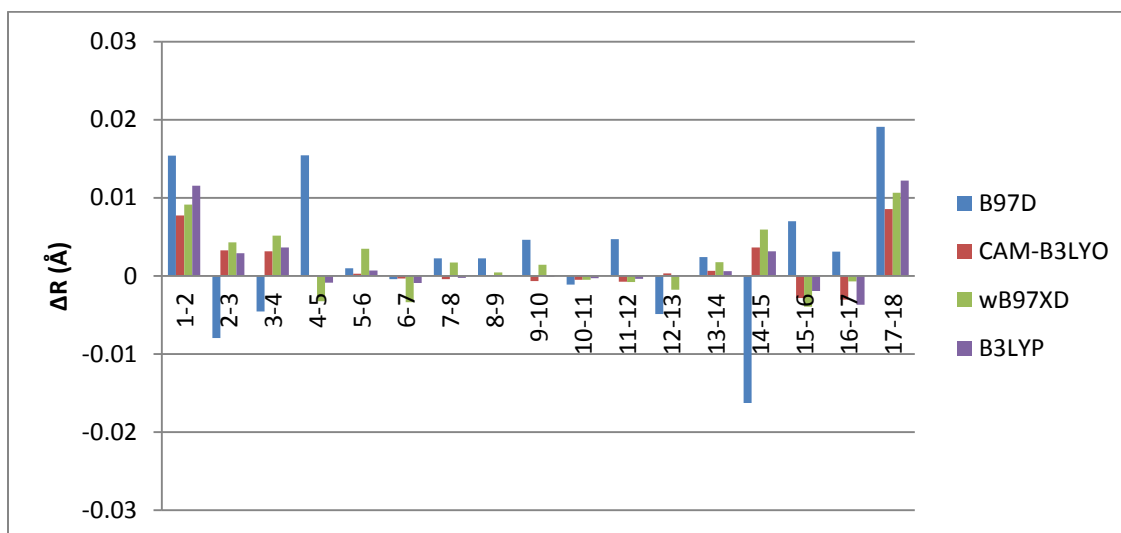


Figure 4.8: Bond length differences between ALD- and DTF-endcapped oligomers as a function of bond length position of oligomers with SCs for different DFT methods.

### 4.3.2 Bond Angles

In the case of end group effect on bond angles, the maximum difference of about  $6^\circ$  (see Figure 4.10) is observed for  $A_{1-2-3}$  ( $C_1-C_2-C_3$ ) angle for oligomers with SCs. In systems with SCs, bond angles in benzene rings as well as the terminal angles are somewhat modified by end groups for the B97D and wB97XD methods. On the other hand, for oligomers without SCs (see Figure 4.9) end groups affect mostly terminal angles ( $A_{1-2-3}$ ,  $A_{2-3-4}$ ,  $A_{15-16-17}$  and  $A_{16-17-18}$ ) and the differences are nearly the same for all methods. For ALD-endcapped oligomers,  $A_{1-2-3}$ ,  $A_{2-3-4}$  and  $A_{15-16-17}$  are smaller and  $A_{16-17-18}$  is larger than corresponding values for DTF-endcapped oligomers (see Figure 4.9). These figures show that different end groups do not produce large changes (in most cases less than  $5^\circ$ ) in bond angles along the backbone (see Appendix A for the actual bond angles).

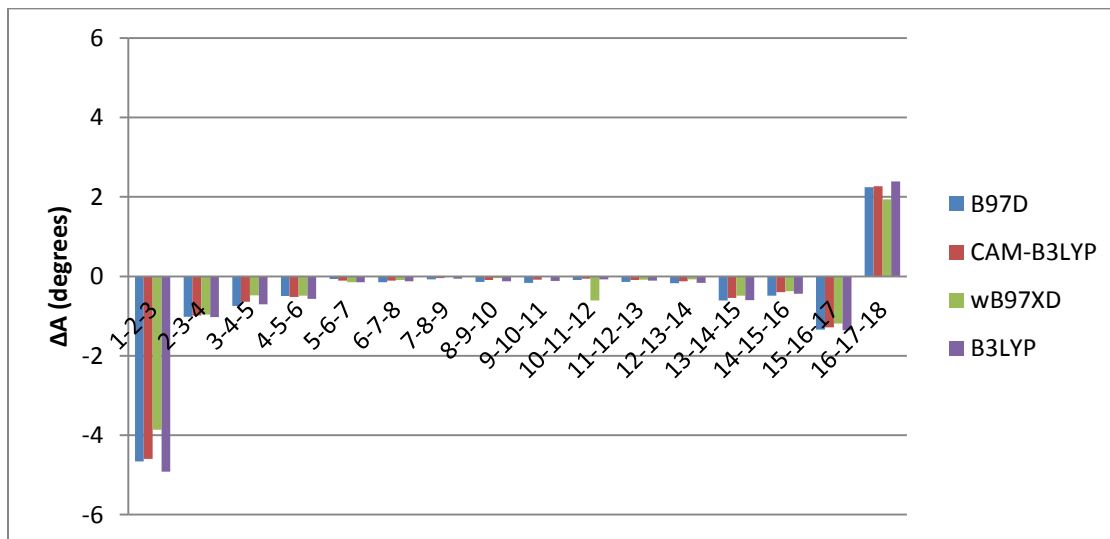


Figure 4.9: Bond angle differences between ALD- and DTF-endcapped oligomers as a function of bond angle position of oligomers without SCs for different DFT methods.

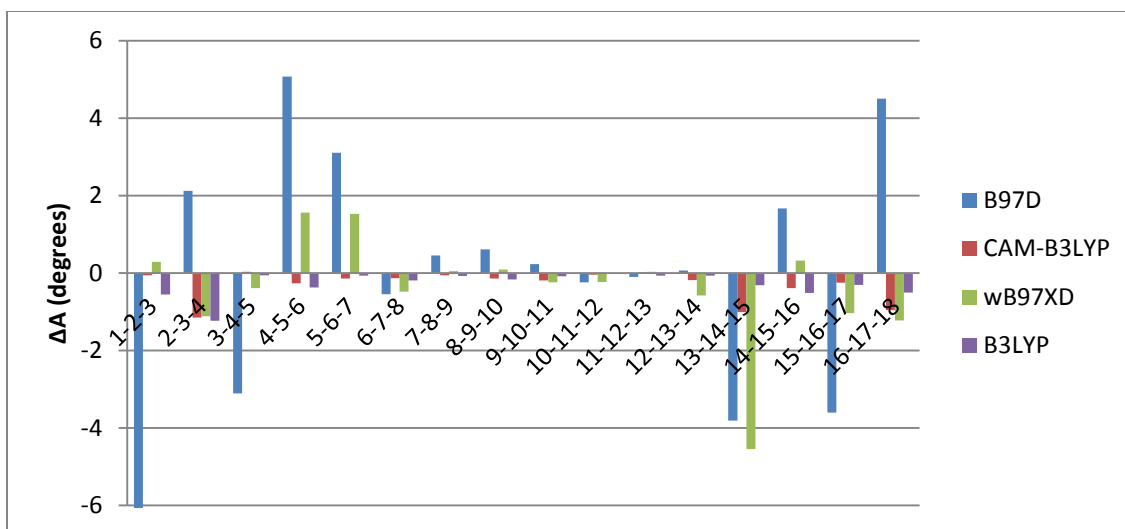


Figure 4.10: Bond angle differences between ALD- and DTF-endcapped oligomers as a function of bond angle position of oligomers with SCs for different DFT methods.

### 4.3.3 Dihedral Angles

Figures 4.11 and 4.12 show the end group effect on backbone dihedral angles of oligomers without and with SCs respectively. In systems with no SCs, Figure 4.11 shows that there is virtually no difference (all differences are less than  $1.6^\circ$ ) between dihedral angles of ALD- and DTF-endcapped oligomers. However, for oligomers with SCs (Figure 4.12), there is a maximum difference of about  $25^\circ$  for  $D_{4-5-6-7}$  (cis) dihedral angle for wB97XD method. Also when SCs are present, the dihedral angles,  $D_{4-5-6-7}$  (cis),  $D_{5-6-7-8}$  (trans),  $D_{11-12-13-14}$  (trans) and  $D_{12-13-14-15}$  (cis) (located primarily between benzene rings and fluorene) are somewhat affected (they tend to be larger for ALD- than for DTF-endcapped oligomers) by the change in end group especially for wB97xD and B97D methods (differences are less than  $10^\circ$  in most cases). In summary it can be said that for oligomers without SCs, the end group (ALD or DTF) has minimal effect on the backbone whereas for oligomers with SCs, dihedral angles between benzene rings and fluorene are

changed somewhat (in most cases by less than  $10^\circ$ ). These results show that oligomers with DTF are more planar than oligomers with ALD end group.

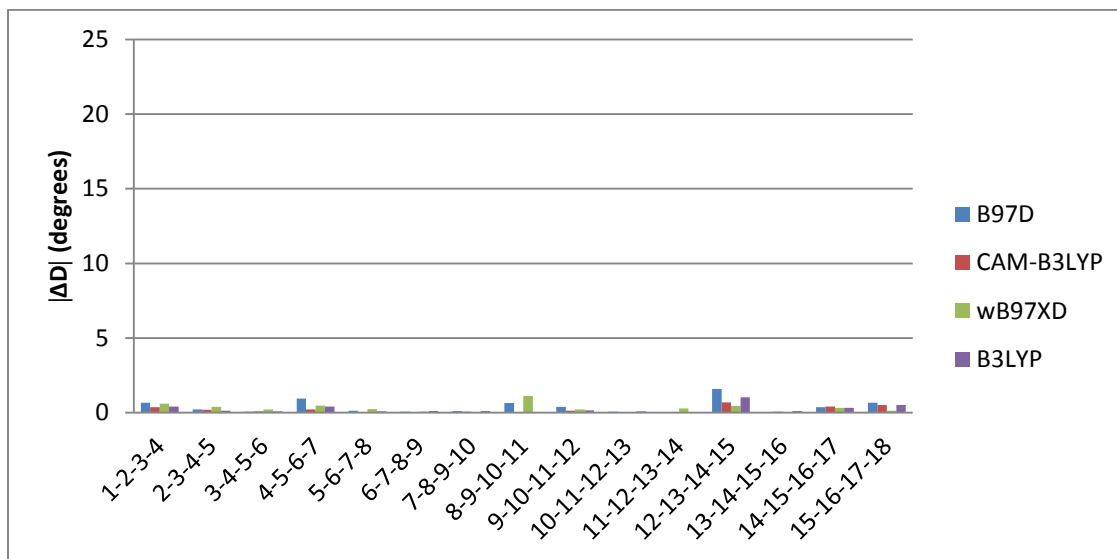


Figure 4.11: Dihedral angle difference between ALD- and DTF-endcapped oligomers as a function of dihedral angle position of oligomer without SCs for different DFT methods.

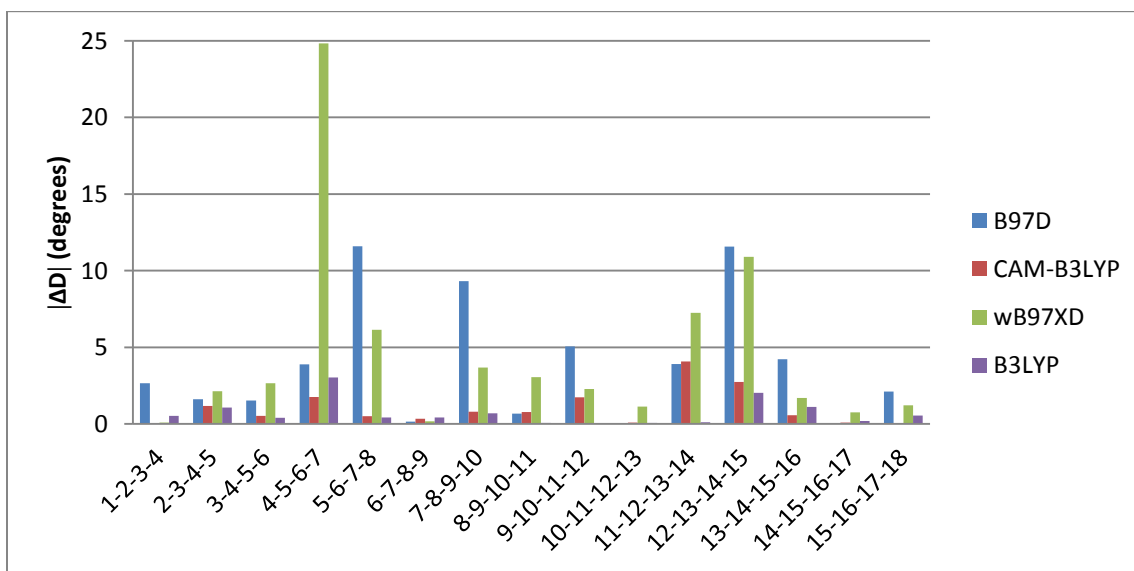


Figure 4.12: Dihedral angle differences between ALD- and DTF-endcapped oligomers as a function of dihedral angles position of oligomers with SCs for different DFT methods.



## 4.4 Side Chain Effect on the Oligomer Backbone

In this section we analyze the effect of long SCs on the backbone of an oligomer with a given end group (ALD or DTF). Our target is to observe the effect of the presence or absences of SCs on the oligomers' backbone for each end group (ALD or DTF). We have subtracted the structures (BLs, BAs and DAs) of oligomers with SCs from those without SCs.

### 4.4.1 Bond Lengths

Figures 4.13 and 4.14 show that the presence of long SCs has a small effect on the bond lengths of oligomers (most differences are less than 0.015 Å for ALD- and less than 0.008 Å for DTF-endcapped oligomers). Maximum difference is approximately 0.015 Å for wB97XD and B97D methods in the oligomers with ALD end group. In the case of DTF end group, SCs effect is negligible. For both oligomers (with ALD and DTF), the biggest differences are observed along the terminal bond lengths such as C<sub>2-3</sub>, C<sub>3-4</sub>, C<sub>4-5</sub>, C<sub>14-15</sub>, C<sub>15-16</sub> and C<sub>16-17</sub> that are part of the benzene rings. The general tendency is to lengthen these bonds when SCs are present. SCs elongate C<sub>1-2</sub> and C<sub>17-18</sub> bond lengths in oligomers with DTF but not with ALD end group.

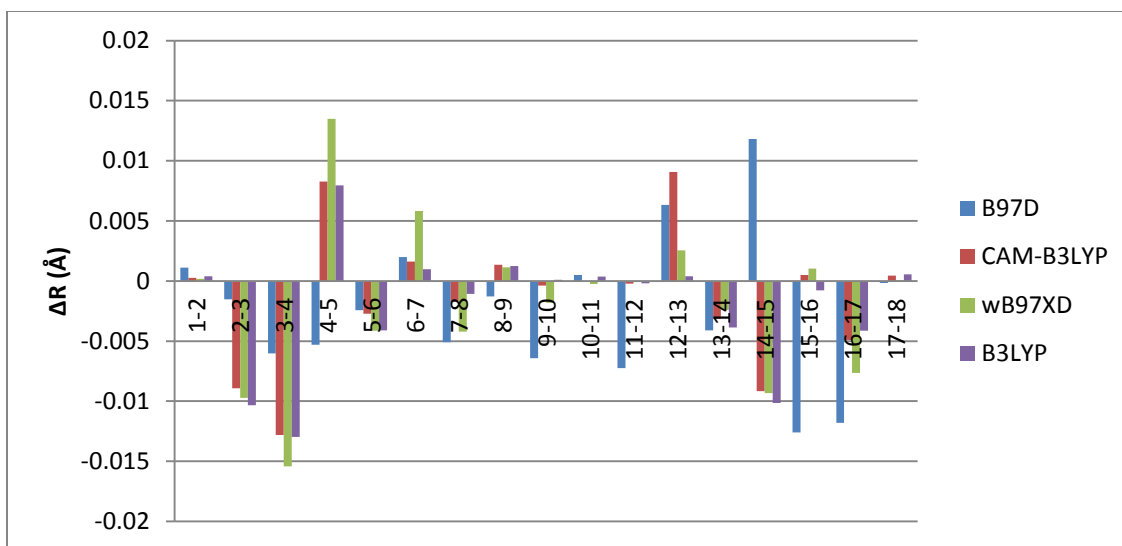


Figure 4.13: Bond length differences between ALD-endcapped oligomers without and with SCs as a function of bond length position of oligomers for different DFT methods.

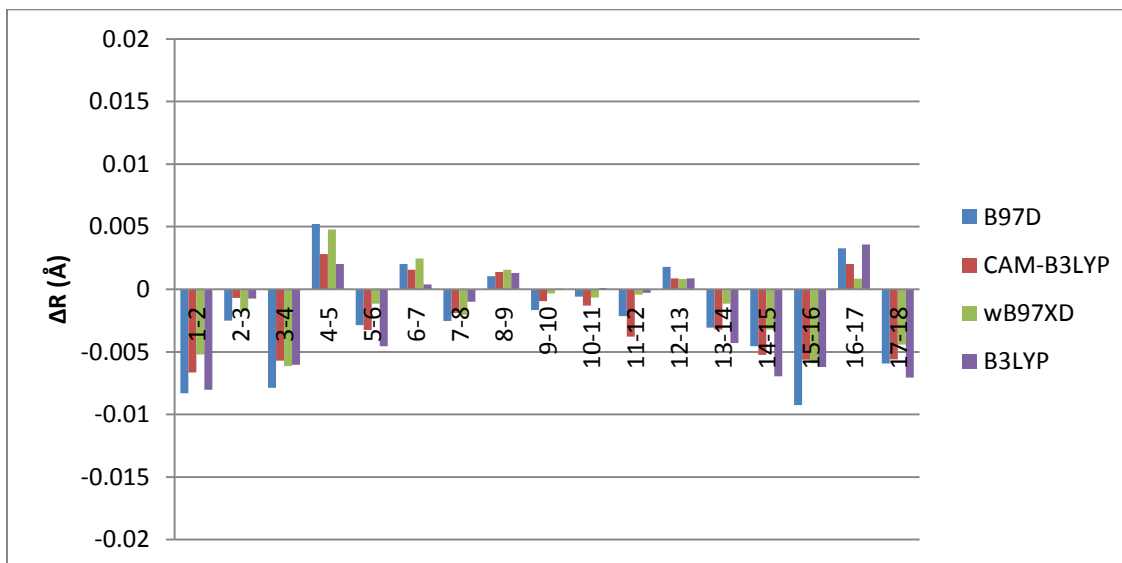


Figure 4.14: Bond length difference between DTF-endcapped oligomers without and with SCs as a function of bond length position of oligomers for different DFT methods.

## 4.4.2 Bond Angles

The changes in bond angles, along the backbone due to the presence of long SCs are somewhat less than those due to the presence of different end groups. The maximum bond angle difference is less than  $4^\circ$  (see Figures 4.15 and 4.16). The biggest differences are observed in ALD-endcapped oligomers for bond angles between end groups and benzene rings ( $A_{1-2-3}$ ,  $A_{16-17-18}$ ), and between benzene rings and fluorene ( $A_{4-5-6}$ ,  $A_{5-6-7}$ ,  $A_{12-13-14}$  and  $A_{13-14-15}$ ) (see Figure 4.15). In the case of DTF-endcapped oligomers (see Figure 4.16) similar bond angles are affected by the presence of SCs but bond angle difference are even smaller (of the order of  $1^\circ$  to  $3^\circ$ ). In summary, the effect of the addition of SCs on the bond angles of the backbone is very small for all DFT methods.

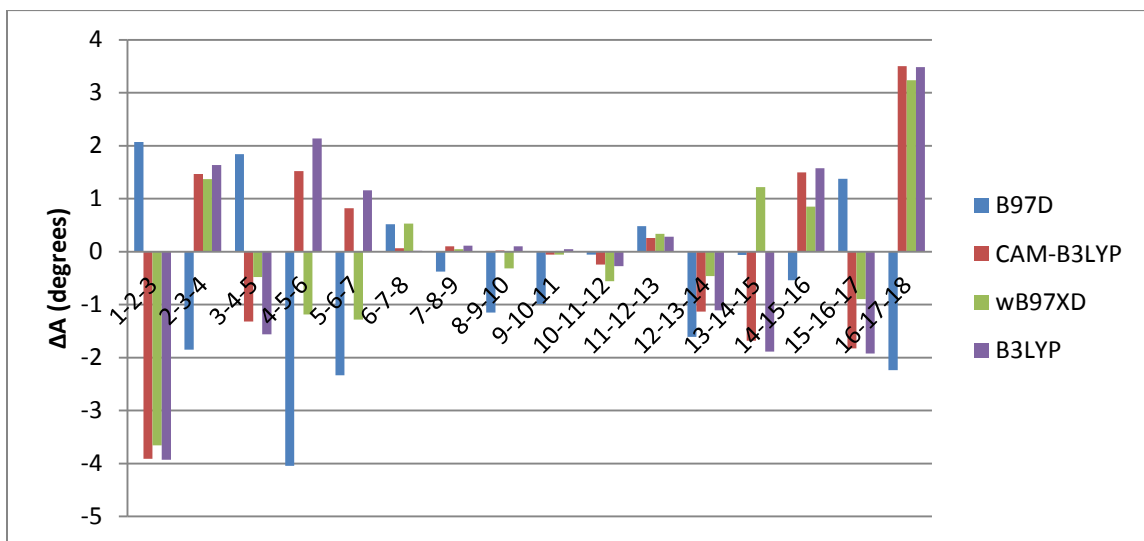


Figure 4.15: Bond angle differences between ALD-endcapped oligomer without and with SCs as a function of bond angle position of oligomers for different DTF methods.

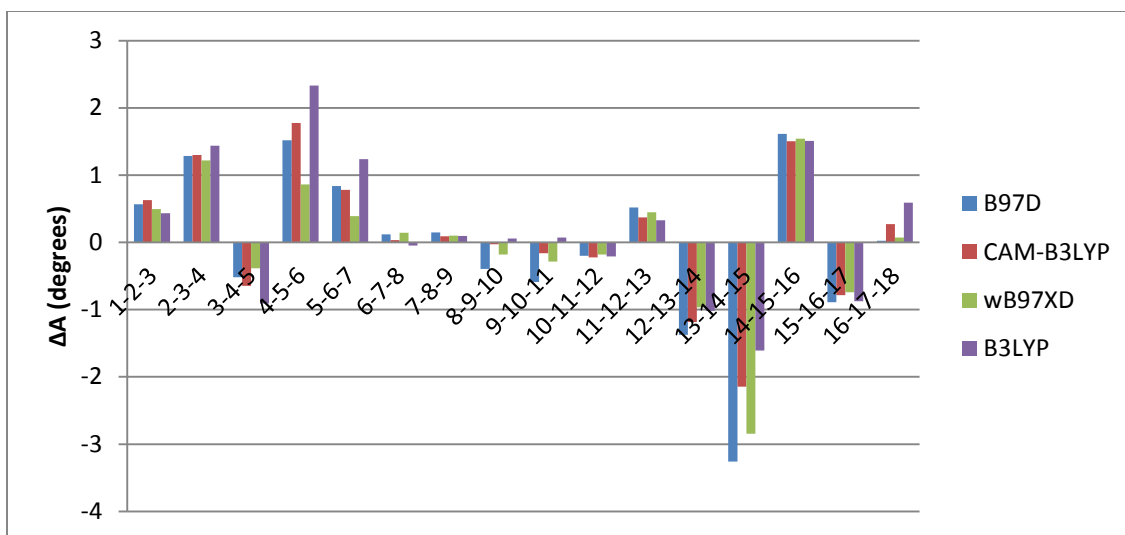


Figure 4.16: Bond angle differences between DTF-endcapped oligomer without and with SCs as a function of bond angle position of oligomers for different DFT methods.

### 4.4.3 Dihedral Angles

When long SCs are present, the maximum dihedral angle difference of  $35^\circ$  (for  $D_{4-5-6-7}$  (cis)) is observed for ALD-endcapped oligomer (see Figure 4.17) for wB97XD. Another angle  $D_{12-13-14-15}$  (cis) is also affected (to a lesser extend) by the presence of SCs. These dihedral angles are located along bonds that connect benzene rings with fluorene. DTF-endcapped oligomer also shows differences at  $D_{4-5-6-7}$  (cis) and  $D_{12-13-14-15}$  (cis) dihedral angles for all DFT methods but they are smaller (less than  $15^\circ$ ) than those for ALD-endcapped oligomers. The above results illustrate that the presence of long SCs make the oligomers less planar.

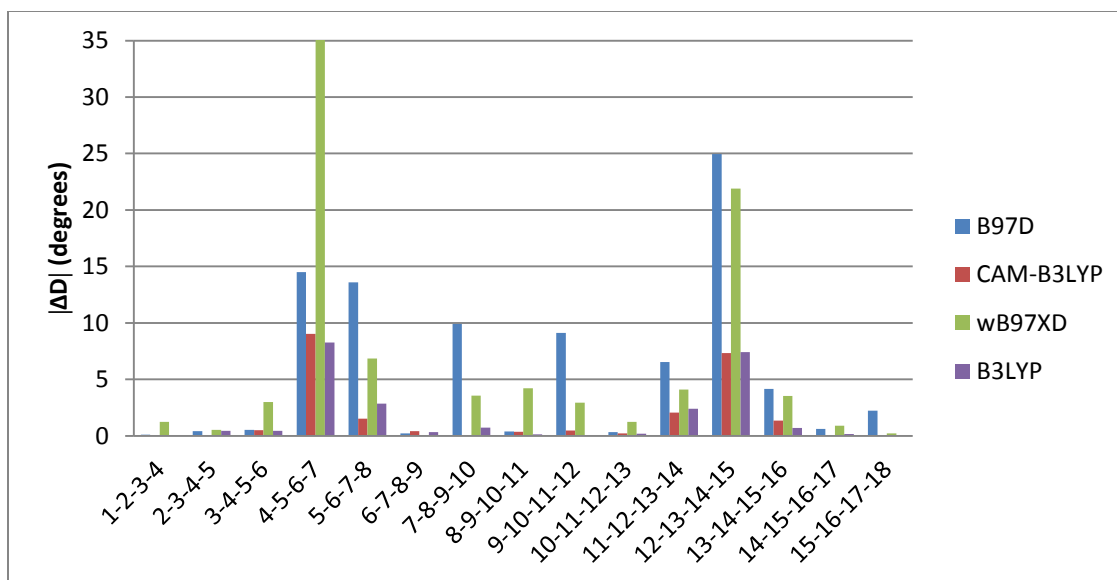


Figure 4.17: Dihedral angle differences between ALD-encapped oligomers without and with SCs as a function of dihedral angle position of oligomer for different DFT methods.

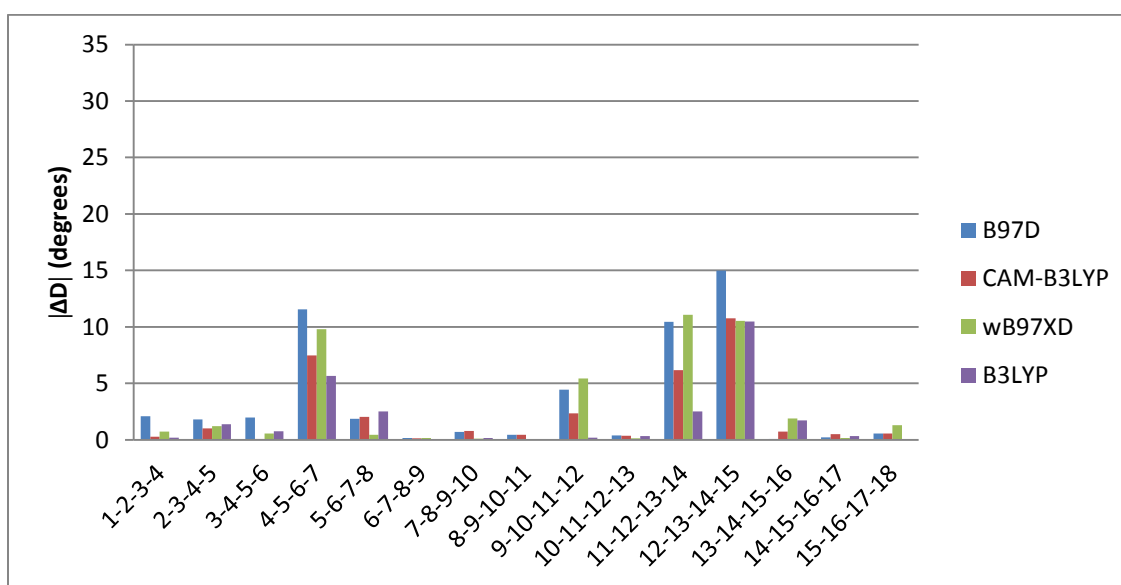
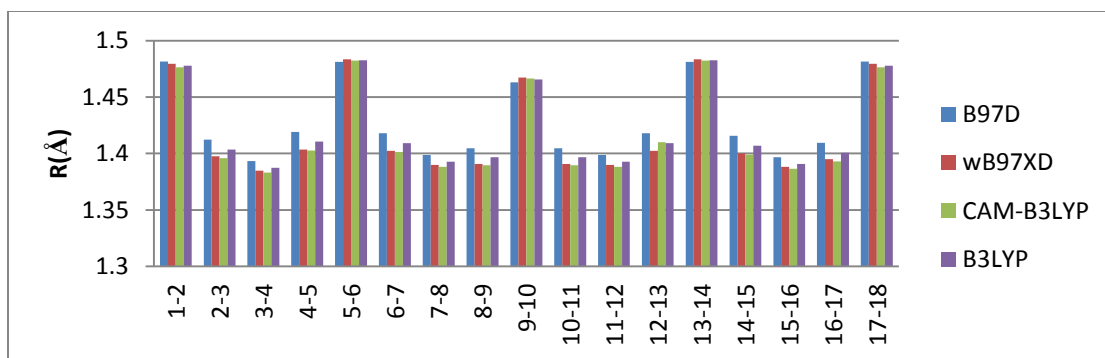


Figure 4.18: Dihedral angle differences between DTF-encapped oligomers without and with SCs as a function of dihedral angle position of oligomer for different DFT methods.

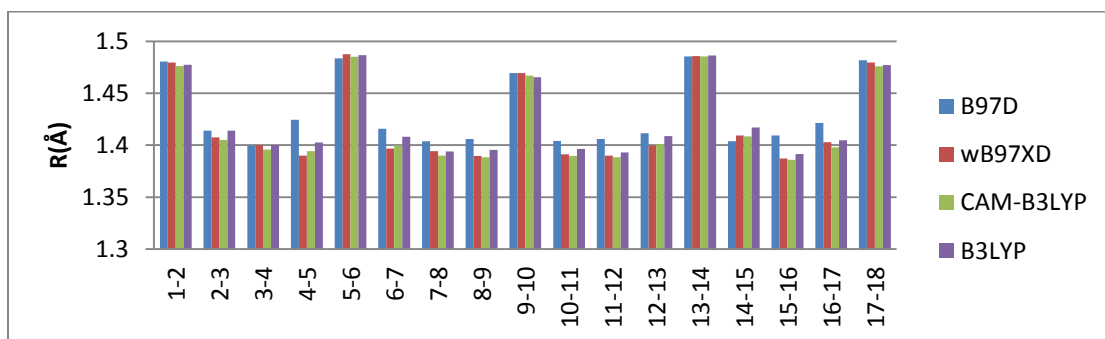
## 4.5 Comparison of DFT Methods

### 4.5.1 Structural Effects

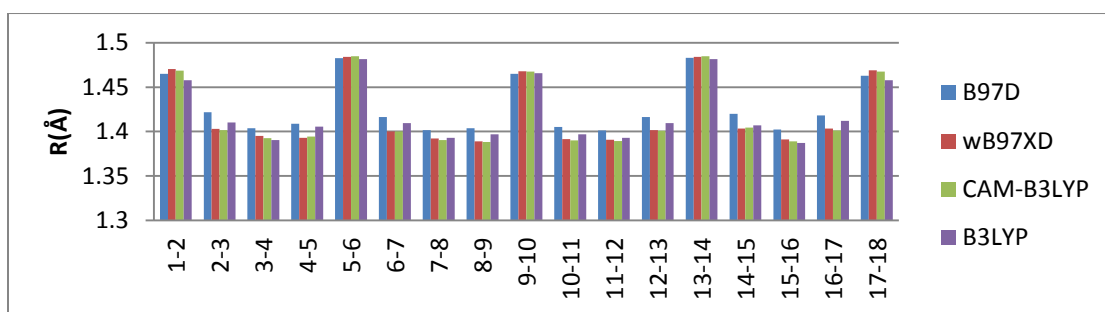
It is known that for isolated molecules, hybrid DFT such as B3LYP, produces their geometrical and electronic structures that are close to the corresponding experimental values [103]. Figures 4.19-4.21 show the bond lengths, bond angles and dihedral angles as a function of the position along the oligomers backbone for different DFT methods. Figure 4.19 ((a)-(d)) illustrates that bond lengths for all methods are close to the B3LYP values except for B97D. For the bond angles, all oligomers give approximately the same result as B3LYP (see Figure 4.20 ((a)-(d))) except for ALD with SCs where B97D gives different values than B3LYP (see Figure 4.20(b)). In the case of dihedral angles (see Figure 4.21), wB97XD gives somewhat different values for two angles (e.g.  $D_{4-5-6-7}$  and  $D_{12-13-14-15}$ ) in comparison to B3LYP for ALD- and DTF-endcapped oligomers without and with SCs.



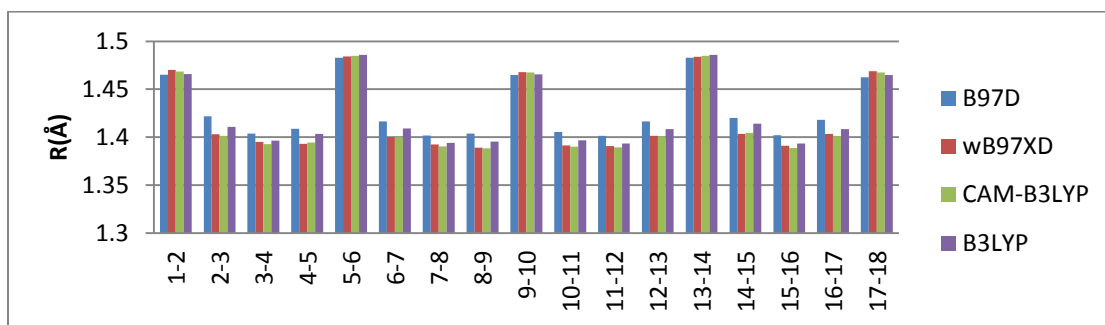
(a)



(b)

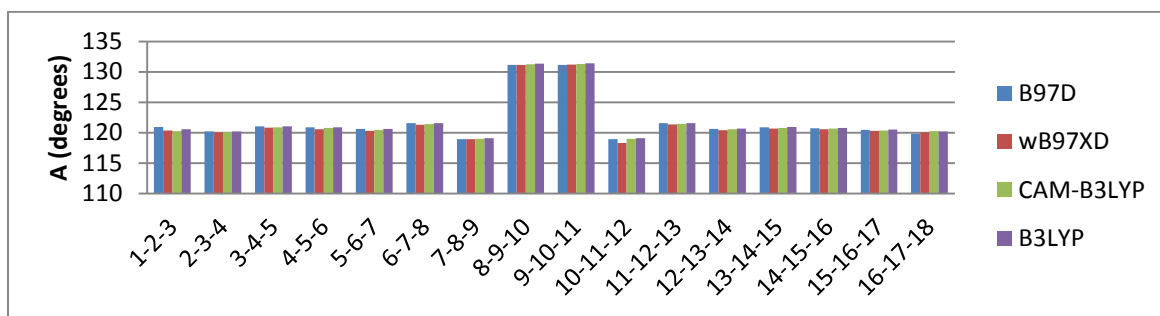


(c)

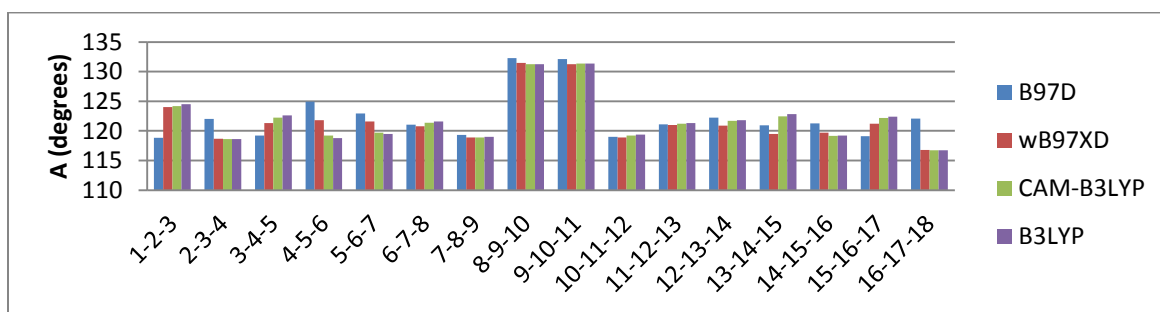


(d)

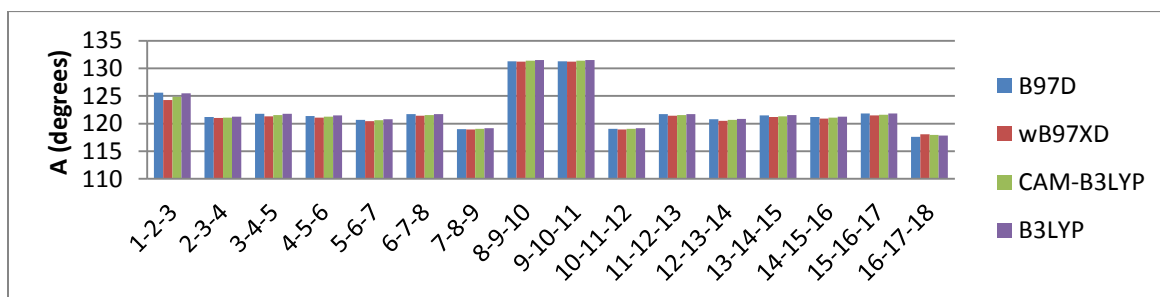
Figure 4.19: Bond lengths for ALD-endcapped oligomers (a) without and (b) with SCs and for DTF-endcapped oligomers (c) without and (d) with SCs along oligomers backbones (see Figure 4.1 and 4.4 respectively) for different DTF methods.



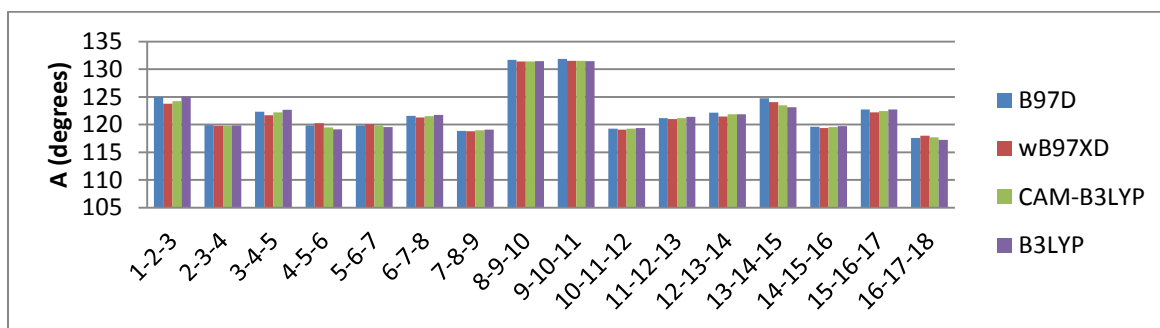
(a)



(b)



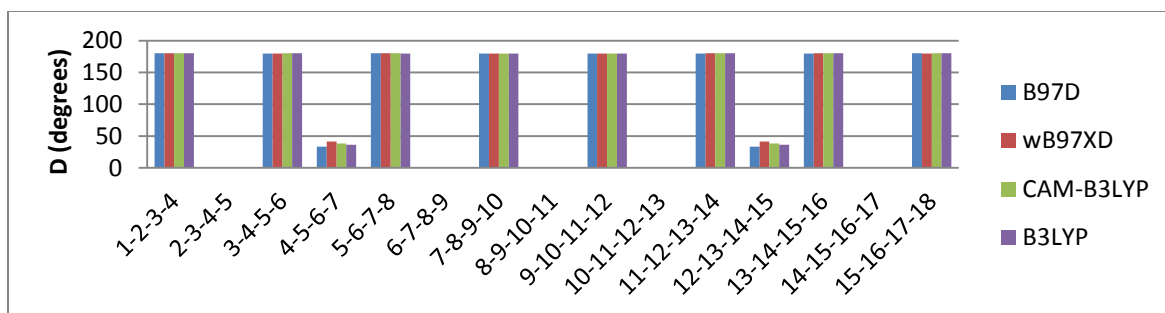
(c)



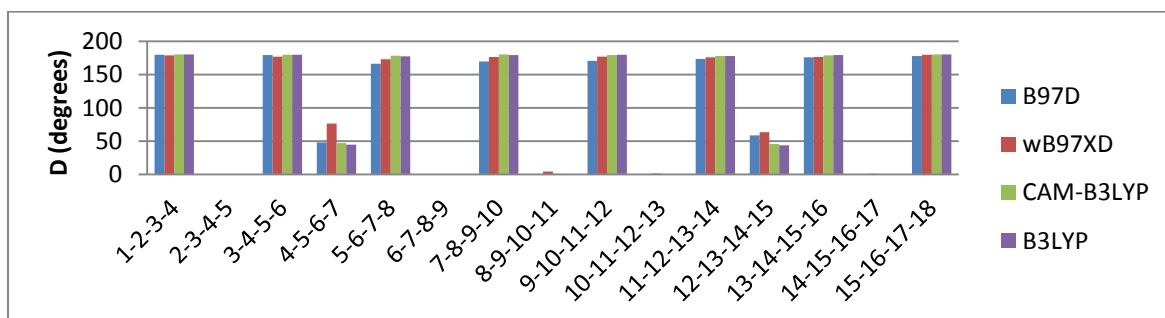
(d)

Figure 4.20: Bond angles for ALD-endcapped oligomers (a) without and (b) with SCs and for DTF-endcapped oligomers (c) without and (d) with SCs along oligomers backbones (see Figure 4.1 and 4.4 respectively) for different DTF methods.

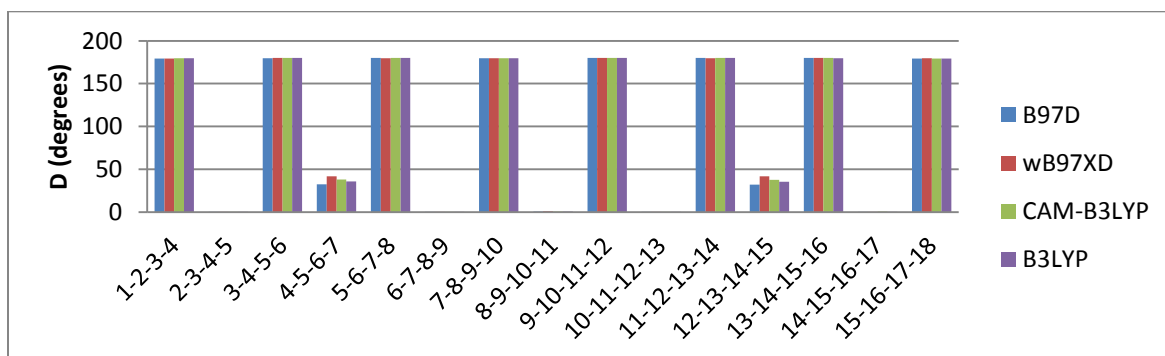




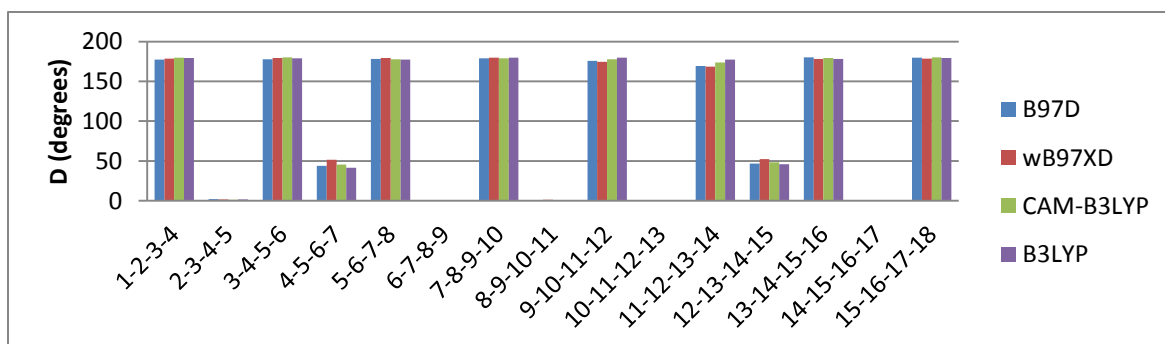
(a)



(b)



(c)



(d)

Figure 4.21: Dihedral angles for ALD-endcapped oligomers (a) without and (b) with SCs and for DTF-endcapped oligomers (c) without and (d) with SCs along oligomers backbones (see Figure 4.1 and 4.4 respectively) for different DTF methods.

### 4.5.2 Standard Deviation

Tables 4.1-4.3 gives the standard deviations (SDs) of BLs, BAs, and DAs for different dispersion corrected and hybrid functional DFT methods as a function of different oligomers (with different end groups, and with and without SCs). The SD measures the amount of variation or dispersion from the average. A low standard deviation indicates that the data points tend to be very close to the mean, a high standard deviation indicates that the data points are spread out over a large range of values. The data given in Tables 4.1-4.3 are plotted in Figures 4.22-4.24. For bond lengths, SD is close to 0.04 Å which is very small for all methods (only B97D values are smaller and are closer to 0.03 Å). In case of bond angles SD, oligomers with SCs have a larger SD (close to 4.1°) than those without SCs (close to 3.8°). The SD for dihedral angles is between 83°-89° and tends to be, in contrast, to SD for bond angles smaller for oligomers with SCs than without SCs.

Table 4.1: Standard deviations of bond lengths (in Angstroms) for different dispersion corrected DFT methods as a function of oligomers with different end groups and with and without SCs

| Bond length     |       |        |           |       |
|-----------------|-------|--------|-----------|-------|
|                 | B97D  | wB97XD | CAM-B3LYP | B3LYP |
| ALD without SCs | 0.034 | 0.040  | 0.040     | 0.037 |
| ALD with SCs    | 0.034 | 0.040  | 0.039     | 0.037 |
| DTF without SCs | 0.030 | 0.038  | 0.038     | 0.033 |
| DTF with SCs    | 0.030 | 0.038  | 0.038     | 0.035 |

Table 4.2: Standard deviations of bond angles (in degrees) for different dispersion corrected DFT methods as a function of oligomers with different end groups and with and without SCs

| Bond angle      |       |        |           |       |
|-----------------|-------|--------|-----------|-------|
|                 | B97D  | wB97XD | CAM-B3LYP | B3LYP |
| ALD without SCs | 3.702 | 3.793  | 3.764     | 3.760 |
| ALD with SCs    | 4.166 | 4.101  | 4.127     | 4.177 |
| DTF without SCs | 3.877 | 3.812  | 3.856     | 3.900 |
| DTF with SCs    | 4.190 | 3.998  | 4.030     | 4.098 |

Table 4.3: Standard deviations of dihedral angles (in degrees) for different dispersion corrected DFT methods as a function of oligomers with different end groups and with and without SCs

| Dihedral Angle  |        |        |           |        |
|-----------------|--------|--------|-----------|--------|
|                 | B97D   | wB97XD | CAM-B3LYP | B3LYP  |
| ALD without SCs | 88.523 | 87.728 | 88.021    | 88.194 |
| ALD with SCs    | 83.651 | 83.360 | 86.771    | 86.858 |
| DTF without SCs | 88.505 | 87.488 | 87.970    | 88.198 |
| DTF with SCs    | 85.614 | 85.135 | 86.346    | 86.764 |

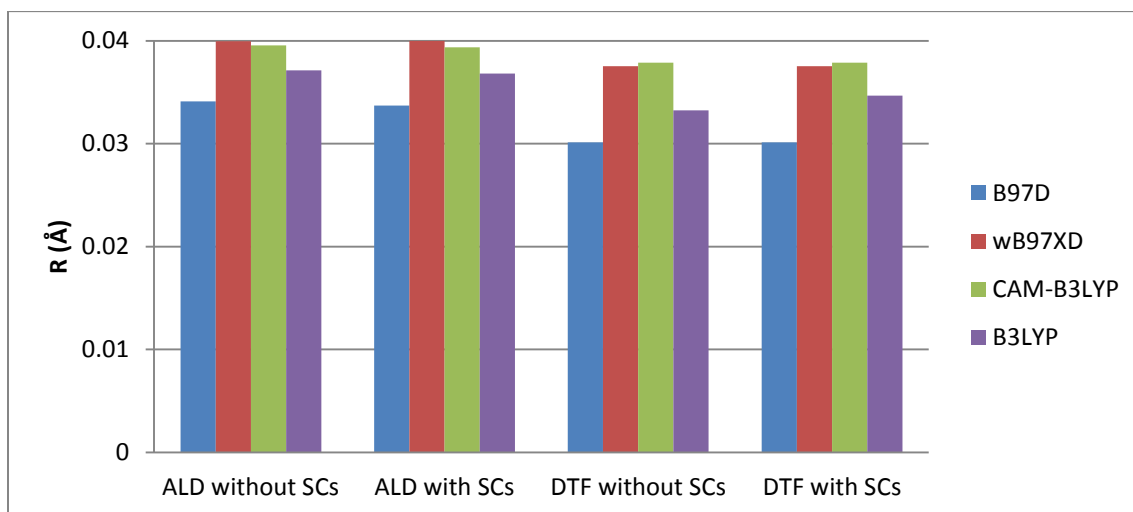


Figure 4.22: Standard deviation for bond length as a function of different oligomer systems for different methods.

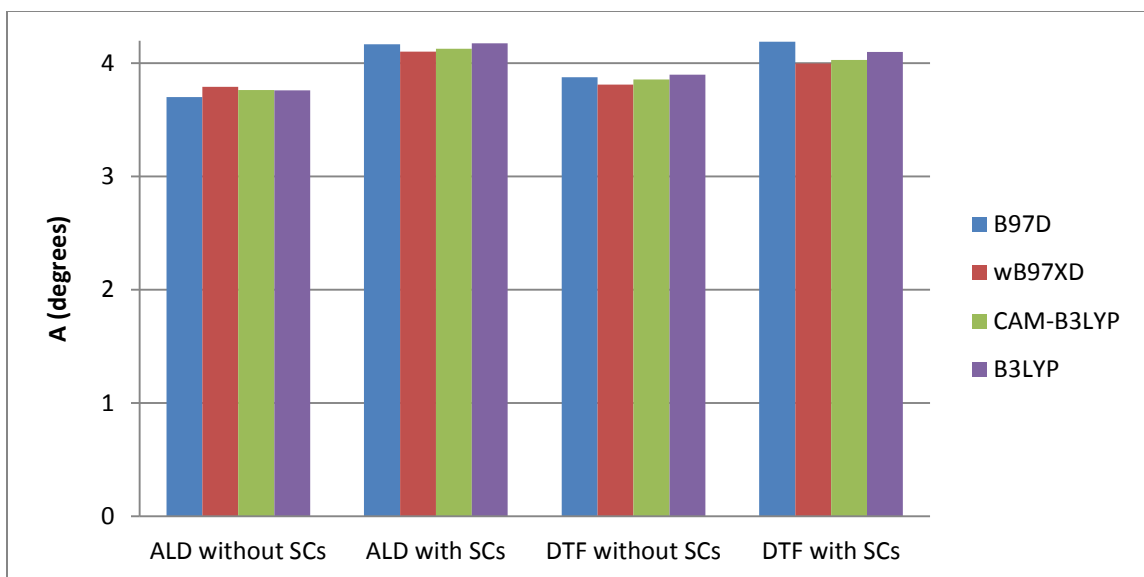


Figure 4.23: Standard deviation for bond angle as a function of different oligomer systems for different methods.

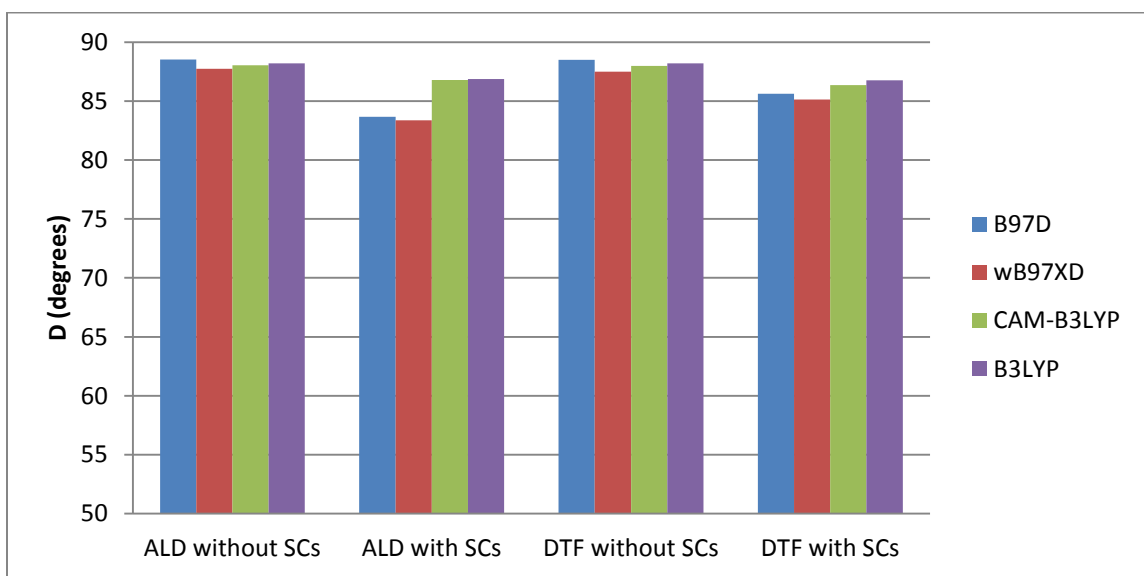


Figure 4.24: Standard deviation for dihedral angle as a function of different oligomer systems for different methods.

## 4.6 Dipole Moments

The magnitude and direction of dipole moments ( $\mu$ ) give the information about the charge polarizations in the polymer. The dipole moment is defined as the sum of the products of the charge  $Q_i$  and the position  $R_i$  of the charge i.e.

$$\mu = \sum_{i=1}^n Q_i R_i . \quad 4.1$$

Table 4.4 gives the magnitudes of the total dipole moments ( $\mu$ 's) and their components ( $\mu_x, \mu_y, \mu_z$ ) as a function of different molecular system for different dispersion corrected and hybrid DFT methods. All dipole moments are calculated relative to the coordinate systems as defined by the standard orientations and point towards positive charge (see Figures 4.25 and 4.26). For the oligomers without SCs  $x$ -,  $y$ - and  $z$ -axes (Figure 4.25) are, respectively, along the backbone, passing through the center of fluorene in plane and perpendicular to the  $x$ -axis and out of plane and perpendicular to the backbone. However, in the presence of SCs, the center of the mass shifts and axis are not as consistently defined. Figure 4.25 (and Table 4.4) show that, for all oligomers without SCs for B97D and wB97XD and for oligomers with DTF end group for B3LYP and CAM-B3LYP, the dipole moments lie almost in the fluorene plane. In contrast, for oligomer with the ALD end group without SCs for B3LYP and CAM-B3LYP, the dipole moment has a significant  $z$ -component (see Table 4.4) which makes dipole moment point out of fluorene plane. It should be noted that dipole moments for ALD- and DTF-endcapped oligomers point in the opposite directions. For oligomers with SCs (see Figure 4.26), dipole moments for both end groups lie nearly in the fluorene plane with exception of oligomer with DTF end group for B3LYP which has a relatively large  $z$  (out of the plane)

component. The trend for the direction of the dipole moments for the oligomers with SCs is similar to what is observed for oligomers without SCs.

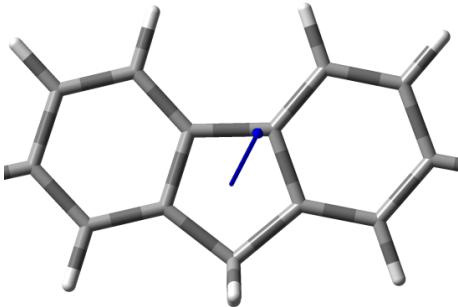
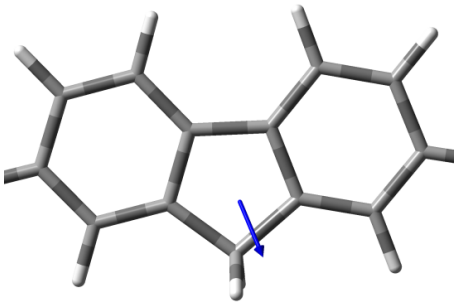
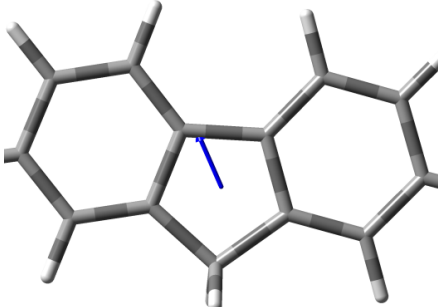
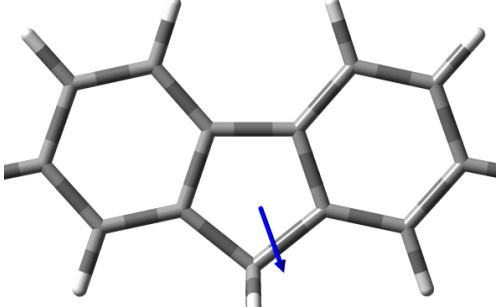
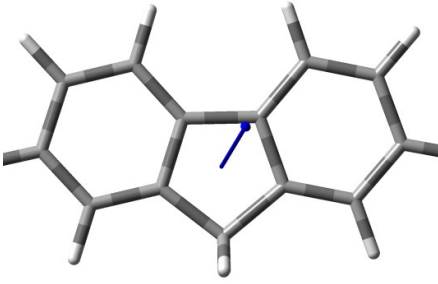
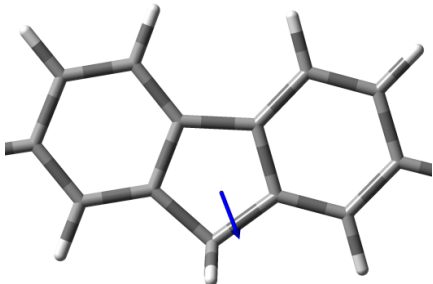
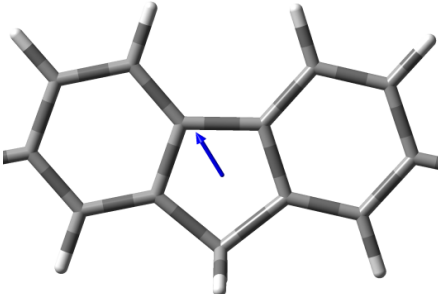
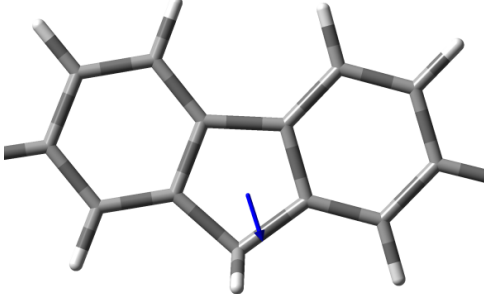
| ALD-endcapped Oligomer   | DTF-endcapped Oligomer  |
|--|---|
|  <p>ALD without SCs-B3LYP</p>       |  <p>DTF without SCs-B3LYP</p>         |
|  <p>ALD without SCs-B97D</p>        |  <p>DTF without SCs- B97D</p>         |
|  <p>ALD without SCs-CAM-B3LYP</p> |  <p>DTF without SCs- CAM-B3LYP</p> |
|  <p>ALD without SCs-wB97XD</p>    |  <p>DTF without SCs- wB97XD</p>     |

Figure 4.25 Total dipole moments (indicated by the blue arrow) of ALD- and DTF-endcapped oligomers without SCs for different dispersion corrected and hybrid functional DFT methods. For clarity, only the relevant portion of the oligomer is shown.

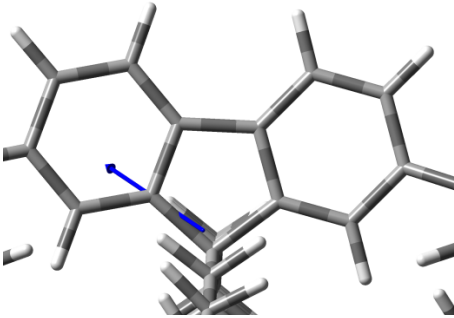
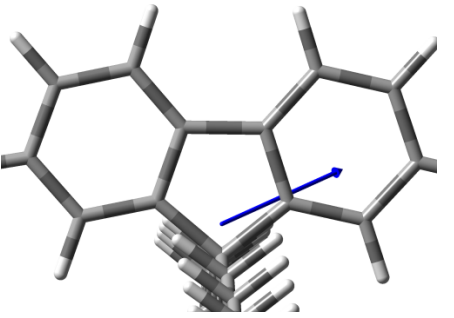
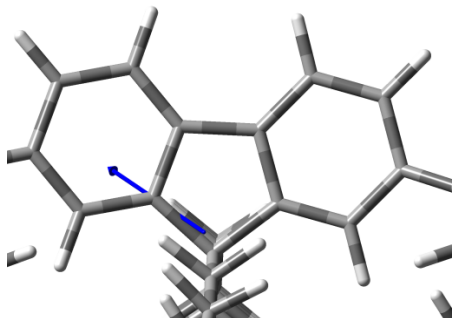
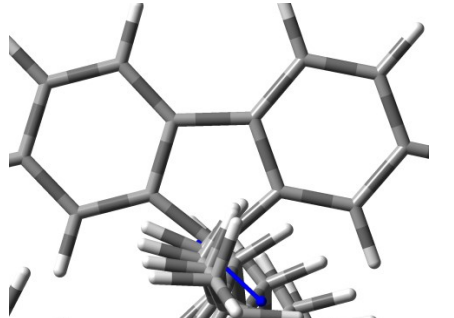
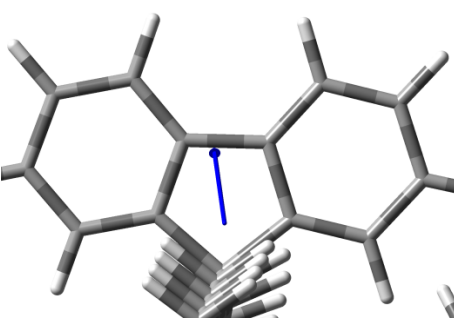
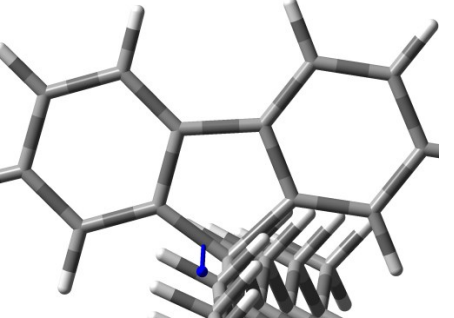
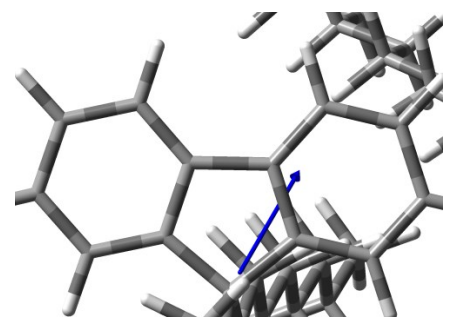
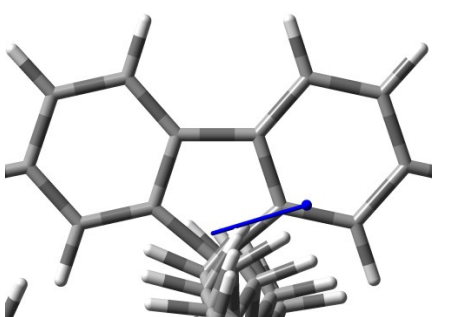
| ALD-endcapped Oligomer  | DTF-endcapped Oligomer   |
|---|--|
| <br>ALD with SCs-B3LYP       | <br>DTF with SCs- B3LYP       |
| <br>ALD with SCs-B97D        | <br>DTF with SCs- B97D        |
| <br>ALD with SCs-CAM-B3LYP | <br>DTF with SCs- CAM-B3LYP |
| <br>ALD with SCs-wB97XD    | <br>DTF with SCs- wB97XD    |

Figure 4.26 Total dipole moments (indicated by the blue arrows) of ALD- and DTF-endcapped oligomers with SCs for different dispersion corrected and hybrid functional DFT methods. For clarity, only the relevant portion of the oligomer is shown.



Table 4.4 Dipole moments (in debyes) with  $x$ ,  $y$  and  $z$  components ( $\mu_x, \mu_y, \mu_z$ ) of different molecule systems as a function of different dispersion corrected DFT methods.

|           | ALD without SCs   | DTF without SCs   | ALD with SCs  | DTF with SCs   |
|-----------|---|---|---|--|
| B97D      | $\mu_x=-0.47$ ,<br>$\mu_y=-0.94$ ,<br>$\mu_z=-0.24$<br>Tot=1.08 | $\mu_x=-0.27$ ,<br>$\mu_y=-1.11$ ,<br>$\mu_z=-0.21$<br>Tot=1.16 | $\mu_x=-3.00$ ,<br>$\mu_y=0.90$ ,<br>$\mu_z=0.29$<br>Tot=3.15   | $\mu_x=1.18$ ,<br>$\mu_y=-6.83$ ,<br>$\mu_z=1.10$<br>Tot=7.02  |
| wB97XD    | $\mu_x=-0.47$ ,<br>$\mu_y=0.75$ ,<br>$\mu_z=-0.21$<br>Tot=0.91  | $\mu_x=0.21$ ,<br>$\mu_y=-0.85$ ,<br>$\mu_z=0.01$<br>Tot=0.88   | $\mu_x=-0.77$ ,<br>$\mu_y=-2.32$ ,<br>$\mu_z=-0.93$<br>Tot=2.62 | $\mu_x=0.90$ ,<br>$\mu_y=-7.06$ ,<br>$\mu_z=0.93$<br>Tot=7.18  |
| CAM-B3LYP | $\mu_x=0.51$ ,<br>$\mu_y=0.89$ ,<br>$\mu_z=2.07$<br>Tot=2.31    | $\mu_x=0.29$ ,<br>$\mu_y=-0.91$ ,<br>$\mu_z=0.13$<br>Tot=0.96   | $\mu_x=1.85$ ,<br>$\mu_y=-1.81$ ,<br>$\mu_z=0.72$<br>Tot=2.69   | $\mu_x=0.32$ ,<br>$\mu_y=-6.23$ ,<br>$\mu_z=0.56$<br>Tot=6.27  |
| B3LYP     | $\mu_x=0.50$ ,<br>$\mu_y=0.97$ ,<br>$\mu_z=1.93$<br>Tot=2.22    | $\mu_x=-0.29$ ,<br>$\mu_y=-1.06$ ,<br>$\mu_z=-0.39$<br>Tot=1.17 | $\mu_x=-1.73$ ,<br>$\mu_y=-1.79$ ,<br>$\mu_z=-0.39$<br>Tot=2.52 | $\mu_x=1.93$ ,<br>$\mu_y=-0.93$ ,<br>$\mu_z=-2.33$<br>Tot=3.17 |

First, we consider the end group effect on the magnitude of the total dipole moments of oligomers without SCs (see Figure 4.27). wB97XD and B97D give almost the same value, whereas B3LYP and CAM-B3LYP give larger magnitudes for oligomers with ALD than with DTF end groups. For oligomers with SCs, the end group effect is significant (see Figure 4.28) since oligomers with DTF end group have larger dipole moment magnitudes (by a factor of two or more in all cases except for B3LYP) than oligomers with ALD end group. Figures 4.29 and 4.30 show that oligomers with SCs have in most cases significantly larger dipole moments than oligomers without SCs (this is especially true for DTF-DPF).

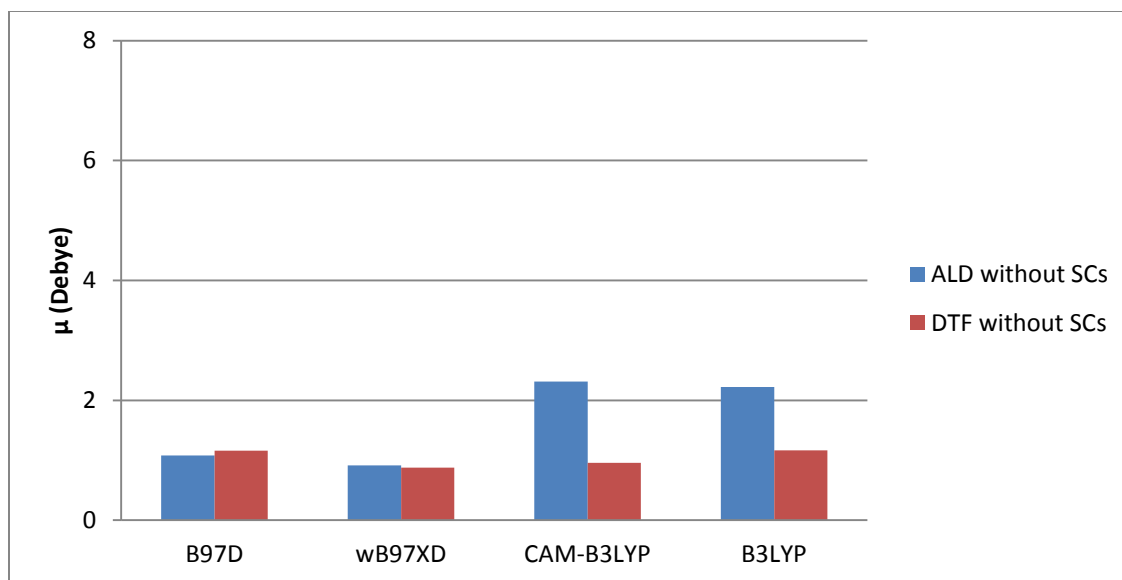


Figure 4.27: Dipole moments as a function of different methods for oligomers with ALD and DTF end groups without SCs.

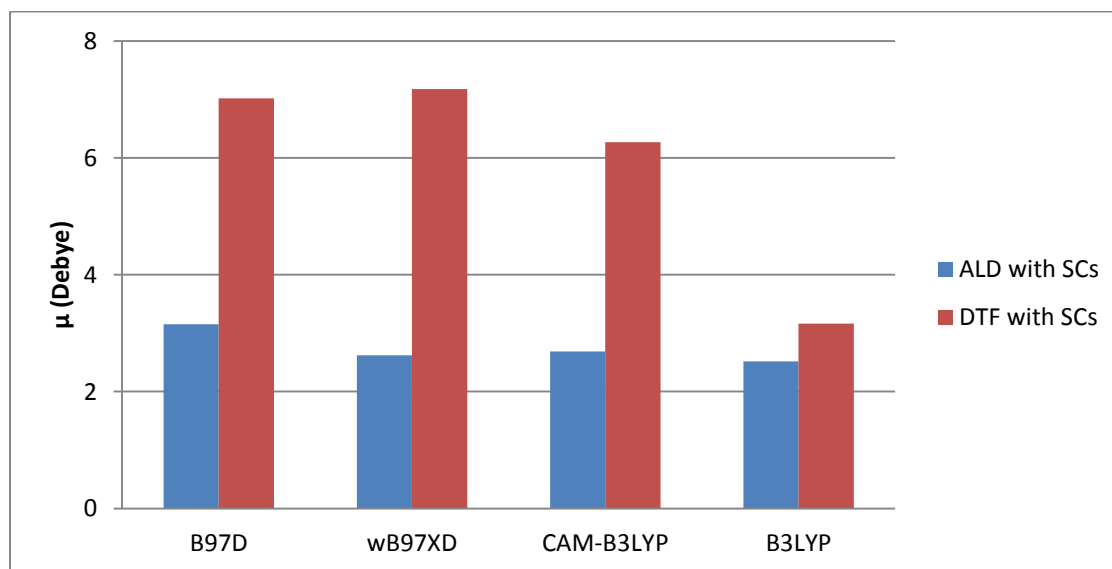


Figure 4.28 Dipole moment magnitudes as a function of different methods for oligomers with ALD and DTF end groups with SCs.

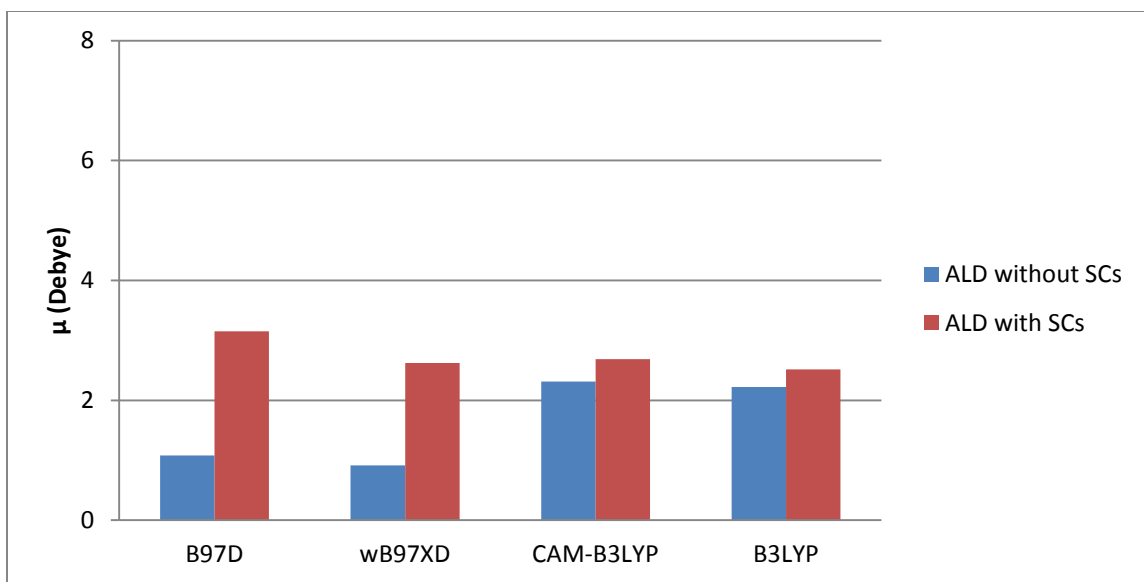


Figure 4.29: Dipole moment magnitudes as a function of different methods for oligomers with ALD end group and without and with SCs.

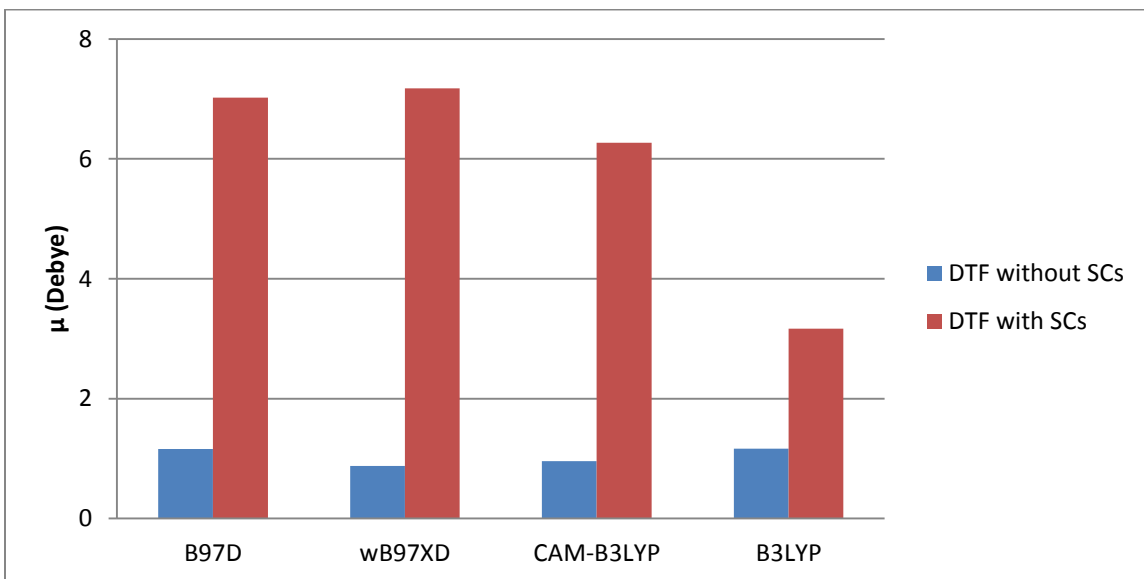


Figure 4.30: Dipole moment magnitudes as a function of different methods for oligomers with DTF end group and without and with SCs.

## 4.7 HOMO, LUMO Eigenvalues and HOMO-LUMO Energy Gaps

Electronic structure of the conjugated oligomers with and without SCs is discussed in this section. Table 4.5 gives the HOMO, LUMO eigenvalues and HOMO-LUMO energy gaps of different molecular systems as a function of different dispersion corrected and hybrid DFT methods. Figures 4.31-4.34 show the HOMO, LUMO eigenvalues and HOMO-LUMO gaps as a function of different oligomer system (1.ALD without SCs, 2.DTF without SCs, 3.ALD with SCs and 4.DTF with SCs) for B97D, wB97XD, CAM-B3LYP and B3LYP methods respectively. These four graphs illustrate clearly that the variations (trends in magnitudes) of HOMO, LUMO eigenvalues and HOMO-LUMO gaps are very similar for all DFT methods. HOMO-LUMO gaps are approximately 2 eV (see Figure 4.31), 8 eV (see Figure 4.32), 6 eV (see Figure 4.33) and 4 eV (see Figure 4.34) for B97D, wB97XD CAM-B3LYP and B3LYP respectively. Since B3LYP method gives good results in comparison to experimental values for band gaps [105], we can say that B97D underestimates, and wB97XD and CAM-B3LYP overestimate the HOMO-LUMO gaps in comparison to corresponding B3LYP values. All four methods show that ALD-endcapped oligomers have larger HOMO-LUMO gaps than DTF-endcapped oligomers. These trends are clearly displayed on Figures 4.35-4.36.

Table 4.5: HOMO, LUMO eigenvalues and HOMO-LUMO energy gap of different molecule system as a function of different dispersion corrected DFT methods.

| Molecule system | Method   | HOMO (eV) | LUMO (eV) | HOMO-LUMO (eV) |
|-----------------|----------|-----------|-----------|----------------|
| ALD without SCs | B97D     | -5.206    | -2.757    | -2.449         |
|                 | wB97XD   | -7.719    | -0.322    | -7.397         |
|                 | CAM-B3YP | -7.110    | -0.878    | -6.231         |
|                 | B3LYP    | -5.881    | -2.136    | -3.744         |
| DTF without SCs | B97D     | -4.073    | -1.931    | -2.142         |
|                 | wB97XD   | -6.680    | 0.347     | -7.027         |
|                 | CAM-B3YP | -6.063    | -0.223    | -5.840         |
|                 | B3LYP    | -4.782    | -1.395    | -3.387         |
| ALD with SCs    | B97D     | -4.601    | -2.318    | -2.283         |
|                 | wB97XD   | -7.429    | 0.123     | -7.552         |
|                 | CAM-B3YP | -6.654    | -0.546    | -6.108         |
|                 | B3LYP    | -5.372    | -1.767    | -3.606         |
| DTF with SCs    | B97D     | -3.903    | -1.724    | -2.179         |
|                 | wB97XD   | -6.620    | 0.521     | -7.141         |
|                 | CAM-B3YP | -6.034    | -0.087    | -5.947         |
|                 | B3LYP    | -4.619    | -1.196    | -3.423         |

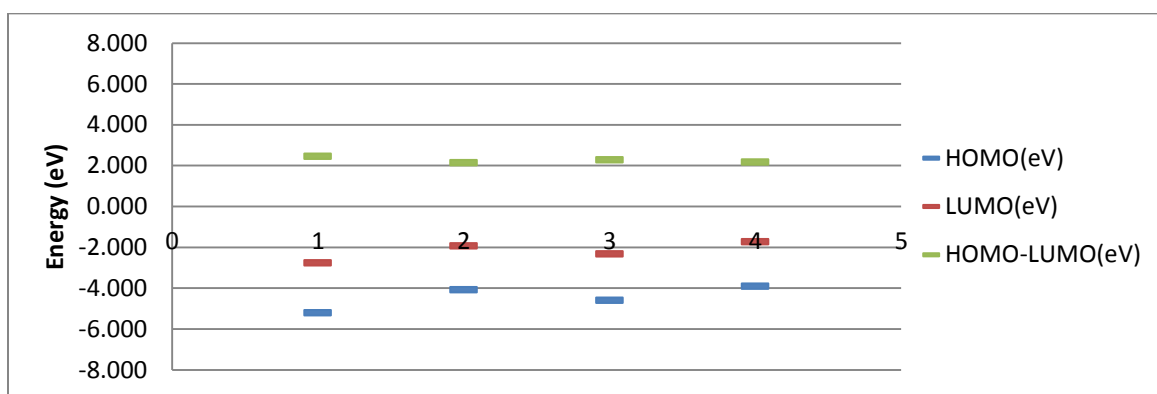


Figure 4.31 HOMO, LUMO eigenvalues and (HOMO-LUMO) gaps as a function of different oligomer systems (1.ALD without SCs, 2.DTF without SCs, 3.ALD with SCs, 4.DTF with SCs) for B97D method.

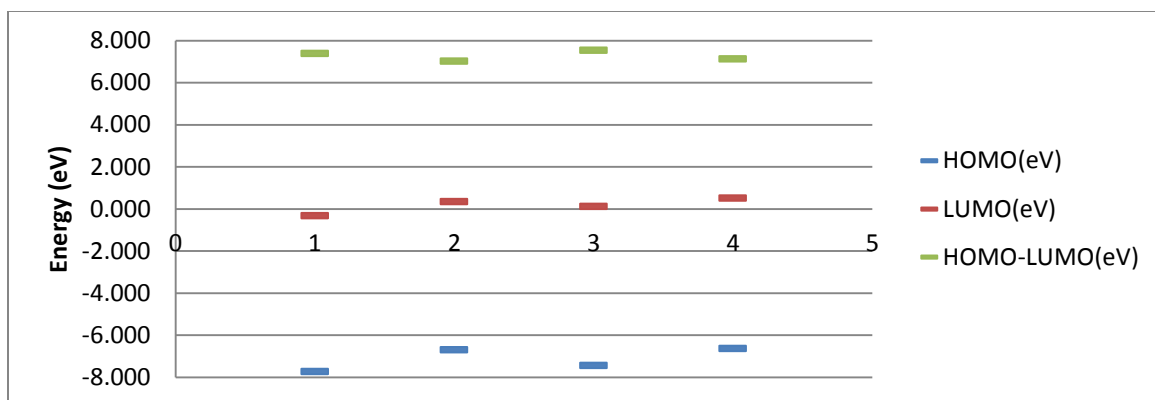


Figure 4.32 Figure 4.26 HOMO, LUMO eigenvalues and (HOMO-LUMO) gaps as a function of different oligomer systems (1.ALD without SCs, 2.DTF without SCs, 3.ALD with SCs, 4.DTF with SCs) for wB97XD method.

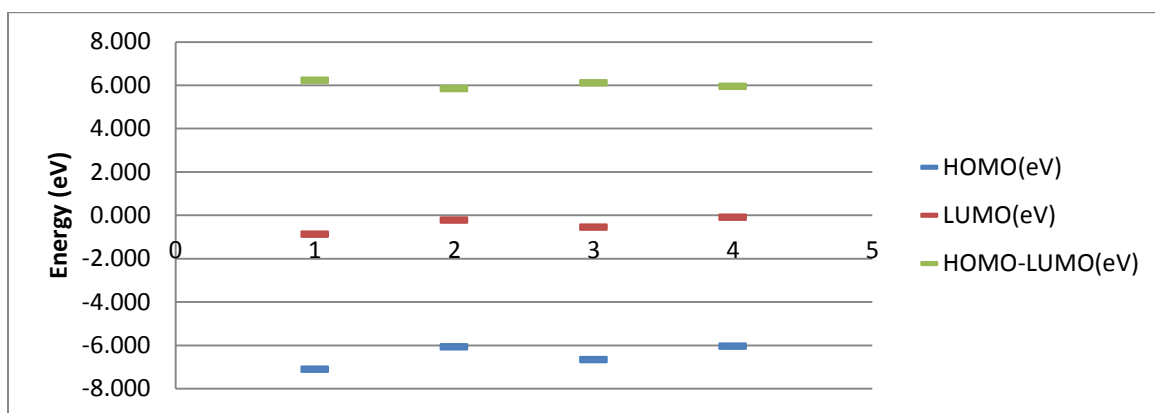


Figure 4.33 Figure 4.26 HOMO, LUMO eigenvalues and (HOMO-LUMO) gaps as a function of different oligomer systems (1.ALD without SCs, 2.DTF without SCs, 3.ALD with SCs, 4.DTF with SCs) for CAM-B3LYP method.

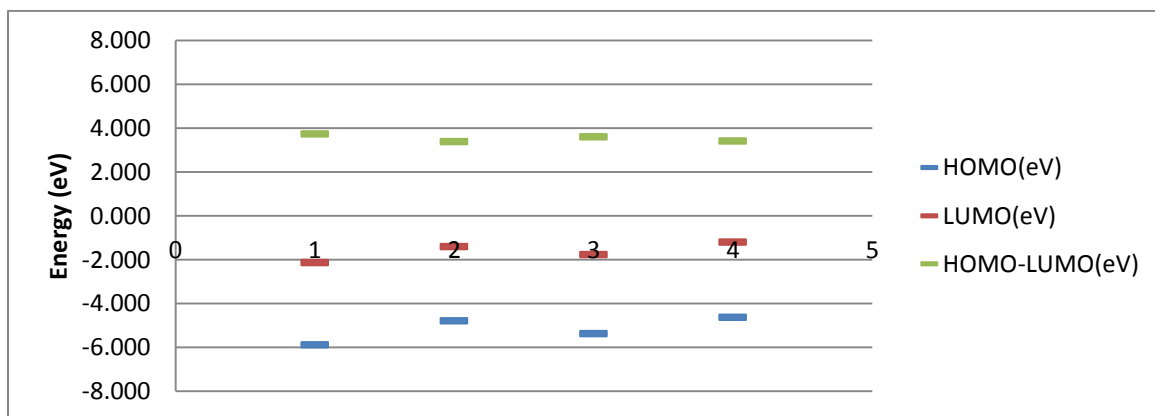


Figure 4.34 Figure 4.26 HOMO, LUMO eigenvalues and (HOMO-LUMO) gaps as a function of different oligomer systems (1.ALD without SCs, 2.DTF without SCs, 3.ALD with SCs, 4.DTF with SCs) for B3LYP method.

In the case of SCs effect, oligomers with ALD without SCs have larger gaps than ALD with SCs (Figure 4.37) except for wB97XD method. In contrast, the oligomers with DTF with SCs have larger gaps (Figure 4.38) than without SCs.

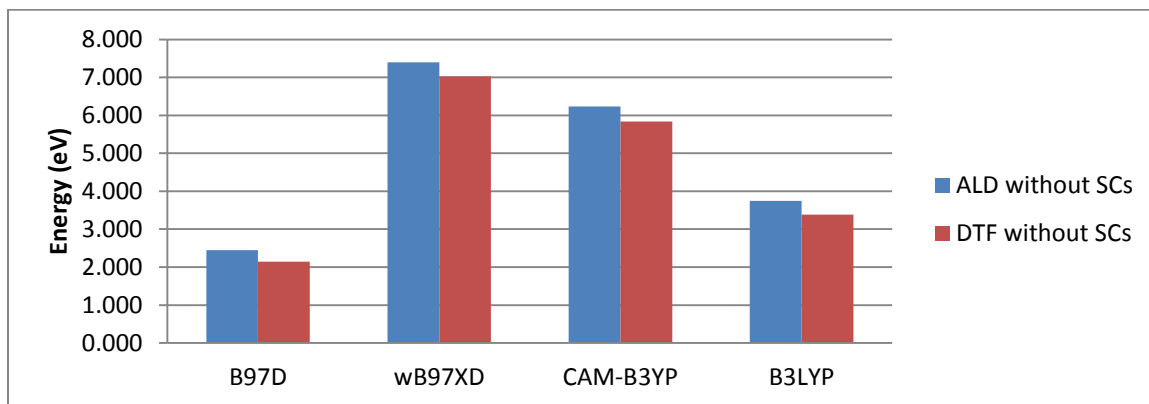


Figure 4.35: HOMO-LUMO gaps of oligomers with ALD and DTF without SCs oligomers as a function of different DFT methods.

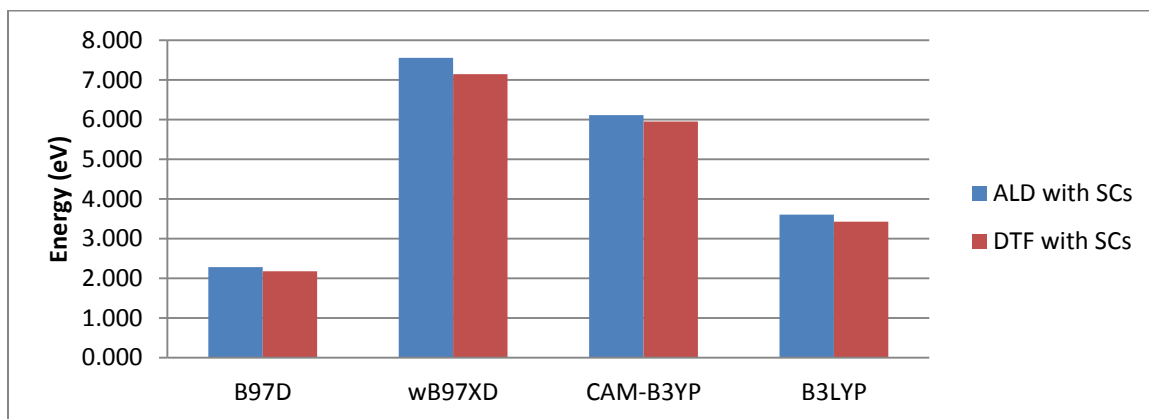


Figure 4.36: HOMO-LUMO gaps of oligomers with ALD and DTF with SCs oligomers as a function of different DFT methods.

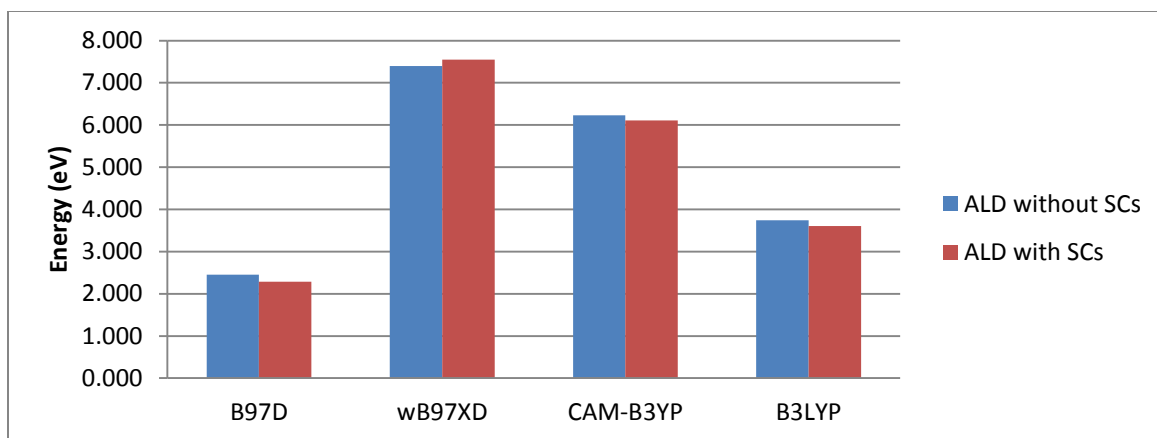


Figure 4.37: HOMO-LUMO gaps of oligomers with ALD without and with SCs oligomers as a function of different DFT methods.

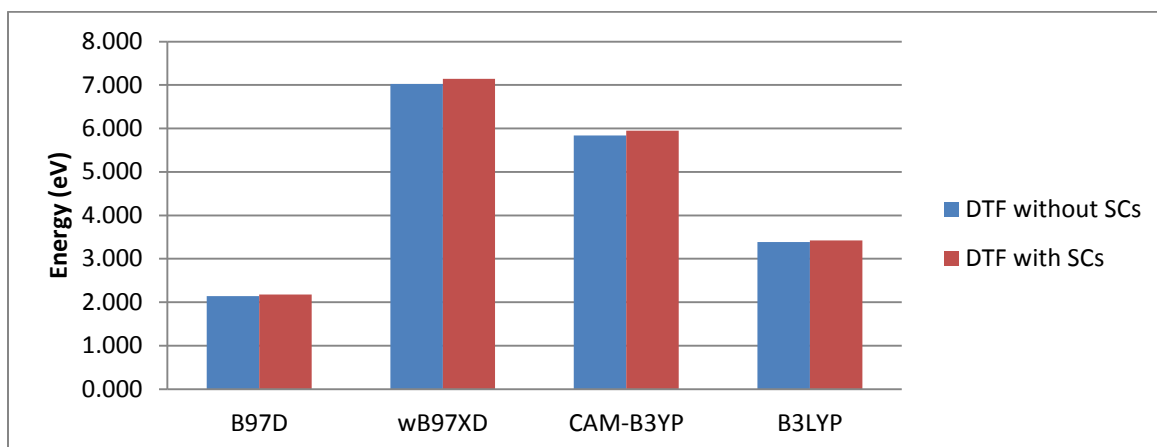


Figure 4.38: HOMO-LUMO gaps of oligomers with DTF without and with SCs oligomers as a function of different DFT methods.

## 4.8 Conclusions

In this chapter we have discussed the ALD- and DTF-endcapped fluorene-based conjugated oligomers with and without SCs using dispersion corrected (B97D, wB97XD, CAM-B3LYP) and hybrid (B3LYP) DTF methods. It is found that SCs reduce the end group effect on the bond lengths of backbone of oligomers with ALD and DTF end



groups. Bond angles of the backbone are not affected very much by the end groups. In contrast dihedral angles are affected by the end groups. Oligomers with DTF are more planar than oligomers with ALD end groups, especially when long SCs are present. That is, oligomers' backbones become more twisted in the presence of SCs and ALD effects structure of the backbone more than DTF end group. Also, for oligomers with SCs, DTF polarizes the oligomers more (i.e. they have larger dipole moments) than ALD end group. The HOMO-LUMO gaps for DTF-encapped oligomers are smaller than for ALD-encapped oligomers without and with SCs. This is consistent with the fact that more planar structures typically have lower HOMO-LUMO gaps due to larger conjugation length. With few exceptions, all DFT methods give structural values (BLs, BAs and DAs) close to each other and to B3LYP results for a given molecular system. Figures 4.7-4.38 also show that different dispersion corrected DFT methods give very similar results for end group and side chain effect on the oligomers' geometric and electronic structures. Where differences are observed, they are usually very small.

## **Chapter 5**

### **Interacting Oligomers - Comparison of Structures Using Different Dispersion Corrected DFT Methods**

#### **5.1 Introduction**

In this chapter, we analyze the structure of the oligomers (as before with two end groups (ALD and DTF), and with and without SCs) in the presence of a SWCNT. Hence these oligomers are referred to as interacting oligomers (since they interact with nanotubes). Structural details (BLs, Bas and DAs) of the interacting oligomers' backbones will be given and the comparison of these results as obtained using the different dispersion corrected DFT methods will be made. In addition, we will give results for the binding energies, dipole moments and the intermolecular distances between oligomer and CNT for the composite systems.

## 5.2 Molecular Structure of Interacting Fluorene-Based Oligomers

We consider two types of composite (oligomer and CNT) systems one with SCs and one without SCs for each ALD- and DTF-endcapped oligomer. Figures 5.1-5.3 show the molecular structures of interacting ALD- and DTF-endcapped oligomers in the presence of SWCNT without SCs and Figures 5.4-5.6 show the molecular structures of interacting ALD- and DTF-endcapped oligomers in the presence of SWCNT with SCs for different DTF methods (B97D, CAM-B3LYP, wB97XD). For each Figure (5.1-5.6) there are three sub-figures ((a), (b), (c)) which show the different views (side, top, top along the backbone) of that molecular system. For the top view along the backbone, the oligomer is colored blue for better identification. Figures 5.1-5.6 show that when SCs are present, oligomers tend to wrap themselves around nanotube more in comparison to oligomers without SCs. The wrapping of oligomers and SCs around nanotube is most pronounced for B97D and wB97XD DFT methods. The SCs do not wrap themselves as much around nanotube in the case of results obtained with CAM-B3LYP suggesting that intermolecular interactions are not as strong for this DFT approximation.

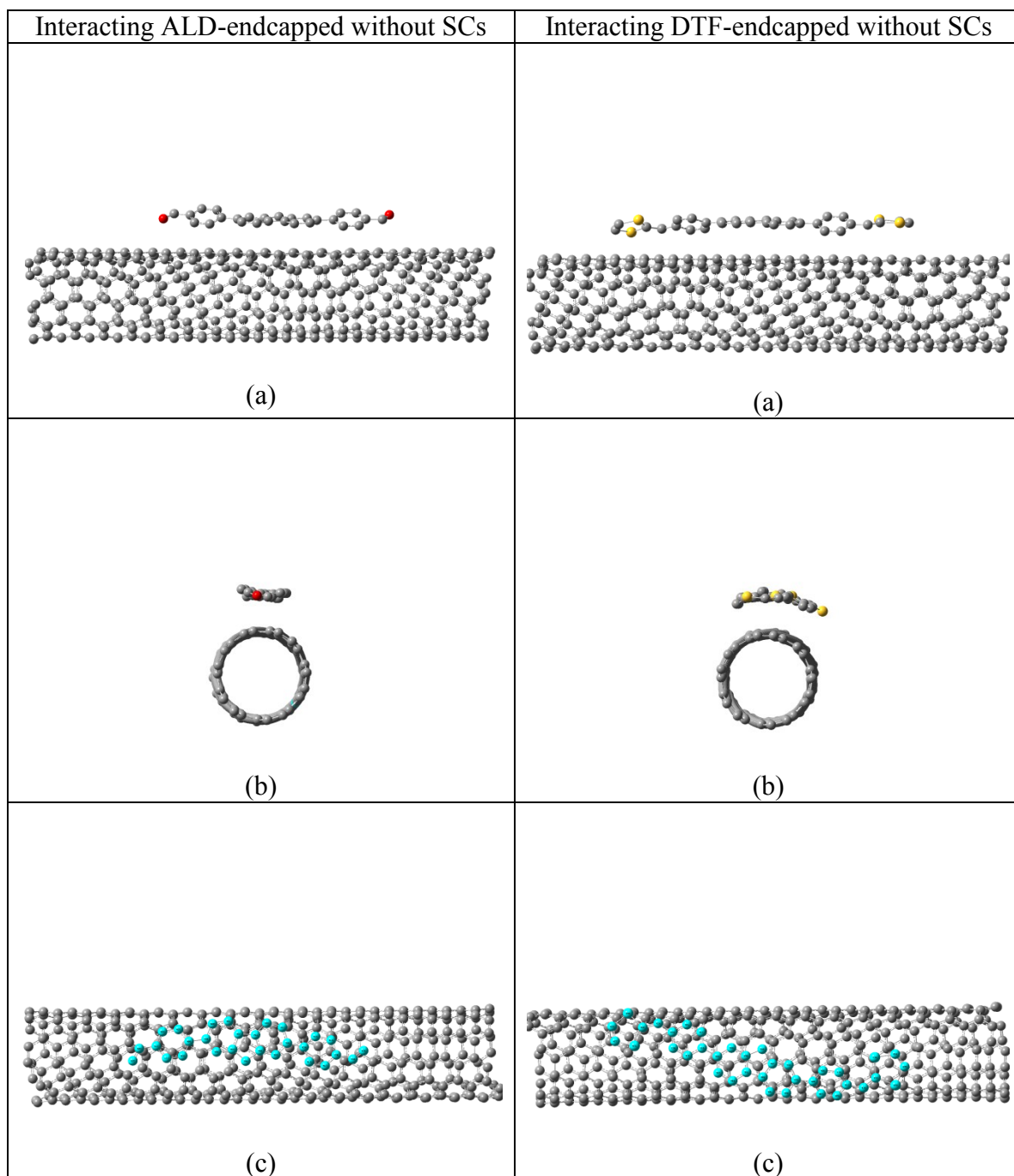


Figure 5.1: Molecular structures of composite fluorene-based ALD- and DTF-endcapped oligomers and SWCNs without SCs (a) side view (b) top view (c) top view along the backbone obtained using DTF/B97D.

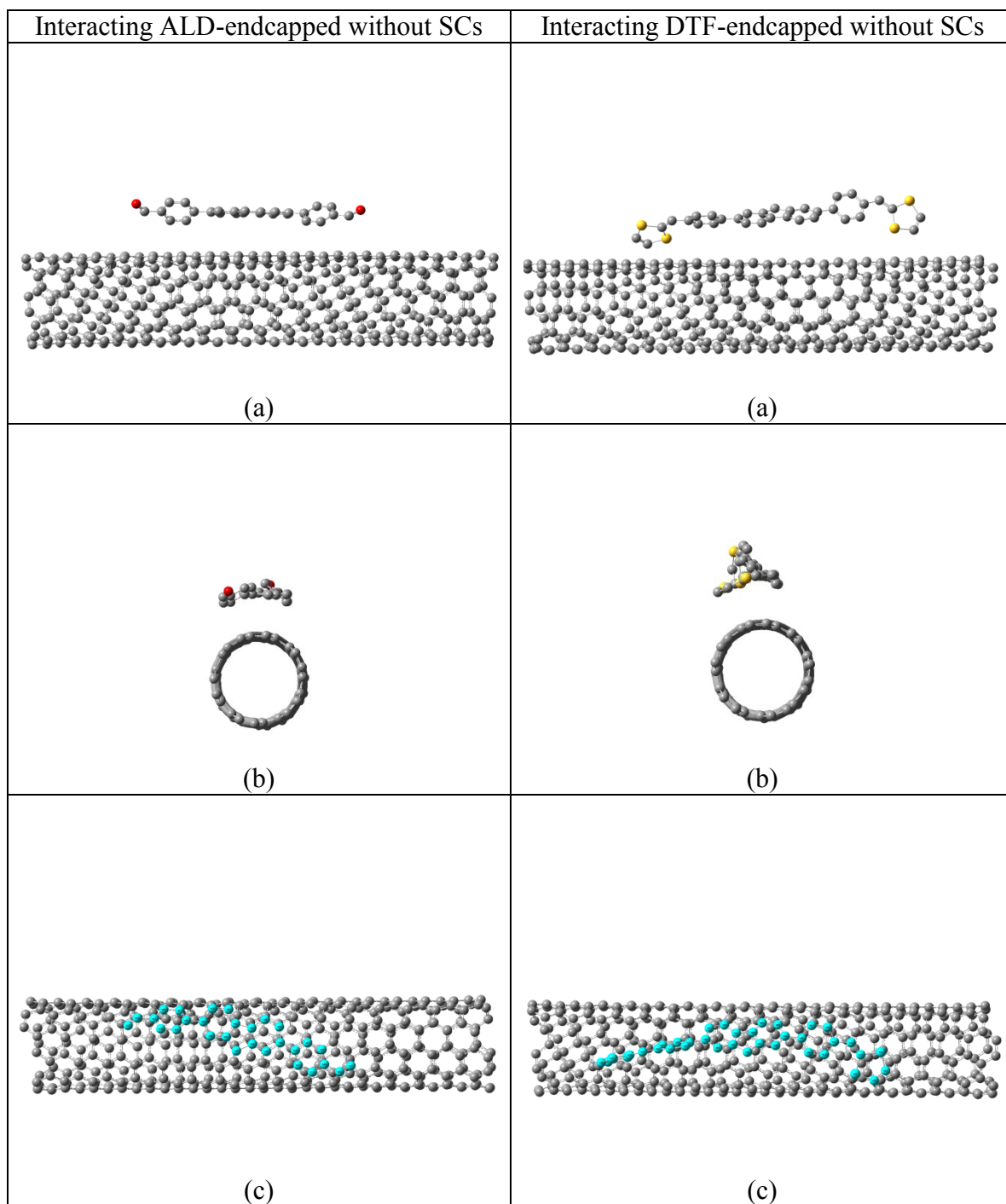


Figure 5.2: Molecular structures of composite fluorene-based ALD- and DTF-endcapped oligomers and SWCNTs without SCs (a) side view (b) top view (c) top view along the backbone obtained using DFT/CAM-B3LYP.

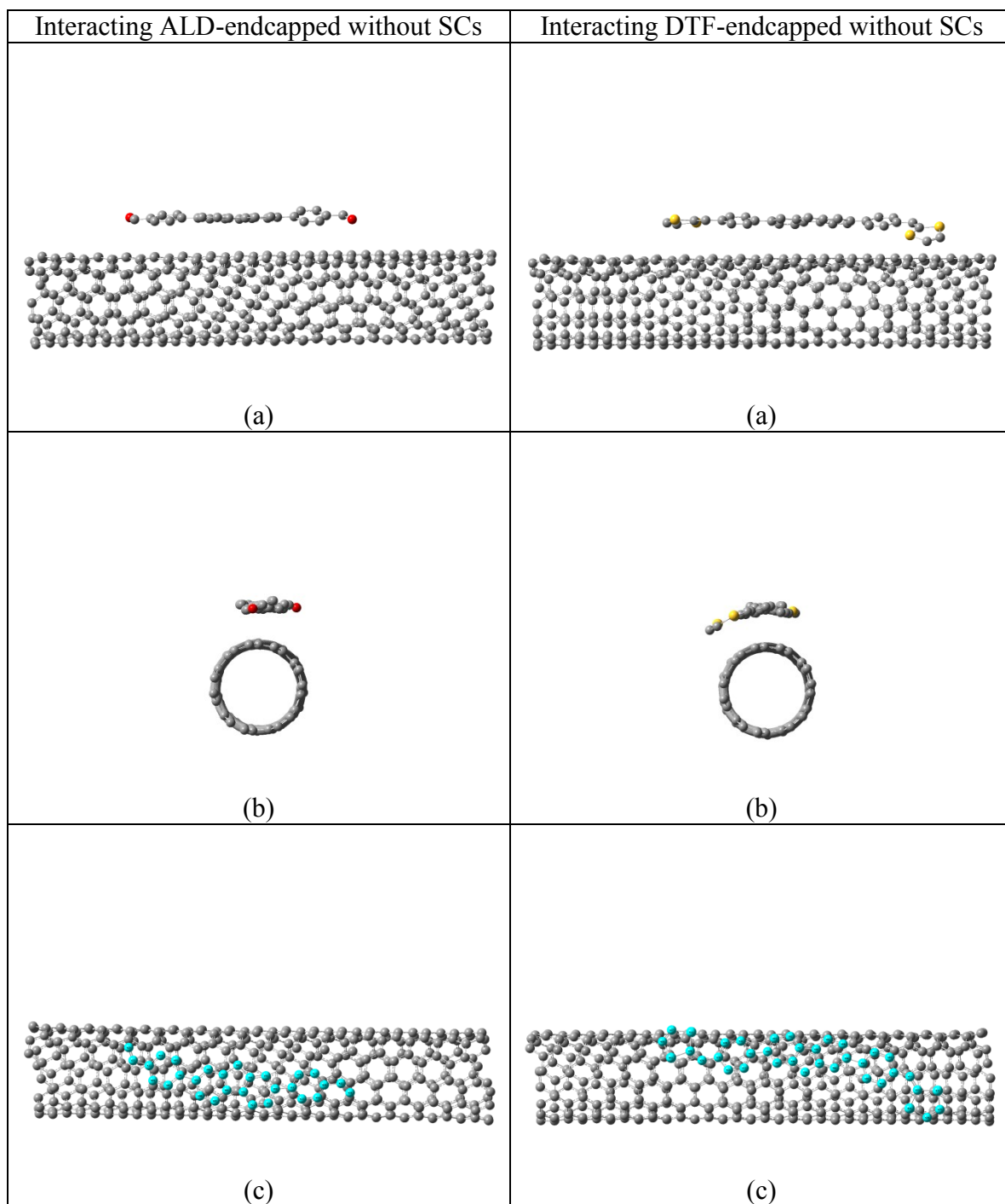


Figure 5.3: Molecular structures of composite fluorene-based ALD- and DTF-endcapped oligomers and SWCNTs without SCs (a) side view (b) top view (c) top view along the backbone obtained using DFT/wB97XD.

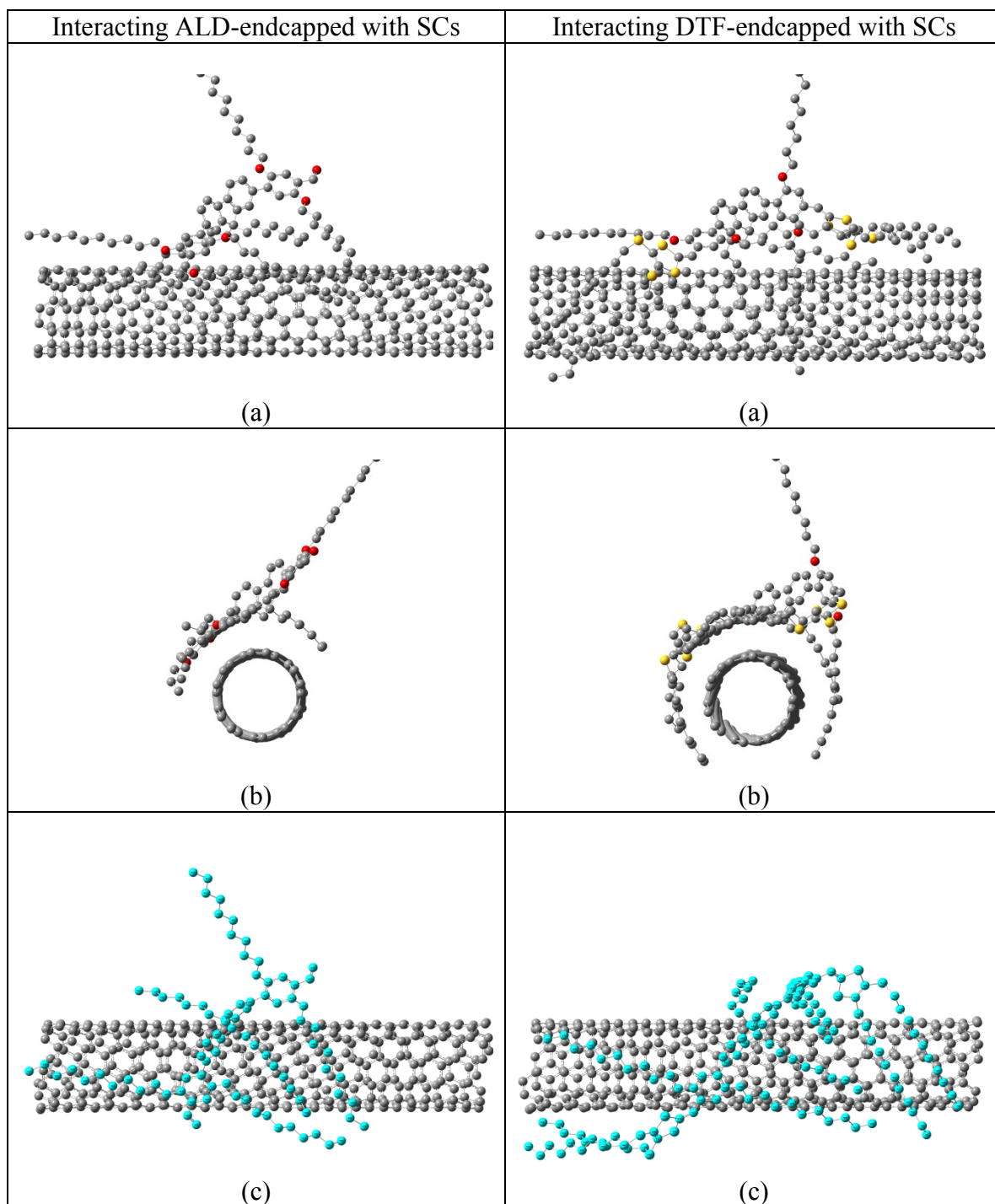


Figure 5.4: Molecular structures of composite fluorene-based ALD- and DTF-endcapped oligomers and SWCNTs with SCs (a) side view (b) top view (c) top view along the backbone obtained using DFT/B97D.

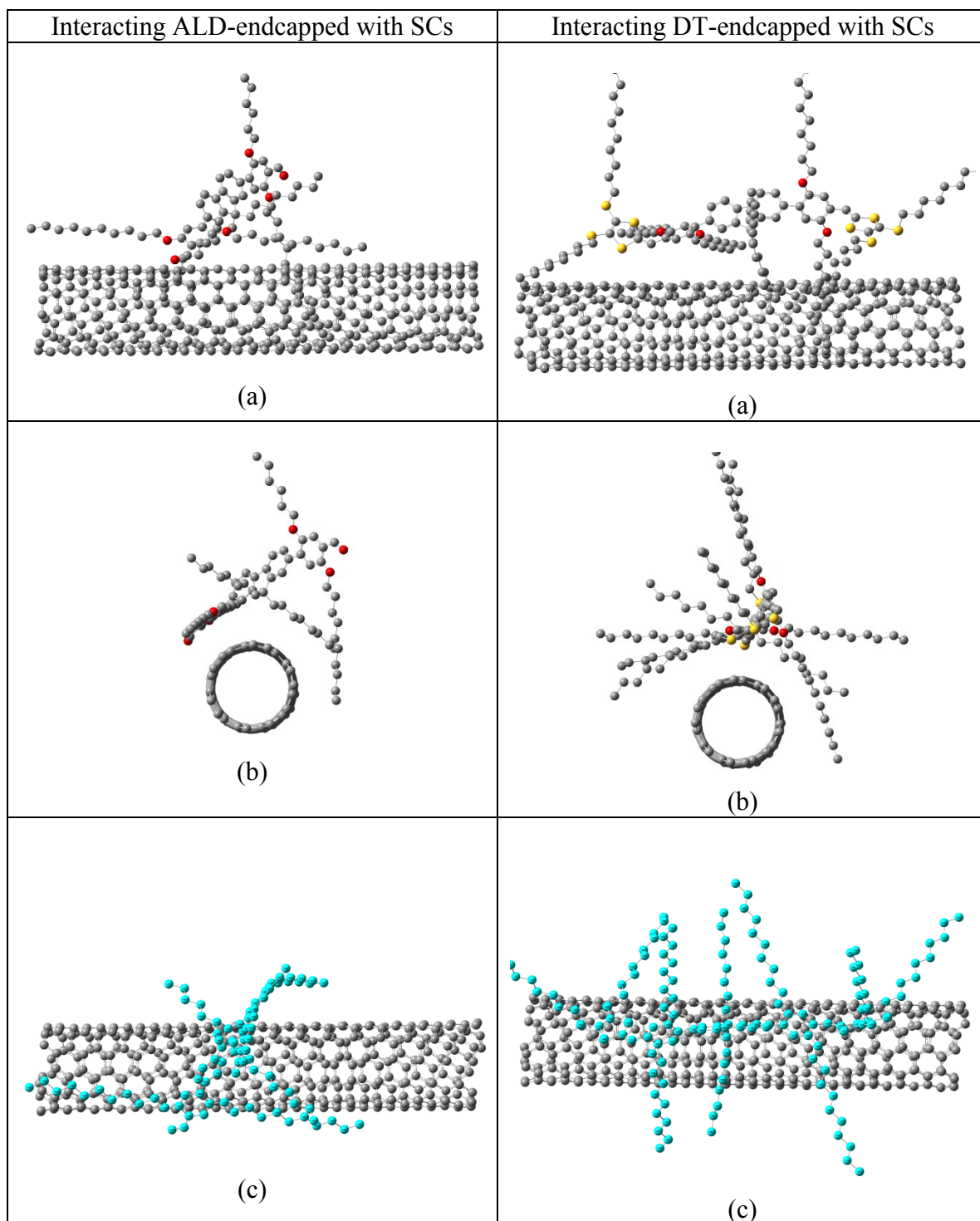


Figure 5.5: Molecular structures of composite fluorene-based ALD- and DTF-endcapped oligomers and SWCNTs with SCs (a) side view (b) top view (c) top view along the backbone obtained using DFT/CAM-B3LYP.



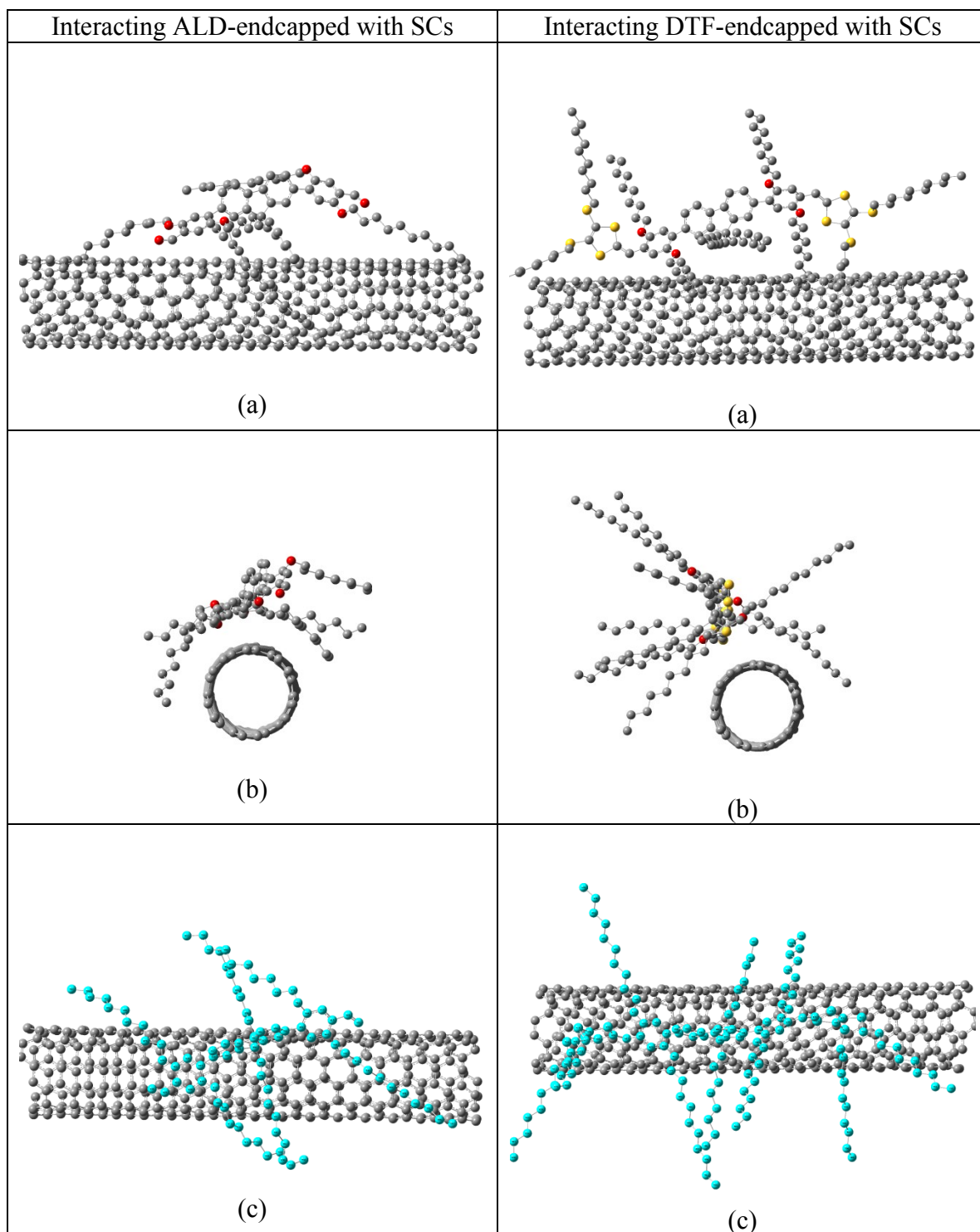


Figure 5.6: Molecular structures of composite fluorene-based ALD- and DTF-endcapped oligomers and SWCNTs with SCs (a) side view (b) top view (c) top view along the backbone obtained using DFT/wB97XD.

## 5.3 End Group Effect on the Oligomer Backbones

In this section, we analyze how the geometry (BLs, and BAs and DAs) of the backbone of the interacting oligomers is affected by different end groups (ALD and DTF).

### 5.3.1 Bond Lengths

Figures 5.7 and 5.8 show the bond length differences between ALD- and DTF-encapped oligomers as a function of bond length position for interacting oligomers without SCs and with SCs respectively for different DFT methods. From Figure 5.7, it can be seen that there is no significant difference for bond lengths between the two end groups except for bonds such as  $C_{1-2}$  and  $C_{17-18}$  that are very close to the end groups. B97D exhibits largest bond lengths differences. In general, oligomers with ALD have  $C_{1-2}$  and  $C_{17-18}$  longer and  $C_{2-3}$  and  $C_{16-17}$  shorter than the respective bond lengths for oligomers with DTF. In the presence of SCs, backbone does not behave same way as without SCs. For systems with SCs (see Figure 5.8) not only the terminal bond lengths are influenced by the end group but also the central bonds are affected. Both B97D and wB97XD give the largest bond length differences.

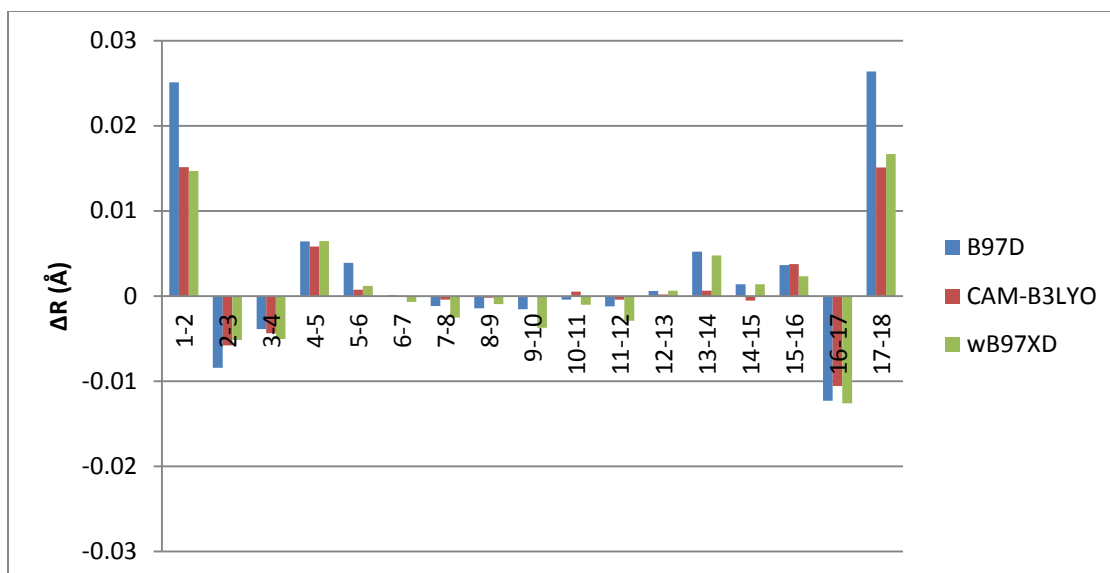


Figure 5.7: Bond length differences between ALD- and DTF-endcapped oligomers as a function of bond length position of interacting oligomers without SCs for different DFT methods.

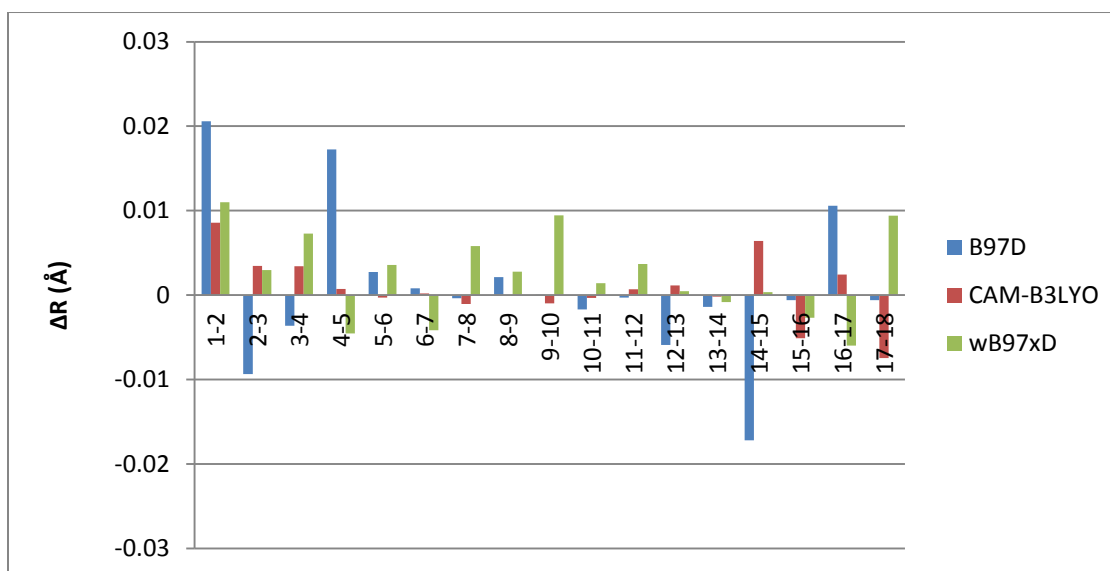


Figure 5.8: Bond length differences between ALD- and DTF-endcapped oligomers as a function of bond length position of interacting oligomers with SCs for different DFT methods.

### 5.3.2 Bond Angles

Figure 5.9 shows the bond angle differences between ALD- and DTF-endcapped oligomers as a function of bond angle position for interacting oligomers without SCs for different DFT methods. Only terminals bond angles are affected by the different end groups for all DFT methods. All bond angle differences are less than  $6^\circ$ . For systems with SCs (Figure 5.10), the end groups change the terminal as well as central (between fluorene and benzene ring) bond angles. Typically B97D bond angles differences are largest (less than  $8^\circ$ ) than those obtained using the other dispersion corrected DFT methods.

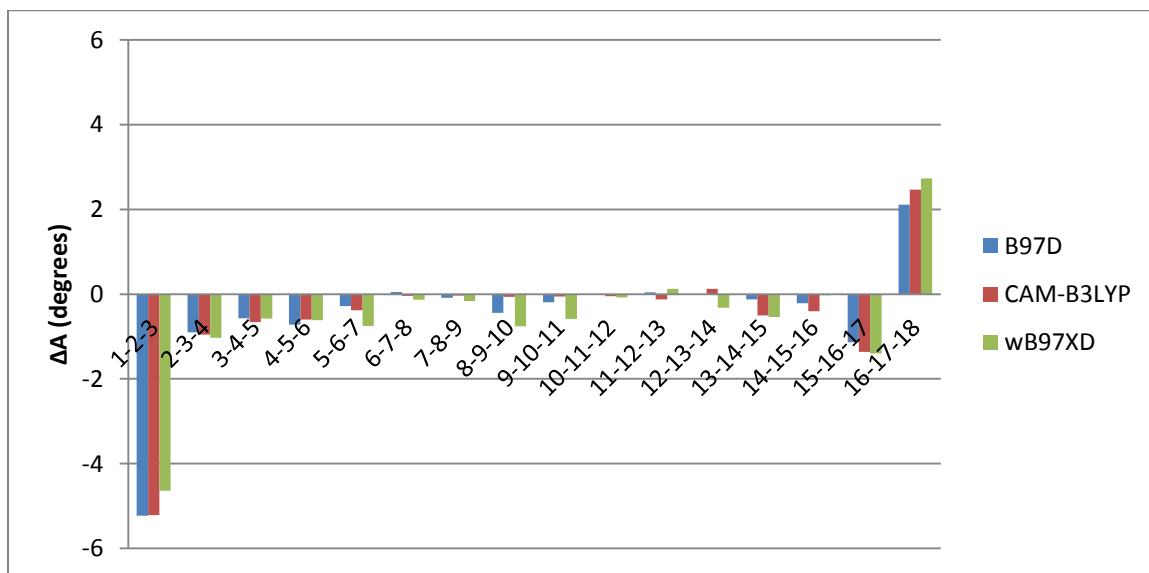


Figure 5.9: Bond angle differences between ALD- and DTF-endcapped oligomers as a function of bond angle position of interacting oligomers without SCs for different DFT methods.

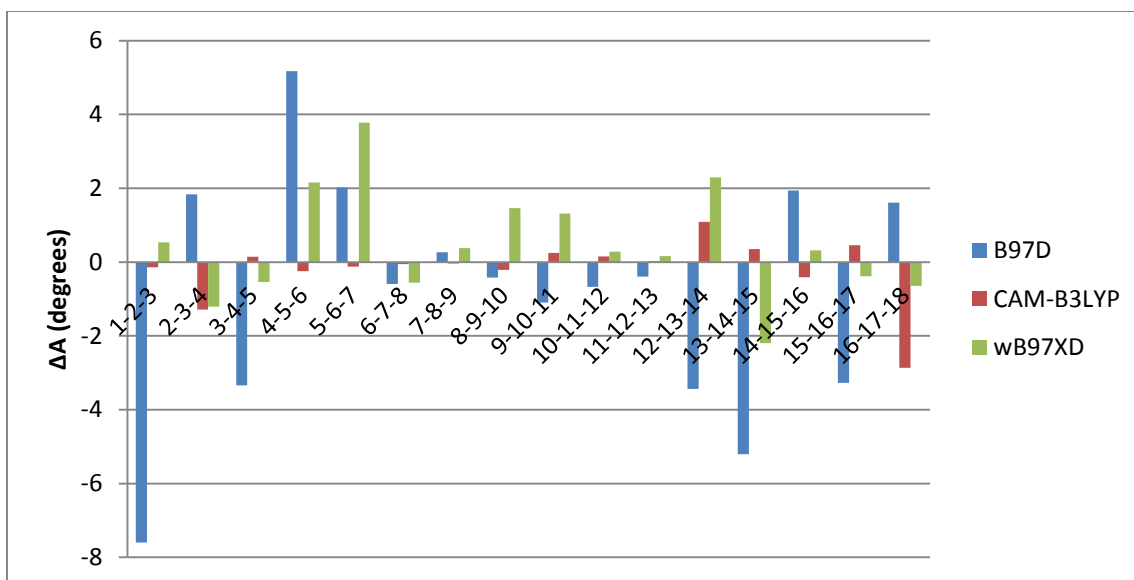


Figure 5.10: Bond angle differences between ALD- and DTF-endcapped oligomers as a function of bond angle position of interacting oligomers with SCs for different DFT methods.

### 5.3.3 Dihedral Angles

Figures 5.11 and 5.12 are the graphs of dihedral angle differences between ALD- and DTF-endcapped oligomers as a function of dihedral angle position of interacting oligomers without SCs and with SCs respectively for different DFT methods. Figure 5.11 shows that for systems without SCs, dihedral angles differences are very small (less than  $10^\circ$ ). The biggest difference has been observed for the central  $D_{4-5-6-7}$  and  $D_{12-13-14-15}$  dihedral angles for B97D and wB97XD. These trends are further enhanced for systems with SCs (Figure 5.12). That is, the dihedral angle differences with SCs are larger than those without SCs. These differences can be as large as  $30^\circ$  (especially for B97D and wB97XD). In general oligomers with ALD tend to be more planar than the ones with DTF for both oligomers with and without SCs.

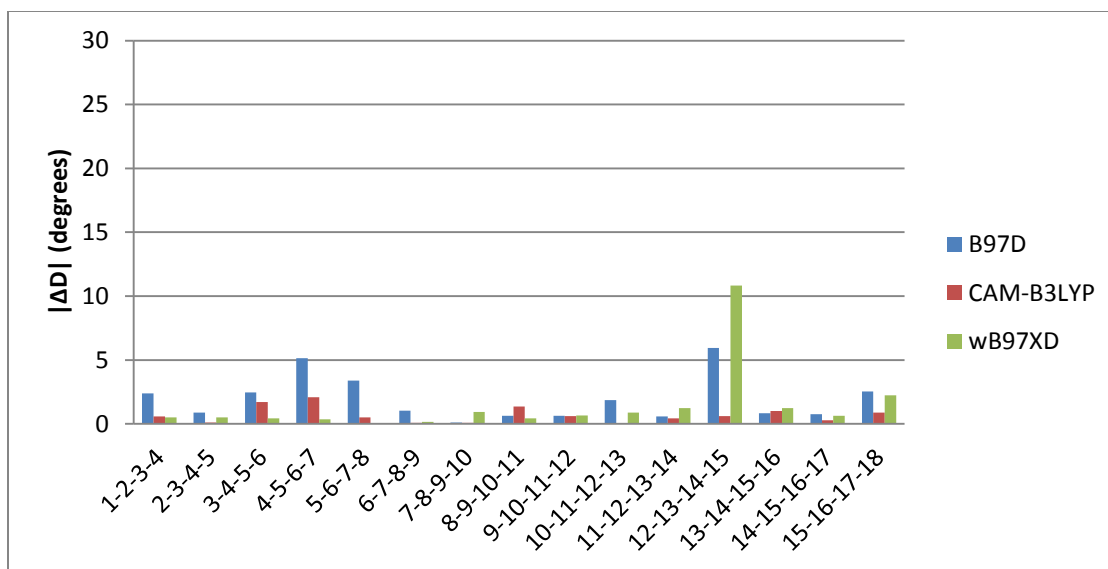


Figure 5.11: Dihedral angle differences between ALD- and DTF-endcapped oligomers as a function of dihedral angles position of interacting oligomers without SCs for different DFT methods.

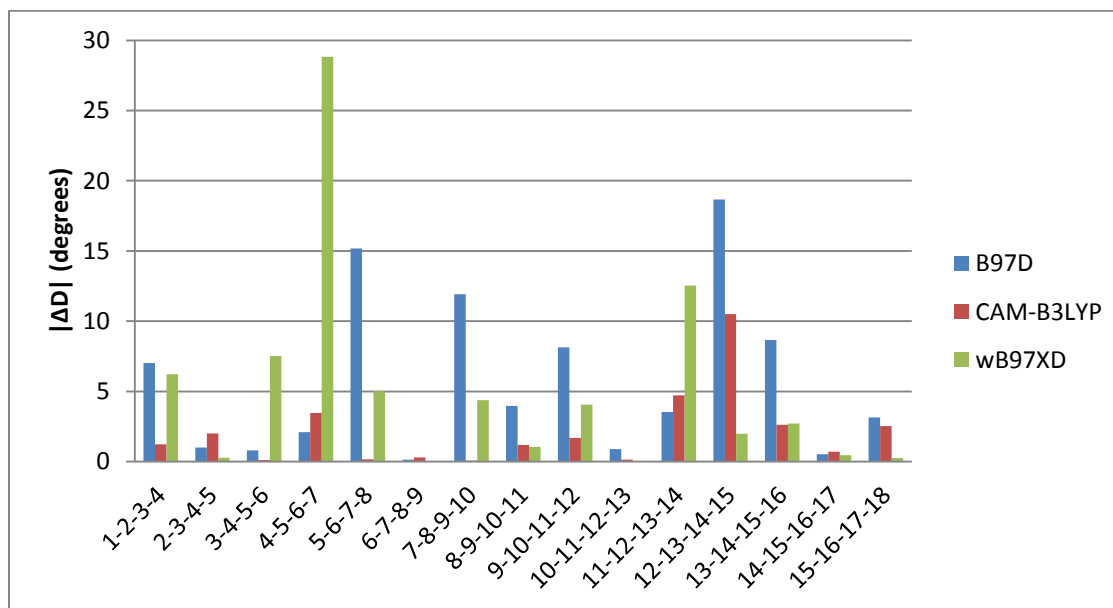


Figure 5.12: Dihedral angle differences between ALD- and DTF-endcapped oligomers as a function of dihedral angles position of interacting oligomers with SCs for different DFT methods.

## 5.4 SCs Effect on the Oligomer Backbones

In this section, we consider the effect of the SCs on the backbone structures of the interacting oligomers for a given oligomer with ALD or DTF end group.

### 5.4.1 Bond Lengths

The effect of SCs on bond lengths is not significant (in general, they are a bit smaller in this (interacting) case than for isolated oligomers). In the case of ALD-endcapped interacting oligomer, the SCs modify the bonds lengths along the backbone by less than 0.02 Å (in most cases bond lengths are decreases) (see Figure 5.13). Similar results were obtained for the DTF-endcapped oligomer (see Figure 5.14). Once again the bond length differences were larger for B97D and wB97XD in comparison to CAM-B3LYP method.

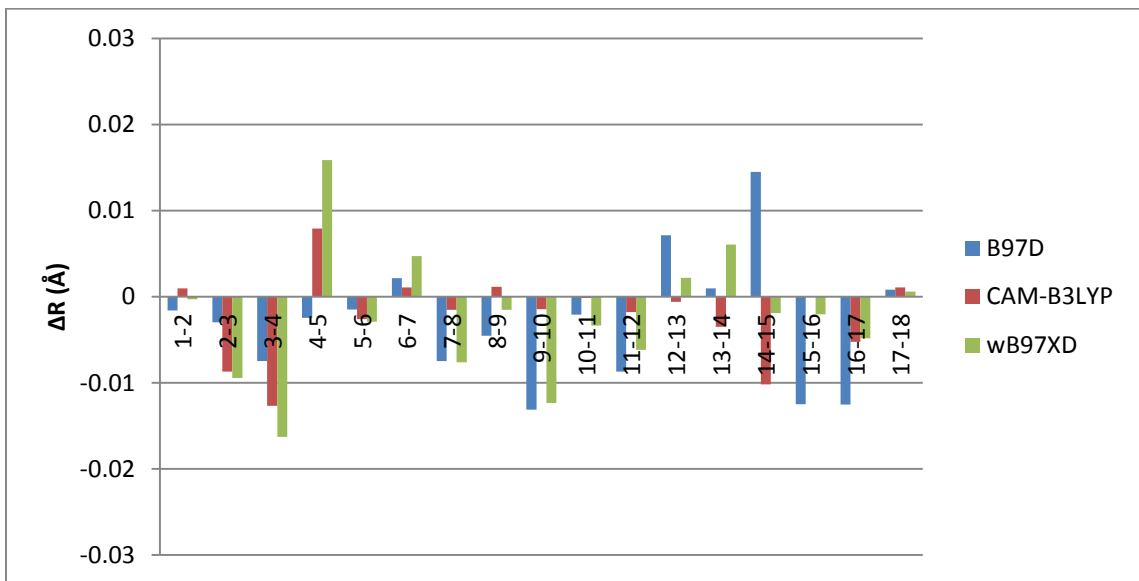


Figure 5.13: Bond length differences between ALD-endcapped oligomer without and with SCs as a function of bond length position of interacting oligomers for different DFT methods.

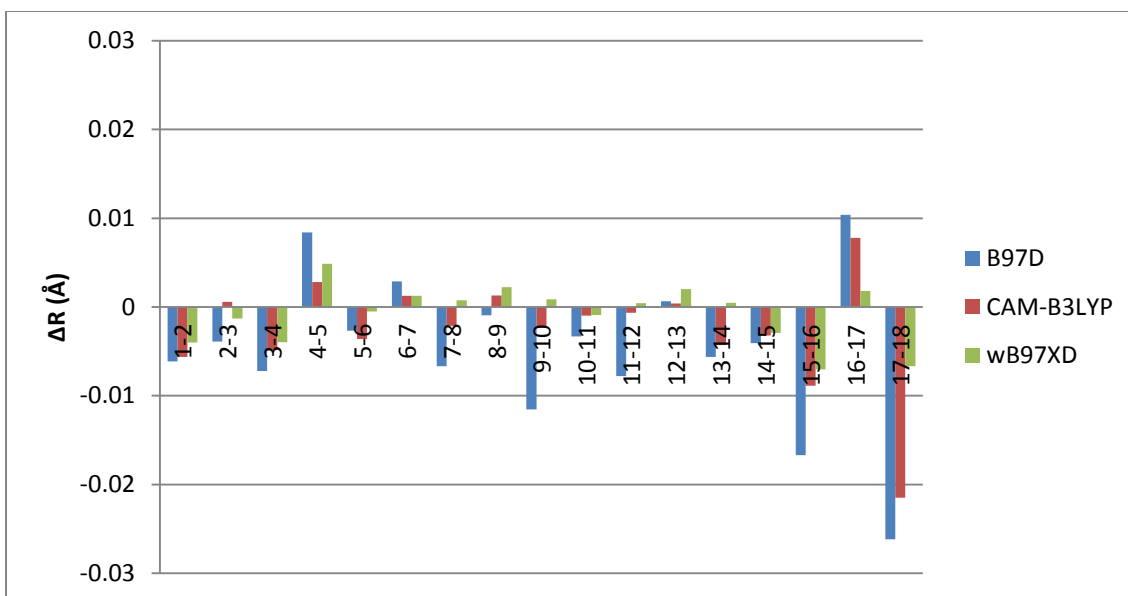


Figure 5.14: Bond length difference between DTF-endcapped oligomer without and with SCs as a function of bond length position of interacting oligomers for different DFT methods.

### 5.4.2 Bond Angles

The presence of SCs changes the bond angles by less than  $5^\circ$  (which are less than the changes due to end group effect) for both oligomers with ALD and DTF end groups. The bond angles that are most affected tend to lie between benzene and end groups and between benzene and fluorene unit. As before B97D and wB97XD, differences are larger than those produced by CAM-B3LYP.



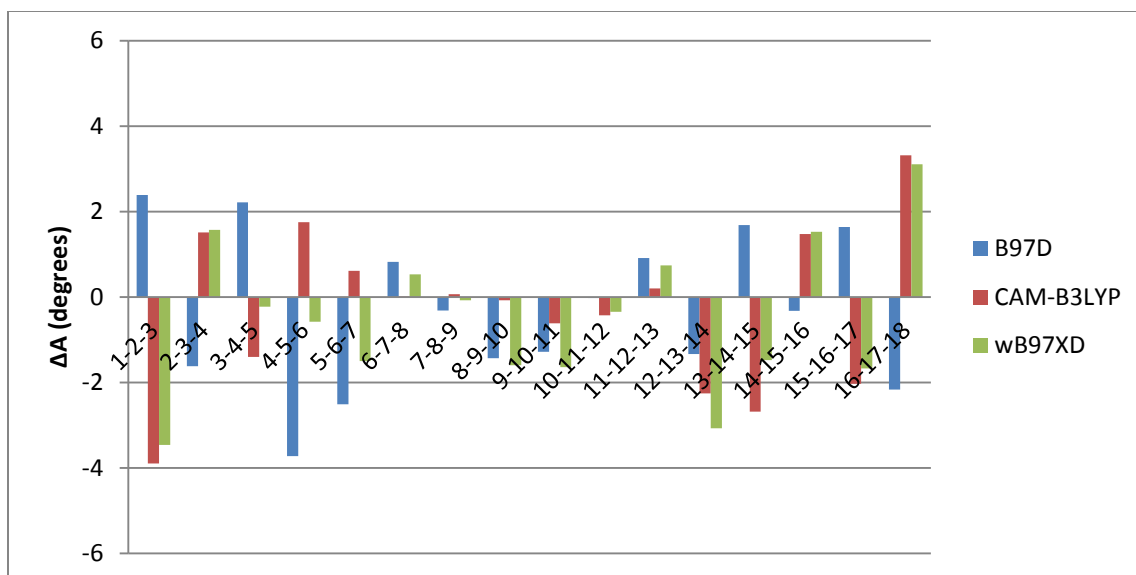


Figure 5.15: Bond angle differences between ALD-endcapped oligomer without and with SCs as a function of bond angle position of interacting oligomers for different DTF methods.

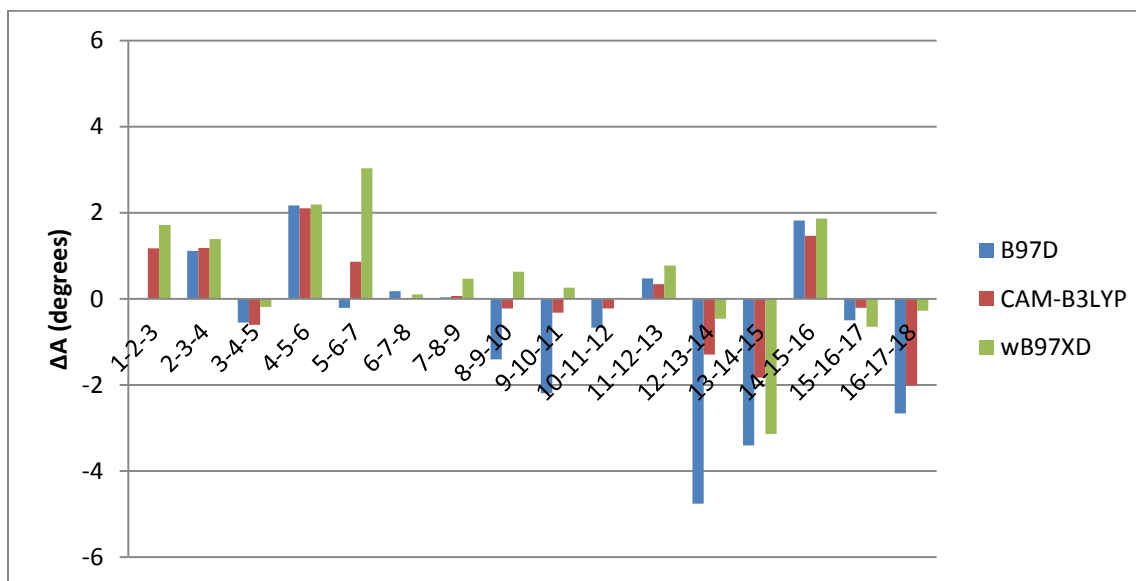


Figure 5.16: Bond angle differences between DTF-endcapped oligomer without and with SCs as a function of bond angle position of interacting oligomers for different DFT methods.

### 5.4.3 Dihedral Angles

As for the isolated oligomers the dihedral angles can be affected significantly by the presence of SCs. The two angles,  $D_{4-5-6-7}$  and  $D_{12-13-14-15}$ , show the biggest differences. These differences are in the range of  $40^\circ$  for B97D and wB97XD methods for oligomers with ALD end group and approximately  $20^\circ$  for oligomers with DTF end group. Both angles lie between benzene ring and fluorene. These results show that in the presence of SCs the backbones of both (ALD and DFT) types of oligomers become more twisted.

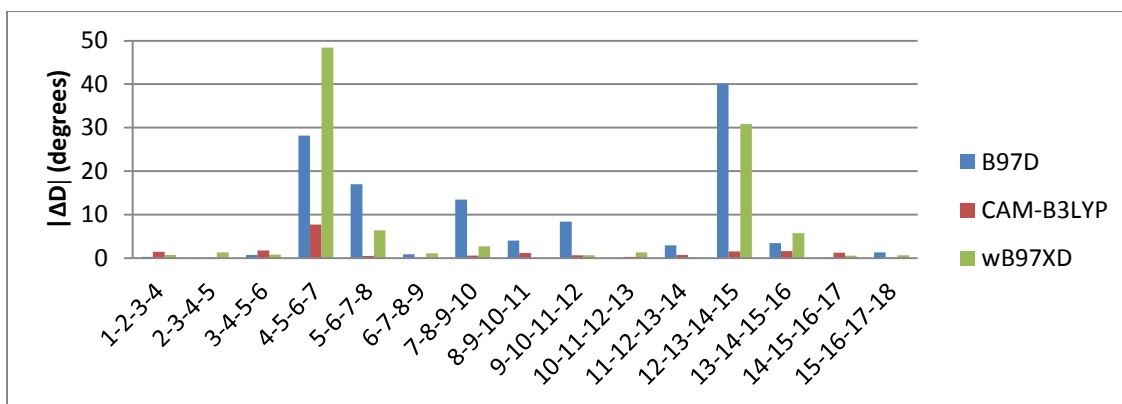


Figure 5.17: Dihedral angle differences between ALD-endcapped oligomers without and with SCs as a function of dihedral angles position of interacting oligomer for different DFT methods.

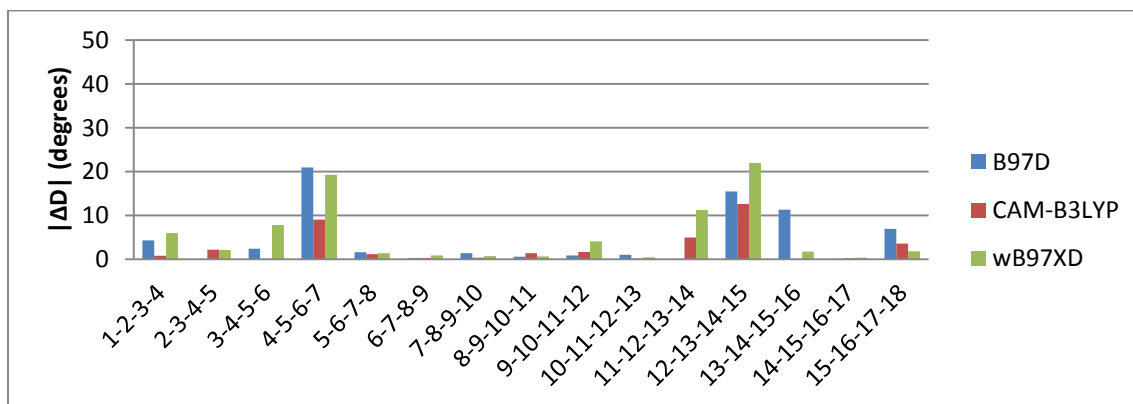
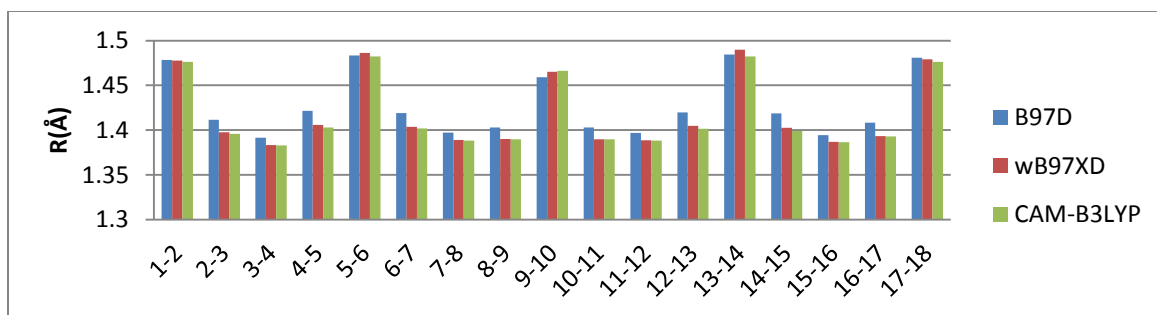


Figure 5.18: Dihedral angle differences between DTF-endcapped oligomers without and with SCs as a function of dihedral angle position of interacting oligomer for different DFT methods.

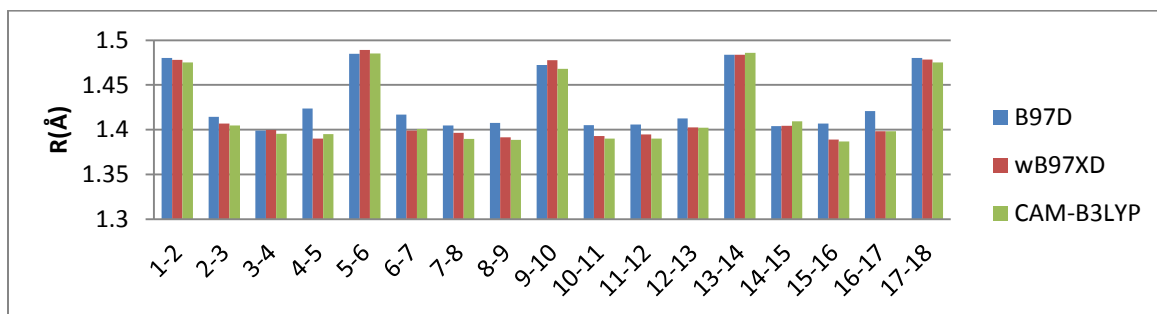
## 5.5 Method Effects

### 5.5.1 Structural Effects

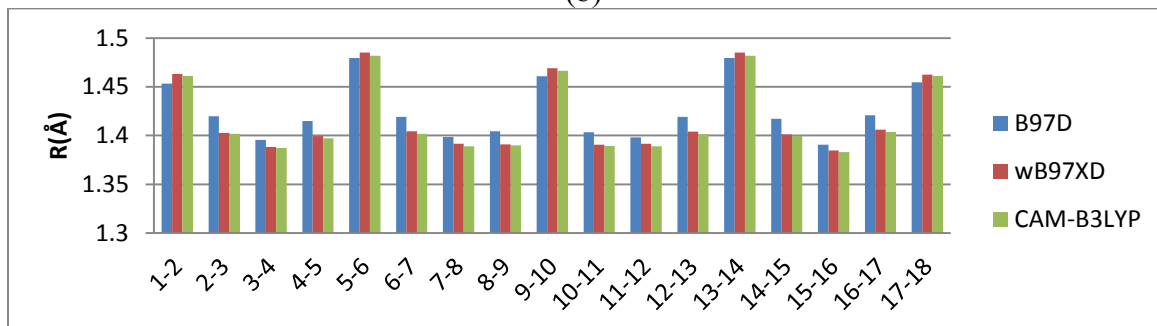
Figures 5.19-5.21 show BLs, BAs and DAs as a function of the position along the oligomers' backbones for different DFT methods. Figure 5.19 (a)-(b) shows that B97D method gives slightly different values than others two methods (wB97XD and CAM-B3LYP). It can be seen from Figure 5.20 for the bond angles along the backbones that for the interacting systems for both end groups, oligomers without SCs have nearly the same values for all methods whereas for oligomers with SCs small differences have been observed (B97D again shows more variability than the other two methods). It is clear that (see Figure 5.19) dihedral angles along the backbones are most affected by the all methods. This is especially true for  $D_{4-5-6-7}$  and  $D_{12-13-14-15}$  which are the angles that lie between benzene and fluorene. The biggest variations in dihedral angles occurs for ALD-endcapped oligomers with SCs (see Figure 5.21(b))



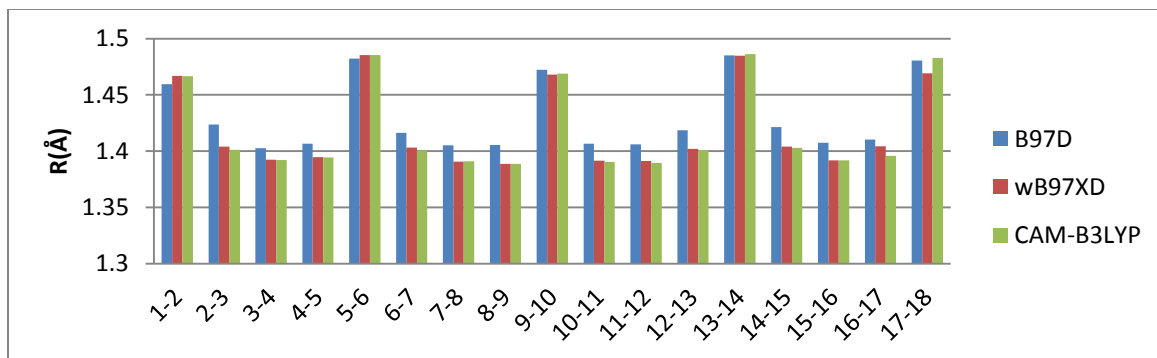
(a)



(b)

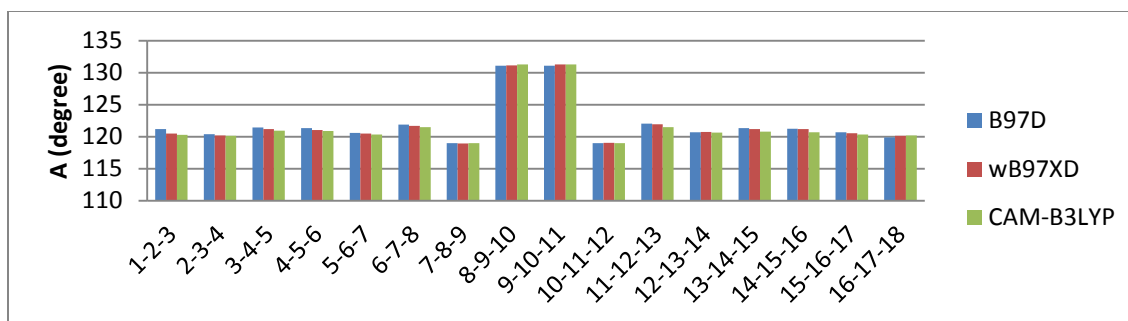


(c)

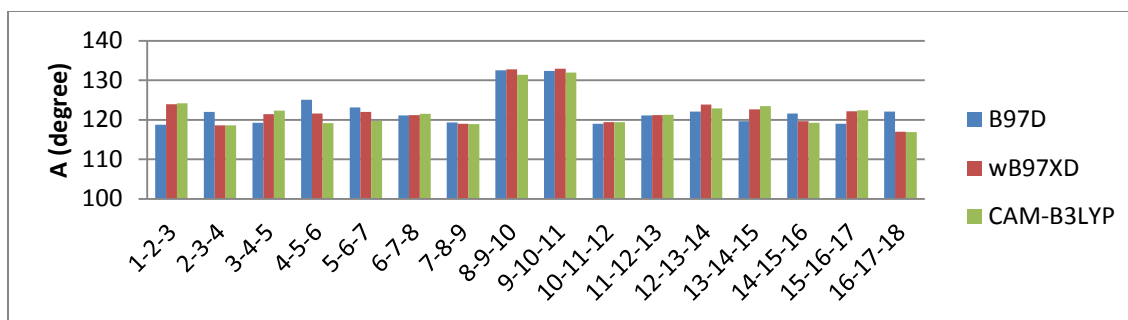


(d)

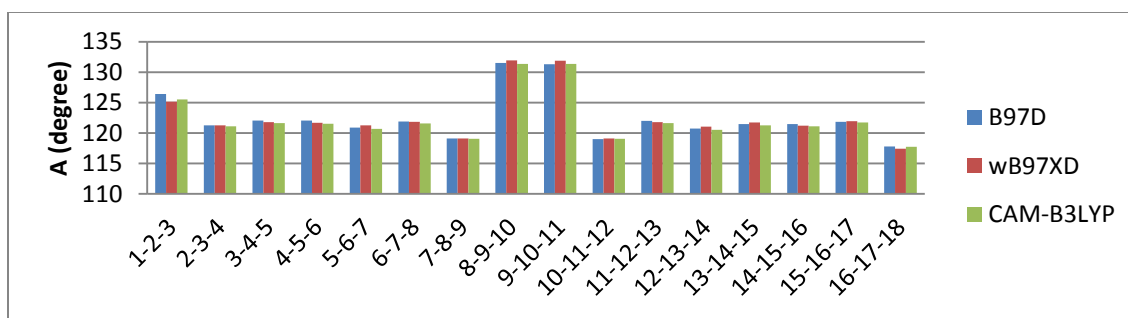
Figure 5.19: Bond lengths for ALD-encapped oligomers (a) without SCs and (b) with SCs. Bond lengths for DTF-encapped oligomers (c) without SCs and (d) with SCs.



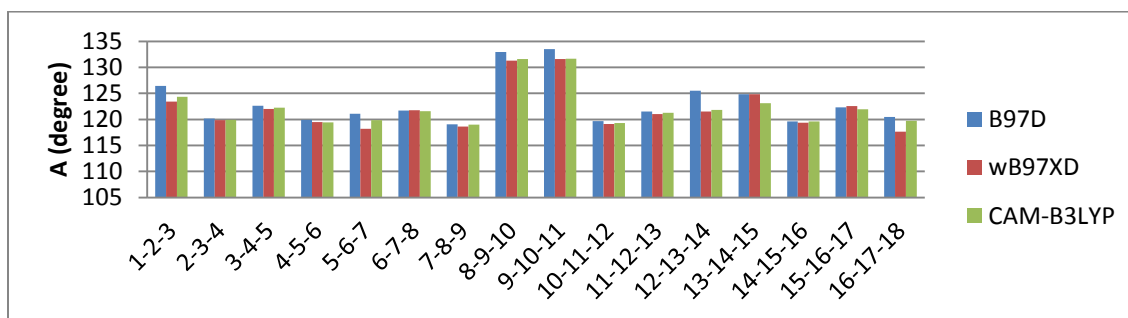
(a)



(b)

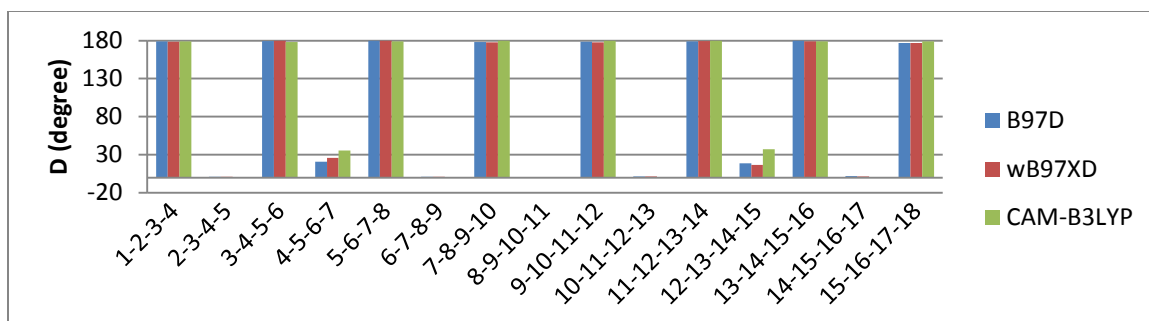


(c)

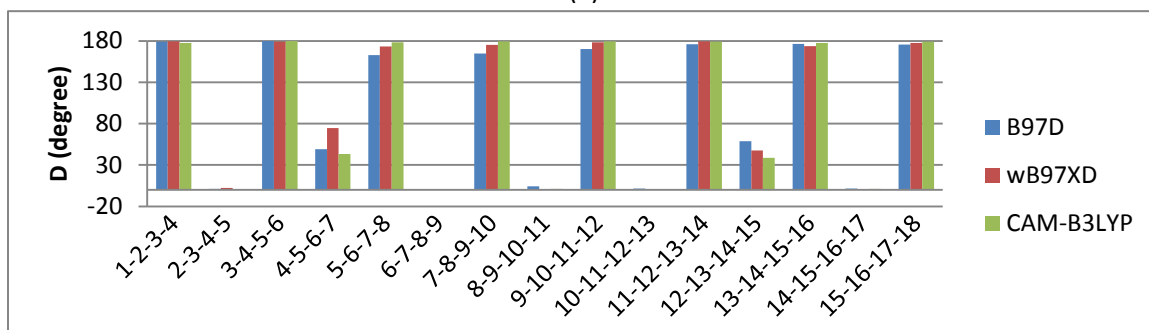


(d)

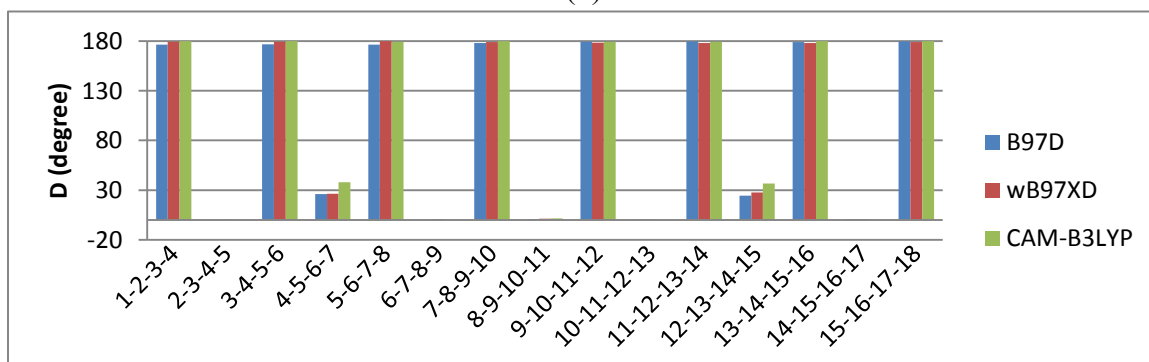
Figure 5.20: Bond angles for ALD-encapped oligomers (a) without SCs and (b) with SCs. Bond angles for DTF-encapped oligomers (c) without SCs and (d) with SCs.



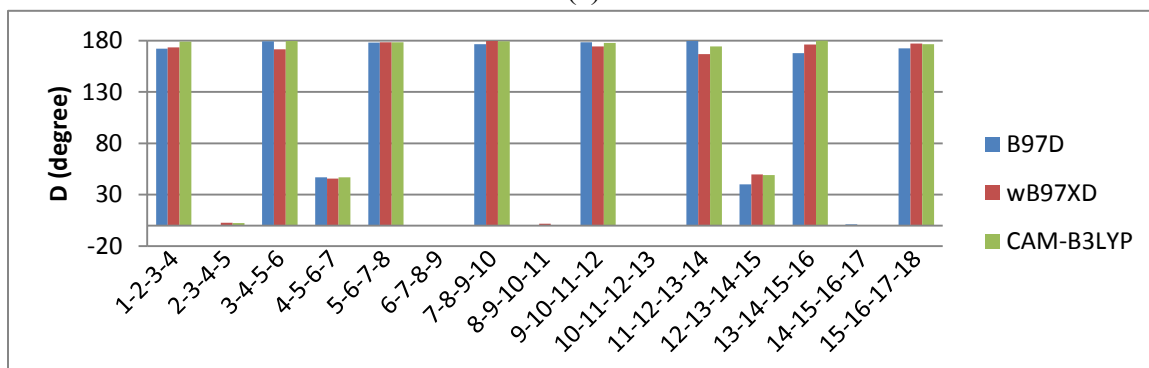
(a)



(b)



(c)



(d)

Figure 5.21: Dihedral angles for ALD-endcapped oligomers (a) without SCs and (b) with SCs. Dihedral angles for DTF-endcapped oligomers (c) without SCs and (d) with SCs.

### 5.5.2 Standard Deviation

Tables 5.1-5.3 show the standard deviations of BLs, BAs, and DAs of different dispersion corrected DFT methods as a function of interacting oligomers with different end groups and SCs. Figures 5.22-5.24 illustrate the standard deviations (as given in Tables 5.1-5.3) for BLs, BAs, and DAs as a function of interacting oligomers with ALD without SCs, ALD with SCs, DTF without SCs and DTF with SCs for different dispersion corrected DFT methods respectively. For bond lengths, Figure 5.22 and Table 5.1 show that maximum deviation is 0.041Å (which is quite small). As observed in subsection 5.5.1 for all composite systems, wB97XD and CAM-B3LYP give nearly the same values for the respective bond lengths. B97D gives smaller standard deviation which indicates that bond lengths obtained using this method have less variability. Figure 5.23 and Table 5.2 show that the maximum BA deviation is less than 5° for all methods and all systems. Only in one case, for oligomers with DTF with SCs the bond angle standard deviation is somewhat different for B97D than for other methods. In the case of dihedral angle (see Figure-5.24 and Table 5.3), interacting oligomers without SCs give almost the same standard deviations whose values are approximately 88°. For system with SCs, different methods give somewhat different values for standard deviations. This is especially true for interacting oligomers with ALD end groups and with SCs which is consistent with what was found in subsection 5.5.1.

Table 5.1: Standard deviations of bond length (in Angstroms) for different dispersion corrected DFT methods as a function of interacting oligomers with different end groups and SCs.

| Bond lengths          |       |        |           |
|-----------------------|-------|--------|-----------|
|                       | B97D  | wB97XD | CAM-B3LYP |
| ALD without SCs & CNT | 0.035 | 0.041  | 0.040     |
| ALD with SCs & CNT    | 0.034 | 0.040  | 0.039     |
| DTF without SCs & CNT | 0.029 | 0.037  | 0.037     |
| DTF with SCs & CNT    | 0.032 | 0.037  | 0.040     |

Table 5.2: Standard deviations of bond angles(in degrees) for different dispersion corrected DFT methods as a function of interacting oligomers with different end groups and SCs.

| Bond angles           |       |        |           |
|-----------------------|-------|--------|-----------|
|                       | B97D  | wB97XD | CAM-B3LYP |
| ALD without SCs & CNT | 3.632 | 3.704  | 3.768     |
| ALD with SCs & CNT    | 4.293 | 4.456  | 4.238     |
| DTF without SCs & CNT | 3.922 | 4.016  | 3.903     |
| DTF with SCs & CNT    | 4.464 | 4.170  | 3.956     |

Table 5.3: Standard deviations of dihedral angles (in degrees) for different dispersion corrected DFT methods as a function of interacting oligomers with different end groups and SCs.

| Dihedral Angle        |      |        |           |
|-----------------------|------|--------|-----------|
|                       | B97D | wB97XD | CAM-B3LYP |
| ALD without SCs & CNT | 89   | 89     | 88        |
| ALD with SCs & CNT    | 83   | 84     | 87        |
| DTF without SCs & CNT | 88   | 88     | 88        |
| DTF with SCs & CNT    | 85   | 84     | 86        |



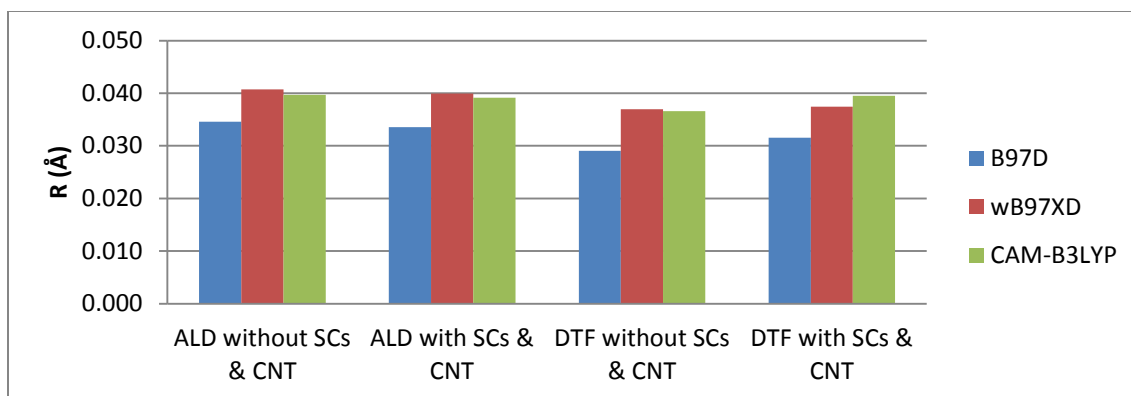


Figure 5.22: Standard deviations for bond lengths as a function of different interacting oligomer systems for different methods.

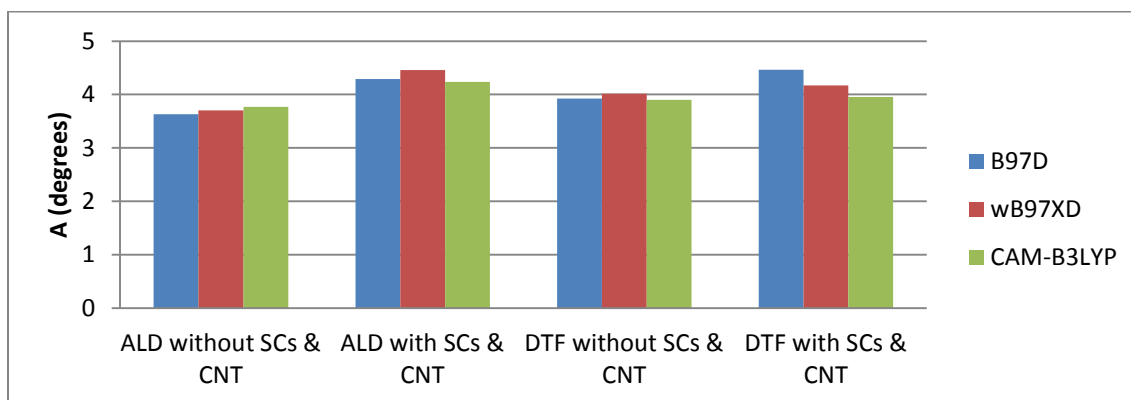


Figure 5.23: Standard deviations for bond angles as a function of different interacting oligomers system for different methods.

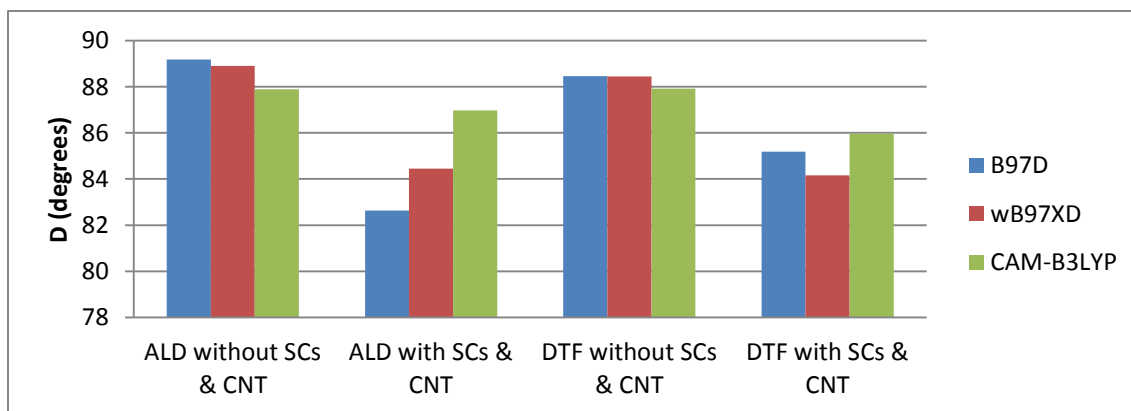


Figure 5.24: Standard deviations for dihedral angles as a function of different interacting oligomers system for different methods.

## 5.6 Binding Energy

In our research, it has been seen that the total energy of isolated oligomer and CNT is not equal to the total energy for the composite system (oligomer and CNT). This energy difference is called the binding energy. Table 5.4 gives the binding energies of different composite systems as a function of different DFT methods. Binding energy is defined (see chapter 2) as

$$BE = (E_O + E_{CNT}) - E_{O+CNT} \quad 5.1$$

where  $E_O$ ,  $E_{CNT}$  and  $E_{O+CNT}$  are the energies of isolated oligomer, isolated CNT and composite oligomer-CNT system respectively.

Table 5.4 Binding energy (eV) of different composite systems as a function of different DFT methods.

|           | ALD without<br>SCs and CNT | DTF without<br>SCs and CNT | ALD with SCs<br>and CNT | DTF with SCs<br>and CNT |
|-----------|----------------------------|----------------------------|-------------------------|-------------------------|
| B97D      | 1.753                      | 2.484                      | 3.899                   | 7.057                   |
| wB97XD    | 1.629                      | 2.402                      | 3.286                   | 2.260                   |
| CAM-B3LYP | 0.177                      | 0.231                      | 0.412                   | 0.110                   |

Figures 5.25 and 5.26 show the end group effect for binding energy of composite systems (with ALD and DTF end groups) without and with SCs as a function of different dispersion corrected DFT methods. It can be seen that systems with ALD end group and without SCs have lower binding energy than those with SCs. This is also true for systems with DTF end group for B97D but not for CAM-B3LYP and wB97XD. For systems without SCs oligomers with DTF end group have higher binding energy than those with ALD end group for all methods. For composite systems with SCs, ALD-encapped

oligomers have higher binding energy for wB97XD and CAM-B3LYP but not for B97D relative to DTF-endcapped oligomers.

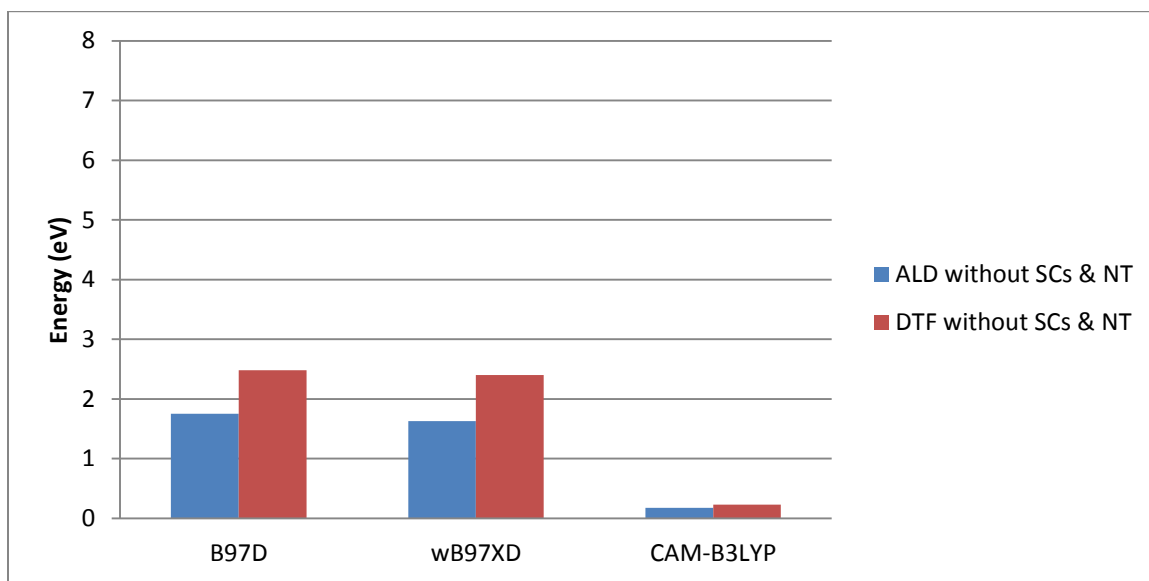


Figure 5.25: End group effect for binding energy of composite systems with (ALD and DTF end group) without SCs as a function of different dispersion corrected DFT methods.

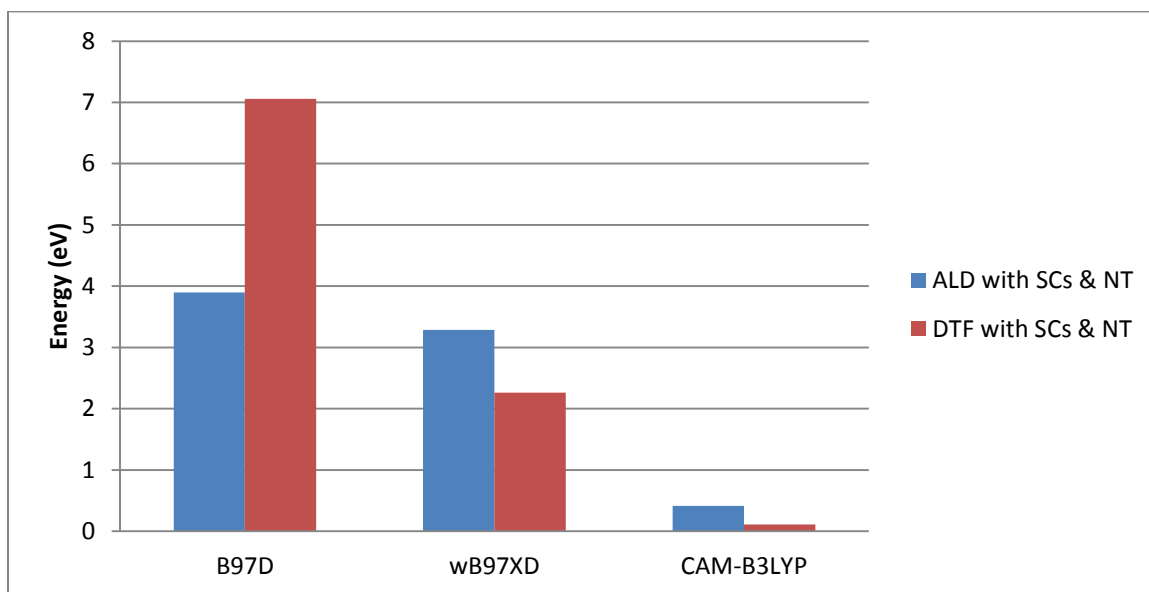


Figure 5.26: End group effect for binding energy of composite systems with (ALD & DTF end group) with SCs as a function of different dispersion corrected DFT methods.

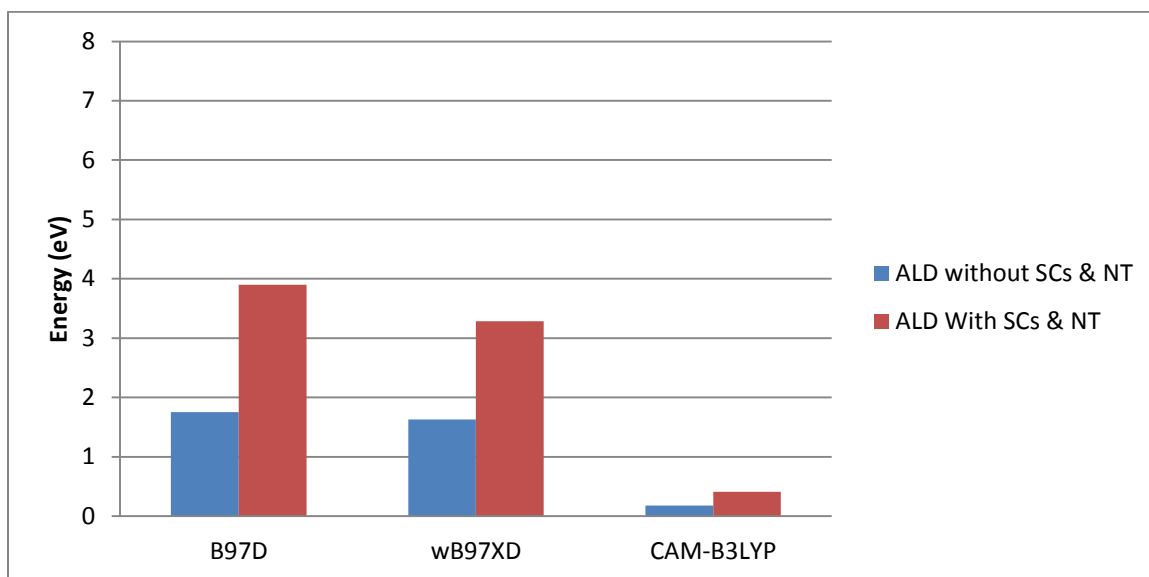


Figure 5.27: SCs effect for binding energy of composite systems with ALD end group without and with SCs as a function of different dispersion corrected DFT methods.

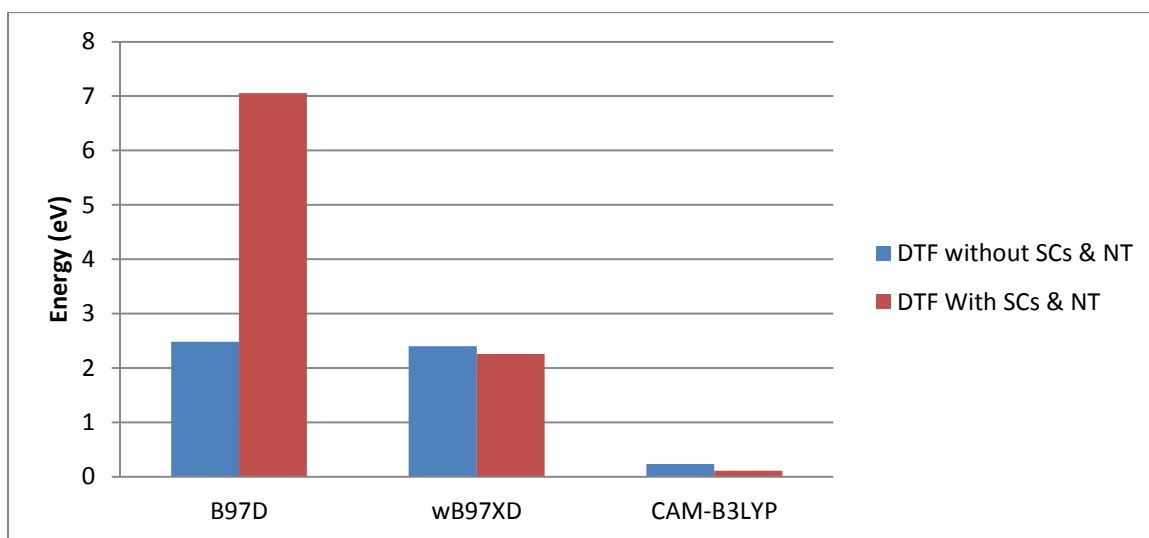


Figure 5.28: SCs effect for binding energy of composite systems with DTF end group without and with SCs as a function of different dispersion corrected DFT methods.

## 5.7 Intermolecular Distance between Oligomer and CNT

Tables 5.5 and 5.6 give the intermolecular distance and the angle of the oligomer relative to the CNT for different composite systems as a function of different dispersion corrected DFT methods. For determining the distance and angle, we consider only fluorene part of the oligomer and its plane and nanotube center and its plane (as shown in Figure 5.29). An angle of  $90^\circ$  and  $0^\circ$  would mean that oligomer lies parallel to the CNT and perpendicular to the CNT respectively. For oligomers, for both end groups and without SCs, CAM-B3LYP method gives the largest intermolecular distance. For oligomer with SCs, for ALD end group CAM-B3LYP gives the largest distance but for DTF, both CAM-B3LYP and wB97XD give comparable values. For oligomers for both end groups and without SCs, wB97XD and B97D methods give oligomer that is nearly parallel to CNT. For oligomers with SCs, for both end groups all three method give oligomer that is nearly perpendicular to plane CNT.

Table 5.5 Distance of the oligomer relative to CNT for different composite systems as a function of different dispersion corrected DFT methods.

| Intermolecular distance (Å)<br>between oligomer to CNT<br>surface | DFT Method | ALD<br>without<br>SCs | DTF<br>without<br>SCs | ALD<br>with SCs | DTF<br>with SCs |
|---|------------|-----------------------|-----------------------|-----------------|-----------------|
|   | B97d       | 3.149                 | 3.068                 | 5.800           | 5.384           |
|   | CAM-B3LYP  | 3.611                 | 4.153                 | 6.240           | 6.666           |
|   | wB97XD     | 3.183                 | 3.122                 | 5.732           | 6.680           |

Table 5.6 Angle of the oligomer relative to CNT for different composite systems as a function of different dispersion corrected DFT methods.

| Angle (degree) between<br>Oligomer to CNT surface<br>plane | DFT Method    | ALD<br>without<br>SCs | DTF<br>without<br>SCs | ALD<br>with SCs | DTF<br>with<br>SCs |
|--|---------------|-----------------------|-----------------------|-----------------|--------------------|
|  | B97d          | 84.44                 | 84.25                 | 28.460          | 24.87              |
|  | CAM-<br>B3LYP | 87.41                 | 47.88                 | 40.714          | 28.24              |
|  | wB97XD        | 87.50                 | 77.28                 | 23.284          | 32.92              |

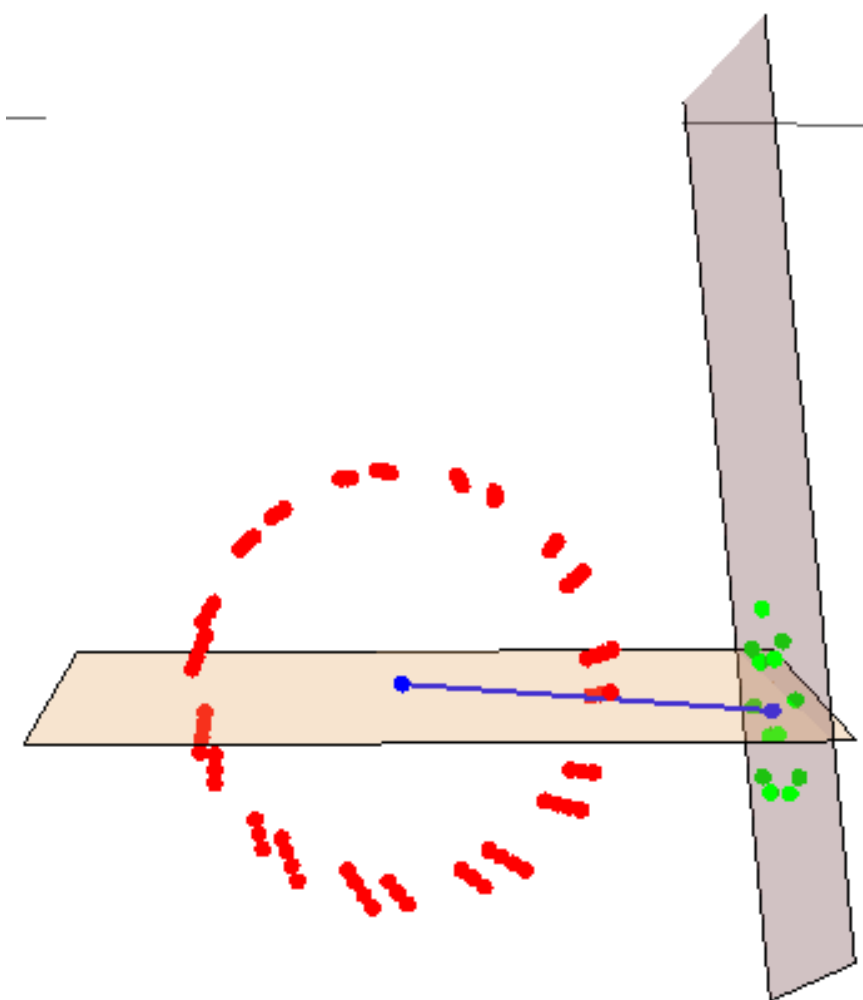


Fig 5.29 Distance of oligomer and CNT.

## 5.8 Dipole Moment

Table 5.7 gives the dipole moments (in Debyes) with components (along the  $x$ ,  $y$ ,  $z$  axis) for different conjugated oligomers as a function of different dispersion corrected DFT methods. The dipole moment orientations are shown in Figures 5.30 and 5.31 where first figure shows the dipole moment (total dipole moment as indicated by the blue arrow) for ALD- and DTF-endcapped oligomers without SCs and CNT and the second figure shows the total dipole moments for ALD- and DTF-endcapped oligomers with SCs and CNT. For the isolated single walled carbon nanotube, dipole moment direction is along the  $z$ -axis (from center to the carbon wall), and other components are zero, which is as expected (see Table 5.7). In the case of composite systems, dipole moment is not directed along the  $z$ -axis (its resultant direction pointing towards positive charge). For the composite systems without SCs, the part of the oligomer facing the nanotube becomes positively polarized for B97D and wB97XD but has a net negative polarity for CAM-B3LYP relative CNT. In the presence of SCs, the direction of the dipole moment becomes more complicated (see Figure 5.31). For oligomers with ALD end groups with SCs, the magnitude dipole is largest with B97D and smallest with wB97XD and all dipoles point away from the oligomer indicating that the oligomers has a net negative charge. For oligomer with DTF end group with SCs, B97D gives the smallest amplitude for the dipole moment and wB97XD the largest. The oligomer has a net positive charge.

Table 5.7: Dipole moments (in Debyes) with components (along  $x$ ,  $y$ ,  $z$  axis) of different conjugated oligomer as a function of different dispersion corrected DFT methods.

|           | Carbon Nanotube   | ALD without SCs & NT | DTF without SCs & NT | ALD with SCs & NT  | DTF with SCs & NT  |
|-----------|-------------------|----------------------|----------------------|--------------------|--------------------|
| B97D      | X=0.0000          | X=0.3507             | X=-0.1495            | X=-1.8447          | X=0.2626           |
|           | Y=0.0000          | Y=1.0420             | Y=1.7359             | Y=-3.6788          | Y=-3.6713          |
|           | Z=0.1412          | Z=0.7727             | Z=-0.5771            | Z=-0.8739          | Z= 1.0988          |
|           | <b>Tot=0.1412</b> | <b>Tot=1.3438</b>    | <b>Tot=1.8354</b>    | <b>Tot= 4.2071</b> | <b>Tot=3.8412</b>  |
| CAM-B3LYP | X=0.0000          | X= -0.1755           | X=-0.2466            | X=0.8434           | X=0.5855           |
|           | Y=0.0000          | Y=-1.8256            | Y=1.2304             | Y= -0.6415         | Y=-1.0420          |
|           | Z=0.1109          | Z=-0.5925            | Z=1.5040             | Z=1.8964           | Z=-4.0246          |
|           | <b>Tot=0.1109</b> | <b>Tot=1.9274</b>    | <b>Tot= 1.9588</b>   | <b>Tot=2.1723</b>  | <b>Tot= 4.1983</b> |
| wB97XD    | X=0.0000          | X= -0.2004           | X=0.1339             | X=0.1111           | X=0.2040           |
|           | Y=0.0000          | Y=0.8290             | Y=1.1361             | Y=-0.0743          | Y=4.1356           |
|           | Z=0.1170          | Z= 0.7486            | Z= 0.4103            | Z=-0.9142          | Z=-4.5245          |
|           | <b>Tot=0.1170</b> | <b>Tot=1.1348</b>    | <b>Tot=1.2154</b>    | <b>Tot=0.9239</b>  | <b>Tot=6.1332</b>  |

The results of this Table 5.7 are shown in Figures 5.30 and 5.31.



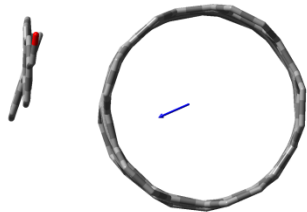
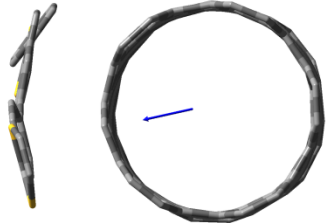
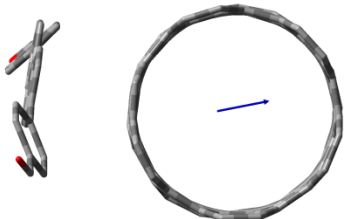
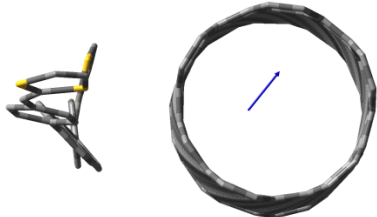
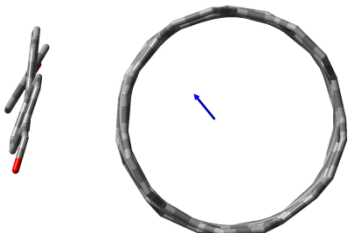
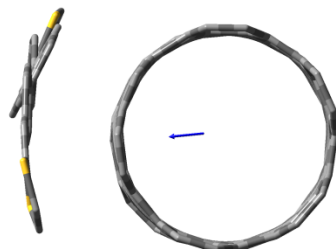
| ALD-endcapped Oligomer   | DTF-endcapped Oligomer  |
|--|---|
|  <p>ALD without SCs &amp; NT B97D</p>       |  <p>DTF without SCs &amp; NT B97D</p>       |
|  <p>ALD without SCs &amp; NT CAM-B3LYP</p> |  <p>DTF without SCs &amp; NT CAM-B3LYP</p> |
|  <p>ALD without SCs s&amp; NT wB97Xd</p>  |  <p>DTF without SCs &amp; NT wB97Xd</p>   |

Figure 5.30: Dipole moments (direction indicated by the blue arrow) for ALD- and DTF -endcapped interacting oligomers without SCs for different dispersion corrected DFT methods. For clarity hydrogens are not shown.

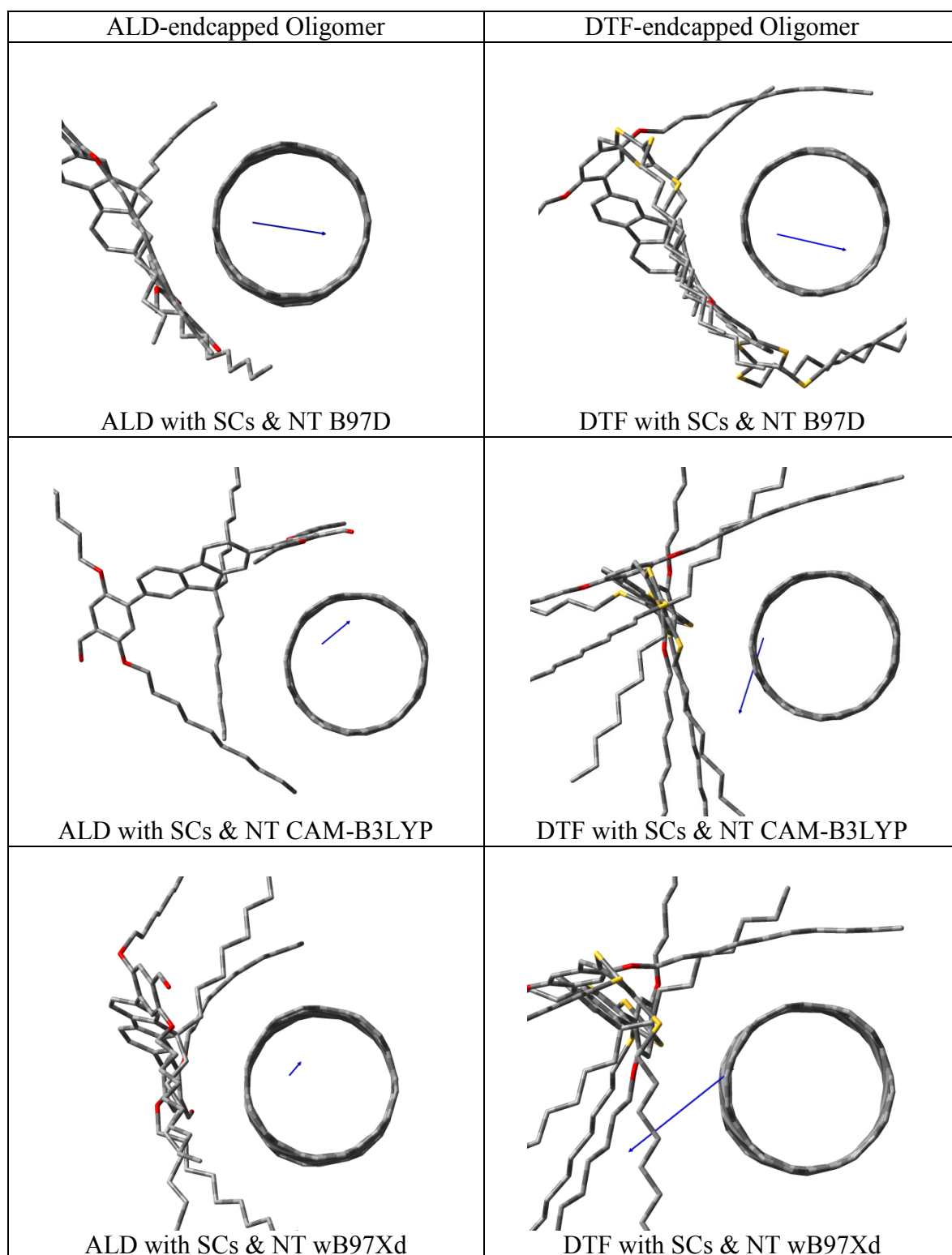


Figure 5.31: Dipole moment (direction indicated by the blue arrow) for ALD- and DTF -endcapped interacting oligomers with SCs for different dispersion corrected DFT methods. For clarity hydrogens are not shown.

### 5.8.1 End Group Effect

Figures 5.32 and 5.33 show the end group effects on dipole moment as a function of different methods for interacting oligomers with ALD and DTF end groups without and with SCs respectively. Without SCs, there is no significant dipole moment difference between ALD- and DTF-endcapped interacting oligomers (but DTF-endcapped without SCs has a dipole that is a bit larger than ALD-endcapped composite system). According to Figure 5.30, CAM-B3LYP method gives different polarity for the dipole moment than other two methods.

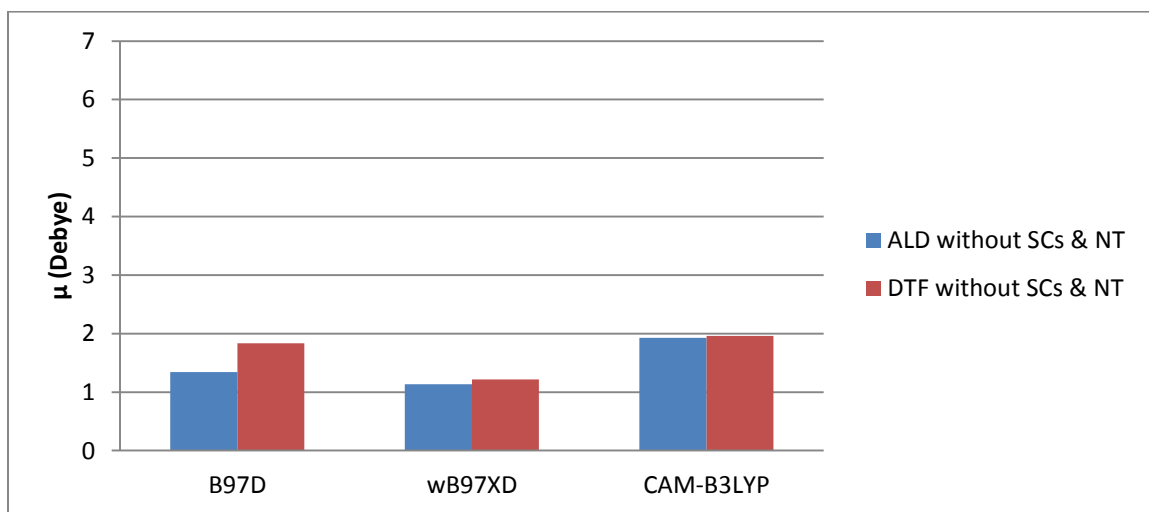


Figure 5.32 Dipole moment as a function of different methods for oligomers with ALD and DTF end group without SCs.

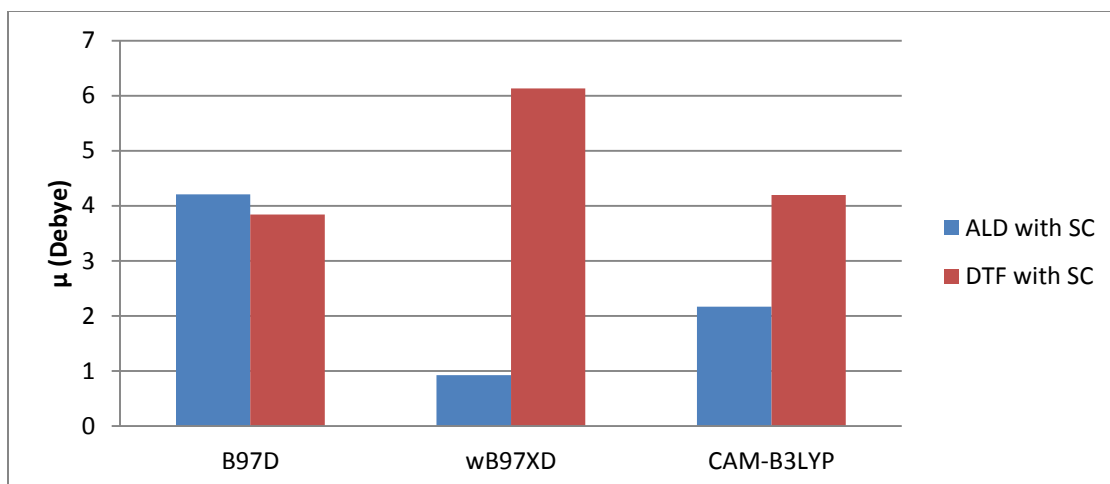


Figure 5.33 Dipole moment as a function of different methods for oligomers with ALD and DTF end group with SCs.

### 5.8.2 Side Chains Effect

The SCs orientations affect the dipole moment magnitude and direction. Figure 5.34 shows that ALD with SCs gives larger dipole moment than ALD without SCs except wB97XD method. For DTF with SCs the dipole moment is always larger than DTF without SCs (see Figure 5.35)

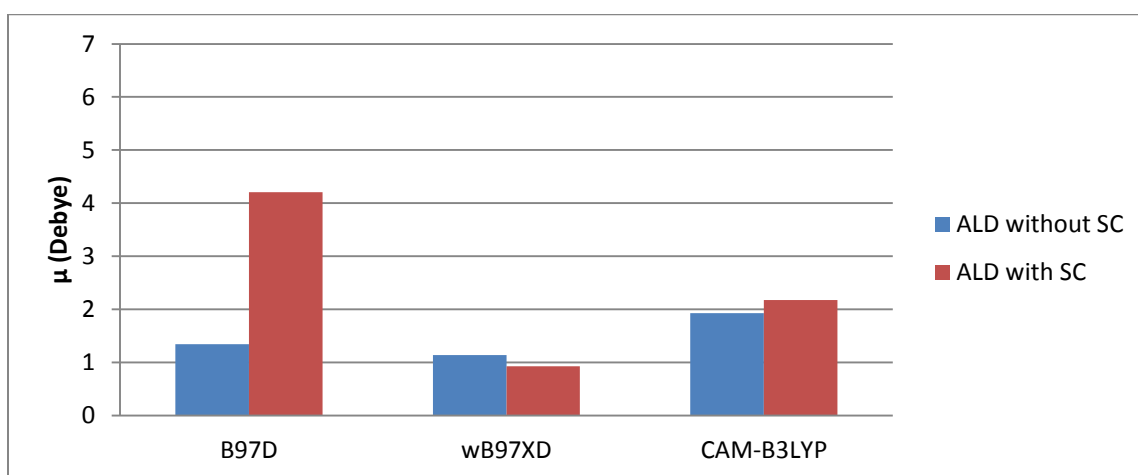


Figure 5.34 Dipole moment as a function of different methods for oligomers with ALD end group without and with SCs.

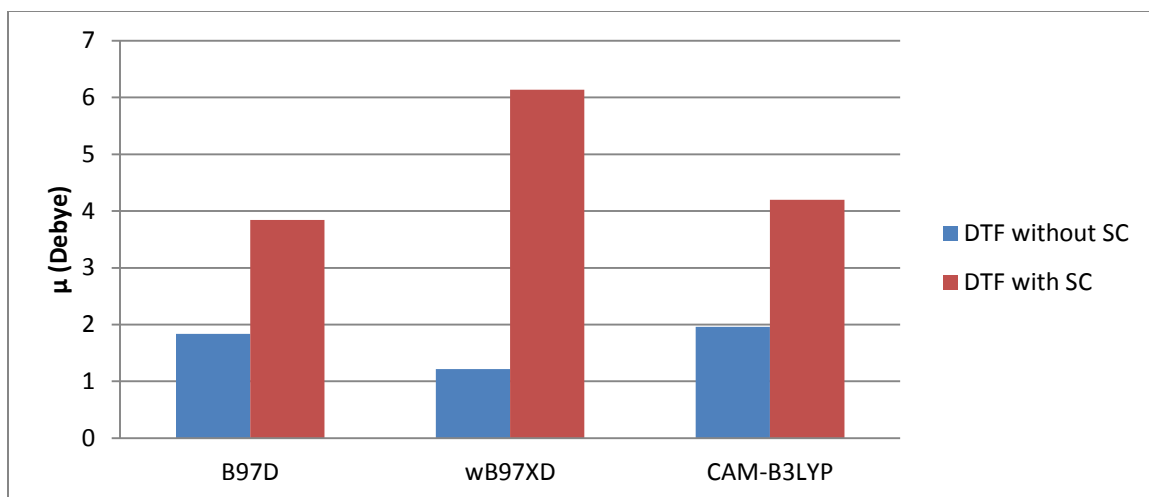


Figure 5.35 Dipole moment as a function of different methods for oligomers with DTF end group without and with SCs.

## 5.9 HOMO, LUMO Eigenvalues and HOMO-LUMO Gaps

In this section we discuss the electronic band structure of the composite systems that consist of the conjugated polymer and CNT with and without SCs. Table 5.8 gives the HOMO, LUMO eigenvalues and HOMO-LUMO gaps of different molecular systems for different dispersion corrected DFT methods. Figures 5.36 to 5.38 show the HOMO, LUMO eigenvalues and HOMO-LUMO gaps as a function of different oligomer system (1. ALD without SCs, 2. DTF without SCs, 3. ALD with SCs, and 4. DTF with SCs) for B97D, WB97XD, CAM-B3LYP methods respectively. These three graphs illustrate clearly that the variations of HOMO, LUMO eigenvalues and HOMO-LUMO gaps are similar for corresponding molecule systems. HOMO-LUMO gaps are close to 1eV, 3.8 eV and 3 eV for B97D, wB97XD and CAM-B3LYP respectively. All three methods show that ALD-endcapped oligomer-CNT composite has larger HOMO-LUMO gaps than DTF-endcapped oligomer-CNT composite.

Table 5.8: HOMO and LUMO eigenvalues and HOMO-LUMO gaps of different composite systems as a function of different dispersion corrected DFT methods.

|                         | DFT Method | HOMO (eV) | LUMO (eV) | HOMO-LUMO (eV) |
|-------------------------|------------|-----------|-----------|----------------|
| ALD without SCs and CNT | B97D       | -4.224    | -3.166    | 1.058          |
|                         | wB97XD     | -5.745    | -1.950    | 3.795          |
|                         | CAM-B3YP   | -5.275    | -2.275    | 3.000          |
| DTF without SCs and CNT | B97D       | -4.072    | -3.129    | 0.943          |
|                         | wB97XD     | -5.698    | -1.903    | 3.795          |
|                         | CAM-B3YP   | -5.256    | -2.254    | 3.003          |
| ALD with SCs and CNT    | B97D       | -4.321    | -3.262    | 1.059          |
|                         | WB97XD     | -5.776    | -1.980    | 3.795          |
|                         | CAM-B3YP   | -5.311    | -2.314    | 2.998          |
| DTF with SC & CNT       | B97D       | -3.751    | -3.275    | 0.476          |
|                         | wB97XD     | -5.746    | -1.946    | 3.801          |
|                         | CAM-B3YP   | -5.273    | -2.273    | 3.000          |

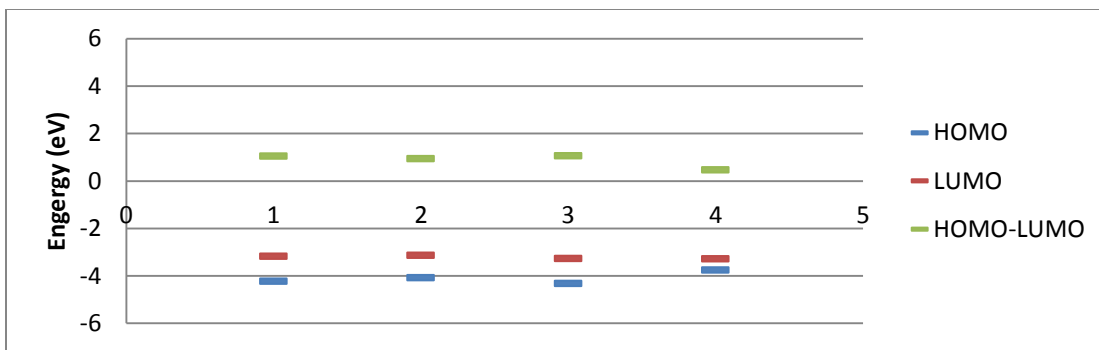


Figure 5.36: HOMO, LUMO eigenvalues and HOMO-LUMO gaps as a function of different composite systems (1. ALD without SCs, 2. DTF without SCs, 3. ALD with SCs, 4. DTF with SCs) for B97D method.

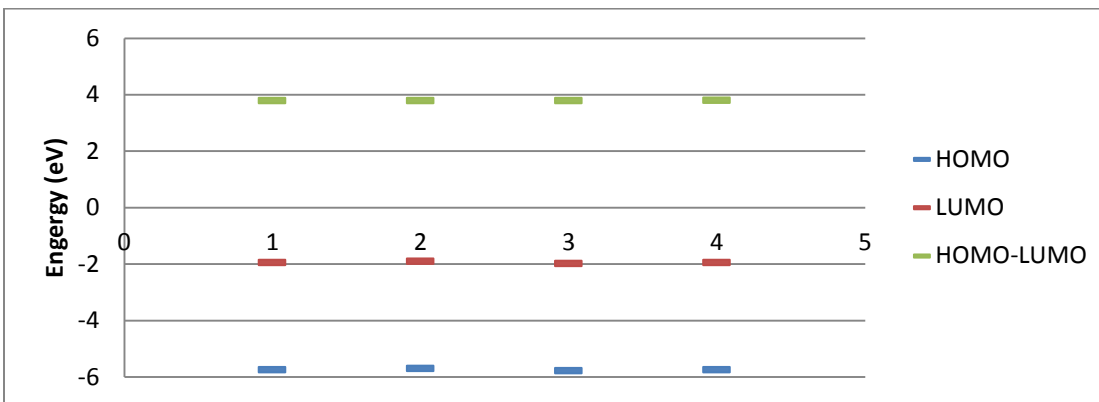


Figure 5.37: HOMO, LUMO eigenvalues and HOMO-LUMO gaps as a function of different composite systems (1. ALD without SCs, 2. DTF without SCs, 3. ALD with SCs, 4. DTF with SCs) for wB97XD method.

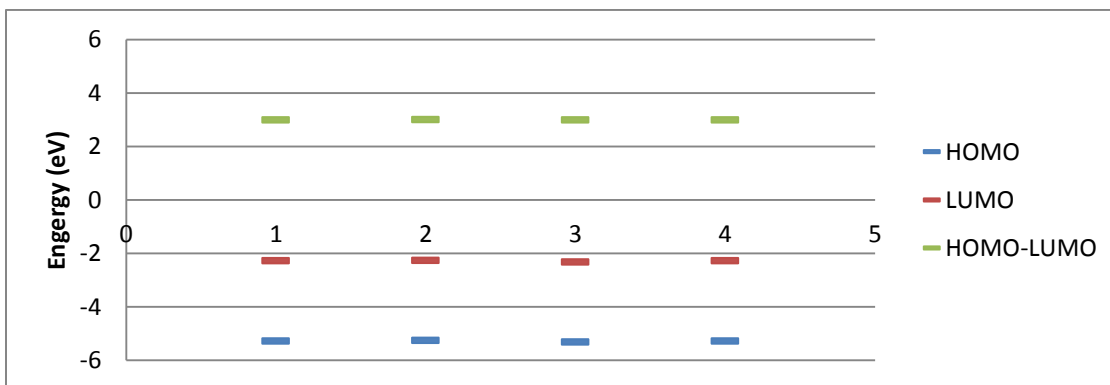


Figure 5.38: HOMO, LUMO eigenvalues and HOMO-LUMO gaps as a function of different composite systems (1. ALD without SCs, 2. DTF without SCs, 3. ALD with SCs, 4. DTF with SCs) for CAM-B3LYP method.

### 5.9.1 End Group Effect

Figures 5.39 and 5.40 show the end group effect on HOMO-LUMO gaps of the ALD- and DTF-endcapped systems without and with SCs for different DFT methods. From these two figures, it is clear that end group has small effect on the gaps (only for oligomers with SCs B97D gives a significant difference in the HOMO-LUMO gaps).

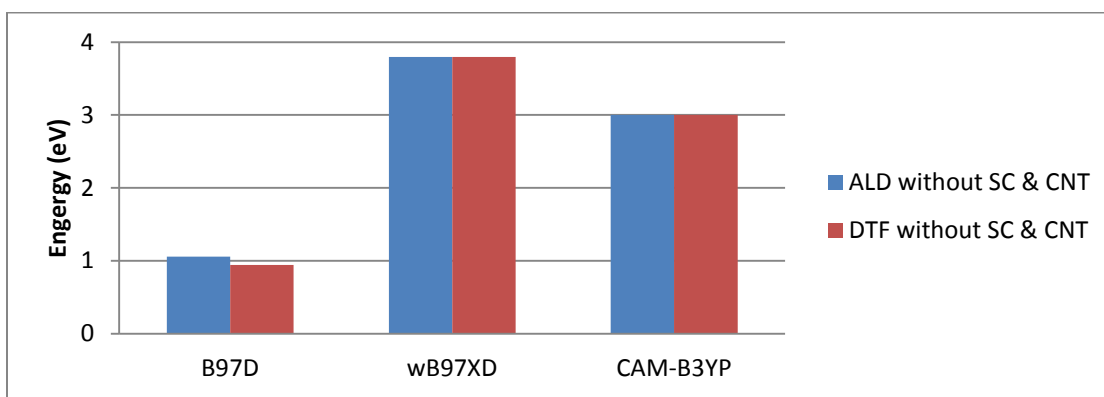


Figure 5.39: HOMO-LUMO gaps of interacting ALD- and DTF-endcapped oligomers without SCs as a function of different DFT methods.

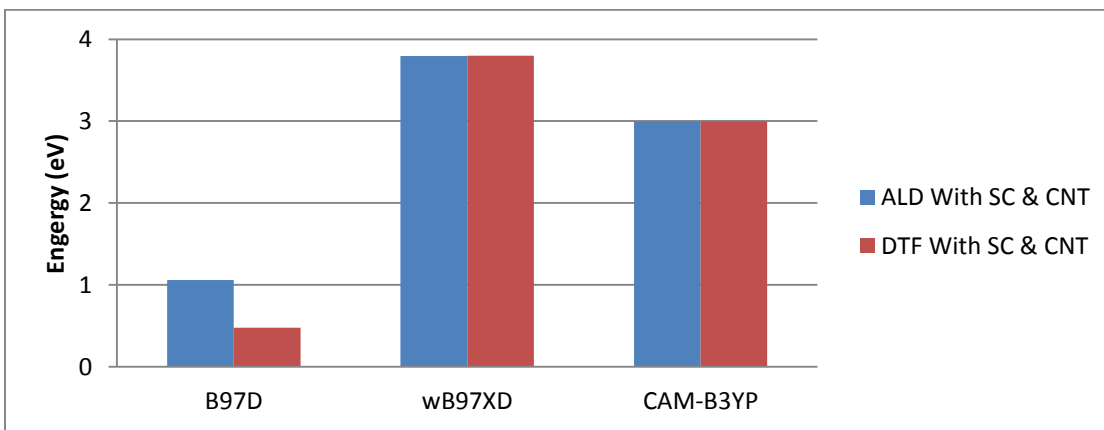


Figure 5.40: HOMO-LUMO gaps of interacting ALD- and DTF-endcapped oligomers with SCs as a function of different DFT methods.



## 5.9.2 Side Chain Effect

Figures 5.41 and 5.42 illustrate that, with exception of oligomers with DTF end group, for B97D, SCs has very small effect on the HOMO-LUMO gaps.

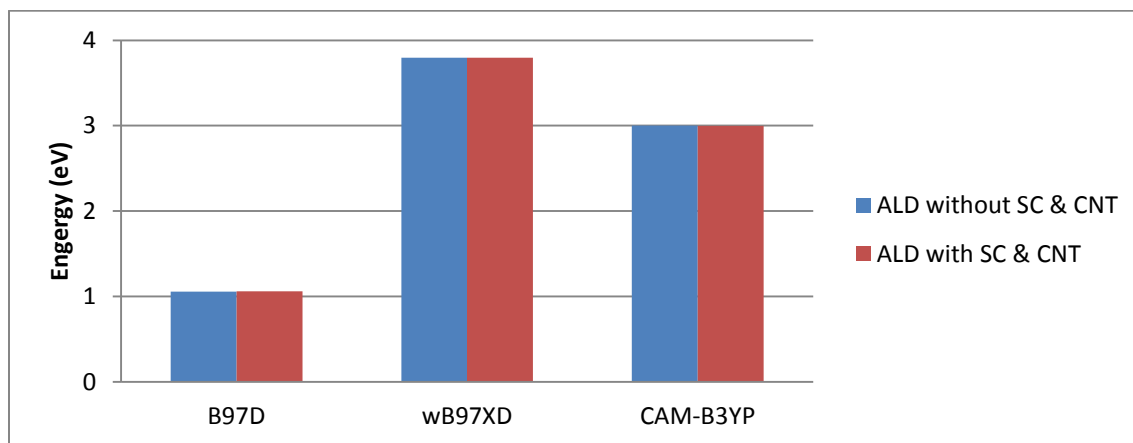


Figure 5.41: HOMO-LUMO gaps of the oligomer with ALD end group without and with SCs as a function of different DFT methods.

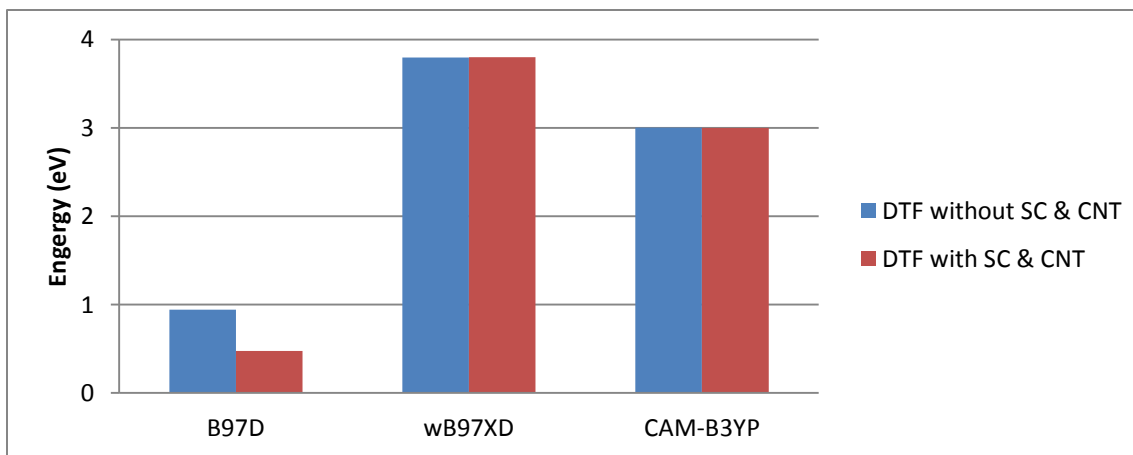


Figure 5.42: HOMO-LUMO gaps of the oligomer with DTF end group without and with SCs as a function of different DFT methods.

## 5. 10 Conclusions

In conclusions, when there are no SCs, there is no significant difference along the backbones between the two endcapped oligomers except for the dihedral angles. In the presence of SCs, bond lengths, bond angles and dihedral angles are affected by the end groups. For the interacting systems, we find some differences in the results that depend on the dispersion corrected DFT methods used in computation. For example, in the case of binding energy, if there are no SCs, the DTF-endcapped oligomer is more tightly bounded around the CNT than ALD-endcapped oligomers whereas in the presence of SCs, ALD-endcapped oligomer wraps more tightly around CNT than DTF-endcapped oligomer except for B97D method. In the presence of SCs, oligomer's backbone moves farther from the CNT and SCs tend to wrap around the CNT (less so for CAM-B3LYP calculations). This makes the oligomer with SCs less parallel to the CNT than without SCs. Dipole moment value and polarity depends on SCs orientations. Moreover, different methods give different value for HOMO-LUMO gaps, however, these values do not depend on the presence or absence of SCs.

## Chapter 6

### The Effect of Dispersion on the Geometrical and Electronic Structure of Interacting Oligomers

In this chapter, we discuss the effect of dispersion on oligomer in the presence of SWCNT. First we compare the dispersion effect on oligomer's backbone structure by considering its BLs, BAs and DAs. Next we compare the dipole moments and HOMO-LUMO gaps. In order to observe the dispersion effect on the geometrical and electronic structure, we subtract the corresponding values of the interacting oligomer from those of the isolated oligomer. In every case, we consider the all ALD- and DTF-endcapped oligomers without and with SCs.

#### 6.1 Bond Length Differences

Figures 6.1-6.4 show the dispersion effects on bond lengths for ALD- and DTF-endcapped oligomers without and with SCs as a function of different bond length position along the backbone for different DFT methods. In the absence of SCs, there are no significant effects (see Figures 6.1 and 6.2) on bond lengths since maximum difference is less than 0.008 Å for CAM-B3LYP and for the other methods the differences are below 0.005 Å. These differences are similar for both end groups and for

all methods. Figures 6.3 and 6.4 show that the bond length differences are also very small when SCs are presents. It should be noted that, for ALD-endcapped oligomer with SCs, wB97XD method gives the largest bond length differences whereas for DTF-endcapped oligomer with SCs, B97D and CAM-B3LYP give the largest corresponding values.

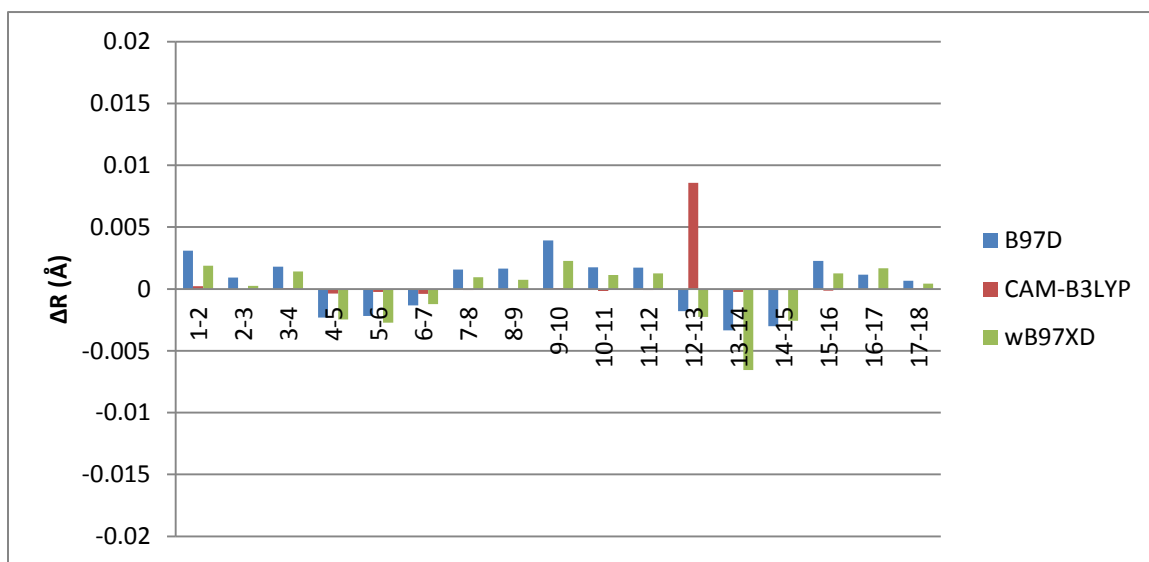


Figure 6.1 Dispersion effect for ALD-endcapped oligomers without SCs for bond length differences as a function of bond length position for different DFT methods.

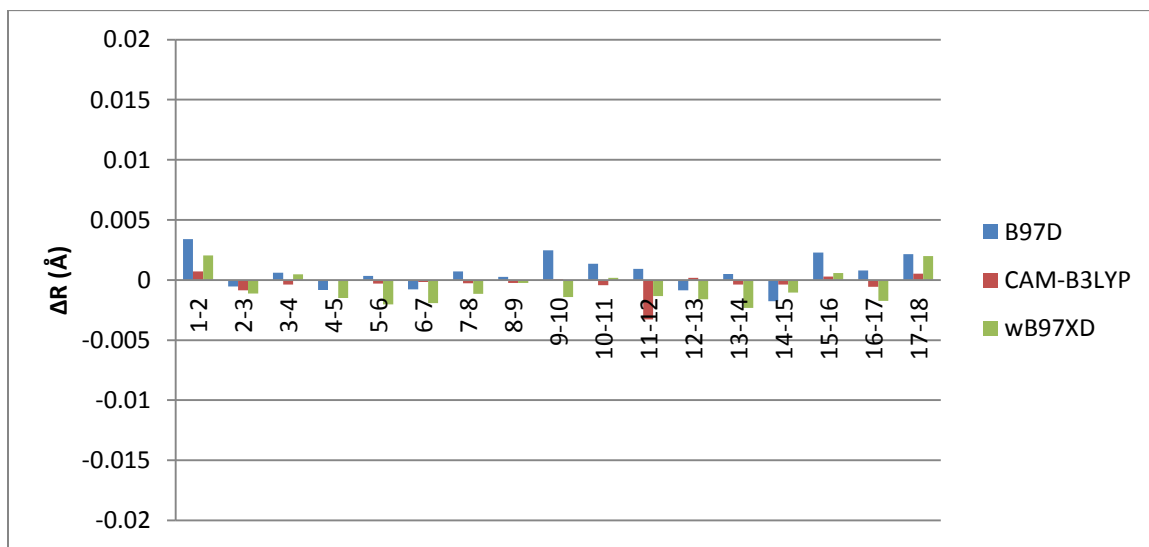


Figure 6.2 Dispersion effect for DTF-endcapped oligomers without SCs for bond length differences as a function of bond length position for different DFT methods.

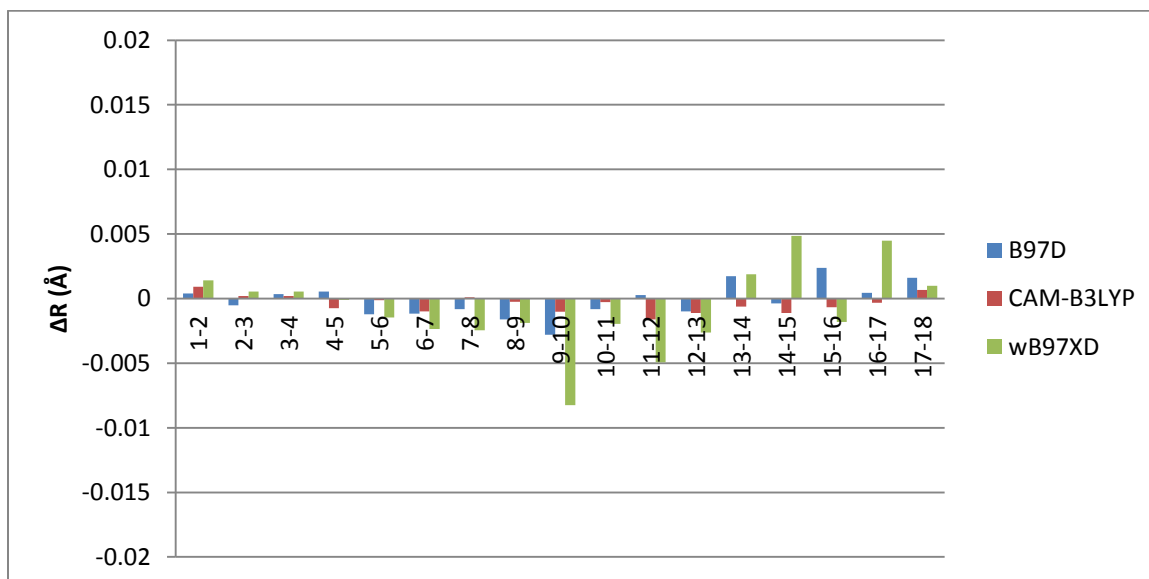


Figure 6.3 Dispersion effect for ALD-endcapped oligomers with SCs for bond length differences as a function of bond length position for different DFT methods.

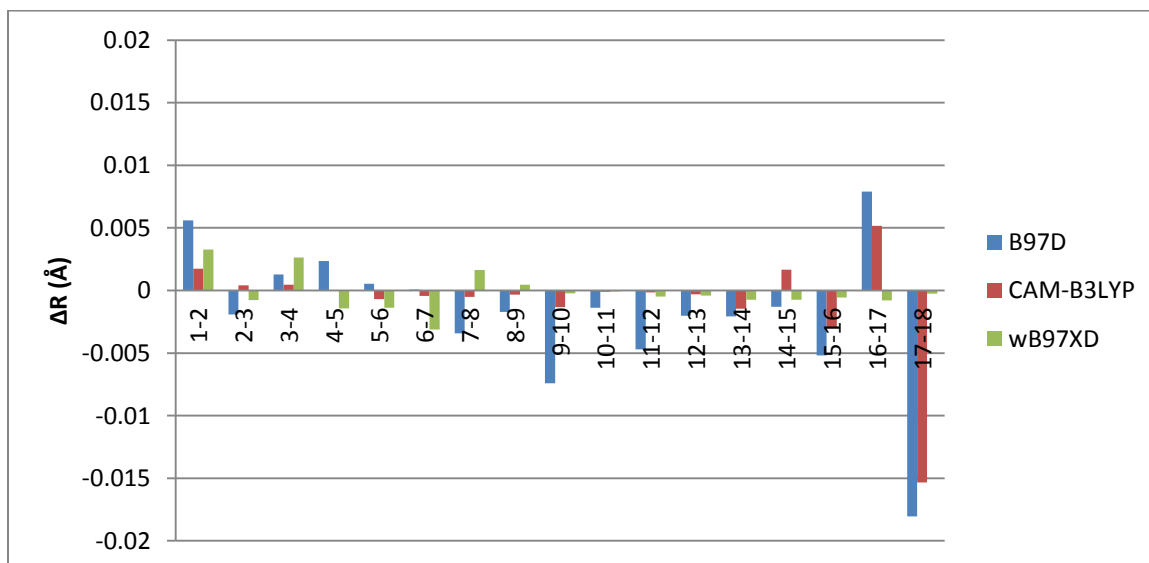


Figure 6.4 Dispersion effect for DTF-endcapped oligomers with SCs for bond length differences as a function of bond length position for different DFT methods

## 6.2 Bond Angle Differences

Figures 6.5-6.8 show the dispersion effect on bond angles for ALD- and DTF-endcapped oligomers without and with SCs for different dispersion corrected DFT methods. Figures 6.5-6.8 show that bond angle differences are smaller for oligomers with SCs in comparison to oligomers without SCs (the maximum difference is  $0.8^\circ$  for wB97XD for oligomers without SCs and  $3.3^\circ$  for B97D for oligomers with SCs). Bond angles along the backbone are bigger for the composite systems than for the isolated systems. This is true for every method and for every molecular system. In general, wB97XD and B97D tend to give somewhat larger bond angle differences than CAM-B3LYP.

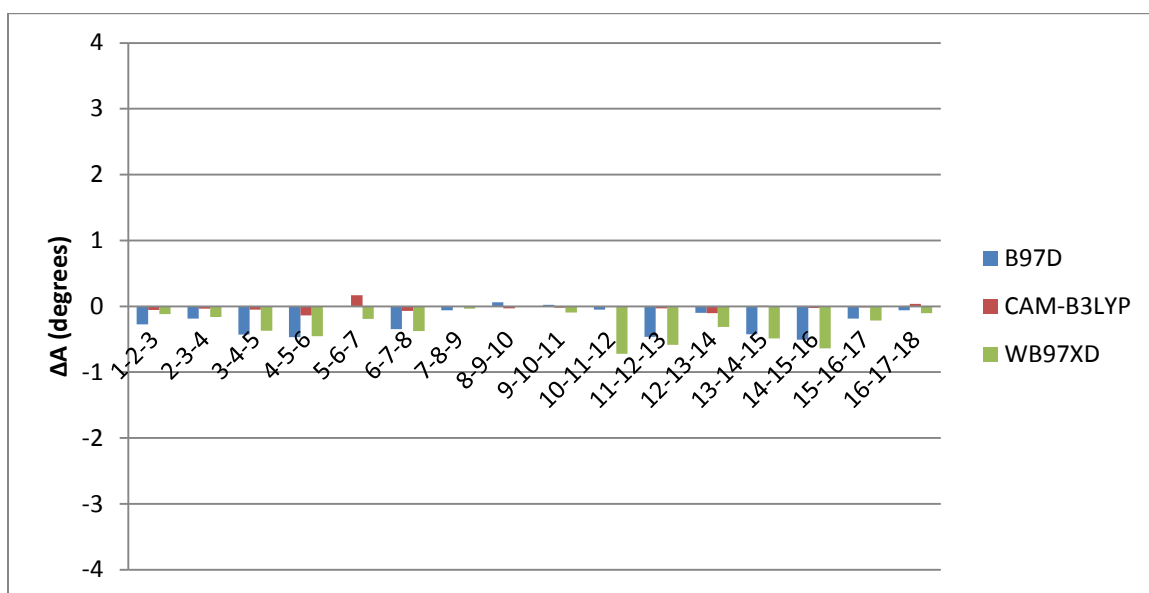


Figure 6.5 Dispersion effect for ALD-endcapped oligomers without SCs for bond angle differences as a function of bond angle position for different DFT methods.

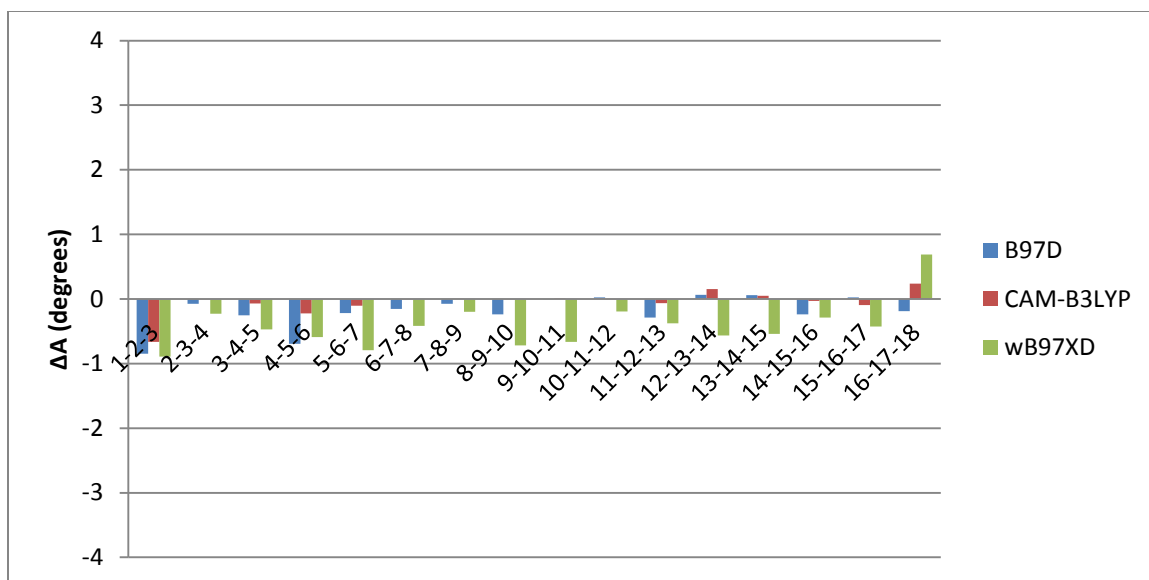


Figure 6.6 Dispersion effect for DTF-endcapped oligomers without SCs for bond angle differences as a function of bond angle position for different DFT methods.

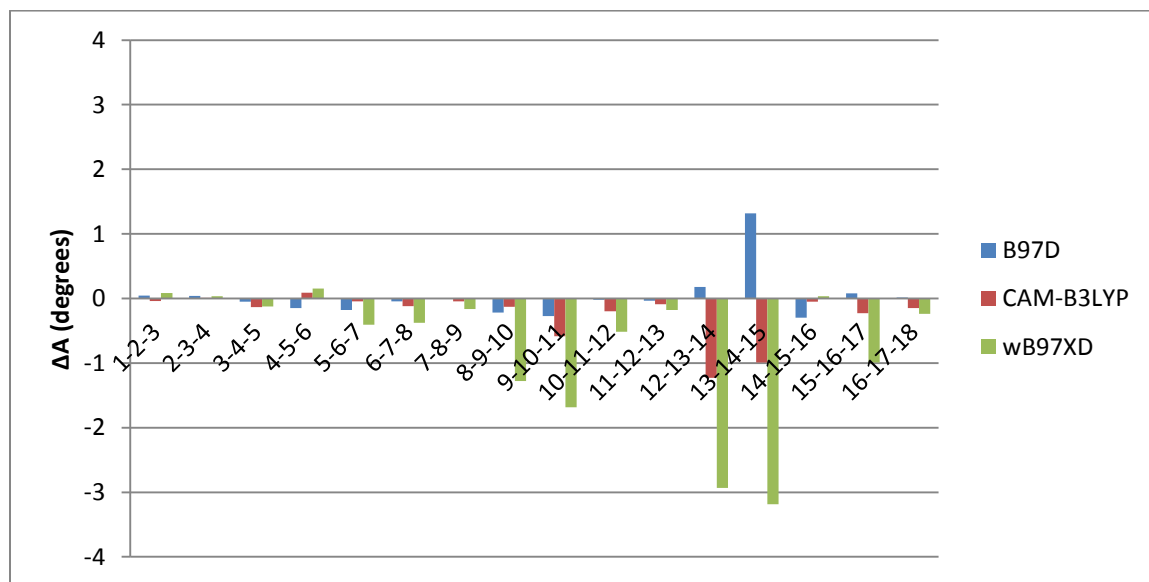


Figure 6.7 Dispersion effect for ALD-endcapped oligomers with SCs for bond angle differences as a function of bond angle position for different DFT methods.

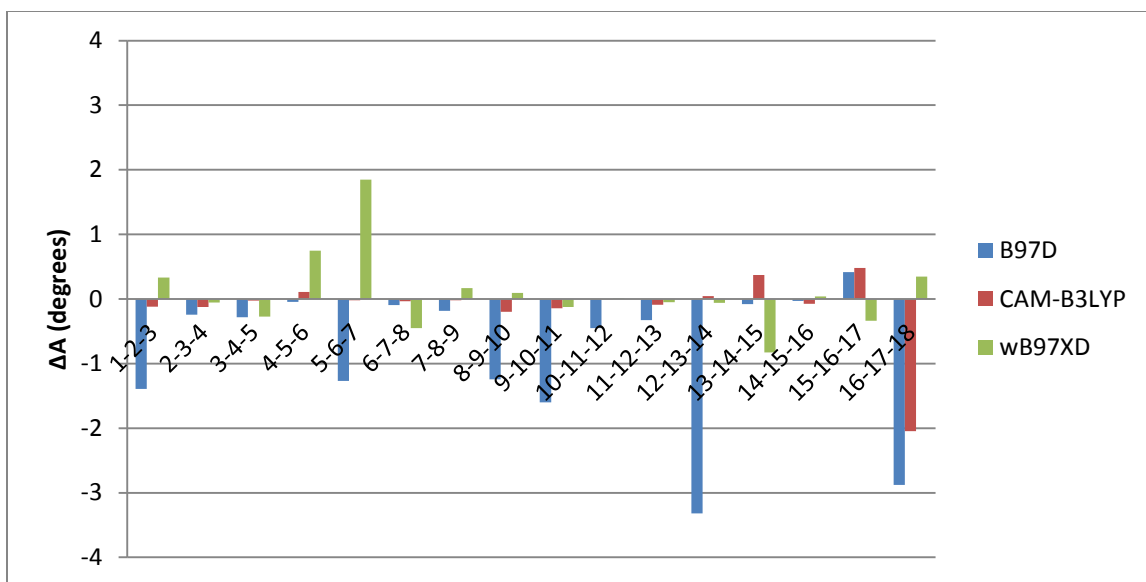


Figure 6.8 Dispersion effect for DTF-endcapped oligomers with SCs for bond angle differences as a function of bond angle position for different DFT methods.

### 6.3 Dihedral Angle Differences

Dispersion effects on dihedral angles for ALD- and DTF-endcapped oligomers without and with SCs are shown in Figures 6.9-6.12. First two figures are for ALD- and DTF-endcapped oligomers without SCs and they show that dihedral angle differences along the backbone between the isolated and interacting oligomers with the exception of  $D_{4-5-6-7}(\text{cis})$  and  $D_{12-13-14-15}(\text{cis})$  are very small (less than  $3^\circ$ ). These two angles ( $D_{4-5-6-7}(\text{cis})$  and  $D_{12-13-14-15}(\text{cis})$ ) are connecting the fluorene with the benzene ring and they show that the interacting oligomers (with ALD and DTF end groups) are more planar (see Appendix, Tables (A.9, A.10, A.21, A.22)) than the isolated oligomers. When the SCs are presents, these two dihedral angle differences decrease. It can also be observed that SCs have minimal effect on the fluorene structure whereas they can make benzene ring less planar



(this is true for oligomers with both end groups). In all cases, interacting oligomers are more planar than isolated oligomers.

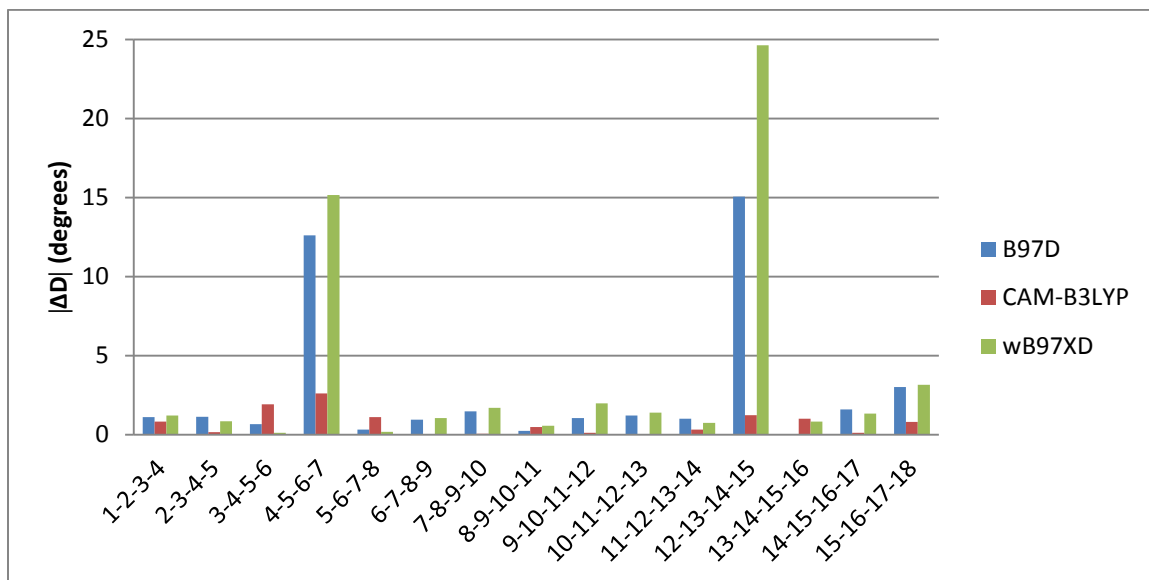


Figure 6.9 Dispersion effect for ALD-endcapped oligomers without SCs for dihedral angle differences as a function of dihedral angle position for different DFT methods.

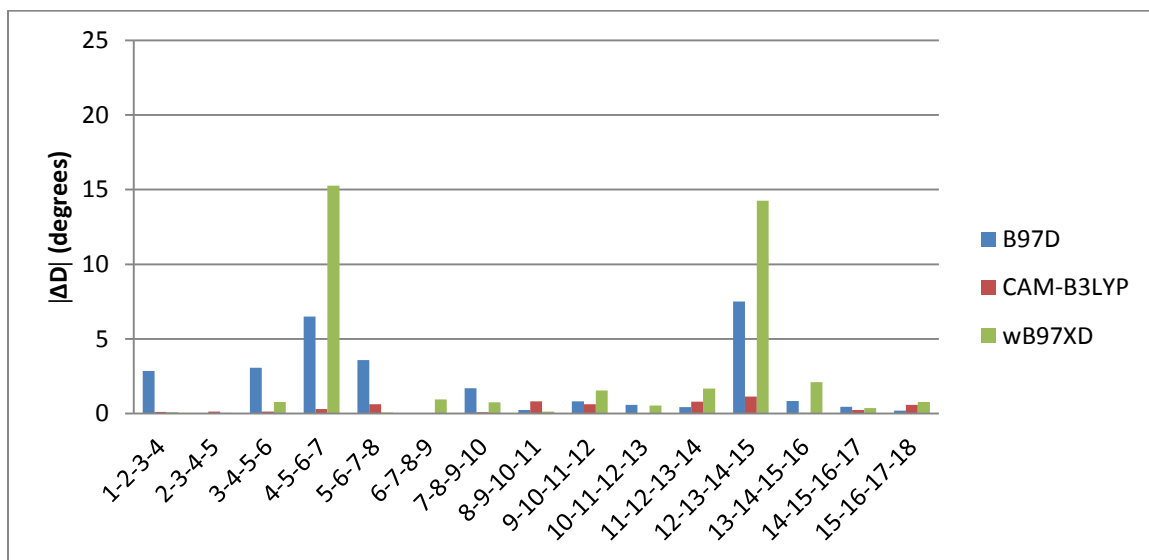


Figure 6.10 Dispersion effect for DTF-endcapped oligomers without SCs for dihedral angle differences as a function of dihedral angle position for different DFT methods.

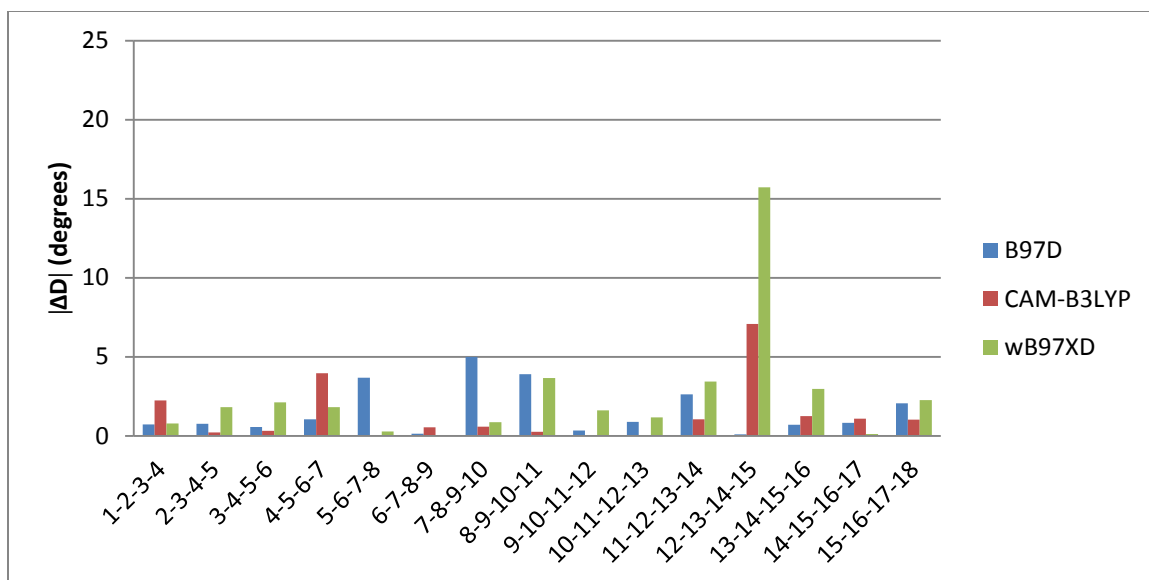


Figure 6.11 Dispersion effect for ALD-endcapped oligomers with SCs for dihedral angle differences as a function of dihedral angle position for different DFT methods.

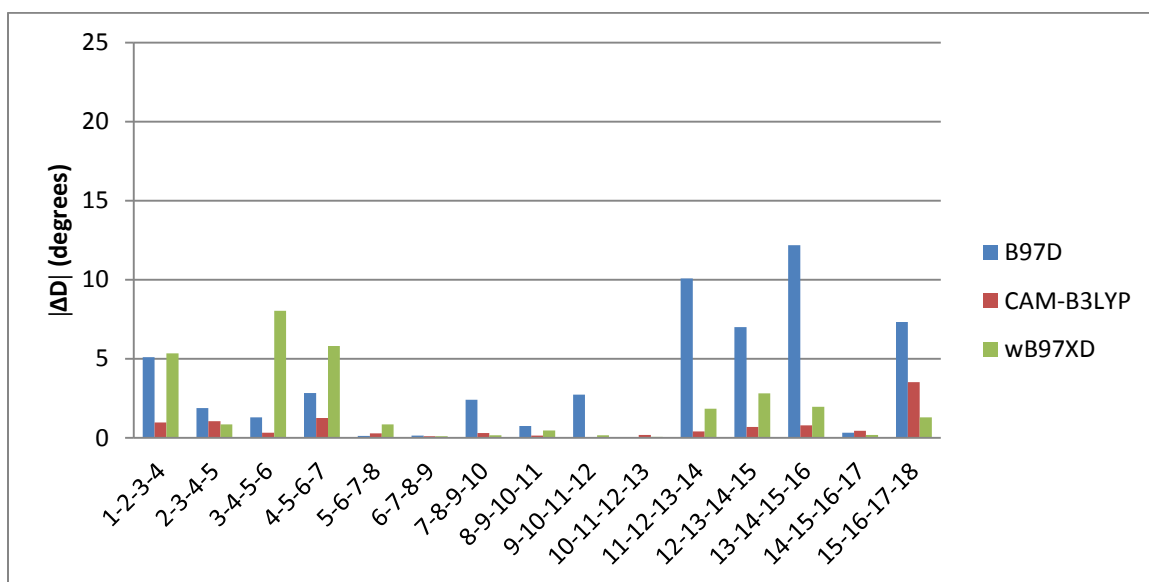


Figure 6.12 Dispersion effect for DTF-endcapped oligomers with SCs oligomer for dihedral angle differences as a function of dihedral angle position for different DFT methods.

## 6.4 Dipole Moments

Figures 6.13-6.16 compare the direction of dipole moments between the isolated oligomers and combinations of SWCNT and oligomers for oligomers with two end groups, and without and with SCs for different dispersion corrected DFT methods. Figures 6.17-6.21 give the corresponding magnitudes of dipole moments. From these figures, it can be seen that for isolated oligomers without SCs, the direction of the dipole moments points away from C-9 position (C-9 position is where alkyl chains are attached to fluorene) for ALD-endcapped oligomers and towards for DTF-endcapped oligomers and the dipole moments lie in the plane of the fluorene for all DFT methods. For the combination systems without SCs, the dipole moments point towards the oligomer from the center of the CNT except for CAM-B3LYP where they point away from oligomer for both ALD and DTF end groups. Figures 6.15 and 6.16 show that for isolated oligomers with SCs, dipole moments are nearly perpendicular to the fluorene plane for all DFT methods and for both end groups. In comparison, the dipole moments of combination systems with SCs tend to point away from the fluorene's SCs for the ALD-endcapped oligomers and towards the fluorene's SCs for the DTF-endcapped oligomers. Figures 6.17 and 6.18 show that for ALD- and DTF-endcapped oligomers without SCs the magnitudes of the dipole moments of the combinations are larger than those for isolated oligomers (except for CAM-B3LYP for ALD end group). For oligomers with SCs (see Figures 6.19 and 6.20) the opposite is true, the magnitude of the dipole moments for isolated systems are larger than those for the combinations (except for B97D for ALD end group).

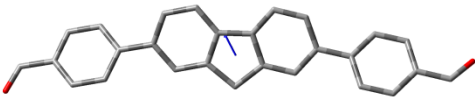

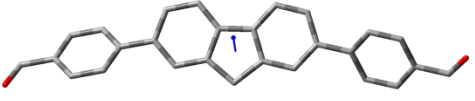
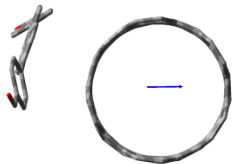
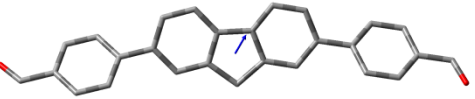

| Isolated ALD-endcapped oligomer without SCs   | Interacting ALD-endcapped oligomer without SCs  |
|---|---|
|  <p>B97D</p>       |  <p>B97D</p>       |
|  <p>CAM-B3LYP</p> |  <p>CAM-B3LYP</p> |
|  <p>wB97XD</p>   |  <p>wB97XD</p>   |

Figure 6.13: Dipole moment directions (see blue arrows) for ALD-endcapped oligomers without SCs for the isolate and the interacting oligomers for different dispersion corrected DFT methods.

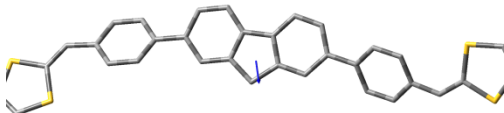
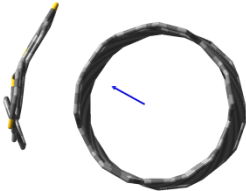
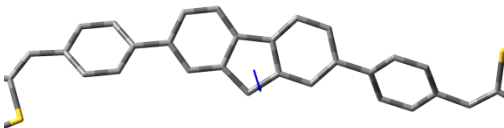

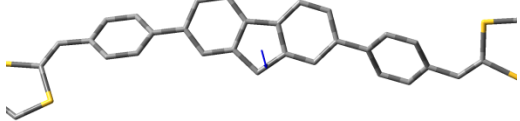
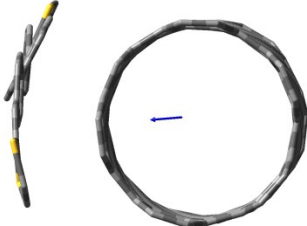
| Isolated DTF-endcapped oligomer without SCs   | Interacting DTF-endcapped oligomer without SCs  |
|---|---|
|  <p>B97D</p>       |  <p>B97D</p>       |
|  <p>CAM-B3LYP</p> |  <p>CAM-B3LYP</p> |
|  <p>wB97XD</p>   |  <p>wB97XD</p>    |

Figure 6.14: Dipole moment directions (see blue arrows) for DTF-endcapped oligomers without SCs for the isolate and the interacting oligomers for different dispersion corrected DFT methods.

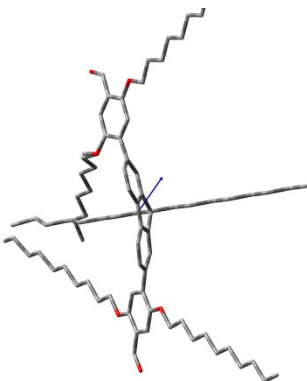
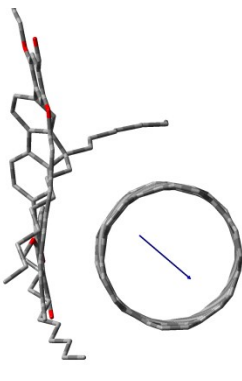
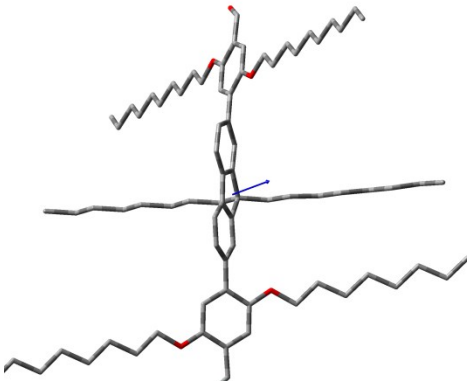
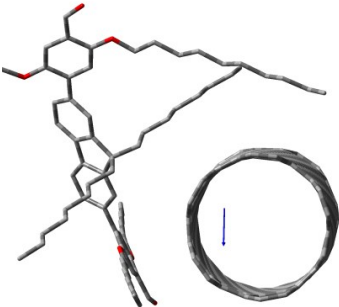
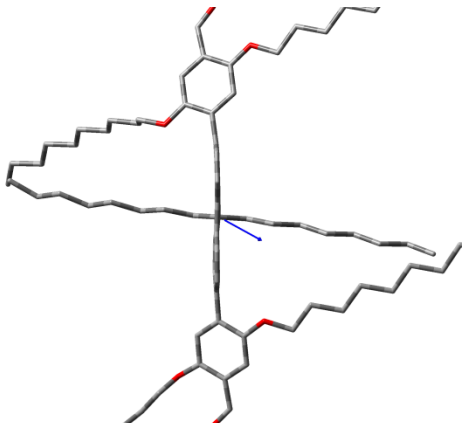
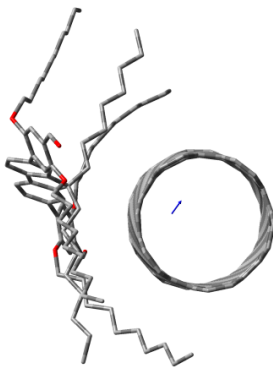
| Isolated ALD-endcapped oligomer with SCs  | Interacting ALD-endcapped oligomer with SCs  |
|---|--|
|  <p>B97D</p>       |  <p>B97D</p>      |
|  <p>CAM-B3LYP</p> |  <p>CAM-B3LYP</p> |
|  <p>wB97XD</p>   |  <p>wB97XD</p>   |

Figure 6.15: Dipole moment directions (see blue arrows) for ALD-endcapped oligomers with SCs for the isolate and the interacting oligomers for different dispersion corrected DFT methods.

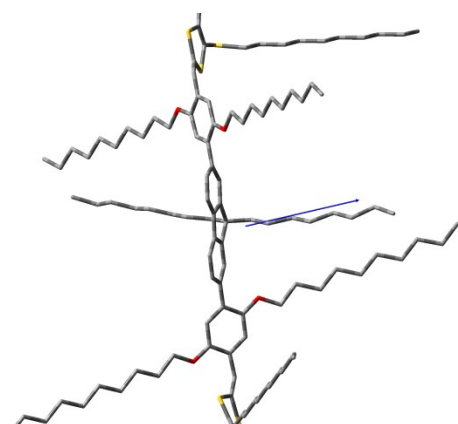
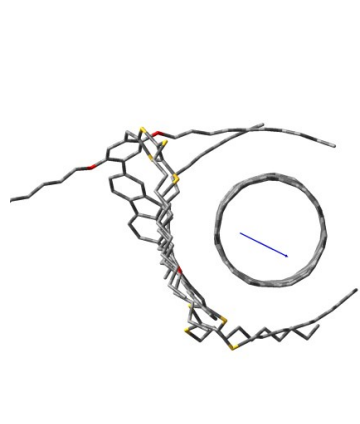
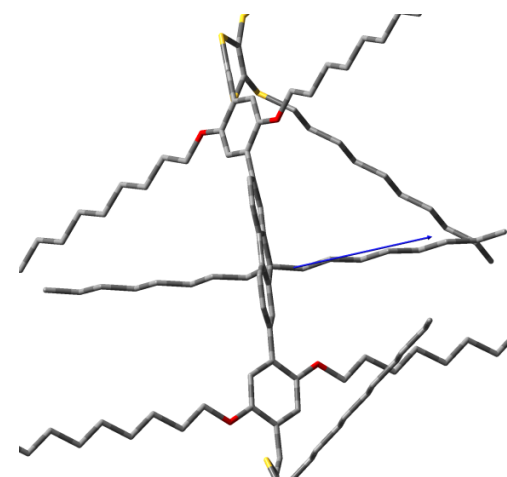
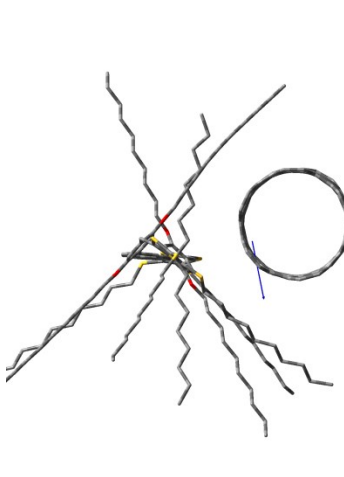
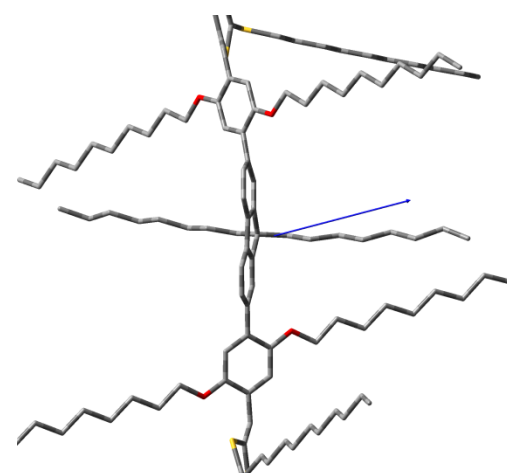
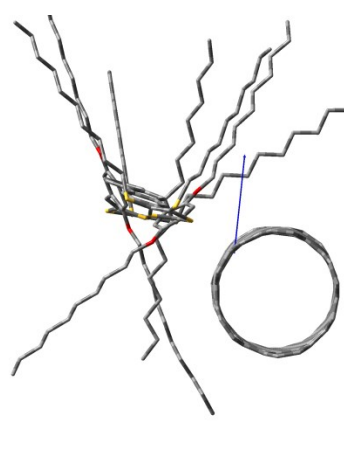
| Isolated DTF-endcapped oligomer with SCs  | Interacting DTF-endcapped oligomer with SCs  |
|---|--|
|  <p data-bbox="519 745 584 777">B97D</p>         |  <p data-bbox="1104 745 1169 777">B97D</p>         |
|  <p data-bbox="470 1281 633 1312">CAM-B3LYP</p> |  <p data-bbox="1055 1281 1218 1312">CAM-B3LYP</p> |
|  <p data-bbox="503 1816 600 1848">wB97XD</p>   |  <p data-bbox="1088 1816 1185 1848">wB97XD</p>   |

Figure 6.16: Dipole moment directions (see blue arrows) for ALD-endcapped oligomers with SCs for the isolate and the interacting oligomers for different dispersion corrected DFT methods.

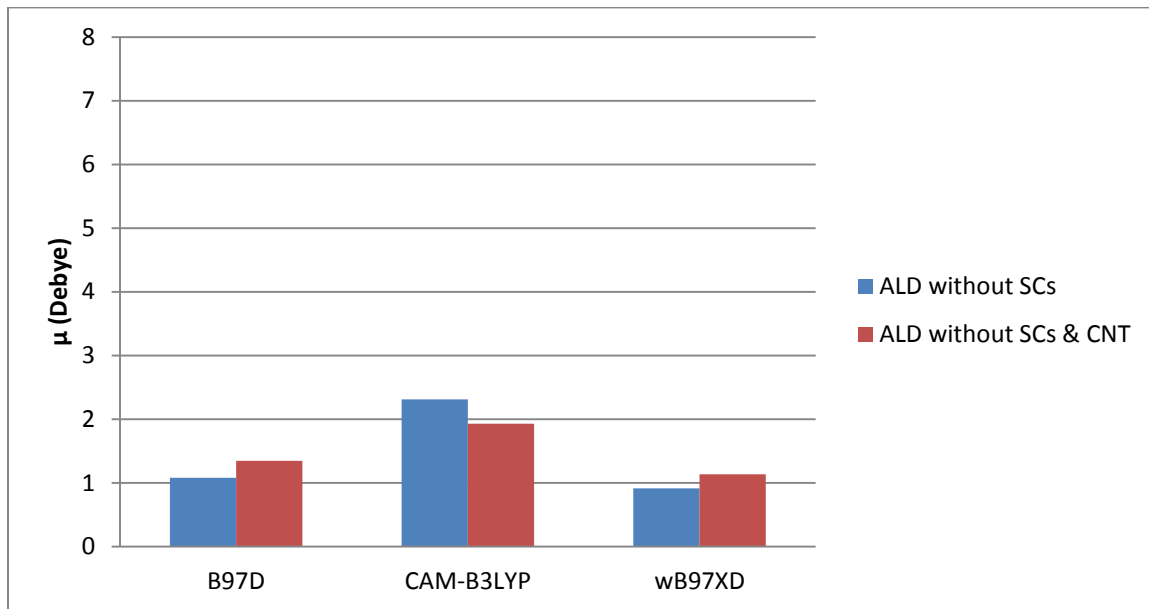


Figure 6.17: Dispersion effect on dipole moments of ALD-endcapped oligomers without SCs as a function of different DFT methods.

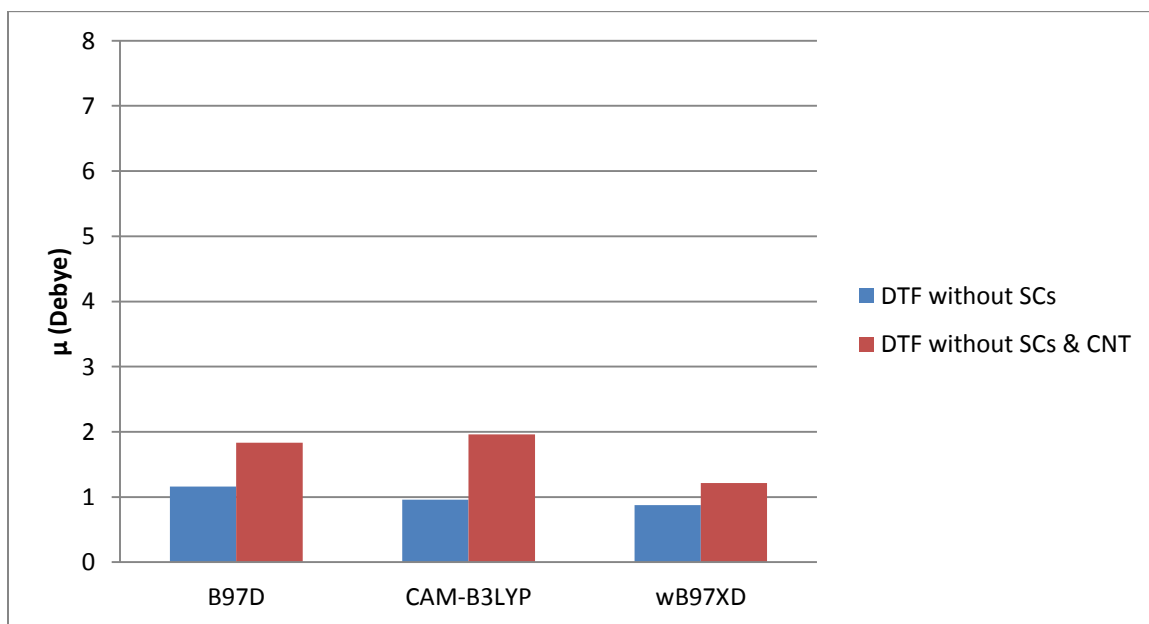


Figure 6.18: Dispersion effect on dipole moments of DTF-endcapped oligomers without SCs as a function of different DFT methods.



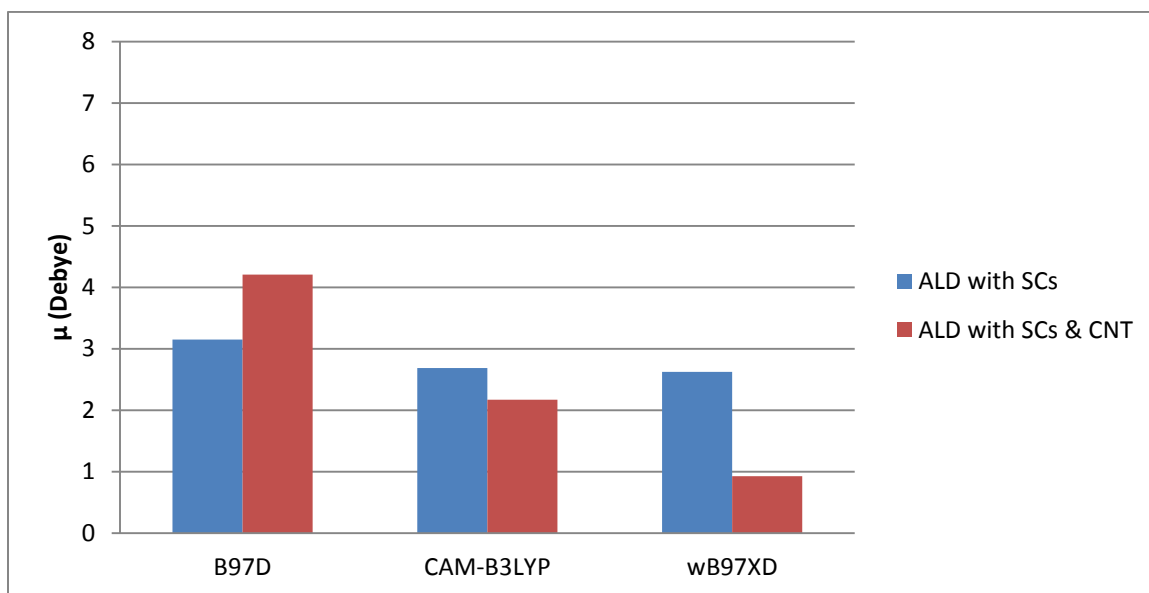


Figure 6.19: Dispersion effect on dipole moments of ALD-endcapped oligomers with SCs as a function of different DFT methods.

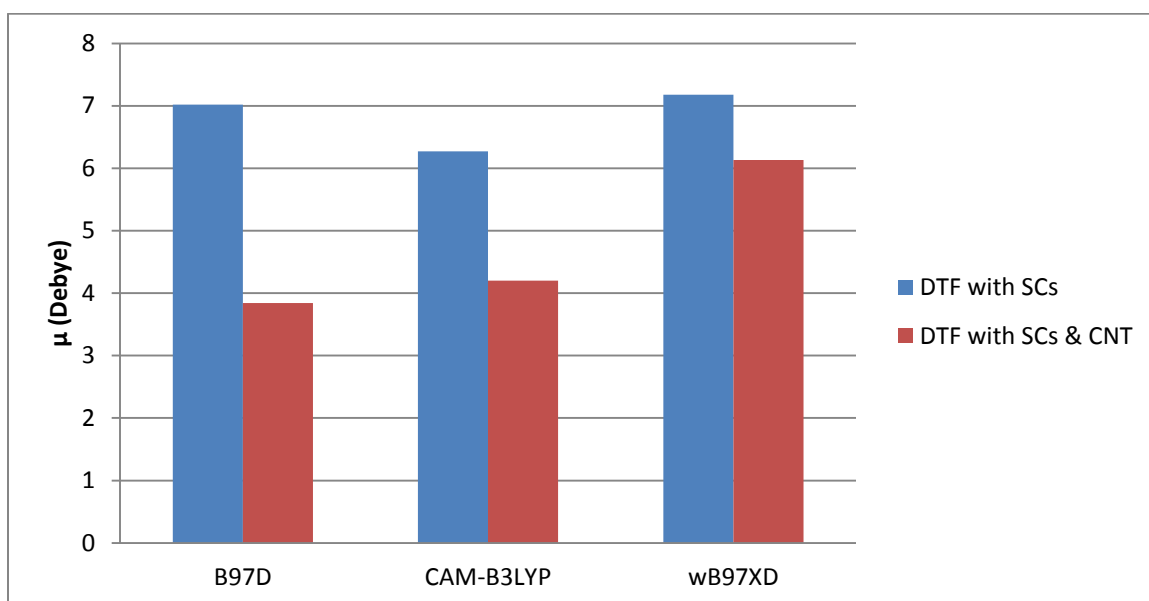


Figure 6.20: Dispersion effect on dipole moments of DTF-endcapped oligomers with SCs as a function of different DFT methods.

## 6.5 HOMO-LUMO Gaps

Figures 6.21-6.24 illustrate the dispersion effect on HOMO-LUMO gaps for different oligomer systems for different dispersion corrected DFT methods. From these figures it is clear that when oligomer interacts with CNT, its HOMO-LUMO gap decreases. All three methods show the same trend. B97D method gives lowest HOMO-LUMO gaps for all systems whereas wB97XD gives the highest and CAM-B3LYP gives the intermediate values.

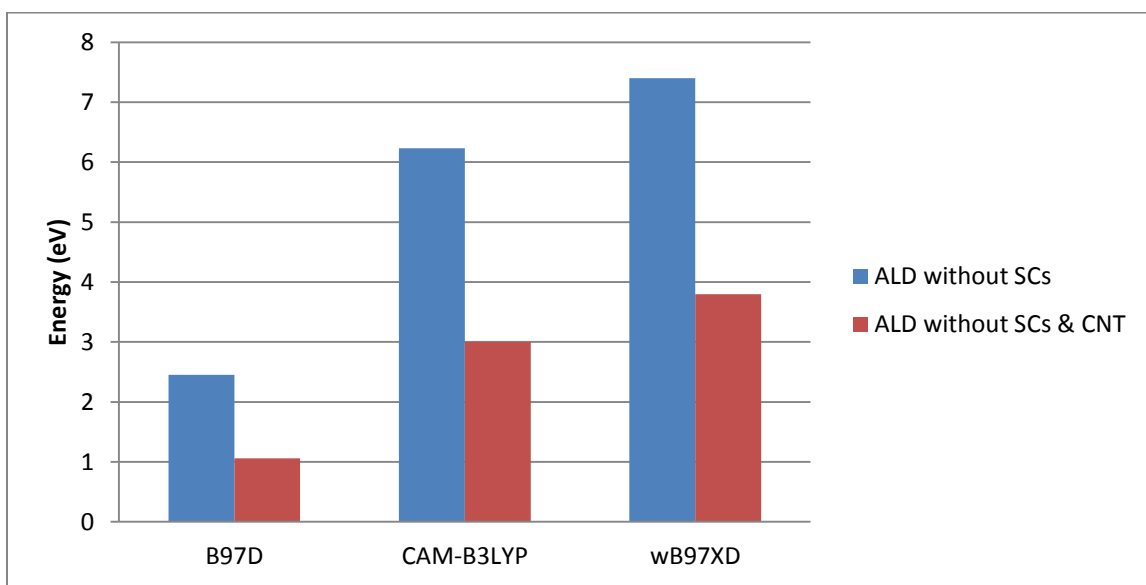


Figure 6.21: Dispersion effect on HOMO-LUMO gaps of ALD-encapped oligomers without SCs as a function of different DFT methods.

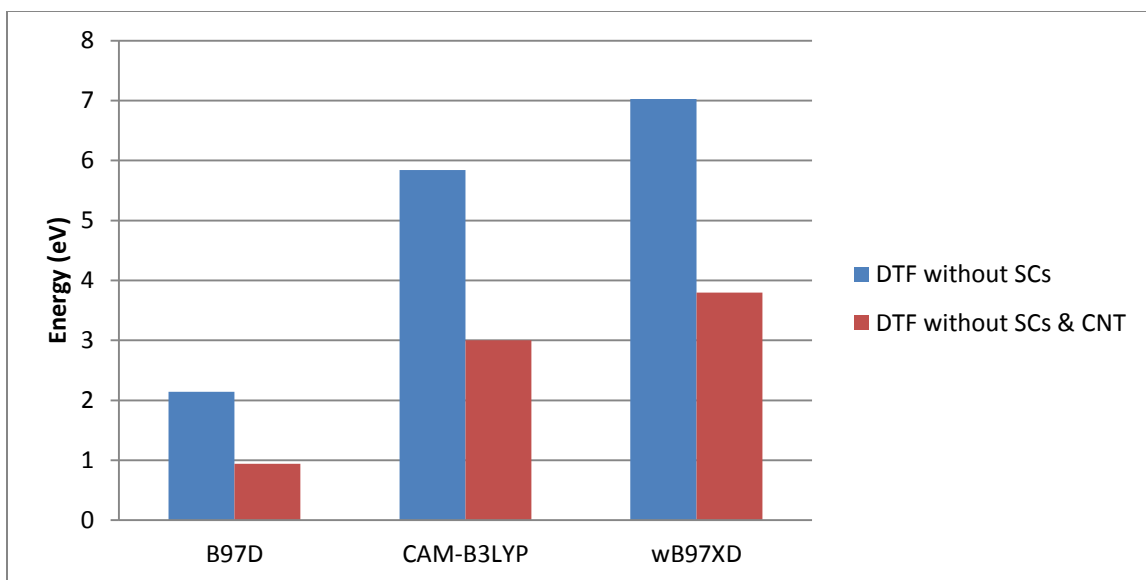


Figure 6.22: Dispersion effect on HOMO-LUMO gaps of DTF-endcapped oligomers without SCs as a function of different DFT methods.

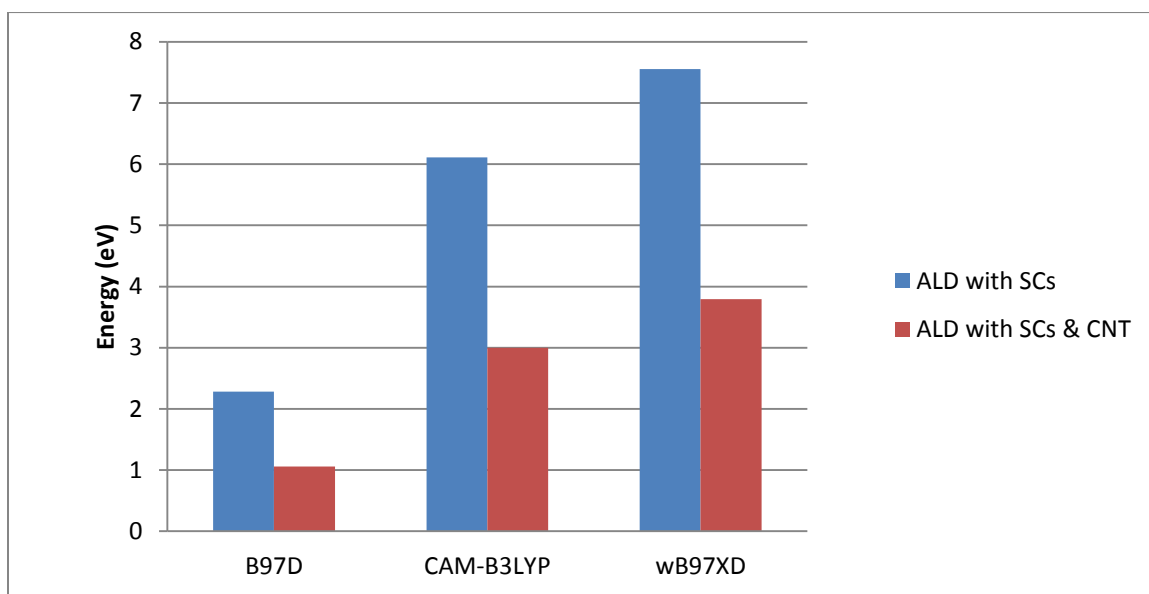


Figure 6.23: Dispersion effect on HOMO-LUMO gaps of ALD-endcapped oligomers with SCs as a function of different DFT methods.

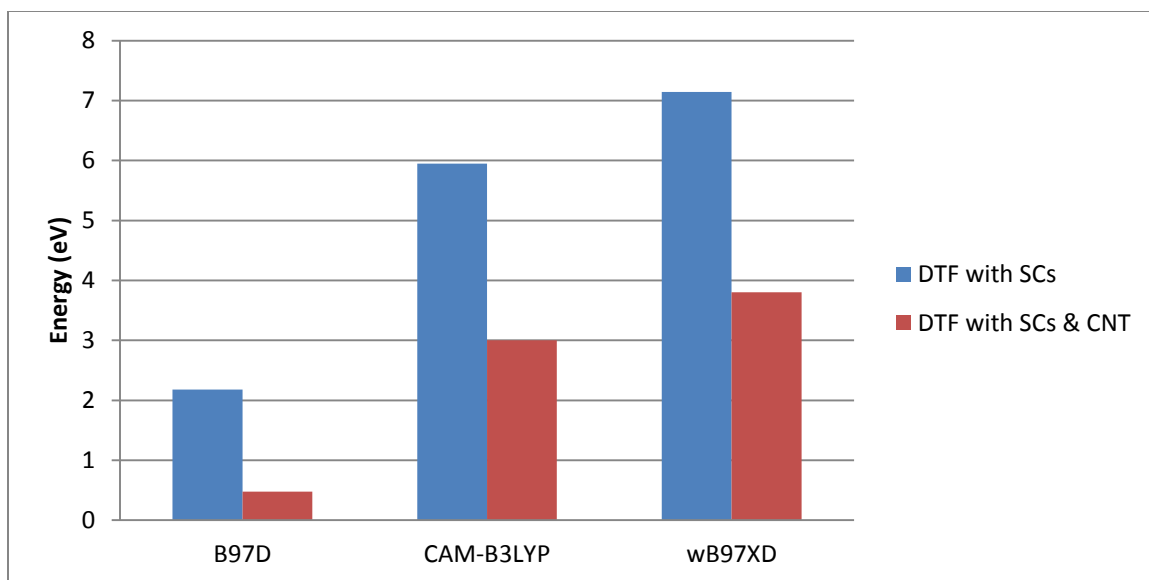


Figure 6.24: Dispersion effect on HOMO-LUMO gaps of DTF-endcapped oligomers with SCs as a function of different DFT methods.

## 6.6 Conclusions

In summary, there is no significant dispersion effect on the bond lengths along the oligomers' backbones however the bond angles for the interacting oligomers are somewhat larger than those for the isolated oligomers and the interacting oligomers are more planer than the isolated oligomers. Dipole moments for interacting oligomers without SCs are larger than those for isolated oligomers without SCs. This is opposite to what is observed for oligomers with SCs. Dipole moments lie in the fluorene plane for oligomer without SCs and their directions depends on the SCs orientations for oligomers with SCs. HOMO-LUMO gaps are decreased in the case of interacting relative to isolated oligomers.

# Chapter 7

## Summary and Conclusions

In this chapter, we summarize the major results of this research work. Our calculations were accomplished using the dispersion corrected DFT methods (B97D, wB97XD and CAM-B3LYP). In our research, we considered the geometrical parameters and electronic properties of isolated ALD- and DTF-endcapped oligomers and ALD- and DTF-endcapped oligomers interacting with the SWCNTs. Our calculations indicate that:

- In the case of isolated system, bond length differences along the backbone between ALD- and DTF-endcapped oligomers are reduced in the presence of SCs relative to oligomers without SCs. The presence of SCs is also responsible for the more twisted oligomers' backbones relative to oligomers without SCs. The DTF-endcapped oligomers are more polarized (have larger dipole moments) than ALD-endcapped oligomers in the presence of SCs. HOMO-LUMO gaps for DTF-endcapped oligomers are smaller than those for ALD-endcapped oligomers.
- In the case of interacting system (oligomer and SWCNT), the largest change is observed in the two dihedral angles connecting the fluorene with benzene and benzenes with the end groups. In general oligomers with DTF are more planar than the ones with ALD for both oligomers with and without SCs. DTF-

endcapped oligomers with SCs have smaller binding energy than ALD-endcapped oligomers with SCs (except for B97D result). That is, in the presence of SCs, DTF-endcapped oligomers move farther away from the SWCNTs and their SCs do not wrap as tightly around the SWCNTs. In contrast ALD-endcapped oligomers move closer to the SWCNTs, and their backbones and SCs wrap around the SWCNTs.

- In general, backbones of the interacting oligomers with SCs are more planar than the backbones of isolated oligomers with SCs. The magnitudes of dipole moments for interacting oligomers with SCs are smaller than those for isolated oligomers with SCs and their directions depend on the SCs' orientations.
- Different dispersion corrected DFT methods give very similar results for geometrical and electronic structures for isolated oligomers whereas some differences are observed (see above discussion) for interacting systems.

In conclusion for combination systems, in most cases, DTF-endcapped oligomer with SCs and SWCNT, has a smaller binding energy than ALD-endcapped oligomer with SCs and SCWCNT. DTF-endcapped combination also has a larger dipole moment and intermolecular distance than ALD-endcapped combination. SCs of the ALD-endcapped oligomer tend to wrap around the SWCNT whereas SCs of the DTF-endcapped oligomer tend to extend farther away from the SWCNT. Because of their smaller binding energies DTF-endcapped fluorene-based oligomers with SCs would be easier to remove from the solution of CNTs and oligomers and hence are recommended more (relative to ALD-endcapped oligomers) for the dispersion SWCNTs.

## Reference

1. Mohd Hamzah Harun, Elias Saion, Anuar Kassim, Noorhana Yahya and Ekramul Mahmud. *Conjugated Conducting Polymers: A Brief Overview*, JASA **2**, 63-68, (2007).
2. Bredas J.L., R.R. Chance, and R. Silbey. *Comparative theoretical study of the doping conjugated polymers; Polarons in polyacetylene and polyparaphenylene*. Physical Review B. **26**, 5843-5854 (1982).
3. Clarke, T.C., R.H. Geiss, J.F.Kwak, and G.B.Street. *Highly conducting transition metal derivatives of polyacetylene*. J. Chem. Soc. Comm. **338**, 489-490. (1978).
4. C. K. Chiang, C. R. Fincher, Jr, Y. W. Park, A, J. Heeger, H. Shirakawa, E, J. Louis, S. C. Gau and A. G. MacDiarmid. *Electrical Conductivity in Doped Polyacetylene*. Phys. Rev. Lett. **39** 1098 (1977).
5. H. Naarman. *Synthesis of New Conductive Polymers*. Synth. Met. **17** 223 (1987).
6. J. H. Burroughs, D. D. C. Bradley, A. R. Brown, R. N. Marks, K. Mackay, R. H. Friend, P. I. Burns and A. B. Holmes. *Light-Emitting Diodes Based on Conjugated Polymers*. Nature **347** 539 (1990).
7. Murat Atesa, Tolga Karazehira and A. Sezai Sarachb. *Conducting Polymers and their Applications*, Cur. Phys. Chem. **2**, 224-240, (2012).
8. Liheng Feng, Chunlei Zhu, Huanxiang Yuan, Libing Liu, Fengting Lv and Shu Wang. *Conjugated polymer nanoparticles: preparation, properties, functionalization and biological applications*. Chem. Soc. Rev. **42**(16) 6620-33 (2013).
9. Bing Wang, Chunlei Zhu, Libing Liu, Fengting Lv, Qiong Yanga and Shu Wan. *Synthesis of a new conjugated polymer for cell membrane imaging by using an intracellular targeting strategy*. Polym. Chem. **4**, 5212-5215, (2013).
10. Winter, M.; Brodd, R.J. *What are batteries, fuel cells, and supercapacitors?* Chem. Rev. **104**(10), 4245-4269, (2004).
11. Miller, J.R.; Simon, P. *Materials science - Electrochemical capacitors for energy management*. Science, **321**(5889), 651-652 (2008).
12. Jim P. Zheng, *Ruthenium oxide for electrochemical capacitors*. J. Electro. chem. Soc. **46**, 2465-2471 (1999).

13. Gupta, V.; Miura, N. *Electrochemically deposited polyaniline nanowire's network a high-performance electrode material for redox supercapacitor*. *Electro. chem. Solid-State Lett.* **8**, A630-A632 (2005).
14. Ebisawa, F.; Kurokawa, T.; Nara, S. *Electrical-properties of polyacetylene polysiloxane interface*. *J. Appl. Phys.* **54**(6), 3255-3259 (1983).
15. Rogers, J.A.; Bao, Z.; Dodabalapur, A. *Organic smart pixels and complementary inverter circuits formed on plastic substrates by casting and rubber stamping*. *IEEE Electron Device Lett.* **21**(3), 100-103 (2000).
16. Torsi, L.; Dodabalapur, A.; Sabbatini, L.; Zamboni, P. *Multiparameter gas sensors based on organic thin-film-transistors*. *Sens. Actuators B-Chemical*, **67**(3), 312-316 (2000).
17. Birks JB, *Photophysics of Aromatic Molecules*. Wiley-Interscience, New York. (1970).
18. Wong K-T, Chien Y-Y, Chen R-T, Wang C-F, Lin Y-T, Chiang H-H, Hsieh P-Y, Wu C-C, Chou CH, Su YO, Lee G-H, Peng S-M, *Ter(9,9-diarylfuorene)s: Highly Efficient Blue Emitter with Promising Electrochemical and Thermal Stability*. *J. Am. Chem. Soc.* **124** 11576, (2002).
19. Wu C-C, Lin Y-T, Wong K-T, Chen R-T, Chien Y-Y. *Efficient Organic Blue-Light-Emitting Devices with Double Confinement on Terfluorenes with Ambipolar Carrier Transport Properties*. *Adv. Mater* **16** 61, (2004).
20. Cornelissen HJ, Huck HPM, Broer DJ, Picken SJ, Bastiaansen CWM, Erdhuisen E, Maaskant. *Polarized Light LCD Backlight Based on Liquid Crystalline Polymer Film: A New Manufacturing Process*. *SID Int Symp Dig Tech Pap* **35** 1178, (2004).
21. Geng Y, Trajkovska A, Culligan SW, Ou JJ, Chen HMP, Katsis D, Chen SH. *Organic Field Effect Transistors Comprising Monodisperse Glassy Nematic Oligofluorenes*. *J Am Chem. Soc.* **125**:14032, (2003).
22. Kauffman JM, Kelley CJ, Ghiorghis A, Neister E, Armstrong L, Prause PR. *Cyclic Ether Auxofluors on Oligophenylene Laser Dyes*. *Laser Chem.* **7** 343, (1987).
23. Seliskar CJ, Landis DA, Kauffman JM, Aziz MA, Steppel RN, Kelley CJ, Qin Y, Ghiorghis A. *Characterization of new excimer pumped UV laser dyes*. *Laser Chem.* **13** 19, (1994).
24. Murphy AR, Fréchet JM, *Organic semiconducting oligomers for use in thin film transistors*. *Chem Rev* **107** 106626, (2007).



25. Meng H, Bao Z, Lovinger AJ, Wang B-C, Mujsce AM. *High field-effect mobility oligofluorene derivatives with high environmental stability*. J Am Chem Soc **123** 9214, (2001).
26. Carrasco-Orozco M, Tsoi WC, O'Neill M, Aldred MP, Vlachos P, Kelly SM. *New Photovoltaic Concept: Liquid-Crystal Solar Cells Using a Nematic Gel Template*. Adv. Mater **18** 1754, (2006).
27. R. Saito, G. Dresselhaus, M. S. Dresselhaus: *Physical Properties of Carbon Nanotubes*. Imperial College Press, London (1998).
28. Sumio Iijima *Helical microtubules of graphitic carbon*, NEC Corporation, Fundamental Research Laboratories, 34 Miyukigaoka, Tsukuba, Ibaraki 305, Japan.
29. P. M. Ajayan, M. Terrones, A. de la Guardia, V. Hue, N. Grobert, B. Q. Wei, H. Lezec, G. Ramanath, T. W. Ebbesen. *Nanotubes in a flash – Ignition and reconstruction*, Science **296**, 705 (2002).
30. E. A. Avallone and T. Baumeister Marks' *Standard Handbook for Mechanical Engineers*. McGraw–Hill, New York, (1991).
31. D. A. Walters, L. M. Ericson, M. J. Casavant, J. Liu, D. T. Colbert, K. A. Smith, R. E. Smalley: *Elastic strain of freely suspended single-wall carbon nanotube ropes*. Appl. Phys. Lett. **74**, 3803–3805 (1999).
32. B Bhushan. Springer. Springer Handbook of Nanotechnology. (2007).
33. J. H. Hafner, C. L. Cheung, A. T. Wooley, C.M. Lieber: *Structural and functional imaging with carbon nanotube AFM probes*, Progr. Biophys. Molec. Biol. **77**, 73–110 (2001).
34. W. A. de Heer, A. Châtelain, D. Ugarte: *A carbon nanotube field-emission electron source*, Science **270**, 1179–1180 (1995).
35. Igor Pochorovski, Huiliang Wang, Jeremy I. Feldblyum, Xiaodong Zhang, Alexander L. Antaris, and Zhenan Bao. *H-Bonded Supramolecular Polymer for the Selective Dispersion and Subsequent Release of Large-Diameter Semiconducting Single-Walled Carbon Nanotubes*. J. Am. Chem. Soc., **137** (13), 4328–4331, (2015).
36. P. G. Collins, P. Avouris, *Nanotubes for electronics*, Sci. Am., **283**, 62, (2000).
37. S. Frank, P. Poncharal, Z. L. Wang, W. A. Heer, *Carbon nanotube quantum resistors*, Science, **280**, 1744, (1998).
38. G. O. Shonaike, S. G. Advani, *Advanced Polymeric Materials: Structure Property Relationships*, CRC Press, Boca Raton, FL, USA (2003).

39. J-H. Du, J. Bai, H-M. Cheng. *The present status and key problems of carbon nanotube based polymer composites*, Express Polymer Lett. **1** 253–273, (2007)
40. Shaffer M. S. P., Windle A. H. *Fabrication and characterization of carbon nanotubes/poly(vinyl alcohol) composites*. Adv. Mater., **11**, 937–941 (1999).
41. Berber S., Kwon Y-K., Tománek D.: *Unusually high thermal conductivity of carbon nanotubes*. Physical Review Letters, **84**, 4613–4616 (2000).
42. Kim P., Shi L., Majumdar A., McEuen P. L.: *Thermal transport measurements of individual multiwalled nanotubes*. Phys. Rev. Lett. **87**, 215502–215505 (2000).
43. Wei C. Y., Srivastava D., Cho K.: *Thermal expansion and diffusion coefficients of carbon nanotube polymer composites*. Nano Letters, **2** 647–650 (2002).
44. Dasari, A.; Yu, Z.Z.; Mai, Y.W. *Electrically conductive and super-tough polyamide-based nanocomposites*. Polymer, **50** (16), 4112–4121, (2009).
45. Jin, Z.; Pramoda, K.P.; Xu, G.; Goh, S.H. *Dynamic mechanical behavior of melt-processed multi-walled carbon nanotube poly(methyl methacrylate) composites*. Chem. Phys. Lett. **337** (1–3), 43–47, (2001).
46. Kwon, J.Y.; Kim, H.D. *Preparation and properties of acid-treated multiwalled carbon nanotube, waterborne polyurethane nanocomposites*. J. Appl. Polym. Sci. **96** (2), 595–604, (2005).
47. Coleman, J.N.; Curran, S.; Dalton, A.B.; Davey, A.P.; McCarthy, B.; Blau, W.; Barklie, R.C. *Percolation-dominated conductivity in a conjugated-polymer-carbon-nanotube composite*. Phys. Rev. B, **58** (12), 7492–7495, (1998).
48. Geng, Y.; Liu, M.Y.; Li, J.; Shi, X.M.; Kim, J.K. *Effects of surfactant treatment on mechanical and electrical properties of CNT/epoxy nanocomposites*. Compos. Pt. A, **39** (12), 1876–1883, (2008).
49. Chunying Min, Xiangqian Shen, Zhou Shi, Lei Chen, and Zhiwei Xu. *The Electrical Properties and Conducting Mechanisms of Carbon Nanotube/Polymer Nanocomposites: A Review*, Polymer-Plastics Tech. and Eng. **49**: 1172–1181, (2010).
50. Jianhua Zou, Liwei Liu, Hui Chen, Saiful I. Khondaker, Richard D. McCullough, Qun Huo,\* and Lei Zhai. *Dispersion of Pristine Carbon Nanotubes Using Conjugated Block Copolymers*, Adv. Mater, **20**, 2055-2060, (2008).
51. Xiao-Lin Xie, b, Yiu-Wing Ma, Xing-Ping Zhou. *Dispersion and alignment of carbon nanotubes in polymer matrix: A review*, Mater. Sci. and Eng. R: Reports, **49** 4 89–112, (2005).

52. D. Qian, E.C. Dickey, R. Andrews, T. Rantell. *Load transfer and deformation mechanisms in carbon nanotube-polystyrene composites*. Appl. Phys. Lett., **76**, p.2868, (2000).
53. J. Sandler, M.S.P. Shaffer, T. Prasse, W. Bauhofer, K. Schulte, A.H. Windle, *Development of a dispersion process for carbon nanotubes in an epoxy matrix and the resulting electrical properties*, Polymer, **40**, 5967, (1999).
54. J.E. Riggs, Z. Guo, D.L. Carroll, Y.P. Sun, *Strong Luminescence of Solubilized Carbon Nanotubes*, J. Am. Chem. Soc. **122** 5879, (2000).
55. Y. Lin, B. Zhou, K.A.S. Fernando, P. Liu, Y.P. Sun, *Polymeric Carbon Nanocomposites from Carbon Nanotubes Functionalized with Matrix Polymer*, Macromolecules, **36**, 7199, (2003).
56. J.H. Fan, M.X. Wan, D.B. Zhu, B.H. Chang, Z.W. Pan, S.S. Xie. J. Appl. Polym. Sci., **74**, p. 2605 (1999).
57. Alexander Star, J. Fraser Stoddart, David Steuerman, Mike Diehl, Akram Boukai, Eric W. Wong, Xin Yang, Sung-Wook Chung, Hyeon Choi, and James R. Heath. *Preparation and Properties of Polymer-Wrapped Single-Walled Carbon Nanotubes*. Angew. Chem. Int. Ed. **40**, No. 9, (2001).
58. Q.F. Xiao, X. Zhou, *The study of multiwalled carbon nanotube deposited with conducting polymer for supercapacitor*, Elec. chem. Act. **48**, 575, (2003).
59. Jianhua Zou, Liwei Liu, Hui Chen, Saiful I. Khondaker, Richard D. McCullough, Qun Huo,\* and Lei Zhai. *Dispersion of Pristine Carbon Nanotubes Using Conjugated Block Copolymers*, 20, 4, 2055–2060 (2008).
60. Karimulla Mulla and Yuming Zhao. *When Dithiafulvenyl functionalized  $\pi$ -conjugated oligomers meet fullerenes and single-walled carbon nanotubes*, J. Mater. Chem. C, **1**, 5116-5127, (2013).
61. E. Torres and G. DiLabio, *Dispersion-Correcting Potentials for DFT functionals*, J. Phys. Chem. Lett. **3**, 1738-1744, (2012).
62. [http://www.gaussian.com/g\\_tech/g\\_ur/k\\_dft.htm](http://www.gaussian.com/g_tech/g_ur/k_dft.htm).
63. V. Barone, M. Casarin, D. Forrer, M. Pavone, M. Sambi, and A. Vittadini, *Role and effective treatment of dispersive forces in materials: polyethylene and graphite crystals as test case*. J. of Compute. Chem. **30** 6 934–939, (2009).
64. H.Dorsett and A. White, *Overview of Molecular Modelling and Ab initio molecular Orbital Methods suitable for Use with Energetic Materials*. DSTO-GD-0253.

65. John P. Perdew, *Density Gradient Expansion of the Electronic Exchange correlation Energy and its Generalization*, **337**, 51-64, (1995).
66. Attila Szabo & Neil S. Ostlund, *Modern Quantum Chemistry, Introduction to Advanced Electronic Structure Theory*.
67. T. Tsuneda, *Density Functional Theory in Quantum Chemistry*, © Springer Japan (2014).
68. I.N. Levine, *Quantum Chemistry*. Prentice Hall, Engelwood Cliff, New Jersey, (2000).
69. C. C. J. Roothaan, *New Developments in Molecular Orbital Theory*. Rev. Mod. Phys. **23** 69-89 (1951).
70. J.B. Foresman and A. Frisch. *Exploring Chemistry with Electronic Structure Methods*. Gaussian Inc. (1994).
71. Amusia, M. Ya., *Atomic Photoeffect* (Plenum Press, New York–London, 1990).
72. Axel D. Becke, Perspective: *Fifty years of density-functional theory in chemical physics*. J. Chem. Phys. **140**, 18A301 (2014).
73. M.Ya. Amusia, A.Z. Msezane, V.R. Shaginyan, *Density Functional Theory versus the Hartree Fock Method: Comparative Assessment*. Physica Scripta. **68**, C133–140, (2003).
74. Kieron Burke and friends, *The ABC of DFT*, Department of Chemistry, University of California, Irvine, April 10, (2007).
75. Klaus Capelle, *A Bird's-Eye View of Density-Functional Theory*, Departamento de Física e Informática, Instituto de Física de São Carlos Universidade de São Paulo.
76. Robert G. Parr and Yang Weitao, *Density-Functional Theory of the electronic structure of molecules*, Ann. Rev. Phys. Chem. **46**: 701-28 (1995)
77. R Peverati, *Advances in Theoretical Description of Molecules and their Environment Density Functional Theory and Continuum Solvation Models*, Zürich, (2010).
78. John P. Perdew and Karla Schmidt, *Jacob's ladder of density functional approximations for the exchange-correlation energy*, AIP Conf. Proc. **577**,1 (2001).
79. T. Ziegler and M. Seth, M. Krykunov, J. Autschbaach, and F. Wang, *On the relation between time-dependent and variational density functional theory approaches for the*

- determination of excitation energies and transition moments, *chem. Phys.* **130**, 154102 (2009).
80. U. von Barth and L. Hedin, *A local exchange-correlation potential for the spin polarized case:I*. J. Phys. C: Solid State Phys.**5**, (1972).
  81. O. Gunnarsson and B. I. Lundqvist, *Exchange and correlation in atoms, molecules, and solids by the spin-density-functional formalism* , Phys. Rev. B **13**, 4274 (1976).
  82. Kohn, W. and Sham, L. J. *Self-Consistent Equations Including Exchange and Correlation Effects*, Phys. Rev. **140**, A1133 (1965).
  83. P. A. M. Dirac *Proc. Note on Exchange Phenomena in the Thomas Atom*, Cambridge Phil. Soc. **26**, 376 (1930).
  84. D. M. Ceperley and B. J. Alder, *Ground State of the Electron Gas by a Stochastic Method*, Phys. Rev. Lett. **45**, 566 (1980).
  85. John P. Perdew, Kieron Burke, and Matthias Ernzerhof, *Generalized Gradient Approximation Made Simple*. Phys. Rev. Lett. **77**, 3865 1996.
  86. John P. Perdew and Wang Yue, *Accurate and simple density functional for the electronic exchange energy: Generalized gradient approximation*. Department of Physics and Quantum Theory Group, Tulane University.
  87. A. D. Becke, *Density-functional exchange-energy approximation with correct asymptotic behavior*, Phys. Rev. A. **38**, 3098 (1988).
  88. C. Lee, W. Yang and R. G. Parr, *Development of the Colle-Salvetti correlation-energy formula into a functional of the electron density*, Phys. Rev. B **37**, 785 (1988).
  89. S. Kraft, A. C. Grimsdale and A. B. Holmes, *Angew. Electroluminescent Conjugated Polymers—Seeing Polymers in a New Light*, Chem. Int. Ed. **37**, 402-428 (1998).
  90. Hobza, P.; Sponer, J.; Reschel, T, *Density functional theory and molecular clusters*, J. Comp. Chem. **11**, 1315. (1995).
  91. Stefan Grimme, *Semiempirical GGA-Type Density Functional Constructed with a Long-Range Dispersion Correction*. J Comp. Chem. **27** 1787–1799, (2006).
  92. Hartmut L. Schmider and Axel D. Becke, *Optimized density functionals from the extended G2 test set*. J. Chem. Phys. **108**, 9624 (1998).

93. Yoshihiro Tawada, Takao Tsuneda, Susumu Yanagisawa, Takeshi Yanai, and Kimihiko Hirao, *A long-range-corrected time-dependent density functional theory*, J. Chem. Phys. **120**, 8425 (2004).
94. Takeshi Yanaia, David P Tewb, Nicholas C Handyb, *A new hybrid exchange–correlation functional using the Coulomb-attenuating method (CAM-B3LYP)*, Chem. Phys Lett, **393** 51–57, (2004).
95. Roger D. Amos, Rika Kobayashi, *The application of CAM-B3LYP to the charge-transfer band problem of the zincbacteriochlorin–bacteriochlorin complex* Chem. Phys Lett. **420** 106-109 (2009).
96. Thierry Leiningera, Hermann Stolla, Hans-Joachim Wernera, Andreas Savin, *Combining long-range configuration interaction with short-range density functionals*. Chem. Phys. Lett. **275**, 151–160 (1997).
97. Jeng-Da Chai and Martin Head-Gordon, *Systematic optimization of long-range corrected hybrid density functionals*. J. Chem. Phys. **128**, 084106 (2008).
98. Gaussian 09, Revision D.01, M. J. Frisch, G. W. Trucks, H. B. Schlegel, G. E. Scuseria, M. A. Robb, J. R. Cheeseman, G. Scalmani, V. Barone, B. Mennucci, G. A. Petersson, H. Nakatsuji, M. Caricato, X. Li, H. P. Hratchian, A. F. Izmaylov, J. Bloino, G. Zheng, J. L. Sonnenberg, M. Hada, M. Ehara, K. Toyota, R. Fukuda, J. Hasegawa, M. Ishida, T. Nakajima, Y. Honda, O. Kitao, H. Nakai, T. Vreven, J. A. Montgomery, Jr., J. E. Peralta, F. Ogliaro, M. Bearpark, J. J. Heyd, E. Brothers, K. N. Kudin, V. N. Staroverov, R. Kobayashi, J. Normand, K. Raghavachari, A. Rendell, J. C. Burant, S. S. Iyengar, J. Tomasi, M. Cossi, N. Rega, J. M. Millam, M. Klene, J. E. Knox, J. B. Cross, V. Bakken, C. Adamo, J. Jaramillo, R. Gomperts, R. E. Stratmann, O. Yazyev, A. J. Austin, R. Cammi, C. Pomelli, J. W. Ochterski, R. L. Martin, K. Morokuma, V. G. Zakrzewski, G. A. Voth, P. Salvador, J. J. Dannenberg, S. Dapprich, A. D. Daniels, Ö. Farkas, J. B. Foresman, J. V. Ortiz, J. Cioslowski, and D. J. Fox, Gaussian, Inc., Wallingford CT, 2009.
99. Austin Dwyer, *Weak interactions and excited states from Coulomb-attenuated DFT*. Department of Chemistry Durham University, 2011.
100. Michelle M. Francl, William J. Pietro, Warren J. Hehre, J. Stephen Binkley, Mark S. Gordon, Douglas J. DeFrees and John A. Pople. *Self-consistent molecular orbital methods. XXIII. A polarization-type basis set for second-row elements*. J. Chem. Phys. **77**, 3654 (1982).
101. GaussView (Version 5.0) Visualization Software. Semichem Inc., Shawnee Mission KS, 2009.

102. VMD for WIN32, version 1.9.1 (February 1. 2012),  
[www.ks.uiuc.edu/Research/vmd](http://www.ks.uiuc.edu/Research/vmd).
103. Ahmad Irfan, Abdullah G. Al-Sehemi, *DFT study of the electronic and charge transfer properties of perfluoroarene–thiophene oligomers*, J Saudi Chem. Soc. **18**, 574–580, (2014).
104. <http://www.wolfram.com/mathematica/>.
105. J. Muscata, A. Wanderb, N.M. Harrisonb. *On the prediction of band gaps from hybrid functional theory*. Chem. Phy. Lett **342**, 397–401, (2001).

# Appendix

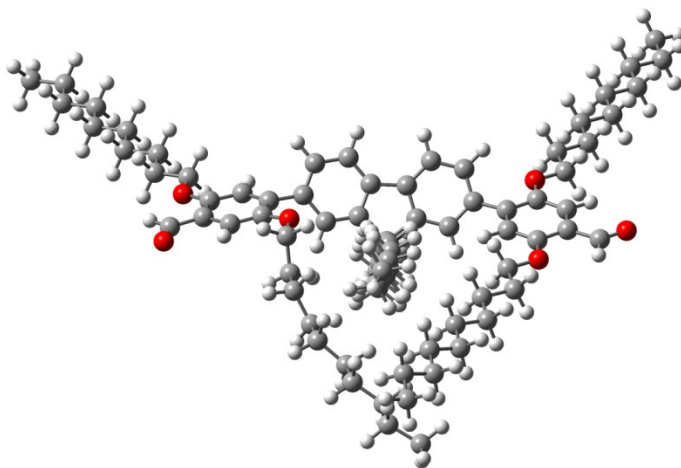


Figure A.1: Molecular (optimized with DFT/B97D) structure of fluorene-based ALD-encapped oligomer with SCs.

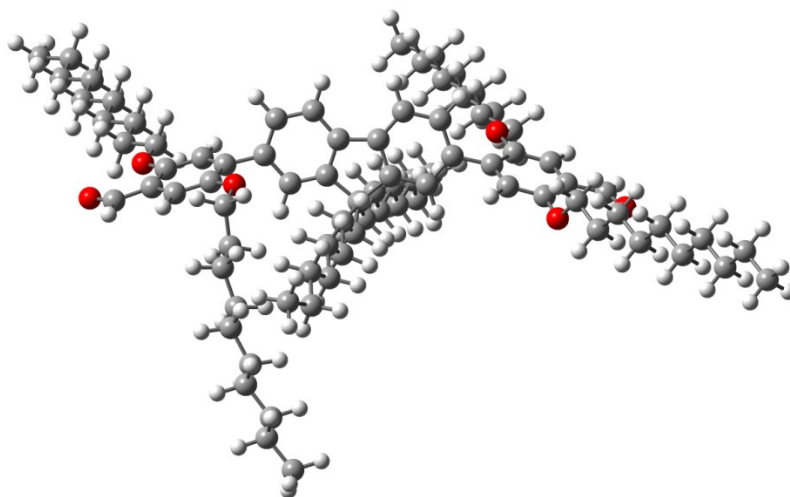


Figure A.2: Molecular (optimized with DFT/wB97XD) structure of fluorene-based ALD-encapped oligomer with SCs.



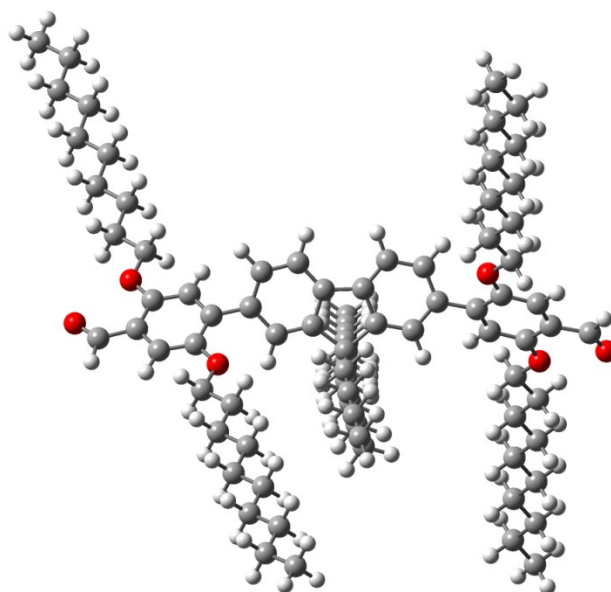


Figure A.3: Molecular (optimized with DFT/CAM-B3LYP) structure of fluorene-based ALD-endcapped oligomer with SCs.

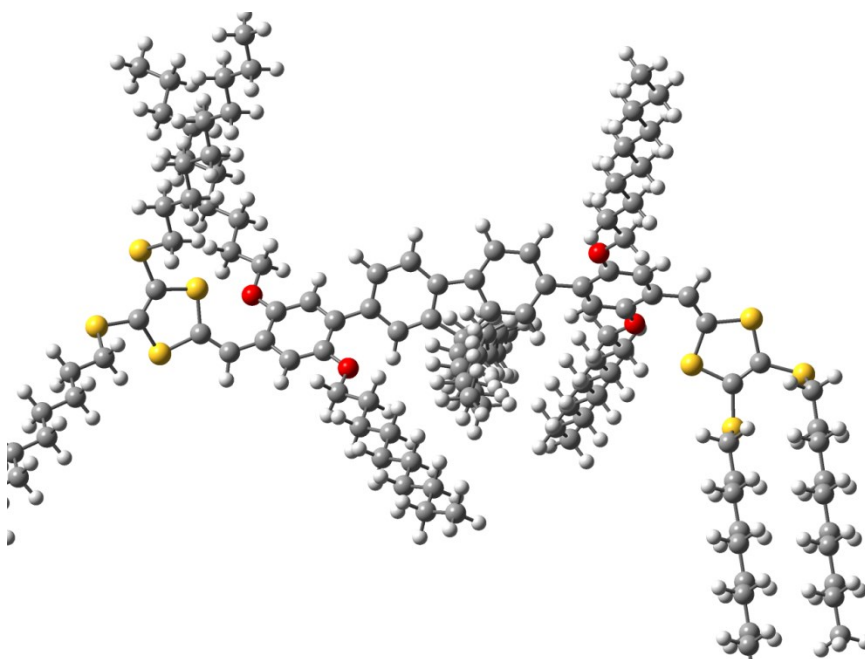


Figure A.4: Molecular (optimized with DFT/B97D) structure of fluorene-based DTF-endcapped oligomer with SCs.

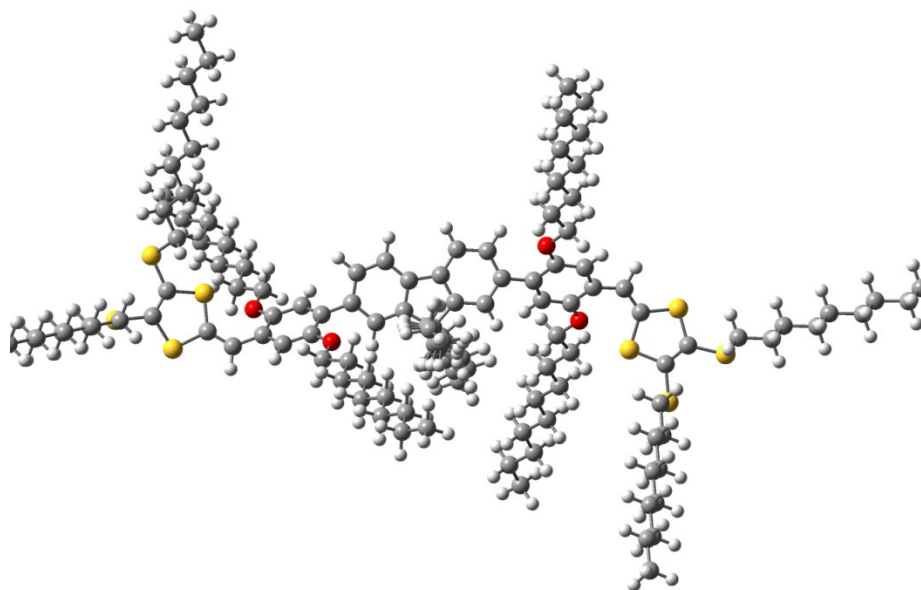


Figure A.5: Molecular (optimized with DFT/wB97XD) structure of fluorene-based DTF-endcapped oligomer with SCs.

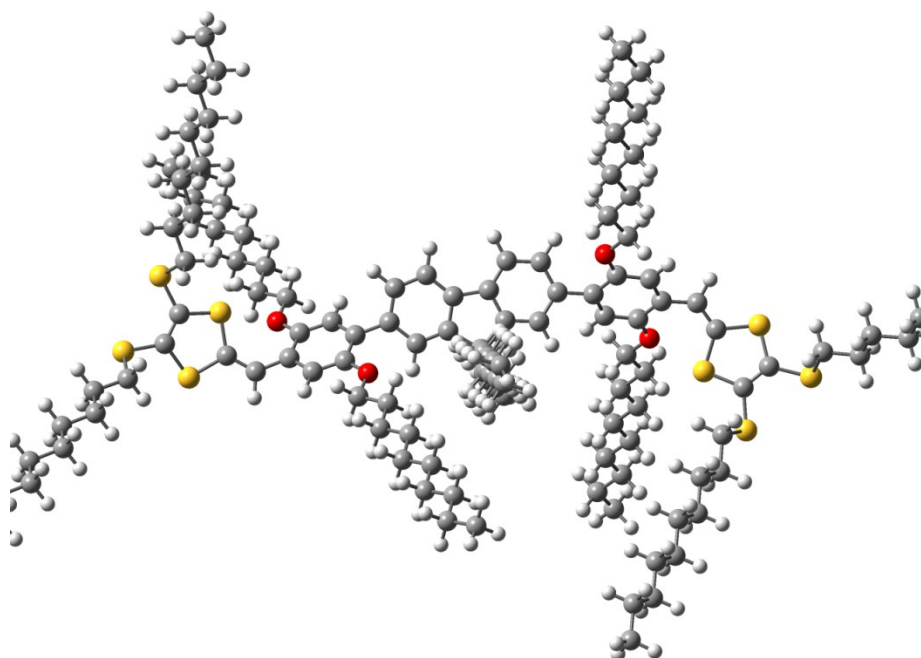


Figure A.6: Molecular (optimized with DFT/CAM-B3LYP) structure of fluorene-based DTF-endcapped oligomer with SCs.

Table A.1: Bond lengths (in Angstrom) for ALD-endcapped oligomers without SCs as a function of different dispersion corrected DFT methods.

| Bond Length<br>(R) | B97D  | wB97XD | CAM-<br>B3LYP | B3LYP |
|--------------------|-------|--------|---------------|-------|
| R <sub>1-2</sub>   | 1.482 | 1.480  | 1.476         | 1.478 |
| R <sub>2-3</sub>   | 1.412 | 1.398  | 1.396         | 1.403 |
| R <sub>3-4</sub>   | 1.393 | 1.385  | 1.383         | 1.387 |
| R <sub>4-5</sub>   | 1.419 | 1.403  | 1.403         | 1.411 |
| R <sub>5-6</sub>   | 1.481 | 1.484  | 1.482         | 1.483 |
| R <sub>6-7</sub>   | 1.418 | 1.403  | 1.401         | 1.409 |
| R <sub>7-8</sub>   | 1.399 | 1.390  | 1.388         | 1.393 |
| R <sub>8-9</sub>   | 1.405 | 1.391  | 1.390         | 1.397 |
| R <sub>9-10</sub>  | 1.463 | 1.467  | 1.466         | 1.465 |
| R <sub>10-11</sub> | 1.405 | 1.391  | 1.390         | 1.397 |
| R <sub>11-12</sub> | 1.399 | 1.390  | 1.388         | 1.393 |
| R <sub>12-13</sub> | 1.418 | 1.402  | 1.410         | 1.409 |
| R <sub>13-14</sub> | 1.481 | 1.483  | 1.482         | 1.482 |
| R <sub>14-15</sub> | 1.416 | 1.400  | 1.399         | 1.407 |
| R <sub>15-16</sub> | 1.397 | 1.388  | 1.387         | 1.391 |
| R <sub>16-17</sub> | 1.410 | 1.395  | 1.393         | 1.401 |
| R <sub>17-18</sub> | 1.482 | 1.480  | 1.476         | 1.478 |

Table A.2: Bond lengths (in Angstrom) for DTF-endcapped oligomers without SCs as a function of different dispersion corrected DFT methods.

| Bond Length<br>(R) | B97D  | wB97XD | CAM-<br>B3LYP | B3LYP |
|--------------------|-------|--------|---------------|-------|
| R <sub>1-2</sub>   | 1.457 | 1.465  | 1.462         | 1.458 |
| R <sub>2-3</sub>   | 1.419 | 1.402  | 1.401         | 1.410 |
| R <sub>3-4</sub>   | 1.396 | 1.389  | 1.387         | 1.391 |
| R <sub>4-5</sub>   | 1.414 | 1.398  | 1.397         | 1.405 |
| R <sub>5-6</sub>   | 1.480 | 1.483  | 1.482         | 1.481 |
| R <sub>6-7</sub>   | 1.418 | 1.403  | 1.402         | 1.410 |
| R <sub>7-8</sub>   | 1.399 | 1.390  | 1.389         | 1.393 |
| R <sub>8-9</sub>   | 1.405 | 1.391  | 1.389         | 1.397 |
| R <sub>9-10</sub>  | 1.463 | 1.468  | 1.467         | 1.466 |
| R <sub>10-11</sub> | 1.405 | 1.391  | 1.389         | 1.397 |
| R <sub>11-12</sub> | 1.399 | 1.390  | 1.386         | 1.393 |
| R <sub>12-13</sub> | 1.418 | 1.402  | 1.402         | 1.409 |
| R <sub>13-14</sub> | 1.480 | 1.482  | 1.482         | 1.481 |
| R <sub>14-15</sub> | 1.416 | 1.400  | 1.399         | 1.407 |
| R <sub>15-16</sub> | 1.393 | 1.385  | 1.383         | 1.387 |
| R <sub>16-17</sub> | 1.422 | 1.404  | 1.403         | 1.412 |
| R <sub>17-18</sub> | 1.457 | 1.464  | 1.462         | 1.458 |

Table A.3: Bond lengths (in Angstrom) for ALD-endcapped oligomers with SCs as a function of different dispersion corrected DFT methods.

| Bond Length<br>(R) | B97D  | wB97XD | CAM-<br>B3LYP | B3LYP |
|--------------------|-------|--------|---------------|-------|
| R <sub>1-2</sub>   | 1.480 | 1.479  | 1.476         | 1.477 |
| R <sub>2-3</sub>   | 1.414 | 1.407  | 1.405         | 1.414 |
| R <sub>3-4</sub>   | 1.399 | 1.400  | 1.396         | 1.400 |
| R <sub>4-5</sub>   | 1.424 | 1.390  | 1.394         | 1.403 |
| R <sub>5-6</sub>   | 1.483 | 1.488  | 1.485         | 1.487 |
| R <sub>6-7</sub>   | 1.416 | 1.400  | 1.380         | 1.408 |
| R <sub>7-8</sub>   | 1.404 | 1.394  | 1.390         | 1.394 |
| R <sub>8-9</sub>   | 1.406 | 1.390  | 1.388         | 1.396 |
| R <sub>9-10</sub>  | 1.470 | 1.469  | 1.467         | 1.465 |
| R <sub>10-11</sub> | 1.404 | 1.391  | 1.390         | 1.396 |
| R <sub>11-12</sub> | 1.406 | 1.390  | 1.389         | 1.393 |
| R <sub>12-13</sub> | 1.412 | 1.400  | 1.401         | 1.409 |
| R <sub>13-14</sub> | 1.485 | 1.486  | 1.485         | 1.486 |
| R <sub>14-15</sub> | 1.404 | 1.409  | 1.408         | 1.417 |
| R <sub>15-16</sub> | 1.409 | 1.387  | 1.386         | 1.392 |
| R <sub>16-17</sub> | 1.421 | 1.403  | 1.398         | 1.405 |
| R <sub>17-18</sub> | 1.482 | 1.480  | 1.476         | 1.477 |

Table A.4: Bond lengths (in Angstrom) for DTF-endcapped oligomers with SCs as a function of different dispersion corrected DFT methods.

| Bond Length<br>(R) | B97D  | wB97XD | CAM-<br>B3LYP | B3LYP |
|--------------------|-------|--------|---------------|-------|
| R <sub>1-2</sub>   | 1.465 | 1.470  | 1.468         | 1.466 |
| R <sub>2-3</sub>   | 1.422 | 1.403  | 1.402         | 1.411 |
| R <sub>3-4</sub>   | 1.404 | 1.395  | 1.393         | 1.397 |
| R <sub>4-5</sub>   | 1.409 | 1.393  | 1.394         | 1.403 |
| R <sub>5-6</sub>   | 1.483 | 1.484  | 1.485         | 1.486 |
| R <sub>6-7</sub>   | 1.416 | 1.400  | 1.400         | 1.409 |
| R <sub>7-8</sub>   | 1.402 | 1.392  | 1.390         | 1.394 |
| R <sub>8-9</sub>   | 1.404 | 1.389  | 1.388         | 1.396 |
| R <sub>9-10</sub>  | 1.465 | 1.468  | 1.468         | 1.465 |
| R <sub>10-11</sub> | 1.405 | 1.391  | 1.390         | 1.397 |
| R <sub>11-12</sub> | 1.401 | 1.390  | 1.389         | 1.393 |
| R <sub>12-13</sub> | 1.417 | 1.402  | 1.400         | 1.409 |
| R <sub>13-14</sub> | 1.483 | 1.484  | 1.485         | 1.486 |
| R <sub>14-15</sub> | 1.420 | 1.404  | 1.405         | 1.414 |
| R <sub>15-16</sub> | 1.402 | 1.391  | 1.389         | 1.393 |
| R <sub>16-17</sub> | 1.418 | 1.403  | 1.401         | 1.409 |
| R <sub>17-18</sub> | 1.463 | 1.469  | 1.467         | 1.465 |

Table A.5: Bond angles (in degree) for ALD-endcapped oligomers without SCs as a function of different dispersion corrected DFT methods.

| Bond angle<br>(A)     | B97D  | wB97XD | CAM-<br>B3LYP | B3LYP |
|-----------------------|-------|--------|---------------|-------|
| A <sub>1-2-3</sub>    | 120.9 | 120.4  | 120.3         | 120.6 |
| A <sub>2-3-4</sub>    | 120.2 | 120.0  | 120.1         | 120.2 |
| A <sub>3-4-5</sub>    | 121.0 | 120.8  | 120.9         | 121.1 |
| A <sub>4-5-6</sub>    | 120.9 | 120.6  | 120.8         | 120.9 |
| A <sub>5-6-7</sub>    | 120.6 | 120.3  | 120.5         | 120.6 |
| A <sub>6-7-8</sub>    | 121.6 | 121.3  | 121.4         | 121.6 |
| A <sub>7-8-9</sub>    | 119.0 | 118.9  | 119.0         | 119.1 |
| A <sub>8-9-10</sub>   | 131.1 | 131.2  | 131.3         | 131.4 |
| A <sub>9-10-11</sub>  | 131.1 | 131.2  | 131.3         | 131.4 |
| A <sub>10-11-12</sub> | 118.9 | 118.3  | 119.0         | 119.1 |
| A <sub>11-12-13</sub> | 121.6 | 121.3  | 121.5         | 121.6 |
| A <sub>12-13-14</sub> | 120.6 | 120.4  | 120.5         | 120.7 |
| A <sub>13-14-15</sub> | 120.9 | 120.7  | 120.8         | 120.9 |
| A <sub>14-15-16</sub> | 120.7 | 120.6  | 120.7         | 120.8 |
| A <sub>15-16-17</sub> | 120.5 | 120.3  | 120.3         | 120.5 |
| A <sub>16-17-18</sub> | 119.8 | 120.0  | 120.2         | 120.2 |

Table A.6: Bond angles (in degree) for DTF-endcapped oligomers without SCs as a function of different dispersion corrected DFT methods.

| Bond angle<br>(A)     | B97D  | wB97XD | CAM-<br>B3LYP | B3LYP |
|-----------------------|-------|--------|---------------|-------|
| A <sub>1-2-3</sub>    | 125.6 | 124.2  | 124.9         | 125.5 |
| A <sub>2-3-4</sub>    | 121.2 | 121.0  | 121.1         | 121.3 |
| A <sub>3-4-5</sub>    | 121.8 | 121.3  | 121.5         | 121.8 |
| A <sub>4-5-6</sub>    | 121.4 | 121.1  | 121.3         | 121.5 |
| A <sub>5-6-7</sub>    | 120.7 | 120.4  | 120.6         | 120.8 |
| A <sub>6-7-8</sub>    | 121.7 | 121.4  | 121.5         | 121.7 |
| A <sub>7-8-9</sub>    | 119.0 | 118.9  | 119.0         | 119.2 |
| A <sub>8-9-10</sub>   | 131.3 | 131.2  | 131.4         | 131.5 |
| A <sub>9-10-11</sub>  | 131.3 | 131.2  | 131.4         | 131.5 |
| A <sub>10-11-12</sub> | 119.0 | 118.9  | 119.1         | 119.2 |
| A <sub>11-12-13</sub> | 121.7 | 121.4  | 121.5         | 121.7 |
| A <sub>12-13-14</sub> | 120.8 | 120.5  | 120.7         | 120.8 |
| A <sub>13-14-15</sub> | 121.5 | 121.2  | 121.3         | 121.5 |
| A <sub>14-15-16</sub> | 121.2 | 120.9  | 121.1         | 121.2 |
| A <sub>15-16-17</sub> | 121.8 | 121.5  | 121.6         | 121.9 |
| A <sub>16-17-18</sub> | 117.6 | 118.1  | 118.0         | 117.8 |



Table A.7: Bond angles (in degree) for ALD-endcapped oligomers with SCs as a function of different dispersion corrected DFT methods.

| Bond angle<br>(A)     | B97D  | wB97XD | CAM-<br>B3LYP | B3LYP |
|-----------------------|-------|--------|---------------|-------|
| A <sub>1-2-3</sub>    | 118.8 | 124.0  | 124.2         | 124.5 |
| A <sub>2-3-4</sub>    | 122.0 | 118.7  | 118.6         | 118.6 |
| A <sub>3-4-5</sub>    | 119.2 | 121.3  | 122.2         | 122.6 |
| A <sub>4-5-6</sub>    | 124.9 | 121.8  | 119.2         | 118.8 |
| A <sub>5-6-7</sub>    | 122.9 | 121.6  | 119.7         | 119.5 |
| A <sub>6-7-8</sub>    | 121.1 | 120.8  | 121.4         | 121.6 |
| A <sub>7-8-9</sub>    | 119.3 | 118.9  | 118.9         | 119.0 |
| A <sub>8-9-10</sub>   | 132.3 | 131.5  | 131.2         | 131.3 |
| A <sub>9-10-11</sub>  | 132.1 | 131.2  | 131.3         | 131.3 |
| A <sub>10-11-12</sub> | 119.0 | 118.9  | 119.2         | 119.4 |
| A <sub>11-12-13</sub> | 121.1 | 121.0  | 121.2         | 121.3 |
| A <sub>12-13-14</sub> | 122.2 | 120.9  | 121.7         | 121.8 |
| A <sub>13-14-15</sub> | 121.0 | 119.5  | 122.5         | 122.8 |
| A <sub>14-15-16</sub> | 121.3 | 119.7  | 119.2         | 119.2 |
| A <sub>15-16-17</sub> | 119.1 | 121.2  | 122.2         | 122.4 |
| A <sub>16-17-18</sub> | 122.1 | 116.8  | 116.7         | 116.7 |

Table A.8: Bond angles (in degree) for DTF-endcapped oligomers with SCs as a function of different dispersion corrected DFT methods.

| Bond angle<br>(A)     | B97D  | wB97XD | CAM-<br>B3LYP | B3LYP |
|-----------------------|-------|--------|---------------|-------|
| A <sub>1-2-3</sub>    | 125.0 | 123.7  | 124.2         | 125.1 |
| A <sub>2-3-4</sub>    | 119.9 | 119.8  | 119.8         | 119.8 |
| A <sub>3-4-5</sub>    | 122.3 | 121.7  | 122.2         | 122.7 |
| A <sub>4-5-6</sub>    | 119.9 | 120.2  | 119.5         | 119.1 |
| A <sub>5-6-7</sub>    | 119.8 | 120.1  | 119.8         | 119.5 |
| A <sub>6-7-8</sub>    | 121.6 | 121.3  | 121.5         | 121.8 |
| A <sub>7-8-9</sub>    | 118.9 | 118.8  | 119.0         | 119.1 |
| A <sub>8-9-10</sub>   | 131.7 | 131.4  | 131.4         | 131.4 |
| A <sub>9-10-11</sub>  | 131.9 | 131.5  | 131.5         | 131.4 |
| A <sub>10-11-12</sub> | 119.2 | 119.1  | 119.3         | 119.4 |
| A <sub>11-12-13</sub> | 121.2 | 121.0  | 121.2         | 121.4 |
| A <sub>12-13-14</sub> | 122.2 | 121.5  | 121.9         | 121.9 |
| A <sub>13-14-15</sub> | 124.8 | 124.0  | 123.5         | 123.1 |
| A <sub>14-15-16</sub> | 119.6 | 119.4  | 119.6         | 119.7 |
| A <sub>15-16-17</sub> | 122.7 | 122.2  | 122.4         | 122.7 |
| A <sub>16-17-18</sub> | 117.6 | 118.0  | 117.7         | 117.2 |

Table A.9: Dihedral angles (in degree) for ALD-endcapped oligomers without SCs as a function of different dispersion corrected DFT methods.

| Dihedral angle<br>(D)    | B97D   | wB97XD | CAM-<br>B3LYP | B3LYP |
|--------------------------|--------|--------|---------------|-------|
| D <sub>1-2-3-4</sub>     | 179.9  | 179.9  | -180.0        | 180.0 |
| D <sub>2-3-4-5</sub>     | 0.1    | -0.1   | -0.1          | 0.1   |
| D <sub>3-4-5-6</sub>     | -179.9 | -179.7 | -180.0        | 179.9 |
| D <sub>4-5-6-7</sub>     | -33.5  | 41.2   | 38.3          | 36.4  |
| D <sub>5-6-7-8</sub>     | -180.0 | 180.0  | 179.9         | 179.9 |
| D <sub>6-7-8-9</sub>     | -0.1   | 0.1    | 0.1           | 0.2   |
| D <sub>7-8-9-10</sub>    | -179.6 | 179.6  | 179.8         | 179.7 |
| D <sub>8-9-10-11</sub>   | 0.0    | 0.1    | 0.5           | 0.6   |
| D <sub>9-10-11-12</sub>  | 179.6  | -179.7 | 179.8         | 179.7 |
| D <sub>10-11-12-13</sub> | 0.1    | -0.1   | 0.1           | 0.2   |
| D <sub>11-12-13-14</sub> | -179.9 | 180.0  | -180.0        | 180.0 |
| D <sub>12-13-14-15</sub> | 33.6   | -41.4  | 38.3          | 36.6  |
| D <sub>13-14-15-16</sub> | 179.9  | -180.0 | 180.0         | 179.9 |
| D <sub>14-15-16-17</sub> | -0.1   | 0.1    | -0.1          | 0.1   |
| D <sub>15-16-17-18</sub> | -179.9 | 179.9  | -179.9        | 179.9 |

Table A.10: Dihedral angles (in degree) for DTF-endcapped oligomers without SCs as a function of different dispersion corrected DFT methods.

| Dihedral angle (D)       | B97D   | wB97XD | CAM-B3LYP | B3LYP |
|--------------------------|--------|--------|-----------|-------|
| D <sub>1-2-3-4</sub>     | 179.3  | 179.3  | 179.6     | 179.6 |
| D <sub>2-3-4-5</sub>     | 0.3    | 0.5    | 0.3       | 0.2   |
| D <sub>3-4-5-6</sub>     | -179.8 | 180.0  | -179.9    | 179.9 |
| D <sub>4-5-6-7</sub>     | 32.6   | 41.7   | 38.1      | 36.0  |
| D <sub>5-6-7-8</sub>     | -179.8 | -179.7 | -179.9    | 180.0 |
| D <sub>6-7-8-9</sub>     | -0.1   | 0.0    | -0.1      | 0.1   |
| D <sub>7-8-9-10</sub>    | 179.7  | 179.6  | 179.8     | 179.8 |
| D <sub>8-9-10-11</sub>   | 0.7    | 1.2    | 0.6       | 0.6   |
| D <sub>9-10-11-12</sub>  | 180.0  | 179.9  | 179.9     | 179.9 |
| D <sub>10-11-12-13</sub> | -0.1   | 0.1    | 0.1       | 0.1   |
| D <sub>11-12-13-14</sub> | 179.9  | 179.7  | 180.0     | 180.0 |
| D <sub>12-13-14-15</sub> | 32.0   | 41.9   | 37.6      | 35.5  |
| D <sub>13-14-15-16</sub> | 179.9  | 180.0  | 179.9     | 179.8 |
| D <sub>14-15-16-17</sub> | -0.5   | -0.4   | -0.5      | 0.4   |
| D <sub>15-16-17-18</sub> | -179.3 | -179.8 | -179.4    | 179.4 |

Table A.11: Dihedral angles (in degree) for ALD-endcapped oligomers with SCs as a function of different dispersion corrected DFT methods.

| Dihedral angle (D)       | B97D   | wB97XD | CAM-B3LYP | B3LYP |
|--------------------------|--------|--------|-----------|-------|
| D <sub>1-2-3-4</sub>     | -179.8 | -178.7 | -179.9    | 179.9 |
| D <sub>2-3-4-5</sub>     | -0.5   | -0.5   | 0.1       | 0.5   |
| D <sub>3-4-5-6</sub>     | -179.4 | 176.7  | -179.4    | 179.5 |
| D <sub>4-5-6-7</sub>     | -48.0  | 76.3   | 47.4      | 44.6  |
| D <sub>5-6-7-8</sub>     | -166.4 | 173.1  | -178.4    | 177.0 |
| D <sub>6-7-8-9</sub>     | -0.4   | 0.0    | 0.5       | 0.5   |
| D <sub>7-8-9-10</sub>    | 169.7  | -176.0 | 179.9     | 179.0 |
| D <sub>8-9-10-11</sub>   | 0.4    | -4.4   | 0.9       | 0.8   |
| D <sub>9-10-11-12</sub>  | -170.5 | -176.7 | 179.3     | 179.7 |
| D <sub>10-11-12-13</sub> | 0.5    | -1.4   | 0.3       | 0.3   |
| D <sub>11-12-13-14</sub> | 173.3  | 175.9  | 177.9     | 177.6 |
| D <sub>12-13-14-15</sub> | 58.5   | -63.3  | 45.6      | 44.0  |
| D <sub>13-14-15-16</sub> | 175.7  | -176.4 | 178.6     | 179.2 |
| D <sub>14-15-16-17</sub> | -0.7   | -1.0   | 0.1       | 0.3   |
| D <sub>15-16-17-18</sub> | -177.7 | 179.7  | 180.0     | 180.0 |

Table A.12: Dihedral angles (in degree) for DTF-endcapped oligomers with SCs as a function of different dispersion corrected DFT methods.

| Dihedral angle<br>(D)    | B97D   | wB97XD | CAM-<br>B3LYP | B3LYP |
|--------------------------|--------|--------|---------------|-------|
| D <sub>1-2-3-4</sub>     | 177.2  | 178.6  | -179.9        | 179.4 |
| D <sub>2-3-4-5</sub>     | 2.1    | 1.7    | 1.3           | 1.6   |
| D <sub>3-4-5-6</sub>     | -177.8 | -179.4 | 180.0         | 179.1 |
| D <sub>4-5-6-7</sub>     | 44.2   | 51.5   | 45.6          | 41.6  |
| D <sub>5-6-7-8</sub>     | 178.0  | 179.3  | -177.9        | 177.5 |
| D <sub>6-7-8-9</sub>     | 0.2    | 0.2    | 0.2           | 0.1   |
| D <sub>7-8-9-10</sub>    | -179.0 | 179.7  | 179.1         | 179.7 |
| D <sub>8-9-10-11</sub>   | -1.1   | -1.3   | 0.1           | 0.7   |
| D <sub>9-10-11-12</sub>  | -175.5 | -174.4 | -177.6        | 179.7 |
| D <sub>10-11-12-13</sub> | 0.5    | 0.2    | 0.4           | 0.4   |
| D <sub>11-12-13-14</sub> | 169.4  | 168.6  | 173.8         | 177.5 |
| D <sub>12-13-14-15</sub> | 47.0   | 52.4   | 48.4          | 46.0  |
| D <sub>13-14-15-16</sub> | -179.9 | -178.1 | 179.2         | 178.1 |
| D <sub>14-15-16-17</sub> | 0.7    | -0.2   | 0.0           | 0.1   |
| D <sub>15-16-17-18</sub> | -179.8 | 178.5  | -179.9        | 179.4 |

Table A.13: Bond lengths (in Angstrom) for ALD-endcapped oligomers without SCs as a function of different dispersion corrected DFT methods for combination system.

| Bond Length<br>(R) | B97D  | wB97XD | CAM-<br>B3LYP |
|--------------------|-------|--------|---------------|
| R <sub>1-2</sub>   | 1.478 | 1.478  | 1.476         |
| R <sub>2-3</sub>   | 1.411 | 1.397  | 1.396         |
| R <sub>3-4</sub>   | 1.392 | 1.383  | 1.383         |
| R <sub>4-5</sub>   | 1.421 | 1.406  | 1.403         |
| R <sub>5-6</sub>   | 1.483 | 1.486  | 1.482         |
| R <sub>6-7</sub>   | 1.419 | 1.404  | 1.402         |
| R <sub>7-8</sub>   | 1.397 | 1.389  | 1.388         |
| R <sub>8-9</sub>   | 1.403 | 1.390  | 1.390         |
| R <sub>9-10</sub>  | 1.459 | 1.465  | 1.466         |
| R <sub>10-11</sub> | 1.403 | 1.390  | 1.390         |
| R <sub>11-12</sub> | 1.397 | 1.389  | 1.388         |
| R <sub>12-13</sub> | 1.420 | 1.405  | 1.402         |
| R <sub>13-14</sub> | 1.485 | 1.490  | 1.482         |
| R <sub>14-15</sub> | 1.419 | 1.403  | 1.399         |
| R <sub>15-16</sub> | 1.394 | 1.387  | 1.387         |
| R <sub>16-17</sub> | 1.408 | 1.393  | 1.393         |
| R <sub>17-18</sub> | 1.481 | 1.479  | 1.476         |

Table A.14: Bond lengths (in Angstrom) for DTF-endcapped oligomers without SCs as a function of different dispersion corrected DFT methods for combination system.

| Bond Length<br>(R) | B97D  | WB97XD | CAM-<br>B3LYP |
|--------------------|-------|--------|---------------|
| R <sub>1-2</sub>   | 1.453 | 1.463  | 1.461         |
| R <sub>2-3</sub>   | 1.420 | 1.403  | 1.402         |
| R <sub>3-4</sub>   | 1.395 | 1.388  | 1.387         |
| R <sub>4-5</sub>   | 1.415 | 1.399  | 1.397         |
| R <sub>5-6</sub>   | 1.480 | 1.485  | 1.482         |
| R <sub>6-7</sub>   | 1.419 | 1.404  | 1.402         |
| R <sub>7-8</sub>   | 1.398 | 1.392  | 1.389         |
| R <sub>8-9</sub>   | 1.404 | 1.391  | 1.390         |
| R <sub>9-10</sub>  | 1.461 | 1.469  | 1.466         |
| R <sub>10-11</sub> | 1.403 | 1.391  | 1.389         |
| R <sub>11-12</sub> | 1.398 | 1.392  | 1.389         |
| R <sub>12-13</sub> | 1.419 | 1.404  | 1.401         |
| R <sub>13-14</sub> | 1.479 | 1.485  | 1.482         |
| R <sub>14-15</sub> | 1.417 | 1.401  | 1.400         |
| R <sub>15-16</sub> | 1.391 | 1.385  | 1.383         |
| R <sub>16-17</sub> | 1.421 | 1.406  | 1.404         |
| R <sub>17-18</sub> | 1.455 | 1.462  | 1.461         |



Table A.15: Bond lengths (in Angstrom) for ALD-endcapped oligomers with SCs as a function of different dispersion corrected DFT methods for combination system.

| Bond Length<br>(R) | B97D  | WB97XD | CAM-<br>B3LYP |
|--------------------|-------|--------|---------------|
| R <sub>1-2</sub>   | 1.480 | 1.478  | 1.475         |
| R <sub>2-3</sub>   | 1.414 | 1.407  | 1.405         |
| R <sub>3-4</sub>   | 1.399 | 1.400  | 1.396         |
| R <sub>4-5</sub>   | 1.424 | 1.390  | 1.395         |
| R <sub>5-6</sub>   | 1.485 | 1.489  | 1.485         |
| R <sub>6-7</sub>   | 1.417 | 1.399  | 1.401         |
| R <sub>7-8</sub>   | 1.405 | 1.397  | 1.390         |
| R <sub>8-9</sub>   | 1.408 | 1.391  | 1.389         |
| R <sub>9-10</sub>  | 1.472 | 1.478  | 1.468         |
| R <sub>10-11</sub> | 1.405 | 1.393  | 1.390         |
| R <sub>11-12</sub> | 1.406 | 1.395  | 1.390         |
| R <sub>12-13</sub> | 1.413 | 1.402  | 1.402         |
| R <sub>13-14</sub> | 1.484 | 1.484  | 1.486         |
| R <sub>14-15</sub> | 1.404 | 1.405  | 1.409         |
| R <sub>15-16</sub> | 1.407 | 1.389  | 1.387         |
| R <sub>16-17</sub> | 1.421 | 1.398  | 1.398         |
| R <sub>17-18</sub> | 1.480 | 1.478  | 1.475         |

Table A.16: Bond lengths (in Angstrom) for DTF-endcapped oligomers with SCs as a function of different dispersion corrected DFT methods for combination system.

| DTF end with SCs & NT |       |        |           |
|-----------------------|-------|--------|-----------|
| Bond Length (R)       | B97D  | wB97XD | CAM-B3LYP |
| R <sub>1-2</sub>      | 1.459 | 1.467  | 1.467     |
| R <sub>2-3</sub>      | 1.424 | 1.404  | 1.401     |
| R <sub>3-4</sub>      | 1.403 | 1.392  | 1.392     |
| R <sub>4-5</sub>      | 1.407 | 1.395  | 1.394     |
| R <sub>5-6</sub>      | 1.482 | 1.485  | 1.485     |
| R <sub>6-7</sub>      | 1.416 | 1.403  | 1.400     |
| R <sub>7-8</sub>      | 1.405 | 1.391  | 1.391     |
| R <sub>8-9</sub>      | 1.405 | 1.389  | 1.389     |
| R <sub>9-10</sub>     | 1.472 | 1.468  | 1.469     |
| R <sub>10-11</sub>    | 1.407 | 1.392  | 1.390     |
| R <sub>11-12</sub>    | 1.406 | 1.391  | 1.389     |
| R <sub>12-13</sub>    | 1.419 | 1.402  | 1.401     |
| R <sub>13-14</sub>    | 1.485 | 1.485  | 1.486     |
| R <sub>14-15</sub>    | 1.421 | 1.404  | 1.403     |
| R <sub>15-16</sub>    | 1.407 | 1.392  | 1.392     |
| R <sub>16-17</sub>    | 1.410 | 1.404  | 1.396     |
| R <sub>17-18</sub>    | 1.481 | 1.469  | 1.483     |

Table A.17: Bond angles (in degree) for ALD-endcapped oligomers without SCs as a function of different dispersion corrected DFT methods for combination system.

| Bond angle<br>(A)     | B97D  | wB97XD | CAM-<br>B3LYP |
|-----------------------|-------|--------|---------------|
| A <sub>1-2-3</sub>    | 121.2 | 120.5  | 120.3         |
| A <sub>2-3-4</sub>    | 120.4 | 120.2  | 120.1         |
| A <sub>3-4-5</sub>    | 121.5 | 121.2  | 121.0         |
| A <sub>4-5-6</sub>    | 121.4 | 121.1  | 120.9         |
| A <sub>5-6-7</sub>    | 120.6 | 120.5  | 120.3         |
| A <sub>6-7-8</sub>    | 121.9 | 121.7  | 121.5         |
| A <sub>7-8-9</sub>    | 119.0 | 119.0  | 119.0         |
| A <sub>8-9-10</sub>   | 131.1 | 131.2  | 131.3         |
| A <sub>9-10-11</sub>  | 131.1 | 131.3  | 131.3         |
| A <sub>10-11-12</sub> | 119.0 | 119.0  | 119.0         |
| A <sub>11-12-13</sub> | 122.0 | 121.9  | 121.5         |
| A <sub>12-13-14</sub> | 120.7 | 120.7  | 120.7         |
| A <sub>13-14-15</sub> | 121.3 | 121.2  | 120.8         |
| A <sub>14-15-16</sub> | 121.2 | 121.2  | 120.7         |
| A <sub>15-16-17</sub> | 120.7 | 120.5  | 120.4         |
| A <sub>16-17-18</sub> | 119.9 | 120.1  | 120.2         |

Table A.18: Bond angles (in degree) for DTF-endcapped oligomers without SCs as a function of different dispersion corrected DFT methods for combination system.

| Bond angle<br>(A)     | B97D  | wB97XD | CAM-<br>B3LYP |
|-----------------------|-------|--------|---------------|
| A <sub>1-2-3</sub>    | 126.4 | 125.1  | 125.5         |
| A <sub>2-3-4</sub>    | 121.3 | 121.2  | 121.1         |
| A <sub>3-4-5</sub>    | 122.0 | 121.8  | 121.6         |
| A <sub>4-5-6</sub>    | 122.1 | 121.7  | 121.5         |
| A <sub>5-6-7</sub>    | 120.9 | 121.2  | 120.7         |
| A <sub>6-7-8</sub>    | 121.9 | 121.8  | 121.6         |
| A <sub>7-8-9</sub>    | 119.1 | 119.1  | 119.0         |
| A <sub>8-9-10</sub>   | 131.5 | 131.9  | 131.4         |
| A <sub>9-10-11</sub>  | 131.3 | 131.9  | 131.3         |
| A <sub>10-11-12</sub> | 119.0 | 119.1  | 119.1         |
| A <sub>11-12-13</sub> | 122.0 | 121.8  | 121.6         |
| A <sub>12-13-14</sub> | 120.7 | 121.1  | 120.5         |
| A <sub>13-14-15</sub> | 121.5 | 121.7  | 121.3         |
| A <sub>14-15-16</sub> | 121.4 | 121.2  | 121.1         |
| A <sub>15-16-17</sub> | 121.8 | 121.9  | 121.7         |
| A <sub>16-17-18</sub> | 117.8 | 117.4  | 117.7         |

Table A.19: Bond angles (in degree) for ALD-endcapped oligomers with SCs as a function of different dispersion corrected DFT methods for combination system.

| Bond angle<br>(A)     | B97D  | wB97XD | CAM-<br>B3LYP |
|-----------------------|-------|--------|---------------|
| A <sub>1-2-3</sub>    | 118.8 | 124.0  | 124.2         |
| A <sub>2-3-4</sub>    | 122.0 | 118.6  | 118.6         |
| A <sub>3-4-5</sub>    | 119.3 | 121.4  | 122.4         |
| A <sub>4-5-6</sub>    | 125.1 | 121.6  | 119.1         |
| A <sub>5-6-7</sub>    | 123.1 | 122.0  | 119.7         |
| A <sub>6-7-8</sub>    | 121.1 | 121.2  | 121.5         |
| A <sub>7-8-9</sub>    | 119.3 | 119.0  | 118.9         |
| A <sub>8-9-10</sub>   | 132.5 | 132.7  | 131.4         |
| A <sub>9-10-11</sub>  | 132.4 | 132.9  | 131.9         |
| A <sub>10-11-12</sub> | 119.0 | 119.4  | 119.4         |
| A <sub>11-12-13</sub> | 121.1 | 121.2  | 121.3         |
| A <sub>12-13-14</sub> | 122.0 | 123.8  | 122.9         |
| A <sub>13-14-15</sub> | 119.7 | 122.7  | 123.5         |
| A <sub>14-15-16</sub> | 121.6 | 119.7  | 119.2         |
| A <sub>15-16-17</sub> | 119.0 | 122.2  | 122.4         |
| A <sub>16-17-18</sub> | 122.1 | 117.0  | 116.9         |

Table A.20: Bond angles (in degree) for DTF-endcapped oligomers with SCs as a function of different dispersion corrected DFT methods for combination system.

| Bond angle<br>(A)     | B97D  | wB97XD | CAM-<br>B3LYP |
|-----------------------|-------|--------|---------------|
| A <sub>1-2-3</sub>    | 126.4 | 123.4  | 124.3         |
| A <sub>2-3-4</sub>    | 120.2 | 119.8  | 119.9         |
| A <sub>3-4-5</sub>    | 122.6 | 122.0  | 122.2         |
| A <sub>4-5-6</sub>    | 119.9 | 119.5  | 119.4         |
| A <sub>5-6-7</sub>    | 121.1 | 118.2  | 119.8         |
| A <sub>6-7-8</sub>    | 121.7 | 121.7  | 121.5         |
| A <sub>7-8-9</sub>    | 119.1 | 118.7  | 119.0         |
| A <sub>8-9-10</sub>   | 132.9 | 131.3  | 131.6         |
| A <sub>9-10-11</sub>  | 133.5 | 131.6  | 131.7         |
| A <sub>10-11-12</sub> | 119.7 | 119.1  | 119.3         |
| A <sub>11-12-13</sub> | 121.5 | 121.0  | 121.3         |
| A <sub>12-13-14</sub> | 125.5 | 121.5  | 121.8         |
| A <sub>13-14-15</sub> | 124.9 | 124.9  | 123.1         |
| A <sub>14-15-16</sub> | 119.6 | 119.4  | 119.6         |
| A <sub>15-16-17</sub> | 122.3 | 122.6  | 121.9         |
| A <sub>16-17-18</sub> | 120.5 | 117.7  | 119.8         |

Table A.21: Dihedral angles (in degree) for ALD-endcapped oligomers without SCs as a function of different dispersion corrected DFT methods for combination system.

| Dihedral Angle (D)       | B97D  | wB97XD | CAM-B3LYP |
|--------------------------|-------|--------|-----------|
| D <sub>1-2-3-4</sub>     | 178.8 | 178.7  | 179.1     |
| D <sub>2-3-4-5</sub>     | 1.2   | 0.9    | 0.3       |
| D <sub>3-4-5-6</sub>     | 179.2 | 179.6  | 178.0     |
| D <sub>4-5-6-7</sub>     | 20.9  | 26.1   | 35.7      |
| D <sub>5-6-7-8</sub>     | 179.6 | 179.8  | 178.8     |
| D <sub>6-7-8-9</sub>     | 1.1   | 1.2    | 0.1       |
| D <sub>7-8-9-10</sub>    | 178.1 | 177.9  | 179.8     |
| D <sub>8-9-10-11</sub>   | 0.3   | 0.7    | 0.1       |
| D <sub>9-10-11-12</sub>  | 178.5 | 177.7  | 179.9     |
| D <sub>10-11-12-13</sub> | 1.4   | 1.5    | 0.1       |
| D <sub>11-12-13-14</sub> | 178.9 | 179.3  | 179.6     |
| D <sub>12-13-14-15</sub> | 18.5  | 16.8   | 37.1      |
| D <sub>13-14-15-16</sub> | 179.9 | 179.1  | 178.9     |
| D <sub>14-15-16-17</sub> | 1.7   | 1.4    | 0.0       |
| D <sub>15-16-17-18</sub> | 176.9 | 176.7  | 179.1     |

Table A.22: Dihedral angles (in degree) for DTF-endcapped oligomers without SCs as a function of different dispersion corrected DFT methods for combination system.

| Dihedral angle<br>(D)    | B97D  | wB97XD | CAM-<br>B3LYP |
|--------------------------|-------|--------|---------------|
| D <sub>1-2-3-4</sub>     | 176.4 | 179.2  | 179.7         |
| D <sub>2-3-4-5</sub>     | 0.3   | 0.4    | 0.2           |
| D <sub>3-4-5-6</sub>     | 176.8 | 179.2  | 179.8         |
| D <sub>4-5-6-7</sub>     | 26.1  | 26.4   | 37.8          |
| D <sub>5-6-7-8</sub>     | 176.3 | 179.8  | 179.3         |
| D <sub>6-7-8-9</sub>     | 0.1   | 1.0    | 0.1           |
| D <sub>7-8-9-10</sub>    | 178.0 | 178.8  | 179.7         |
| D <sub>8-9-10-11</sub>   | 0.9   | 1.1    | 1.4           |
| D <sub>9-10-11-12</sub>  | 179.1 | 178.4  | 179.3         |
| D <sub>10-11-12-13</sub> | -0.5  | 0.6    | 0.1           |
| D <sub>11-12-13-14</sub> | 179.5 | 178.0  | 179.2         |
| D <sub>12-13-14-15</sub> | 24.5  | 27.6   | 36.5          |
| D <sub>13-14-15-16</sub> | 179.0 | 177.9  | 179.9         |
| D <sub>14-15-16-17</sub> | 0.9   | 0.8    | 0.3           |
| D <sub>15-16-17-18</sub> | 179.5 | 179.0  | 180.0         |



Table A.23: Dihedral angles (in degree) for ALD-endcapped oligomers with SCs as a function of different dispersion corrected DFT methods for combination system.

| Dihedral angle<br>(D)    | B97D  | wB97XD | CAM-<br>B3LYP |
|--------------------------|-------|--------|---------------|
| D <sub>1-2-3-4</sub>     | 179.1 | 179.4  | 177.7         |
| D <sub>2-3-4-5</sub>     | 1.2   | 2.3    | 0.4           |
| D <sub>3-4-5-6</sub>     | 179.9 | 178.9  | 179.8         |
| D <sub>4-5-6-7</sub>     | 49.1  | 74.5   | 43.4          |
| D <sub>5-6-7-8</sub>     | 162.7 | 173.4  | 178.3         |
| D <sub>6-7-8-9</sub>     | 0.2   | 0.1    | 0.0           |
| D <sub>7-8-9-10</sub>    | 164.7 | 175.1  | 179.3         |
| D <sub>8-9-10-11</sub>   | 4.3   | 0.7    | 1.2           |
| D <sub>9-10-11-12</sub>  | 170.1 | 178.4  | 179.3         |
| D <sub>10-11-12-13</sub> | 1.4   | 0.2    | 0.4           |
| D <sub>11-12-13-14</sub> | 176.0 | 179.3  | 178.9         |
| D <sub>12-13-14-15</sub> | 58.6  | 47.6   | 38.6          |
| D <sub>13-14-15-16</sub> | 176.4 | 173.4  | 177.3         |
| D <sub>14-15-16-17</sub> | 1.6   | 0.9    | 1.2           |
| D <sub>15-16-17-18</sub> | 175.6 | 177.4  | 178.9         |

Table A.24: Dihedral angles (in degree) for ALD-endcapped oligomers with SCs as a function of different dispersion corrected DFT methods for combination system.

| Dihedral Angle (D)       | B97D  | wB97XD | CAM-B3LYP |
|--------------------------|-------|--------|-----------|
| D <sub>1-2-3-4</sub>     | 172.1 | 173.2  | 178.9     |
| D <sub>2-3-4-5</sub>     | 0.2   | 2.5    | 2.4       |
| D <sub>3-4-5-6</sub>     | 179.1 | 171.4  | 179.7     |
| D <sub>4-5-6-7</sub>     | 47.0  | 45.7   | 46.9      |
| D <sub>5-6-7-8</sub>     | 177.8 | 178.4  | 178.2     |
| D <sub>6-7-8-9</sub>     | 0.4   | 0.1    | 0.3       |
| D <sub>7-8-9-10</sub>    | 176.6 | 179.5  | 179.3     |
| D <sub>8-9-10-11</sub>   | 0.4   | 1.7    | 0.0       |
| D <sub>9-10-11-12</sub>  | 178.2 | 174.3  | 177.6     |
| D <sub>10-11-12-13</sub> | 0.5   | 0.2    | 0.2       |
| D <sub>11-12-13-14</sub> | 179.5 | 166.8  | 174.2     |
| D <sub>12-13-14-15</sub> | 40.0  | 49.6   | 49.1      |
| D <sub>13-14-15-16</sub> | 167.8 | 176.1  | 179.9     |
| D <sub>14-15-16-17</sub> | 1.0   | 0.4    | 0.5       |
| D <sub>15-16-17-18</sub> | 172.5 | 177.2  | 176.4     |

### Standard Deviations

Table A.25: Standard deviations for the bond lengths of isolated systems for different molecule systems as function of different dispersion corrected DFT methods.

| Bond length     |       |        |           |       |
|-----------------|-------|--------|-----------|-------|
|                 | B97D  | wB97XD | CAM-B3LYP | B3LYP |
| ALD without SCs | 0.034 | 0.04   | 0.04      | 0.037 |
| ALD with SCs    | 0.034 | 0.04   | 0.039     | 0.037 |
| DTF without SCs | 0.03  | 0.038  | 0.038     | 0.033 |
| DTF with SCs    | 0.03  | 0.038  | 0.038     | 0.035 |

Table A.26: Standard deviations for the bond angles of isolated systems for different molecule systems as function of different dispersion corrected DFT methods.

| Bond angle      |      |        |           |       |
|-----------------|------|--------|-----------|-------|
|                 | B97D | wB97XD | CAM-B3LYP | B3LYP |
| ALD without SCs | 3.7  | 3.8    | 3.8       | 3.8   |
| ALD with SCs    | 4.2  | 4.1    | 4.1       | 4.2   |
| DTF without SCs | 3.9  | 3.8    | 3.9       | 3.9   |
| DTF with SCs    | 4.2  | 4.0    | 4.0       | 4.1   |

Table A.27: Standard deviations for the dihedral angles of isolated systems for different molecule systems as function of different dispersion corrected DFT methods.

| Dihedral Angle  |      |        |           |       |
|-----------------|------|--------|-----------|-------|
|                 | B97D | wB97XD | CAM-B3LYP | B3LYP |
| ALD without SCs | 88.5 | 87.7   | 88.0      | 88.2  |
| ALD with SCs    | 83.7 | 83.4   | 86.8      | 86.9  |
| DTF without SCs | 88.5 | 87.5   | 88.0      | 88.2  |
| DTF with SCs    | 85.6 | 85.1   | 86.3      | 86.8  |

Table A.28: Standard deviations for the bond lengths of interacting systems for different molecule systems as function of different dispersion corrected DFT methods.

| Bond length           |       |        |           |
|-----------------------|-------|--------|-----------|
|                       | B97D  | wB97XD | CAM-B3LYP |
| ALD without SCs & CNT | 0.035 | 0.041  | 0.040     |
| ALD with SCs & CNT    | 0.034 | 0.040  | 0.039     |
| DTF without SCs & CNT | 0.029 | 0.037  | 0.037     |
| DTF with SCs & CNT    | 0.032 | 0.037  | 0.040     |

Table A.29: Standard deviations for the bond angles of interacting systems for different molecule systems as function of different dispersion corrected DFT methods.

| Bond angle            |      |        |           |
|-----------------------|------|--------|-----------|
|                       | B97D | wB97XD | CAM-B3LYP |
| ALD without SCs & CNT | 3.6  | 3.7    | 3.8       |
| ALD with SCs & CNT    | 4.3  | 4.5    | 4.2       |
| DTF without SCs & CNT | 3.9  | 4.0    | 3.9       |
| DTF with SCs & CNT    | 4.5  | 4.2    | 4.0       |

Table A.30: Standard deviations for the dihedral angles of interacting systems for different molecule systems as function of different dispersion corrected DFT methods.

| Dihedral Angle        |      |        |           |
|-----------------------|------|--------|-----------|
|                       | B97D | wB97XD | CAM-B3LYP |
| ALD without SCs & CNT | 89.2 | 88.9   | 87.9      |
| ALD with SCs & CNT    | 82.6 | 84.5   | 87.0      |
| DTF without SCs & CNT | 88.5 | 88.4   | 87.9      |
| DTF with SCs & CNT    | 85.2 | 84.2   | 86.0      |